Analysis of metabolic pathways controlling cAMP-regulated aquaporin-2 trafficking in renal principal cells

vorgelegt von

Dipl.-Ing. Maike Schulz

geb. in Berlin

von der Fakultät III - Prozesswissenschaften
der Technischen Universität Berlin
zur Erlangung des akademischen Grades

Doktor der Naturwissenschaften
- Dr. rer. nat. -

genehmigte Dissertation

Promotionsausschuss:
Vorsitzender: Prof. Dr. Peter Neubauer
Gutachter: Prof. Dr. Jens Kurreck
Gutachter: Prof. Dr. Roland Lauster
Gutachter: PD Dr. Enno Klußmann

Tag der wissenschaftlichen Aussprache: 18.07.2018

Berlin 2018

Diese Arbeit wurde von Februar 2014 bis Mai 2018 am Max-Delbrück-Centrum für Molekulare Medizin in der Helmholtz-Gemeinschaft (MDC) in Berlin unter der Leitung von PD Dr. Enno Klußmann angefertigt.

DANKSAGUNG

Zunächst möchte ich mich bei PD Dr. Enno Klußmann für die Bereitstellung des Themas und die tolle Unterstützung über all die Jahre bedanken. Danke, dass du, im wahrsten Sinne des Wortes, immer eine offene Tür für deine Doktoranden hast.
Vielen Dank an Prof. Dr. Jens Kurreck und Prof. Dr. Roland Lauster für die Begutachtung dieser Arbeit, sowie Prof. Dr. Peter Neubauer für den Vorsitz der Promotionskommission.
Ein großes Dankeschön auch an alle Kooperationspartner, mit denen ich in meiner Doktorandenzeit zusammenarbeiten durfte, allen voran Prof. Dr. Karsten Hiller, Dr. Andre Wegner, Tobias Ludwig und Yannic Nonnenmacher von der TU Braunschweig für die Metabolomanalyse der IMCD Zellen und, dass ihr mich so freundlich und offen in eurem Labor willkommen geheißen habt, sowie Dr. Daniela Panáková und Kitti Csályi am MDC Berlin und Prof. Nathan Dascal und Dr. Shimrit Oz von der Universität Tel Aviv für die sehr angenehme Zusammenarbeit.
Vielen Dank, Jenny Eichhorst und Dr. Burkhardt Wiesner, dass ihr mir bei allen Fragen und Problemen rund ums LSM geholfen habt.
Ich danke allen aktuellen und ehemaligen Mitgliedern der AG Klußmann für eine tolle Arbeitsatmosphäre, schöne gemeinsame Ausflüge und dass ihr mir einfach immer mit Rat und Tat zur Seite standet. Ein paar Kollegen gilt besonderer Dank: Caro, danke, dass du über meine gesamte Doktorandenzeit an meiner Seite warst und mich so unermüdlich unterstützt hast. Kathi, danke für deine wundervolle positive Art, du hast ein bisschen Sonnenschein in den Laboralltag gebracht. Alessandro, danke für deinen fachlichen Rat, sowie aufmunternde Worte und Schafe :) Maria, danke, dass du immer ein offenes Ohr für mich hattest und das Schreiben dieser Arbeit durch Pizza und Kaffeepausen verschönert hast. Andrea und Beate, danke für eure wunderbare Unterstützung im Labor.
Fürs Korrekturlesen und die konstruktive Kritik ein großes Dankeschön an Ryan, Enno, Alessandro, Leonie und Katharina.
Ich danke meiner Familie und meinen Freunden, dass sie mich immer unterstützt und an mich geglaubt haben. Yannick, du hast so maßgeblich zu dieser Arbeit beigetragen, mich immer wieder aufgemuntert, mir Kraft gegeben. Danke, dass es dich gibt!

TABLE OF CONTENTS

LIST OF FIGURES

LIST OF TABLES

ABBREVIATIONS AND ACRONYMS

Common abbreviations and SI units are not listed

2DG	2-deoxyglucose
4AD	4-acetyldiphyllin
aa	amino acid
AC	adenylyl cyclase
ACE	angiotensin-converting enzyme
A. dest.	aqua destillata
AE1	anion exchanger 1
AICAR	5-aminoimidazole-4-carboxamide-1-β-d-ribofuranoside
AKAP	A-kinase anchoring protein
AKB domain	A-kinase binding domain
AMP	adenosine monophosphate
AMPK	AMP-activated protein kinase
Ang I / II	angiotensin I / II
ANP	atrial natriuretic peptide
ATP	adenosine triphosphate
AQP2	aquaporin-2
AVP	arginine-vasopressin
BafA1	bafilomycin A1
BNP	brain natriuretic peptide
BSA	bovine serum albumin
C subunit	catalytic subunit of PKA
CAII	carbonic anhydrase II
cAMP	cyclic adenosine-3',5'-monophosphate
cDNA	complementary deoxyribonucleic acid
cGMP	cyclic guanosine-3',5'-monophosphate
CHIP	C terminus of HSC70-Interacting Protein
COX2	cyclooxygenase-2
CRE	cAMP-responsive element
Da	dalton
DAPI	4', 6-diamidine-2'-phenylindole dihydrochloride
dbcAMP	dibutyryl-cAMP
D/D domain	dimerisation/docking domain
dDAVP	1-Desamino-8-D-Arginin-Vasopressin / Desmopressin
DMEM	Dulbecco's modified eagle medium
DNA	desoxyribonucleic acid
EDTA	ethylenediaminetetraacetic acid
ER	endoplasmic reticulum
ERGIC	ER- Golgi intermediate compartment
F-actin	filamentous actin
FBP	fructose-1,6-bisphosphate
FCS	fetal calf serum
FSK	forskolin
fwd	forward (primer)
G protein	guanine nucleotide-binding protein
G-actin	globular actin
G6PDH	glucose-6-phosphate dehydrogenase
GAPDH	glyceraldehyde-3-phosphate dehydrogenase
GC-MS	gas chromatography coupled to mass spectrometry
GDP	guanosine diphosphate
GEF	guanine nucleotide-exchange factor
GFP	green fluorescent protein
GMP	guanosine monophosphate
GPCR	G-protein-coupled receptor
GTP	guanosine triphosphate
HMG-CoA	3-hydroxy-3-methyl-glutaryl-coenzyme A

Hsp90	heat-shock protein 90
IC	intercalated cell
IF	immunofluorescence
IP	immunoprecipitation
IMCD	inner medulla collecting duct
LB medium	lysogeny broth medium
LC3	short for MAP1LC3B
LDH	lactate dehydrogenase
LKB1	liver kinase B1
LSM	laser scanning microscope
MAL	myelin and lymphocyte-associated protein
MAP1LC3B	microtubule-associated proteins 1A/1B light chain 3B
MCD4	mouse collecting duct (cell line)
MDCK	Madin-Darby canine kidney (cell line)
MID	mass isotopomer distribution
MLB	mild lysis buffer
mRNA	messenger RNA
mTORC1	mechanistic target of rapamycin complex 1
NADH	nicotinamide adenine dinucleotide
NDI	nephrogenic diabetes insipidus
NHE	Na+/H+-exchanger
NKCC	Na-K-2Cl-Cotransporter
NO	nitric oxide
NP	natriuretic peptides
NP40	Nonidet P-40
ns	not significant
NSIAD	nephrogenic syndrome of inappropriate antidiuresis
OAA	oxaloacetate
p	value used for statistic assessment
PBS	phosphate-buffered saline
PC	pyruvate carboxylase
PCR	polymerase chain reaction
PDE	phosphodiesterase
PDH	pyruvate dehydrogenase
PEI	polyethylenimine
PEP	phosphoenolpyruvate
PFK	phosphofructokinase
PGK	phosphoglycerate kinase
pH value	negative of the logarithm to base 10 of the molar concentration of hydrogen ions
PKA	protein kinase A, cAMP-dependent protein kinase
PKM	pyruvate kinase, muscle isozyme
POD	peroxidase
PP	protein phosphatase
PPI	protein – protein interaction
PPP	pentose phosphate pathway
PVDF	polyvinylidene fluoride
qPCR	quantitative PCR
RAAS	renin-angiotensin-aldosterone system
rev	reverse (primer)
RhoGDI	Rho protein GDP dissociation inhibitor
RISC	RNA-induced silencing complex
RNA	ribonucleic acid
rpm	revolutions per minute
R subunit	regulatory subunit of PKA
RT	room temperature
sAC	soluble adenylyl cyclase
SD	standard deviation
SDS	sodium dodecyl sulfat
SDS-PAGE	SDS-polyacrylamide gel electrophoresis

SEM	standard error of mean
SERCA	sarco/endoplasmic reticulum Ca^{2+} ATPase
SGLT	sodium-glucose cotransporter
shRNA	small hairpin RNA
SIADH	syndrome of inappropriate antidiuretic hormone secretion
siRNA	small interfering RNA
SLB	standard lysis buffer
SNAP23	synaptosome-associated protein
SO	sodium oxamate
TBS	tris-buffered saline
TBS-T	TBS + tween
TCA	trichloroacetic acid
TM5b	tropomyosin 5b
UT-A1	urea transporter A1
V-ATPase	vacuolar H^+-ATPase
V2R	vasopressin receptor type 2
VAMP2/3	vesicle-associated membrane protein 2/3
WB	Western blotting
WT	wild-type

SUMMARY

One of the main effectors of the second messenger cyclic adenosine monophosphate (cAMP) is the ubiquitously expressed serine/threonine protein kinase, cAMP-dependent protein kinase (PKA). Binding of cAMP to the regulatory subunits of PKA results in a conformational change and the release of the catalytic subunits to phosphorylate nearby targets. To ensure spatially and temporally controlled phosphorylation of a subset of its substrates, PKA is tethered to intracellular compartments by A-kinase anchoring proteins (AKAPs). Around 50 different AKAPs have been described that compartmentalize PKA signalling in various cell types. Canonical AKAPs share a consensus PKA binding motif, which encompasses hydrophilic anchor points that were recently identified by our group. The results of this thesis show that the constituent amino acids are crucial for PKA binding. Detailed knowledge of the AKAP-PKA interaction site will help to develop AKAP-specific strategies for pharmacological interference.

A pathway that requires AKAP-controlled PKA activity is the antidiuretic hormone arginine-vasopressin (AVP)-regulated water reabsorption from primary urine in the kidneys collecting duct. Binding of AVP to its receptor on the surface of renal principal cells causes intracellular cAMP elevation, PKA activation and translocation of the water channel aquaporin-2 (AQP2) from intracellular vesicles into the plasma membrane. The insertion of AQP2 increases the water permeability of the distal part of the nephron, which enables fine-tuning of body water homeostasis. The molecular pathways that underlie controlled AQP2 redistribution are only partially understood. Especially the metabolic control of the vesicle transport is still unknown. In this thesis, a global metabolic analysis of primary inner medullary collecting duct (IMCD) cells shows that AVP stimulation does not modulate major metabolic pathways. Yet, identification of the metabolic enzyme glucose-6-phosphate dehydrogenase (G6PDH) and the metabolic sensors AMP-activated kinase (AMPK) and vacuolar H^+-ATPase (V-ATPase) on AQP2-bearing vesicles indicates local metabolic control of AQP2 trafficking. Recent findings by our group showed that treatment of renal principal cells with the V-ATPase inhibitor 4-acetyl-diphyllin (4AD) diminishes vesicular acidification and interferes with the AVP-induced AQP2 translocation into the plasma membrane. The results of this thesis show that 4AD inhibits V-ATPase in its assembled state and thus not only impairs its proton pumping activity, but also its reversible disassembly. The data suggest that this regulatory mechanism might play a role in AQP2-bearing vesicle fusion with the plasma membrane and metabolic regulation.

The identification of proteins that control AQP2 trafficking is critical for the development of pharmacological agents that target AQP2 localisation for therapeutic purposes. Defective translocation of AQP2 causes water balance disorders, such as nephrogenic diabetes insipidus, which is characterized by incomplete urinary concentration. In contrast, a predominant localization of AQP2 in the plasma membrane is associated with excessive water retention in heart failure patients.

ZUSAMMENFASSUNG

Die cAMP-abhängige Serin/Threonin Proteinkinase A (PKA) ist ubiquitär exprimiert und der Haupteffektor des sekundären Signalmoleküls cAMP. Die Bindung von cAMP an die regulatorischen Untereinheiten von PKA bewirkt eine Konformationsänderung, durch die sich die katalytischen Untereinheiten vom Holoenzym lösen und Zielproteine phosphorylieren. A-Kinase Ankerproteine (AKAP) halten PKA in definierten Zellkompartimenten und ermöglichen so die räumliche und zeitliche Kontrolle der Phosphorylierung. Etwa 50 verschiedene, zum Teil zelltyp-spezifische AKAPs wurden bislang beschrieben. Klassische AKAPs binden PKA durch ein Motiv hydrophober Aminosäuren, das kürzlich von unserer Arbeitsgruppe um polare Ankerpunkte erweitert wurde. In dieser Doktorarbeit wird gezeigt, dass diese Ankerpunkte entscheidend für die Binding von regulatorischen Untereinheiten der PKA sind. Ein detailliertes Bild der AKAP-PKA Interaktion ist für die Entwicklung AKAP-spezifischer Pharmazeutika von großer Bedeutung.

Ein Signalweg, der die Kontrolle der PKA-Aktivität durch AKAPs benötigt, ist die vom antidiuretischen Hormon Arginin-Vasopressin (AVP) regulierte Rückresorption von Wasser aus dem Primärharn im Sammelrohr der Niere. Die Binding von AVP an seinen von renalen Prinzipalzellen exprimierten Rezeptor bewirkt die Erhöhung des intrazellulären cAMP-Spiegels, die Aktivierung von PKA und die dadurch induzierte Umverteilung von AQP2-haltigen Vesikeln in die Plasmamembran. Der Einbau von AQP2 in die Plasmamembran erhöht die Wasserdurchlässigkeit des distalen Bereichs des Nephrons und trägt so zur Feinregulation des Wasserhaushalts bei. Die der AQP2-Umverteilung zugrunde liegenden Signalwege sind noch nicht in vollem Umfang untersucht und vor allem Untersuchungen zur metabolischen Regulation des Vesikeltransports fehlen gänzlich. Die für diese Doktorarbeit durchgeführte Metabolomanalyse von primär isolierten Zellen aus dem renalen Sammelrohr der Ratte, IMCD Zellen, zeigt, dass die Stimulierung mit AVP keine substanziellen Änderungen der zellulären Stoffwechselwege induziert. Jedoch deutet die Identifizierung des metabolischen Enzyms Glucose-6-phosphat-Dehydrogenase (G6PDH), sowie der Stoffwechselsensoren AMP-aktivierte Kinase (AMPK) und vakuoläre H^+-ATPase (V-ATPase) auf AQP2-haltigen Vesikeln auf eine lokale Regulierung des Vesikeltransports durch Bestandteile des Metabolismus hin. Ergebnisse vorangegangener Studien unserer Arbeitsgruppe zeigen, dass ein Inhibitor der V-ATPase, 4-acetyldiphyllin (4AD), die Ansäuerung von intrazellulären Vesikeln hemmt und die AVP-induzierte Umverteilung von AQP2 in die Plasmamembran beeinträchtigt. In dieser Arbeit wird gezeigt, dass 4AD die reversible Dissoziation der V-ATPase-Untereinheiten hemmt. Dadurch wird nicht nur die Etablierung des Protonengradienten inhibiert, sondern auch regulatorische Mechanismen beeinflusst, die potenziell von einer Dissoziation der V-ATPase abhängen, wie Vesikelfusion und Stoffwechselsensorik. Die Erforschung von Proteinen und Signalwegen, die den AQP2-Transport kontrollieren, ist entscheidend für die Wirkstoffentwicklung zur Behandlung von Krankheiten, die mit einem gestörten Wasserhaushalt assoziiert sind, wie beispielsweise nephrogener Diabetes insipidus oder Herzinsuffizienz.

1. INTRODUCTION

Parts of this introduction are adapted from the review “The Trafficking of the Water Channel Aquaporin-2 in Renal Principal Cells - a Potential Target for Pharmacological Intervention in Cardiovascular Diseases.” Vukicevic, T., M. Schulz, D. Faust and E. Klussmann (2016) Front Pharmacol 7: 23. First authorship was shared with Tanja Vukicevic. I hereby declare that only the parts that I contributed to the publication were used for this thesis.

1.1 The kidney

The kidney filters blood to excrete toxins, control blood pressure, and to regulate body water, solute and pH homeostasis. This filtration takes place at an average rate of 120 ml/min, which creates a final volume of more than 170 L of primary urine per day. The nephron is the functional unit of the kidney, and along its length, primary urine is concentrated approximately 100-fold, resulting in the excretion of two to four liters of urine per day in adults (Figure 1). The kidney contains around 1–2 million nephrons. These tubular systems comprise several functionally distinct segments. Within the nephron, blood first enters the glomerulus, and passes through a three-layer filtration barrier built up by vascular fenestrated endothelial cells, the glomerular basement membrane and podocytes into the surrounding Bowman´s capsule. The filtrate flows from there through the proximal convoluted tubule, where organic nutrients and the main portion of water and ions are absorbed into the blood by co-transport with sodium. The major luminal sodium transporters in the proximal tubule are the sodium-glucose cotransporter (SGLT) and the Na^+/H^+-exchanger (NHE). Sodium flow through the epithelial cells is ensured by Na^+/K^+-ATPases on their basolateral site. Along the proximal convoluted tubule and descending limb of Henle most of the water is constitutively reabsorbed following an osmotic gradient that is established by high salt concentrations in the medullary interstitium due to active solute transport in the ascending limb of Henle. The ascending limb of Henle is impermeable to water and a major site of sodium reabsorption from the concentrated filtrate, mainly *via* $Na^+/K^+/Cl^-$ (NKCC) - symport. This builds up the driving force for passive water reabsorption from the descending limb as a countercurrent system. In the distal nephron, aldosterone and vasopressin allow defined hormonal control of remaining sodium and water reabsorption, respectively. The concentrated urine leaves the collecting duct through the ureter and enters the bladder, where it is stored until it is released.

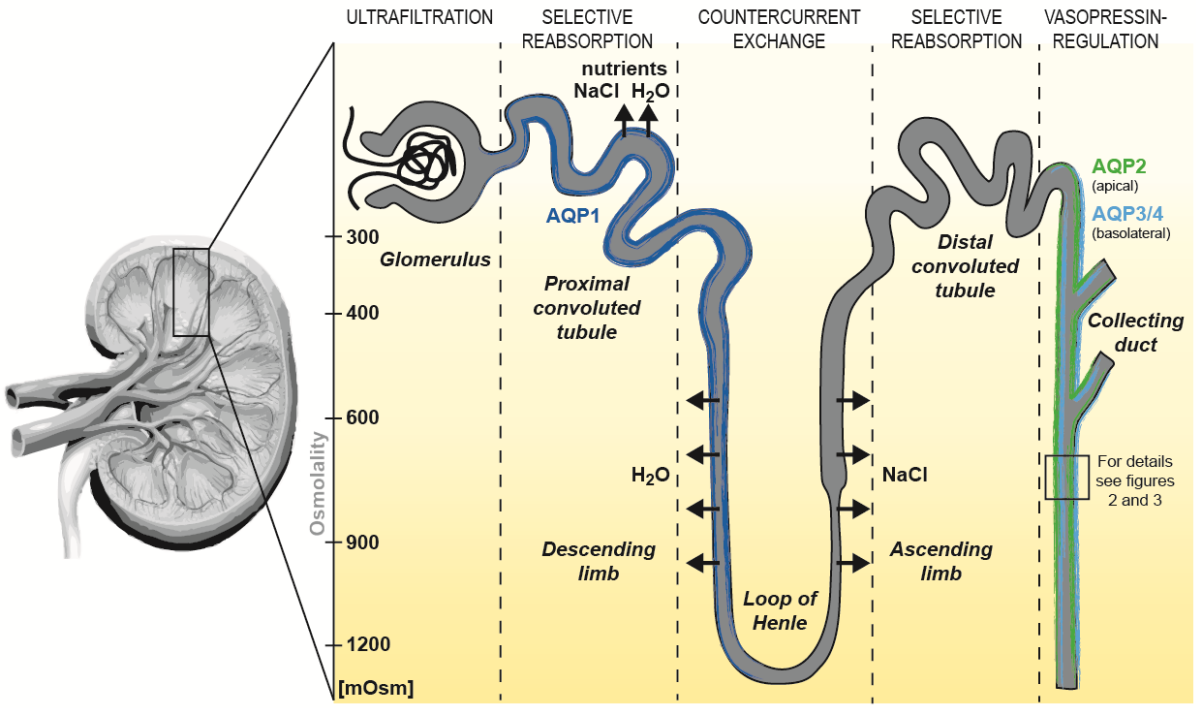

Figure 1: The nephron is the functional unit of the kidney. Blood is filtered through the glomerulus to discharge toxins, allow electrolyte and water homeostasis, and to control blood pressure. Along the proximal tubule and descending limb of Henle the majority of water is constitutively reabsorbed, following the osmotic gradient established by active sodium transfer. In the water-impermeable ascending limb of Henle and distal tubule, sodium is reabsorbed. The distal part of the nephron and collecting duct enables hormone-dependent differential reabsorption of sodium and water according to the demand signaled through aldosterone and arginine-vasopressin (AVP), respectively. Aquaporin water channels 1-4 (AQP1-4) mediate water flow across the plasma membrane of renal epithelial cells.

1.1.1 Blood pressure regulation

The renin-angiotensin-aldosterone system (RAAS) is the main regulator of blood pressure and the interface between cardiovascular and renal function. Low blood pressure, hypovolemic conditions and low tubular sodium induce the secretion of renin from renal juxtaglomerular cells. Tubular sodium is sensed by the macula densa, a chemoreceptor regulating the glomerular filtration rate and renin secretion according to distal tubular osmolality (not shown in Figure 1). Renin hydrolyzes the precursor angiotensinogen to angiotensin I (Ang I), which in turn is converted to angiotensin II (Ang II) by the angiotensin-converting enzyme (ACE). Ang II acts as a vasoconstrictor to increase blood pressure. In addition, Ang II stimulates aldosterone and AVP secretion, which increases renal sodium and water reabsorption, respectively. This, in turn, raises blood volume and consequently blood pressure. *Vice versa*, hypervolemic conditions cause stretching of the vasculature and are sensed by baroreceptors that induce the release of natriuretic peptides (NP). The main classes of NPs are the atrial natriuretic peptide (ANP), which is synthesized by atrial myocytes, and brain natriuretic peptide (BNP), released from ventricular walls. BNP was named following its initial identification in the brain, but is today often referred to as B-type NP. The ANP and BNP prohormones give rise to different cleaved versions that have mainly

vasodilative, natriuretic, kaliuretic or diuretic effects (reviewed in Pandit *et al.* 2011). As a result, decreased systemic vascular resistance and increased diuresis due to enhanced glomerular filtration rate, natriuresis and kaliuresis lowers blood pressure and hypervolemia. Additionally, NPs diminish renin secretion, which suppresses the RAA system.

1.1.2 Aquaporin water channels

Aquaporin (AQP) water channels render tubular epithelial membranes permeable to water, which is the key component of renal filtrate concentration. Active sodium transport establishes the osmotic gradient that enables water flow. In mammals, 13 structurally highly similar AQPs, AQP0-AQP12, are expressed. All AQPs occur as homotetramers with each monomer forming a water pore. Six transmembrane domains form the central AQP structure. A seventh pseudo transmembrane domain composed of the dual conserved signature motif asparagine-proline-alanine (NPA) forms the water pore (Jung *et al.* 1994, Walz *et al.* 1997).
Selectivity of the water channel is achieved by an electrostatic barrier formed by a conserved arginine residue and the dual NPA motifs that prevent passage of ions (de Groot *et al.* 2003). Water molecules pass through the channel as a hydrogen bond-connected chain (Kosinska Eriksson *et al.* 2013).
Along the nephron, nine AQPs (AQP1-8 and AQP11) are expressed with distinct localization to specific segments. AQP1-4 play crucial roles in water reabsorption from primary urine (Figure 1). AQP1 is localized in the apical plasma membrane of epithelial cells of the proximal tubule and the descending limb of Henle (Nielsen *et al.* 1993, Schnermann *et al.* 1998). There it facilitates reabsorption of 80-90 % of filtrate water. The ascending limb of Henle does not express AQPs and is therefore impermeable to water. The cells of the distal convoluted tubule and the collecting duct constitutively express AQP3 and AQP4 in the basolateral plasma membrane. The apical plasma membrane is generally water impermeable, however, collecting duct principal cells additionally express AQP2 that is inserted into the apical plasma membrane when supplementary water reabsorption is required (Fushimi *et al.* 1993, Ecelbarger *et al.* 1995, Terris *et al.* 1995).

1.1.3 Cell types of the collecting duct

The main cell types of the collecting duct are intercalated cells (ICs) type A (α-IC) and B (β-IC), which regulate acid-base homeostasis, as well as principal cells, which are important regulators of water homeostasis. Principal and intercalated cells line the collecting duct in an alternating pattern with a ratio of approximately 2:1 in the cortex ranging to 4:1 in the inner medulla (Guo *et al.* 2015).

Figure 2 gives an overview about the major transport proteins controlling water and ion flux between lumen and interstitial space in the collecting duct. α-ICs secrete protons into the tubular lumen, thereby increasing primary urine acidity and reabsorbing bicarbonate. Conversely, β-ICs recycle protons into the circulation by secreting bicarbonate. The main enzyme for proton transport across the membrane is the vacuolar H^+-ATPase (V-ATPase), which is expressed in the plasma membrane of ICs. The localization of the V-ATPase to the plasma membrane underlies the regulation of cAMP-dependent protein kinase (PKA) and AMP-activated kinase (AMPK), and will be covered in more depth in chapter 1.2.2.1. Briefly, alkaline luminal pH raises intracellular bicarbonate levels, which is sensed by soluble adenylyl cyclases (sAC). sACs in turn increase cAMP levels, activating PKA to induce V-ATPase apical membrane localization in α-ICs (Pastor-Soler *et al.* 2003, Paunescu *et al.* 2008, Paunescu *et al.* 2010). This regulation is counteracted by AMPK to avoid excessive ATP-consumption (Gong *et al.* 2010). Intercalated cells are unique in their capability to use active proton transport through V-ATPase to maintain the membrane potential for secondary solute transport, which is dependent on Na^+/K^+ P-type ATPase in other cell types (Chambrey *et al.* 2013).

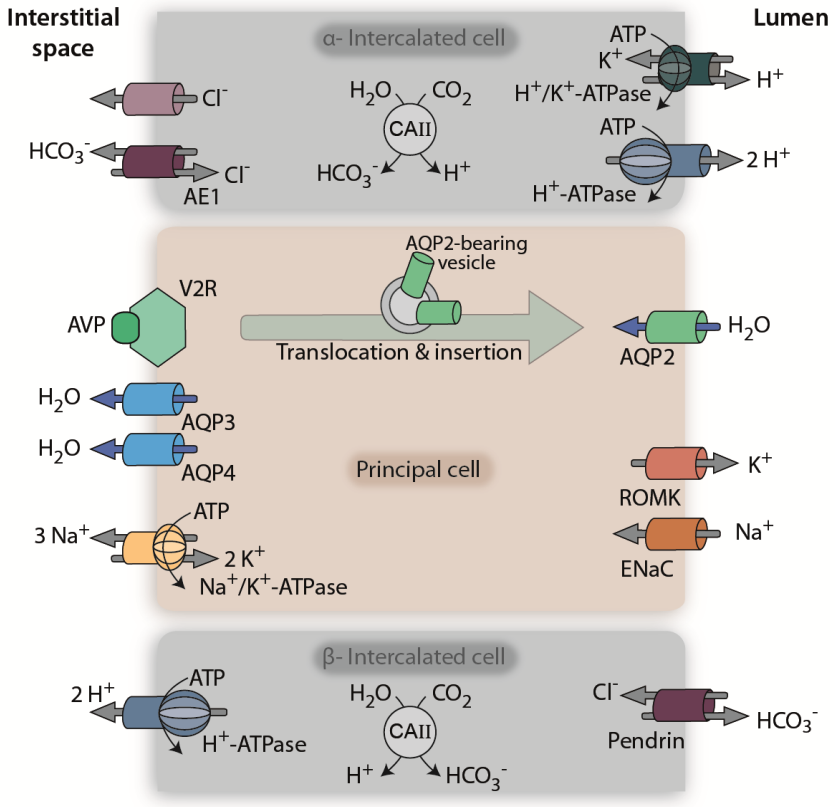

Figure 2: Cell types of the collecting duct. The distal part of the nephron is lined by principal and intercalated cells, which are specialized cells for water and acid-base homeostasis, respectively. Type A ICs (α-ICs) can increase primary urine acidity through the secretion of protons, along with bicarbonate incorporation into the circulation. Conversely, type B ICs (β-ICs) can increase blood acidity by secreting bicarbonate into primary urine. Carbonic anhydrase (CAII), the proton pump vacuolar H^+-ATPase (V-ATPase) and the chloride-bicarbonate exchanger anion-exchanger 1 (AE1) and pendrin are required for acid-base homeostasis. The potassium channel ROMK, the sodium channel ENaC and the sodium-potassium ATPase ensure solute homeostasis of renal principal cells.

Interplay between ICs and principal cells in the control of water homeostasis is not well understood. Choi *et al.* (2015) observed a reduction of AVP-induced AQP2 plasma membrane localization after exposure of inner medullary collecting duct (IMCD) cells to an acidic pH, indicating that there is a connection between IC function and principal cell-mediated water reabsorption.

1.1.4 Water homeostasis regulated by renal collecting duct principal cells

The folding of AQP2 and its assembly into homotetramers takes place in the endoplasmic reticulum (ER), from which the channels are transported through the Golgi and finally stored on perinuclear vesicles. AVP stimulation of principal cells induces a translocation of AQP2 into the apical plasma membrane, where it facilitates water re-uptake from primary urine (Hayashi *et al.* 1994, Katsura *et al.* 1995). This process permits fine-tuning of approximately 10 % of water reabsorption, accounting for 10 to 20 L of final daily urine, that can be modulated by the release of antidiuretic hormones according to the body`s water demand. An increase in blood osmolality from either hypovolemia or solute changes such as hypernatremia are sensed by osmoreceptors in the hypothalamus that promote the release of AVP into the circulation (Verney 1947). AVP is synthesized as a preprohormone that undergoes enzymatic cleavage, which results in its activation. The active peptide hormone is stored in the pituitary gland, from which it is secreted into the circulation to induce collecting duct water reabsorption. Consequently, blood volume rises, osmolality is adjusted and body water homeostasis is re-established. Aldosterone regulates the sodium and potassium balance in renal principal cells and in this way participates in constitutive water reabsorption (reviewed in Pearce *et al.* 2015).

1.1.5 AVP-regulated water transport – The AQP2 shuttle

On the surface of collecting duct principal cells, AVP binds to the G-protein-coupled receptor (GPCR) vasopressin type 2 receptor (V2R), which is located in the basolateral plasma membrane (Figure 3). The GPCR undergoes a conformational change upon ligand binding, which enables the binding of heterotrimeric guanine nucleotide-binding proteins (G proteins) to the intracellular domains. G protein activation is characterized by the exchange of one molecule GDP for GTP within its α-subunit, which promotes the dissociation of its βγ-subunit. Both subunits, the Gα and the Gβγ dimer, stimulate intracellular effectors, including adenylyl cyclases (ACs). G proteins can be divided into four main families according to their α subunits: AC-stimulatory G_s, AC-inhibitory $G_{i/o}$, phospholipase C-activating $G_{q/11}$ and small G protein-linked $G_{12/13}$. ACs convert adenosine triphosphate into the second messenger cAMP and pyrophosphate. AC3 and AC6 are the major AC isoforms in principal cells. $G_s\alpha$ or Gβγ activate AC3 and AC6, whereas $G_i\alpha$ inhibits them. In order to mimic AVP-induced rises

in intracellular cAMP levels, a direct activator of ACs, forskolin (FSK), is often used in experimental settings.

The main cAMP effector enzyme is the cAMP-dependent protein kinase, PKA. The PKA holoenzyme is composed of a dimer of regulatory subunits (RIα, RIβ, RIIα, or RIIβ), each of which binds to one catalytic subunit (Cα, Cβ, Cγ, or PrKX) in the inactive state, creating a tetrameric holoenzyme. The binding of two molecules of cAMP to each R subunit induces a conformational change that releases the C subunits, which are then active to phosphorylate nearby targets, as for example, AQP2 (Figure 3).

AQP2 undergoes constitutive recycling. Its trafficking from intracellular vesicles into the plasma membrane and endocytic retrieval to its intracellular storage site is in dynamic equilibrium under resting conditions. Post-translational modifications influence AQP2's intracellular localization. Four serine residues, at positions 256, 261, 264 and 269 in the AQP2 C terminus, are subject to phosphorylation by various kinases, and lysine 270 is an ubiquitination site. During maturation AQP2 is glycosylated in the endoplasmic reticulum and Golgi, but the role of AQP2 glycosylation for trafficking is still unclear.

The phosphorylation sites are associated with differential regulation of AQP2 trafficking and stability, but the exact mechanisms are not yet well understood. AVP-induced increases in intracellular cAMP levels activate PKA, which phosphorylates AQP2 at S256, and shifts the equilibrium towards plasma membrane insertion (Fushimi *et al.* 1997, Katsura *et al.* 1997, Arnspang *et al.* 2016). At least three monomers of the AQP2 tetramer need to be phosphorylated to enable translocation (Kamsteeg *et al.* 2000). It is also of note that S256 is described as a Casein kinase 2 site, presumably regulating AQP2 maturation (Procino *et al.* 2003). The general model indicates that phosphorylation at S256 is necessary, but not sufficient for AQP2 membrane localization. Treatment of Madin-Darby canine kidney (MDCK) cells expressing the phosphomimic mutant S256D with the protein kinase inhibitor H89 induces AQP2 internalization, suggesting that phosphorylation of other PKA substrate proteins is required for membrane localization of AQP2 (Nejsum *et al.* 2005). However, mutations of S256 or R254 in the PKA consensus sequence R-R-Q-S cause severe urine concentration defects (see chapter 1.1.7.1 and Figure 5). Also, an AQP2 mutant missing all serines and threonines at potential C-terminal phosphorylation sites, but including the phosphomimic S256D was shown to accumulate in the plasma membrane when expressed in LLC-PK1 cells (Arthur *et al.* 2015). Interestingly, inhibition of endocytosis leads to AQP2 accumulation in the apical plasma membrane of cultured collecting duct cells, regardless of S256 phosphorylation, which emphasizes the importance of the recycling pathway under baseline conditions (Lu *et al.* 2004a). The phosphorylation state of the other three C-terminal residues of AQP2, S261, S264 and S269, also changes in response to AVP stimulation (Hoffert *et al.* 2007, Fenton *et al.* 2008, Hoffert *et al.* 2008).

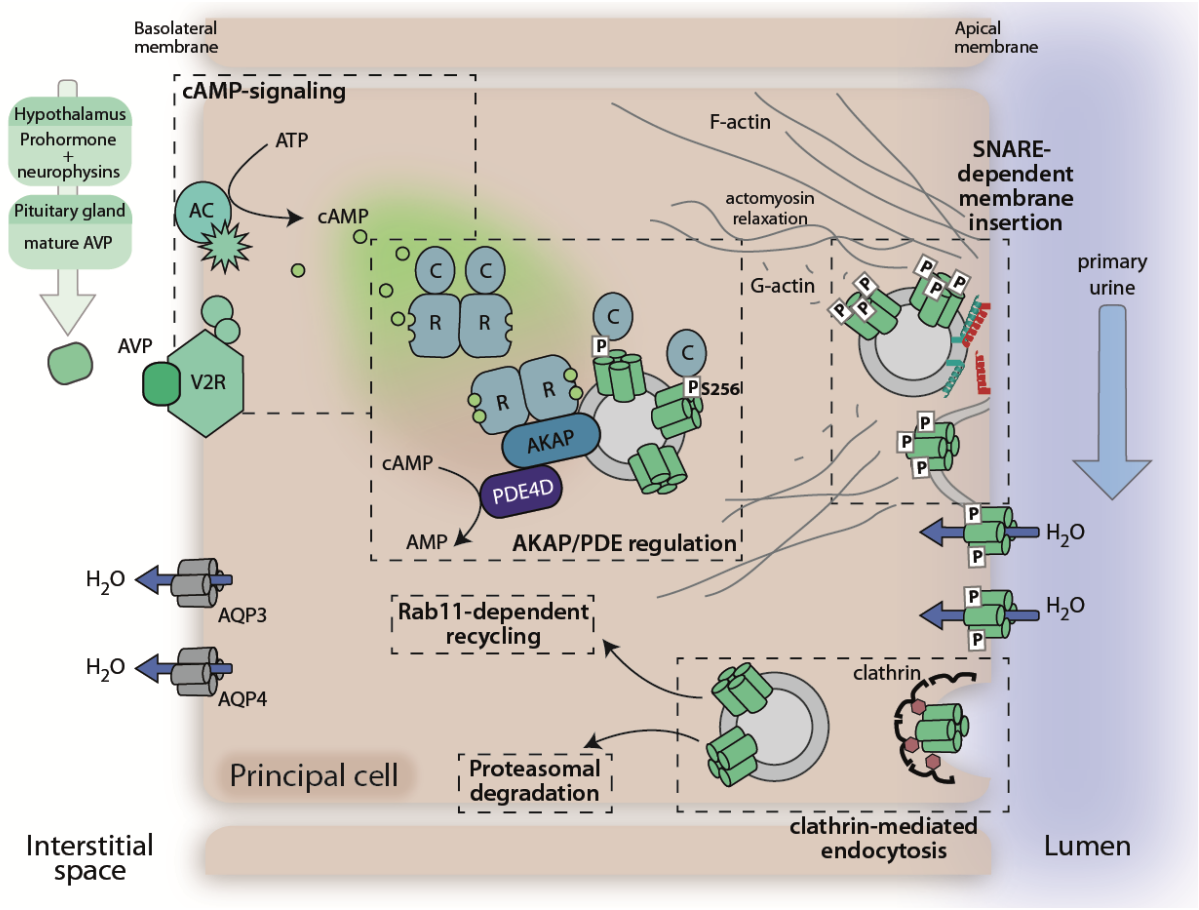

Figure 3: The AVP-stimulated redistribution of AQP2 in renal principal cells. Antidiuretic stimuli, for example hypovolemia, cause AVP release from the pituitary gland. In renal collecting duct principal cells, AVP induces the translocation of AQP2 from intracellular vesicles into the plasma membrane, which facilitates water reabsorption from primary urine. The dashed lines highlight major signaling and trafficking principles that regulate the translocation process. AVP binding to the GPCR vasopressin type 2 receptor (V2R) induces ACs to produce cAMP, which in turn activates AKAP-tethered PKA. Catalytic subunits of PKA phosphorylate AQP2 at serine 256, which favors vesicle transport to the apical plasma membrane and soluble *N*-ethylmaleimide-sensitive factor attachment protein receptor (SNARE)-dependent, exocytosis-like plasma membrane insertion. Hydrolysis of cAMP to AMP by phosphodiesterases (PDEs) terminates the cAMP signal and causes retrieval of AQP2 from the plasma membrane by clathrin-mediated endocytosis. Internalized AQP2 is either degraded or passes through the Rab11-dependent recycling compartment to replenish perinuclear stores. F-actin – filamentous actin, G-actin – globular actin

Under resting conditions S261 is phosphorylated and AVP triggers its de-phosphorylation (Hoffert *et al.* 2007). In contrast, AVP induces the phosphorylation of S264 and S269, which are associated with AQP2 plasma membrane retention. However, phosphorylation of any single one of these sites is not sufficient for AQP2 membrane translocation, and phosphorylation of both sites seems to be dependent on initial S256 phosphorylation (Fenton *et al.* 2008, Hoffert *et al.* 2008, Moeller *et al.* 2009, Arthur *et al.* 2015).

Short-chain ubiquitination at K270 increases upon retrieval of the cAMP-elevating signal and favors endocytosis and sorting of AQP2 to multivesicular bodies. Furthermore, ubiquitinated AQP2 undergoes enhanced lysosomal degradation (Kamsteeg *et al.* 2006). Interplay

between the effects by phosphorylation and ubiquitination further defines AQP2 localization. For example, S269 phosphorylation was shown to override ubiquitination and prolongs AQP2 membrane localization (Moeller *et al.* 2014). Dephosphorylation of S261 does not modulate AQP2 localization, but its ubiquitination and is associated with an increase in AQP2 stability and abundance upon cAMP elevation (Nedvetsky *et al.* 2010).

In addition to regulating the localization of AQP2, AVP also increases its total protein abundance (DiGiovanni *et al.* 1994). This occurs in the short-term through stabilization of AQP2 protein by decreased proteasomal degradation (Nedvetsky *et al.* 2010), and in the long-term through changes at the transcriptional level (Matsumura *et al.* 1997). Umenishi *et al*. (2006) proposed a PKA-independent mechanism, showing that Erk, but not PKA inhibition, diminished the AVP-mediated increase in AQP2 protein abundance. Early studies identified several transcriptional regulator sites, including cAMP-responsive element (CRE), in the 5' UTR of *AQP2* (Hozawa *et al.* 1996, Yasui *et al.* 1997). Screenings for transcriptional regulators specific for IMCD cells identified members of the CREB, ETS, NFAT, and HOX families as transcriptionally controlling AQP2 expression (Yu *et al.* 2009, Tchapyjnikov *et al.* 2010). Independently of AVP, the nuclear factor NFκB and extracellular hypertonicity also modulate AQP2 transcription (Storm *et al.* 2003, Hasler *et al.* 2008). Hypertonic conditions activate the tonicity-responsive enhancer binding protein (TonEBP), which increases AQP2 transcription through a TonE element upstream of AQP2 (Hasler *et al.* 2006).

1.1.6 Proteins and pathways controlling AQP2 trafficking

In addition to the described PKA-based pathway, several proteins participate in the control of AQP2 localization and by extension AVP-directed water homeostasis. This chapter highlights the most relevant principles of AQP2 regulation.

1.1.6.1 A-kinase anchoring proteins and phosphodiesterases

PKA is ubiquitously expressed and phosphorylation of its targets can have adverse effects on cellular pathways. Consequently, its activity needs to be tightly regulated in order to enable phosphorylation of only desired subsets of target proteins. This is achieved by the association of PKA with scaffolding proteins of the A-kinase anchoring protein (AKAP) family that form signaling hubs to organize spatiotemporal control of PKA activity, as exemplified by Figure 4 (Skroblin et al. 2010, Dema et al. 2015).

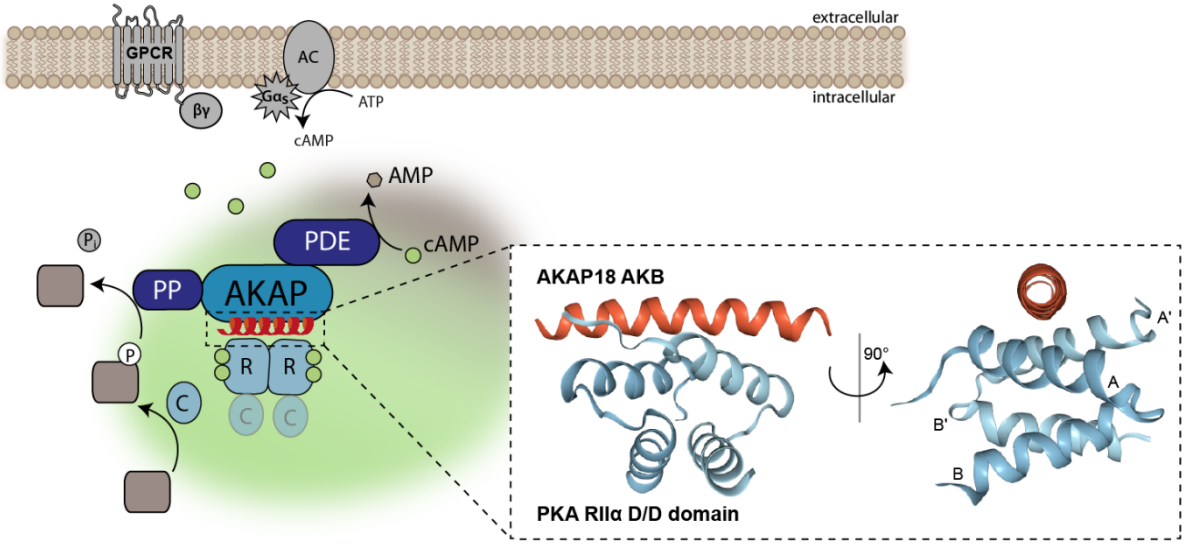

Figure 4: The AKAP signalosome. In addition to tethering PKA near its substrates, AKAPs orchestrate local cAMP signaling hubs by coordinating the localization of PKA, PDEs and protein phosphatases (PPs) in sub-cellular compartments. The interaction of AKAPs with PKA occurs through a conserved helical domain, the A-kinase binding (AKB) domain, that binds the PKA dimer at its docking/dimerization (D/D) domain, exemplified here for the AKAP18:PKA interaction (RCSB protein data bank entry 4ZP3, (Götz *et al.* 2016)).

AKAPs are a family of anchoring proteins that are defined by the presence of a binding site for PKA, but vary in secondary interaction partners, intracellular localization and expression levels in different cell types and organs. Through the compartmentalization by AKAPs, PKA activity is constrained to certain cellular compartments and a defined subset of substrates. AKAPs can be RI-specific, RII-specific or belong to the class of dual specificity AKAPs, which can bind both types of regulatory subunits (Herberg *et al.* 2000, Gold *et al.* 2006). In concert with cAMP-degrading phosphodiesterases (PDEs), protein phosphatases (PP) and organelle-specific interaction proteins, AKAPs integrate PKA signaling hubs into locally defined cAMP-gradients that are shaped by PDEs. A conserved amphipathic helix within the AKAP structure forms the A-kinase binding (AKB) domain that interacts with the dimerization and docking (D/D) domain of PKA regulatory subunits (Figure 4). Bioinformatics screening of AKAPs defined the RII-binding AKAP motif as:
(AVLISE)XX(AVLIF)(AVLI)XX(AVLI)(AVLIF)XX(AVLISE), in which X represents any amino acid and alternative amino acids for a position are given in single letter code in parentheses (Hundsrucker *et al.* 2010). The crystal structure of AKAP18β with PKA-RIIα-D/D revealed hydrophilic anchor points encompassed by the AKB to be crucial for binding of the D/D domain (Götz *et al.* 2016). Manipulation of anchor points might allow for specific targeting of RI- or RII-specific AKAPs. Disruptor peptides or small molecules that specifically interfere with a subset of AKAP-PKA interactions are sought for therapeutic use (Dema *et al.* 2015). The identification of anchor points further defines the interaction site and may help to improve the specificity of AKAP-PKA disruptors.

For renal principal cells, it was shown that AKAP-PKA interactions are crucial for AQP2 trafficking to the plasma membrane, as global interference with a disruptor peptide inhibited the AVP-induced AQP2 membrane localization (Klussmann *et al.* 1999). AKAP18δ and AKAP220 have been detected on AQP2-bearing vesicles, where they tether PKA in close proximity to its target AQP2-S256 (Henn *et al.* 2004, Okutsu *et al.* 2008).

PDEs terminate the cAMP-mediated signal and restore basal concentrations by hydrolyzing cAMP to AMP. On AQP2-bearing vesicles, PDE4D directly interacts with AKAP18δ. PDE4 inhibition alone does not induce AQP2 membrane localization and water permeability of primary inner medullary collecting duct cells, but it augments the response when these changes are induced by FSK application. Subcellular distribution of PDE4D, as detected by immunofluorescence microscopy, resembles that of AQP2. AVP stimulation induces the redistribution of both proteins from a cytosolic location into the plasma membrane (Stefan *et al.* 2007).

Phosphatases counteract kinase activity through dephosphorylation of their substrates. In accordance with this, inhibition of the serine/threonine phosphatases 1 and 2A (PP1 and PP2A) by okadaic acid in cultured renal collecting duct (CD8) cells increases AQP2 phosphorylation by about 60 % (Valenti *et al.* 2000). However, Cheung *et al.* (2017) recently showed that okadaic acid treatment does not significantly interfere with AVP-induced dephosphorylation of p-S261 and AQP2 membrane insertion in LLC-AQP2 cells. They identified PP2C to be the responsible phosphatase, as specific inhibition of PP2C by sanguinarine impedes reduction of p-S261 upon AVP stimulation.

1.1.6.2 Cytoskeletal components

A tight network of cytoskeletal fibers physically hinders the translocation of AQP2 into the plasma membrane and supports AQP2 perinuclear positioning. Generally, the actin cytoskeleton interferes with the exocytosis-like transport towards the membrane, whereas microtubular structures control the endocytic retrieval of AQP2.

AVP induces apical depolymerization of filamentous (F-) actin (Simon *et al.* 1993). There are two main pathways controlling the actin cytoskeleton that are involved in AQP2 trafficking. In the first of which, AQP2 binds monomeric globular (G-) actin under resting conditions. Polymeric actin is stabilized by tropomyosin-5b (TM5b). Phosphorylation of S256 by PKA weakens the interaction with G-actin, while its affinity for TM5b increases. This leads to the withdrawal of TM5b from F-actin, favoring its depolymerization (Noda *et al.* 2004, Noda *et al.* 2008).

In the second pathway, the small GTPase RhoA mediates the formation of actin stress fibers. Upon cAMP-elevation induced by AVP, active PKA phosphorylates RhoA, leading to its inhibition and therefore the destabilization of the actin cytoskeleton (Lang *et al.* 1996,

Klussmann *et al.* 2001, Tamma *et al.* 2001). Riethmüller *et al.* (2008), however, hypothesized that the underlying effect is instead the relaxation of actomyosin, reducing overall cell stiffness to facilitate apical vesicle trafficking. A similar study on Golgi-based intracellular vesicle transport revealed that stiffness of the actin cytoskeleton impedes budding of Rab6-positive vesicles from Golgi-compartments, wherein rigidity is conferred by myosin II-contraction (Guet *et al.* 2014). Interestingly, from a biophysical point of view, actin networks are seen as active polymer gels that constantly hydrolyze ATP, and changes in fluidity are required to allow vesicle transport (Joanny *et al.* 2009). AKAP220, which is associated with AQP2-bearing vesicles, was suggested to play a role in the maintenance of the actin network at apical plasma membranes (Whiting *et al.* 2016). Despite low AVP levels in water-loaded animals, AKAP220 knock-out mice show distinct apical accumulation of AQP2 and a reduction in active GTP-bound RhoA, compared to the more dispersed AQP2 localization in WT animals. Phosphatase inhibition by okadaic acid not only augments AQP2 phosphorylation, as described above, but also induces the disassembly of the actin network, similarly to the cAMP-elevating FSK, and favors AQP2 translocation into the plasma membrane. The finding that PKA inhibition by H89 does not reverse the effect of phosphatase inhibition on the cytoskeleton indicates that PKA-independent phosphorylation events play a role in controlling the actin network dynamics that regulate AQP2 trafficking (Valenti *et al.* 2000).

1.1.6.3 Proteins controlling AQP2 vesicle fusion and apical membrane insertion

After the transport to the plasma membrane, AQP2 vesicles fuse with it in an exocytosis-like manner. The fusion process is controlled by the soluble *N*-ethylmaleimide sensitive factor attachment protein receptor (SNARE) machinery (Gouraud *et al.* 2002). On AQP2-bearing vesicles, the v-SNAREs vesicle-associated membrane proteins (VAMP) 2 and 3 were identified to coordinate vesicle fusion with the corresponding apical plasma membrane located t-SNAREs syntaxin 3 and synaptosome-associated protein (SNAP) 23 (Procino *et al.* 2008). Although presumably not present on AQP2-bearing vesicles, VAMP8 seems to play a role in plasma membrane insertion of AQP2 as VAMP8-deficient mice fail to accumulate AQP2 in the apical collecting duct principal cell membrane upon cAMP elevation. Despite higher AQP2 protein levels than in wild-type (WT) animals, VAMP8 knockout mice show defects in urinary concentration and develop hydronephrosis. In addition, pulldown assays confirmed that VAMP8 is able to form a complex with syntaxins 3, 4 and SNAP23 (Barile *et al.* 2005, Wang *et al.* 2010).

1.1.6.4 Proteins controlling AQP2 internalization

Once body water homeostasis is adjusted, serum AVP levels decline and AQP2 is retrieved from the plasma membrane. AQP2 internalization occurs through clathrin-mediated endocytosis, followed by either degradation or recycling of the channel. Accordingly, dominant-negative dynamin mutants induce AQP2 plasma membrane-accumulation in clathrin-coated pits (Sun *et al.* 2002). Phosphorylation of AQP2-S256 and S269 stabilizes its membrane localization and reduces endocytosis. Their respective phosphomimetic mutants, S256D and S269D, present decreased interaction with endocytic proteins such as clathrin heavy chain, dynamin and Hsc70, as well as diminished internalization and proteasomal degradation (Moeller *et al.* 2010). In line with this, p-S256 confers increased binding to the myelin and lymphocyte-associated protein (MAL) that is associated with apical plasma membrane localization, which explains its abated endocytic internalization (Kamsteeg *et al.* 2007). Appropriate perinuclear positioning of endocytosed AQP2-bearing vesicles requires intact microtubules (Vossenkamper *et al.* 2007). In rat primary collecting duct cells, Rab11 and myosin Vb co-localize with AQP2 under basal conditions as well as upon AVP-mediated translocation. Motor protein myosin Vb binding to its vesicular receptor Rab11, either directly or *via* the Rab11 adaptor protein FIP2, is necessary for transfer of AQP2 through the Rab11-positive recycling compartment (Nedvetsky *et al.* 2007, Vossenkamper *et al.* 2007). Several myosin motor proteins were identified on AQP2-bearing vesicles, e.g. myosin IIA, IIB and VI that enable microtubular transport (Barile *et al.* 2005).

1.1.7 Pathological dysregulation of the AQP2 localization

Dysregulated water homeostasis under control of AVP is associated with several diseases. Patients with nephrogenic diabetes insipidus (NDI) show defective water retention mechanisms. The urine concentration defect causes abnormally high retention of solutes, leading to polyuria, polydipsia and in severe cases dehydration, hypernatremia and hyperchloremia. In contrast, patients suffering from late stage heart failure and liver cirrhosis often display excessive water retention, resembling the syndrome of inappropriate antidiuretic hormone secretion (SIADH), which presents with highly elevated AVP levels independent of serum osmolality. In all cases the molecular pathways that regulate the intracellular AQP2 translocation in collecting duct cells are dysregulated. The next paragraphs will present a brief overview on AQP2-centered water balance disorders, and their underlying molecular defects and treatment strategies.

1.1.7.1 Nephrogenic diabetes insipidus

A variety of defects can cause NDI, which can be categorized as either congenital or acquired NDI. Figure 5 summarizes several forms of NDI and identifies their respective animal models, if applicable. On the molecular level, AQP2 insertion into the plasma membrane is either reduced or absent in patients with NDI. This causes hypervolemic urine of low osmolality and systemic water loss that needs to be compensated by daily water intake of approximately 10-20 L. Treatment strategies vary fundamentally between NDI types. Central DI can be treated by administration of the AVP analog desmopressin (dDAVP) either as orodispersable or normal tablet, intranasal spray or injection. Prospectively, gene therapy might also be a feasible option, but has only been tested in Brattleboro rats (Yoshida *et al.* 2004). For type I or X-linked NDI the options are less abundant. Firstly, water intake needs to be adjusted to avoid dehydration. However, as this can immensely reduce life quality, other options are also considered. To reduce solute load, a low-salt diet is advised. Cyclooxygenase-2 (COX2) inhibitors in combination with diuretics such as hydrochlorothiazide and amiloride can paradoxically reduce urine volume (Pattaragarn *et al.* 2003, Soylu *et al.* 2005). COX2 inhibition increases Na-K-2Cl cotransporter 2 (NKCC2) expression in the thick ascending limb of Henle and AQP2 abundance in principal cells of the collecting duct (Fernandez-Llama *et al.* 1999, Kim *et al.* 2008). In distal parts of the nephron, the diuretics hydrochlorothiazide and amiloride block the sodium chloride co-transporter and EnaC sodium channel, respectively. Sodium reabsorption declines and induces hypovolemia that in turn activates the renin-angiotensin-aldosterone system. As a consequence, more sodium is reabsorbed from the proximal tubule, and water reabsorption through AQP1 increases. Treatment of lithium-induced acquired NDI with COX2 inhibitors also increases urine output through increased NKCC2 and AQP2 expression (Kim *et al.* 2008).

In X-linked NDI, mutations of the gene encoding V2R, *AVPR2,* cause defects in ligand binding (type 1), improper maturation and consequent retention in the ER (type 2), or unstable mRNA due to transcriptional defects (type 3) (reviewed in Bichet *et al.* 2016). Type 2 accounts for approximately 45 % of the mutations causing X-linked NDI. As approximately two-thirds of type 2 mutations give rise to intrinsically functional proteins, cell-permeable antagonists are employed as pharmacological chaperones that promote protein stability, plasma membrane localization and thus restore receptor function (Morello *et al.* 2000, Bernier *et al.* 2004, Robben *et al.* 2007, reviewed in Los *et al.* 2010). Screening for suitable antagonists has to be balanced between high-affinity binding candidates and the requirement to be effectively replaced by endogenous AVP upon successful membrane insertion (Los *et al.* 2010). Alternative agonists that intracellularly activate the receptor can be sought to circumvent the latter difficulty (Robben *et al.* 2009).

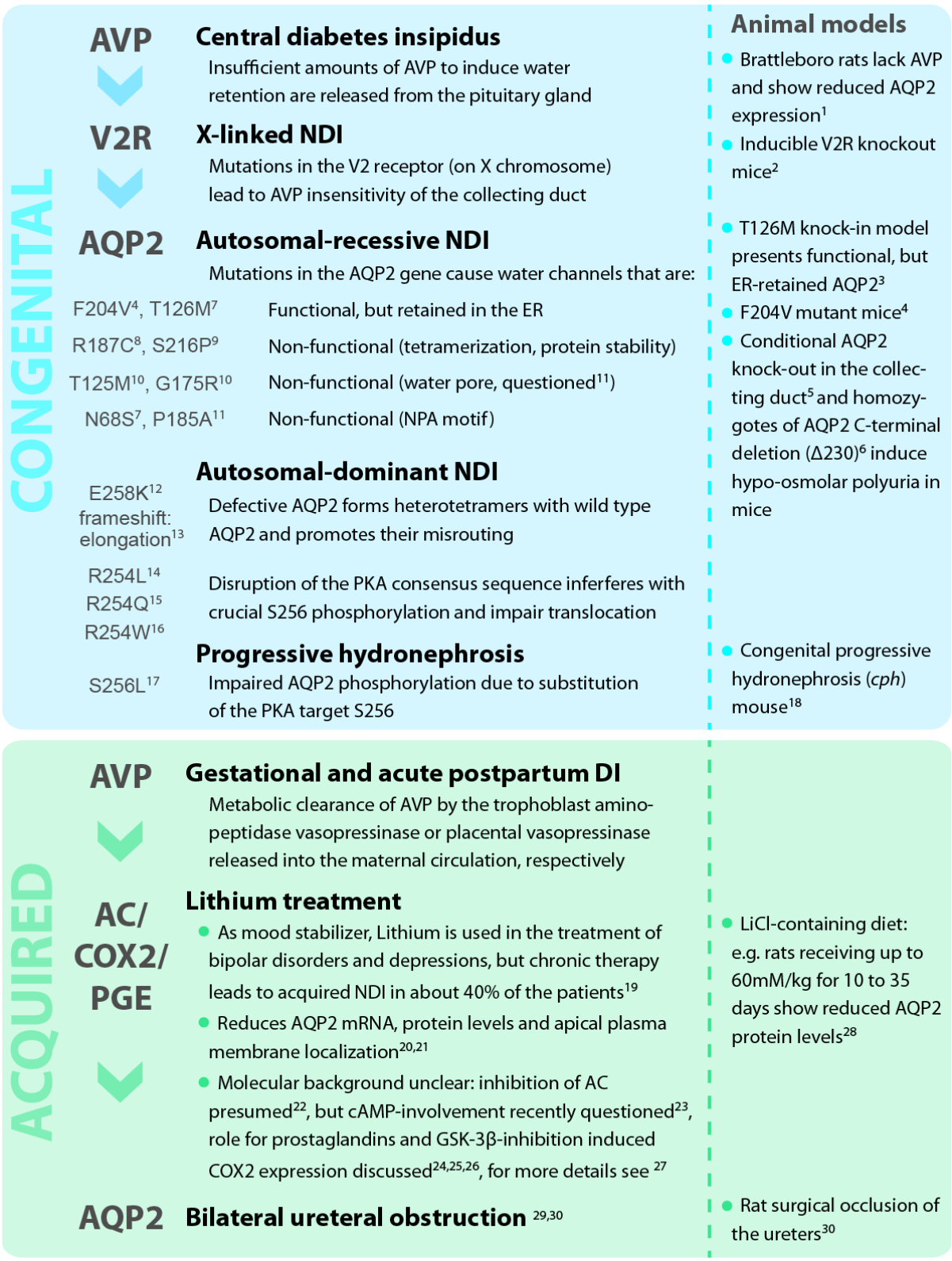

Figure 5: Causes of nephrogenic diabetes insipidus. Summarized are the common subtypes of congenital and acquired NDI with their underlying disease-causing mutation and animal models, if applicable. Literature: 1 (Valtin et al. 1965), 2 (Li et al. 2009), 3 (Yang et al. 2001), 4 (Lloyd et al. 2005), 5 (Rojek et al. 2006), 6 (Shi et al. 2007), 7 (Mulders et al. 1997), 8 (Marr et al. 2001), 9 (Deen et al. 1995), 10 (Goji et al. 1998), 11 (Marr et al. 2002), 12 (Kamsteeg et al. 1999), 13 (Kuwahara et al. 2001), 14 (de Mattia et al. 2005), 15 (Savelkoul et al. 2009), 16 (Dollerup et al. 2015), 17 (McDill et al. 2006), 18 (Horton et al. 1988), 19 (Stone 1999), 20 (Marples et al. 1995), 21 (Li et al. 2006), 22 (Goldberg et al. 1988), 23 (Li et al. 2006), 24 (Zhang et al. 2012), 25 (Rao et al. 2005), 26 (Kortenoeven et al. 2012), 27 (Kishore et al. 2013), 28 (Marples et al. 1995), 29 (Frokiaer et al. 1996), 30 (Stodkilde et al. 2011)

Other treatment strategies employ the induction of AQP2 translocation independent of V2R activation including PDE inhibitors, prostanoid receptor EP2 and EP4 agonists (Olesen *et al.* 2011), nitric oxide donors via cGMP stimulation (Bouley *et al.* 2000) and statins (Procino *et al.* 2011). Statins are inhibitors of 3-hydroxy-3-methyl-glutaryl-coenzyme A (HMG-CoA) reductase that limit cholesterol synthesis by competition with HMG-CoA in the production of mevalonate, a precursor of cholesterol. The effect on AQP2 translocation in collecting duct principal cells is based on inhibition of RhoA and other signaling proteins involved in vesicle trafficking, including Rab and Rac proteins, due to reduced prenylation (Procino *et al.* 2011). Subsequent depolymerization of the actin cytoskeleton reduces the physical barrier to AQP2 vesicles and enables plasma membrane trafficking (Klussmann *et al.* 2001, Tamma *et al.* 2003, Schrade *et al.* 2018). A study with simvastatin identified reduced clathrin-mediated endocytosis as a cause of AQP2 membrane accumulation (Li *et al.* 2011).
Recently, metformin, a standard treatment for type 2 diabetes, was shown to increase AQP2 membrane abundance in rat inner medullae. In V2R knockout mice and tolvaptan-treated rats, metformin elevates urine osmolality, potentially through activation of the metabolic regulator AMPK and increased AQP2 and urea transporter (UT-A1) phosphorylation (Efe *et al.* 2016, Klein *et al.* 2016). An initial study with a small number of healthy volunteers did not show a significant change in urine osmolality upon water load after one week of metformin treatment (Bech *et al.* 2018).

1.1.7.2 Disorders with abnormally elevated AVP-mediated water reabsorption

The main cause of diseases associated with increased water retention is abnormally high levels of AVP in the circulation, either due to uncontrolled elevated secretion from the pituitary gland as in SIADH or following activation of vasoconstrictor systems as the RAAS (heart failure and liver cirrhosis). Both presents a non-osmotic up-regulation of the antidiuretic stimulus. Prolonged AVP stimulation not only induces translocation, but also increased expression of AQP2. For instance, heart failure model rats display increased renal AQP2 expression (Xu *et al.* 1997). Additionally, mutations in the gene encoding for the V2R can establish constitutively active receptor signaling independent of AVP levels, referred to as nephrogenic syndrome of inappropriate antidiuresis (NSIAD). Excessive water retention due to profuse AQP2 translocation into the plasma membrane causes serum dilution and, if not counter-regulated by sodium, systemic hypervolemia (Feldman *et al.* 2005). The physiological response of declining serum sodium is classified as the electrolyte disorder hyponatremia when sodium levels fall below 135 mEg/L. In recent years, investigations of rat models of heart failure have unveiled increased recycling of the V2R to the cell surface after AVP stimulation leading to an amplified antidiuretic signal (Brond *et al.* 2013). For the treatment of hyponatremic diseases with or without hypervolemia, V2R antagonists, such as

tolvaptan, are used. Tolvaptan increases serum sodium and solute-free aquaresis in both short- and long-term studies, and was found to be adequately safe in patients (Gheorghiade *et al.* 2004, Schrier *et al.* 2006, Berl *et al.* 2010).

Despite the general up-regulation of antidiuresis upon AVP stimulation, collecting duct cells can undergo an "escape" from excess stimulation in case of dilutional hyponatremia. After prolonged high levels of AVP and water load, model animals show increased diuresis that potentially protects the kidney from further damage. Over more than 50 years of investigation, several theories pointing towards a central role for extracellular fluid volume expansion have been suggested to explain this phenomenon (Levinsky *et al.* 1959, Chan 1973, Hall *et al.* 1986). The down-regulation of AQP2 protein expression, reduced AVP binding and V2R sensitivity, diminished intracellular cAMP levels, and regulation by nitric oxide and prostaglandins seem to be involved (Ecelbarger *et al.* 1997, Tian *et al.* 2000, Murase *et al.* 2003).

1.2 Metabolic control of intracellular transport systems

1.2.1 Comparisons to neuronal transport systems

In neurons, transport processes from the cell body towards axon terminals are classified as "fast" (0.5 – 4 μm/s) and "slow" (< 0.1 μm/s) axonal transport. Organelles and vesicles are moved most rapidly, cytosolic proteins are moved more slowly and cytoskeletal and filamentous proteins are transported with the lowest velocity (reviewed by Maday *et al.* 2014). Tang *et al.* (2013) suggest that slow axonal transport of cytosolic proteins may depend on transient interactions with fast moving vesicles. Some of the pathways employed for slow transport are similar to vesicular trafficking in other cell systems. For example, active transport along the axon is microtubule-dependent, as it was shown for AQP2 perinuclear positioning (Nedvetsky *et al.* 2007, Vossenkamper *et al.* 2007). In axons, different motor proteins define the direction of the transport. Anterograde movement requires kinesin and retrograde movement is promoted by dynein (Hirokawa *et al.* 1990, Hirokawa *et al.* 1991). Transport of AQP2-bearing vesicles towards the plasma membrane was shown to be mediated by myosin motor proteins and perinuclear positioning depends on dynein (Nedvetsky *et al.* 2007). The activity of motor proteins requires a continuous supply of ATP. The movement of one vesicle along a 40 mm axon consumes about 5×10^6 molecules of ATP (Maday *et al.* 2014).

Glycolysis, with a focus on the involvement of glyceraldehyde-3-phosphate dehydrogenase (GAPDH), was shown to be the source of energy underlying axonal transport. Oxidative phosphorylation is the more efficient source of ATP, but mitochondria are only abundant in cell bodies, whereas unevenly distributed within the neurites. Glycolytic enzymes are

distributed in the cytosol, which makes glycolysis the more accessible source of ATP. Motile vesicles contain both GAPDH and phosphoglycerate kinase (PGK), which produce ATP independently of mitochondrial respiration. The use of a catalytically inactive GAPDH expression construct to rescue a GAPDH siRNA-mediated transport defect indicates that GAPDH enzymatic activity is crucial for vesicle transport (Zala *et al.* 2013). Recent proteomic investigations confirmed the localization of glycolytic enzymes, including GAPDH and PGK, on mouse forebrain motile vesicles (Hinckelmann *et al.* 2016).

In parallel to the work of Hinckelmann and colleagues, other findings on how glycolysis regulates presynaptic processes were published. Lujan and coworkers (2016) describe impaired excitatory postsynaptic currents resulting from the inhibition of glycolysis at the pre-synaptic terminal, while Jang *et al.* (2016) identified a “glycolytic metabolon” that ensures correct synaptic function, even in case of elevated energy demand. The glycolytic couple GAPDH/PGK was found on synaptic vesicles, where it supplies ATP for the uptake of neurotransmitters. These studies mainly focus on glutamate, but similar findings in dopamine and serotonin containing vesicles indicate that there may be a universal mechanism (Ikemoto *et al.* 2003, Ishida *et al.* 2009). The vacuolar H^+-ATPase pumps protons into the lumen of synaptic vesicles at the expense of ATP, in order to establish the needed electrochemical gradient for neurotransmitter uptake through their vesicular transporters (Wolosker *et al.* 1996, Farsi *et al.* 2017).

Several studies have explored a variety of cellular functions of GAPDH, beyond its role as a housekeeping protein (reviewed in Tristan *et al.* 2011). In terms of intracellular transport processes, GAPDH is crucial for the early secretory pathway at the interface between the ER and the Golgi, independently of its enzymatic activity (Tisdale 2001, Tisdale *et al.* 2004). In a complex with Rab2, and dependent on phosphorylation by PKCι/λ, GAPDH regulates microtubule organization and recruitment of the motor protein dynein (Tisdale 2002, Tisdale *et al.* 2009). As Rab2 also localizes to AQP2-bearing vesicles (Barile *et al.* 2005), the question arises, whether GAPDH also controls their transport from the ER to the Golgi complex. It is already known that AQP2 perinuclear positioning depends on microtubules and dynein (Marples *et al.* 1998, Vossenkamper *et al.* 2007). This suggests that GAPDH may also be involved in the AQP2 regulatory pathway. Aldolase, phosphoglycerate kinase, phosphoglycerate mutase and pyruvate kinase co-localize with VAMP2-positive synaptic precursor vesicles (Hinckelmann *et al.* 2016). VAMP2 also associates with AQP2-bearing vesicles, which might indicate that the metabolic drive provided by glycolytic ATP production plays a role in the control of AQP2 intracellular trafficking similarly to neuronal vesicles (Barile *et al.* 2005, Procino *et al.* 2008).

1.2.2 The vacuolar ATPase as a metabolic sensor

The vacuolar ATPase is a multi-subunit enzyme that pumps protons across membranes through its transmembrane domain, v0, which is fueled by ATP hydrolysis through the rotary cytosolic subunit V1. Subunits of the v0 domain are denoted by lower-case letters (a, c, c'', d, e), whereas V1 subunits are written in capital letters (A_3B_3 hexamer, C, D, E, F, G, H). V-ATPases occur ubiquitously on intracellular vesicles, where they serve for example to acidify lysosomes. In specialized cells, V-ATPases additionally localize to the plasma membrane. For example, in osteoclasts V-ATPases establish an acidic extracellular space for bone resorption, and in kidney intercalated cells they participate in the maintenance of acid-base homeostasis (see Figure 2).

Reversible disassembly of the functional domains v0 and V1 controls V-ATPase activity. In yeast, its re-assembly is glucose-dependent, suggesting the presence of a cellular protection mechanism to reduce ATP consumption in cases of low energy supply (Kane 1995). Functional regulation of V-ATPase through assembly and disassembly was also identified in mammalian cells, where it was first studied in relation to the maturation of dendritic cells (Trombetta *et al.* 2003). In both yeast and mammalian cells, V-ATPase interaction with glycolytic enzymes has been shown. V-ATPase directly interacts with the glycolytic enzymes phosphofructokinase and aldolase, potentially in a complex with GAPDH (Lu *et al.* 2001, Su *et al.* 2003, Lu *et al.* 2004b). Yeast aldolase deletion mutants have a pH-dependent growth defect similar to V-ATPase mutants and display negligible V-ATPase activity (Lu *et al.* 2004b).

In addition, V-ATPase assembly and activity is central to metabolic sensing of amino acids through mechanistic target of rapamycin complex 1 (mTORC1) in mammalian cells (Zoncu *et al.* 2011). As depicted in Figure 6, translocation of mTORC1 to the lysosome along with its activation relies on amino acid-dependent V-ATPase interaction with the Ragulator complex that is an anchoring complex and guanine nucleotide exchange factor (GEF) for Rag GTPases (Bar-Peled *et al.* 2012). Rag GTPases sense amino acids, whereby GDP or GTP loading of RagA/B indicates low or high amino acid abundance, respectively. Conversely, inhibition of the mTOR pathway by rapamycin interferes with V-ATPase assembly in dendritic cells (Liberman *et al.* 2014). Efeyan *et al.* (2013) suggest that glucose levels are also sensed by that mechanism. V-ATPase interaction with Ragulator is not only modified by amino acids but also by glucose in the context of neonatal nutrient sensing upon interrupted maternal supply. They propose that Rag GTPases are "multi-input nutrient sensors". Additionally, this highlights the role of V-ATPase as a sensor for various metabolic pathways.

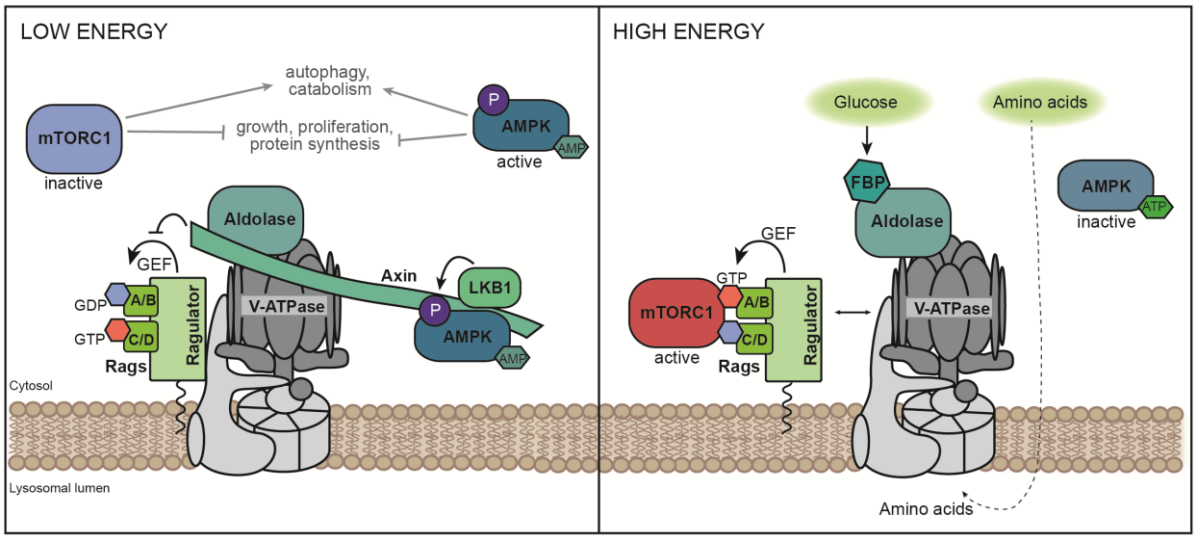

Figure 6: The V-ATPase organizes metabolic sensing of glucose and amino acids on the lysosome. Left: In the case of low energy abundance, the scaffolding protein axin is recruited to the lysosomal V-ATPase-aldolase complex, where it interferes with the guanine exchange factor (GEF) activity of the Ragulator complex, so that mTORC1 is not recruited and remains inactive. In addition, recruitment of AMPK to the lysosome facilitates its activating phosphorylation by liver kinase B1 (LKB1). Inactive mTORC1 and active AMPK repress cell growth and anabolic processes such as protein synthesis, and favor autophagy and catabolic processes, such as glycolysis. Right: High abundance of glucose is sensed through its glycolytic intermediate fructose-1,6-bisphosphate (FBP). FBP-bound aldolase releases axin, enables Ragulator activation and subsequent recruitment of mTORC1. Amino acid abundance is sensed by the V-ATPase though an “inside-out” mechanism, which is not yet fully understood. Active mTORC1 induces cellular pathways that favor cell growth and proliferation. For reasons of simplicity, V-ATPase reversible assembly was neglected in this scheme.

Independent of the described mTOR pathway, amino-acid starvation enhances V-ATPase assembly and activity. This might be a metabolic feedback mechanism to increase lysosomal degradation in order to adjust amino acid availability (Stransky *et al.* 2015).

AMPK is a major sensor for cellular energy status. When energy supplies are low, the ratio of ADP and AMP relative to ATP increases. In the canonical pathway, AMP allosterically activates AMPK (Moore *et al.* 1991, Gowans *et al.* 2013). The upstream kinase LKB1 phosphorylates and activates AMPK (Woods *et al.* 2003). Both AMP and ADP promote the phosphorylation of AMPK at Thr172 by blocking the access of phosphatases to this region. The interaction between AMPK and LKB1 is facilitated by the scaffolding protein Axin (Zhang *et al.* 2013). Zhang *et al.* (2014) showed that a complex comprised of V-ATPase, Ragulator, Axin and LKB1 localizes AMPK to endosomes/lysosomes and induces AMPK activation, which switches the cellular metabolic program towards catabolism (Figure 6). Recent findings indicate that aldolase acts as a sensor for glucose availability through fructose-1,6-bisphosphate (FBP). In the case of low glucose and consequent low FBP, aldolase facilitates AMPK activation *via* the V-ATPase-Ragulator-Axin-LKB1 complex and independently of the cellular energy status signaled though the AMP/ATP ratio (Zhang *et al.* 2017). In summary, V-ATPase is a central player of metabolic control that senses both amino acid as well as glucose availability and integrates mTORC1 activation when nutrients are abundant, as well as AMPK activation upon nutrient shortage.

1.2.2.1 Intracellular trafficking of the vacuolar ATPase

Similarly to AQP2, V-ATPase can be shuttled from intracellular stores to the plasma membrane if elevated proton secretion is required. This translocation is regulated by PKA and AMPK phosphorylation of V-ATPase (Hallows *et al.* 2009, Gong *et al.* 2010).
In type A intercalated cells, PKA phosphorylates the cytosolic V1A domain at S175 and stimulates apical membrane accumulation of V-ATPase (Alzamora *et al.* 2010). In contrast, AMPK activation by the AMP-mimicking agonist Aminoimidazole-carboxamide ribonucleotide (AICAR) in epididymal clear and kidney intercalated cells interferes with PKA-induced apical membrane localization and extracellular acidification, wherein S384 is the crucial AMPK phosphorylation site on V1A (Hallows *et al.* 2009, Alzamora *et al.* 2013).

1.2.3 PKA-AMPK crosstalk

PKA and AMPK pathways have antagonistic effects to one another. With respect to metabolic pathways, PKA phosphorylation induces anabolic enzymes, whereas AMPK favors energy generating-mechanisms and down-regulates ATP-consuming pathways. PKA phosphorylation of AMPK at S173 prevents the activating phosphorylation at T172 by LKB1. However, long-term PKA stimulation by isoproterenol induces p-T172-mediated AMPK activation in adipocytes, apparently serving as a negative feedback mechanism to avoid energy depletion (Djouder *et al.* 2010). Recently, crosstalk between PKA and AMPK in hepatocytes was found to occur through AMPK-mediated phosphorylation of PDE4B and subsequent increased cAMP hydrolysis, which diminishes PKA activation (Johanns *et al.* 2016). This is in line with the findings that the anti-diabetic drug metformin, which leads to AMPK activation (Meng *et al.* 2015), impedes glucagon-induced cAMP elevation and subsequent hepatic gluconeogenesis (He *et al.* 2016). However, the direct involvement of AMPK in metformin-mediated blood sugar reduction through reduced hepatic gluconeogenesis has recently been questioned. Liver-specific AMPK and LKB1 knockout animals show a similar reduction in hepatocyte glucose production upon metformin as wild-type controls (Foretz *et al.* 2010). Metformin-induced AMPK activation occurs indirectly through inhibition of the ATP-producing mitochondrial complex I of the respiratory chain and subsequent increased AMP:ATP ratio. The current model suggests that metformin-increased AMP levels decrease adenylyl cyclase activity, thus blunting glucagon signaling and decreasing cAMP-PKA-mediated gluconeogenesis (Miller *et al.* 2013, reviewed by Rena *et al.* 2013).
Recently, PKA-AMPK crosstalk was also found to play a role for AQP2 translocation in collecting duct principal cells, indicating a link between AQP2 function and cellular metabolism (Al-Bataineh *et al.* 2016). However, the exact role of AMPK remains controversial. Two studies using metformin, also published in 2016, contradict Al-Bataineh *et*

al. (2016) and suggest that AMPK activation instead induces AQP2 plasma membrane accumulation in rat inner medulla and augments urine osmolality in V2R knockout mice (Efe *et al.* 2016, Klein *et al.* 2016). Nonetheless, the molecular effects of metformin are versatile and AMPK activation only occurs indirectly, which could explain the opposing study results.

1.3 Aim of the thesis

The translocation of AQP2 within renal principal cells is crucial for the fine-tuning of body water homeostasis. Stimulation of renal principal cells by antidiuretic hormone induces a rise of intracellular cAMP levels, an increase in PKA activity and the subsequent redistribution of AQP2 from perinuclear vesicles into the plasma membrane. The insertion of AQP2 in the apical plasma membrane facilitates water uptake from primary urine and increases body fluid volume.

The exact molecular mechanisms underlying the redistribution of AQP2, are not yet fully understood. Especially pathways that provide the energy required for the transport of AQP2-bearing vesicles, still have to be elucidated. In neurons, vesicle-associated metabolic complexes were identified that can locally supply energy for the transport along cytoskeletal structures. The aim of this thesis was to determine, which metabolic pathways are involved in the control of AQP2 trafficking. As AQP2 translocation depends on cAMP signaling, a hypothesis was that yet uncharacterized AKAPs link the cAMP/PKA axis with the metabolic control of vesicular transport processes. One candidate was the V-ATPase that pumps protons across membranes in an ATP-dependent manner and is a sensor of the metabolic status of the cell. The small molecule 4-acetyldiphyllin (4AD), an inhibitor of the V-ATPase, prevents acidification of vesicles in renal principal cells and interferes with the AVP/FSK-mediated plasma membrane accumulation of AQP2 (Bogum *et al.* 2013). In the presence of 4AD, total cAMP levels and PKA activity are unchanged, yet the crucial AQP2 phosphorylation at S256 is reduced. This suggests that V-ATPase might be localized on AQP2-bearing vesicles, where it serves as an AKAP to tether PKA in close proximity to its substrate AQP2-S256.

Summarized, the goals of this thesis were:

- To identify metabolic enzymes and pathways that are active in the control of AQP2 trafficking in renal principal cells.
- To discover and characterize new AKAPs that link cAMP/PKA signaling with cellular metabolism.
- To elucidate molecular pathways underlying 4AD-mediated inhibition of AQP2 redistribution in renal principal cells.

2. MATERIAL AND METHODS

2.1 Material

2.1.1 Equipment

Table 1: Equipment

Equipment	Supplier
AutoSpot-Robot ASS 222 peptide spotter	Intavis Bioanalytical Instruments AG (Köln, DE)
Axiovert 25 microscope	Carl Zeiss MicroImaging GmbH (Jena, DE)
Beckmann Coulter Large Scale Centrifuge	Beckmann Coulter GmbH (Krefeld, DE)
Centrifuge Universal 320 R	Hettich (Tuttlingen, DE)
Cryo-container 5100-0001	Thermo Fisher Scientific/NALGENE (Bonn, DE)
Duomax 1030 shaking device	Heidolph Instruments (Schwabach, DE)
Enspire® 2300 microplate reader	PerkinElmer (Rodgau, DE)
GFL 1072 waterbath	Gesellschaft für Labortechnik mbH (Burgwedel, DE)
Incubator CB210	Binder (Tuttlingen, DE)
LSM780 confocal microscope	Carl Zeiss MicroImaging GmbH (Jena, DE)
Miccra D-4 tissue homogenizer	ART Prozess- & Labortechnik GmbH (Müllheim, DE)
MiniProtean® Polyacrylamide gel electrophoresis cell	Bio-Rad Laboratories GmbH (München, DE)
Odyssey Imager Western blot detection system	LI-COR Biosciences (Bad Homburg, DE)
PowerPac 3000	Bio-Rad Laboratories GmbH (München, DE)
Professional TRIO PCR cycler	Biometra/ Analytik Jena
PTR 35 Eppi rotator	Gran Instruments Ltd (Cambridgeshire, UK)
Safe 2020 Sterile bench	Thermo Electron LED GmbH (Langenselbold, DE)
SevenEasy pH meter	Mettler-Toledo (Columbus, US)
Sonopuls HD 2070 ultrasound homogenizer	Bandelin electronic GmbH& Co. KG (Berlin, DE)
Thermomixer Compact Shaking heater	Eppendorf (Hamburg, DE)
Titramax 100 Plate shaking device	Heidolph Instruments (Schwabach, DE)
Typhoon FLA9500 Phosphoimager	GE Healthcare (Little Chalfont, UK)
xMark Microplate Absorbance Spectrophotometer	Bio-Rad Laboratories GmbH (München, DE)

Table 2: Disposables

Disposables	Supplier
96-well plates for absorbance assays	Greiner bio-one (Kremsmünster, AT)
Cell culture flasks	TPP (Trasadingen, CH)
Centrifugation tubes	Corning Falcon (Corning, US)
Coverslips	Thermo Fisher Scientific Gerhard Menzel B.V. &

	Co. KG (Braunschweig, DE)
Cryovials	Carl Roth GmbH & Co KG (Karlsruhe, DE)
Dolphin tubes	Carl Roth GmbH & Co KG (Karlsruhe, DE)
Filter tips	StarLab (Hamburg, DE)
Microscope slides	Thermo Fisher Scientific Gerhard Menzel B.V. & Co. KG (Braunschweig, DE)
Multiwell plates for cell culture	TPP (Trasadingen, CH)
Pipette tips	StarLab (Hamburg, DE)
PVDF membrane	Carl Roth GmbH & Co KG (Karlsruhe, DE)
Reaction tubes	Sarstedt (Nümbrecht, DE)
SDS-PAGE gradient gels Mini Protean® TGX™ 4-12 % Precast Gel	Bio-Rad Laboratories GmbH (München, DE)
Microlance Syringes 0.4 mm x 19 mm	BD Biosciences (Heidelberg, DE)

2.1.2 Chemicals and buffers

2.1.2.1 Chemicals

Table 3: Chemicals

Substance	**Supplier; article number (#)**
4', 6-Diamidine-2'-phenylindole dihydrochloride (DAPI)	Roche Diagnostics GmbH (Mannheim, DE); #10236276001
Alexa Fluor 647 Phalloidin	Invitrogen (Darmstadt, DE); #A22287
Adenosine 3´:5´-Cyclic Monophosphate (cAMP) sodium Salt	Biolog (Bremen, DE); #A-001S
Blocking buffer (Western blot, AQP2 vesicle IP)	EasyBlocker, GeneTex (Irvine, US), #GTX425858
Complete mini EDTA-free	Roche Diagnostics (Mannheim, DE); #REF0693159001
Coomassie PlusTM Protein Assay Reagent	Thermo Fisher Scientific (Bonn, DE); #1856210
EZ-LinkTM Sulfo-NHS-SS-Biotin (Biotin)	Thermo Fisher Scientific (Bonn, DE); #21328
ImmobilonTM Western Chemiluminescent HRP substrate	Merck Millipore (Schwalbach, DE); #WBKLS0500
Immu-MountTM	Thermo Fisher Scientific (Bonn, DE); #99-904-12
PhosSTOP *EASY* pack	Roche Diagnostics (Mannheim, DE); #REF04906837001
Power SYBR green PCR master mix	Life Technologies (Woolston, UK); #4367659
Precision Plus Protein Standard Dual Color	Bio-Rad Laboratories GmbH (München, DE); #1610374
Sodium oxamate (SO)	Sigma-Aldrich (St. Louis, US); #O2751

2.1.2.2 Buffers

All chemicals used for preparing buffers and solutions were obtained from Sigma- Aldrich (St. Louis, US) or Carl Roth GmbH & Co. KG (Karlsruhe, DE), unless indicated. All buffers were prepared with distilled water (*A. dest*).

Table 4: Buffers and solutions

Buffer/solution	Composition
Biotinylation buffer	500 µg Biotin per well; 10 mM triethanolamine; 150 mM NaCl; 1 mM $MgCl_2$; 0.1 mM $CaCl_2$; pH 8.0
Bio Quenching buffer	50 mM NH_4Cl in PBS
Bio Lysis buffer 1	SLB; 0.5 % Triton X-100; 0.2 % BSA; Complete mini EDTA-free)
Bio Lysis buffer 2	SLB; 0.5 % Triton X-100; Complete mini EDTA-free
Blocking buffer (IF)	0.27 % fish skin gelatin; 1x PBS
Blocking buffer (RII overlay)	5 % skim milk powder; 0.1 % BSA; 0.002 % NaN_3; 1x PBS
Blocking buffer (Western blot)	1 % bovine serum albumine (BSA); 1x TBS-T
Fractionation buffer 1	PIPES, pH 6.8 10 mM; Sucrose 300 mM; NaCl 100 mM; $MgCl_2$ 3 mM; EDTA 5 mM; PMSF 1 mM; Digitonin 0.3 mg/ml
Fractionation buffer 2	PIPES, pH 6.8 10 mM; Sucrose 300 mM; NaCl 100 mM; $MgCl_2$ 3 mM; EDTA 5 mM; PMSF 1 mM; Triton X-100 0.5 %
Homogenization buffer	250 mM Sucrose, 3 mM Imidazol, pH 7.4
Lämmli sample buffer	40 % glycerine; 8 % SDS; 0.4 % bromophenol blue; 312.5 mM Tris-HCl; 200 mM DTT; pH 6.8
LDH assay buffer	Tris-HCl 0.2 M; NADH 220 µM; sodium pyruvate 1 mM
Lysis buffer	MLB/SLB; PhosSTOP EASY; Complete mini EDTA-free
Mild lysis buffer (MLB)	2 mM EDTA; 2 mM EGTA; 0.2 % Triton X-100; 1xPBS
Phosphate-buffered saline (PBS)	137 mM NaCl; 2.7 mM KCl; 1.5 mM KH_2PO_4; 8.1 mM Na_2HPO_4; pH 7.4
RIPA buffer	50 mM Tris-HCl, pH 7.4; 150 mM NaCl; 1 % Triton X-100; 1 % sodium deoxycholate; 0.1 % SDS; 1 mM EDTA
SDS-polyacrylamide gel electrophoresis (PAGE) running buffer	25 mM Tris ; 192 mM glycine ; 0.1 % SDS
Separating gel buffer (SDS-PAGE)	0.625 M Tris-HCl; pH 6.8
Standard lysis buffer (SLB)	10 mM K_2HPO_4; 150 mM NaCl; 5 mM EDTA; 5 mM EGTA; 0.5 % Triton X-100; pH 7.4; 0.2 % sodium deoxycholate
Stacking gel buffer (SDS-PAGE)	0.75 M Tris-HCl; pH 8.8
Tank blot buffer	20 mM Tris; 150 mM glycin; 10 % methanol, 0.02 % SDS

TBS + Tween (TBS-T)	1x TBS; 0.05 % Tween-20
Tris-buffered saline (TBS)	10 mM Tris-Hcl, pH 7.4; 150 mM NaCl

2.1.3 Commercial Kits

Table 5: Commercial kits

Kit	Supplier
GeneMATRIX Universal RNA Purification Kit	EURx Ltd. (Gdansk, PL)
NucleoSpin® Extract II kit	Macherey-Nagel (Düren, DE)
Nucleospin® Plasmid QuickPure	Macherey-Nagel (Düren, DE)
NucleoBond® Xtra Midi / Maxi	Macherey-Nagel (Düren, DE)
qScript cDNA synthesis kit	Quanta Biosciences (Beverly, MA, US)

2.1.4 Immunoprecipitation beads

Table 6: Immunoprecipitation beads

Beads type	Supplier, Article number (#)
8AHA-cAMP agarose	Biolog, #A028
Anti-FLAG® M2 Magnetic Beads	Sigma-Aldrich, #M8823
Dyna beads- ProteinA	Invitrogen, #10002D
ProteinA- sepharose	Sigma-Aldrich, #P3391
ProteinG-PLUS-agarose	Santa Cruz Biotechnology, #sc-2002
Sp8-cAMP agarose	Biolog, #A013
Streptavidin agarose beads	Invitrogen, #15942-050

2.1.5 Antibodies

Table 7: Antibodies I Abbreviations: App. – Application, IF – immunofluorescence, IP – immunoprecipitation, POD – peroxidase, WB – Western Blot

Primary antibody	App.	Species	Supplier, Article number (#)
AMPK	WB	mouse	Cell Signaling Technology, #2793
AMPK-phosphoT172	WB	rabbit	Cell Signaling Technology, #2535
AQP2	WB	goat	Santa Cruz Biotechnology, #sc-9882
AQP2 (m)	IF	mouse	Santa Cruz Biotechnology, #sc-515770
AQP2 (r)	IP/IF	rabbit	Custom-made, (Maric *et al.* 1998)
AQP2-phosphoS261	WB	rabbit	Abcam, #ab72383
α-tubulin	WB	mouse	Calbiochem, #CP06

Calnexin	WB	rabbit	Stressgen Biotechnologies, #SPA-865
ERGIC-53	IF	rabbit	SIGMA, #E1031
Flag-tag	WB	mouse	Origene, #TA50011
G6PDH	WB	rabbit	Cell Signaling Technology, #12263
GAPDH	WB	rabbit	Cell Signaling Technology, #2118
Hsp90	WB	mouse	Stressgen Biotechnologies, #SPA-830
LC3A/B	WB	rabbit	Cell Signaling Technology, #4108
LDHA	WB	rabbit	GeneTex, #GTX101416
LDHB	WB	rabbit	GeneTex, #GTX101747
Pan-Cadherin	WB	mouse	Abcam, #ab6528
PDH	WB	rabbit	Cell Signaling Technology, #3205
PFK-C	WB	rabbit	Acris Antibodies, #C10836
PKA-RIα	WB	mouse	BD Biosciences, #610610
PKA-RIIα (m)	WB	mouse	BD Biosciences, #612243
PKA-RIIα (r)	WB	rabbit	Abcam, #ab38949
PKA-RIIβ	WB	mouse	BD Biosciences, #610626
PKM	WB	mouse	Santa Cruz Biotechnology, #sc-365684
Rab11	WB	mouse	BD Biosciences, #610657
V-ATPase v0a1 (m)	WB/IP	mouse	Santa Cruz Biotechnology, #sc-374475
V-ATPase v0a1 (r)	WB	rabbit	Abcam, #ab105937
V-ATPase v0d1	WB/IP	rabbit	Proteintech, #18274-1-AP
V-ATPase V1A	WB	rabbit	GeneTex, #GTX110815
V-ATPase V1H	WB	mouse	Santa Cruz Biotechnology, #sc-166227
ZO-1	IF	rat	Santa Cruz Biotechnology, #sc-33725
Secondary antibody			
Cy2- anti-Rabbit IgG	IF	goat	Immuno Research, #111-225-144
Cy3-F(ab)$_2$-anti-Mouse IgG	IF	goat	Immuno Research, # 115-166-003
Cy5- anti-Rat IgG	IF	donkey	Immuno Research, # 712-175-153
POD-anti-Goat IgG	WB	donkey	Immuno Research, #705-035-147
POD-anti-Mouse IgG	WB	donkey	Immuno Research, # 715-035-151
POD-anti-Mouse IgG (EasyBlot)	WB	-	GeneTex, #GTX221667-01
POD-F(ab)2-anti-Rabbit-IgG	WB	donkey	Immuno Research, # 711-036-152
POD-anti-Rabbit IgG, light-chain-specific	WB	mouse	Immuno Research, #211-032-171

2.1.6 Proteins

Table 8: Purified proteins

Protein	Supplier, Article number (#)
LDH from bovine heart	Sigma-Aldrich, #L2625
LDH from rabbit muscle	Roche Applied Science, #10127230001

2.1.7 Plasmid DNA

Table 9: Plasmid DNA All DNA fragments were cloned into pCMV entry (Origene, PS100001); full plasmid sequences are given in the Appendix.

Expressed gene	Species	Supplier
AKAP18γ WT	human	GeneArt Strings fragment, Life Technologies
AKAP1	human	Tagged ORF clone, Origene, # RC200506
smAKAP WT	human	GeneStrands, Eurofins Genomics
smAKAP mut(D72A/Q76A)	human	GeneStrands, Eurofins Genomics

2.1.8 Primers

Primers were purchased from BioTeZ GmbH (Berlin, DE) in 10 nmol scale, dissolved in *A. dest.* and stored as 50 µM stocks.

Table 10: Primers for quantitative polymerase chain reaction (PCR)

Target gene	Orientation	Sequence
GAPDH, mouse	fwd	AGGTTGTCTCCTGCGACTTCA
	rev	CCAGGAAATGAGCTTGACAAAGTT
AQP2, human	fwd	GAATTCATGTGGGAGCTCCGC
	rev	GCGGCCGCTCAGGCCTTGGTACC

Table 11: Primers for site-directed mutagenesisl Primers were designed using the Agilent QuickChange Primer Design Online Tool (https://www.genomics.agilent.com/primerDesignProgram.jsp). All primer sequences are indicated as 5' to 3'.

Target gene	Mutation	Orientation	Sequence
AKAP18γ	E318A	fwd	GTCCA GCAGT ATCTG GAGGC AACAC AGAAT AAAAAC
		rev	GTTTT TATTC TGTGT TGCCT CCAGA TACTG CTGGAC
AKAP18γ-E318A	Q314A	fwd	GCTCA AGGCT GTCCA GGCGT ATCTG GAGGC AACA

		rev	TGTTG CCTCC AGATA CGCCT GGACA GCCTT GAGC
AKAP18γ-(Q314A/E318A)	D293A	fwd	GAGCC CGATG CCGCT GAACT AGTAA GGC
		rev	GCCTT ACTAG TTCAG CGGCA TCGGG CTC
AKAP1, AKAP1-(Q354A/E358A)	N341A	fwd	CGCTT AATCT CCTCA GCTCT ATCCA AGCCC TCCTC ATTTC TATCC
		rev	GGATA GAAAT GAGGA GGGCT TGGAT AGAGC TGAGG AGATT AAGCG
AKAP1-N341A	Q362A/ T366A	fwd	CCAAC CGTGG CGGCC AGCAC CGCTT CGGTT GCTTC TG
		rev	CAGAA GCAAC CGAAG CGGTG CTGGC CGCCA CGGTT GG
AKAP1	Q354A	fwd	GGTTG CTTCT GAGAT CACTG CGGAG ATTAT CTGGA AGGCA
		rev	TGCCT TCCAG ATAAT CTCCG CAGTG ATCTC AGAAG CAACC
AKAP1-(Q354A)	E358A	fwd	ACCTG TTCGG TTGCT GCTGA GATCA CTGCG G
		rev	CCGCA GTGAT CTCAG CAGCA ACCGA ACAGG T

2.1.9 Cloning reagents and enzymes

Table 12: Cloning reagents

Reagent / enzyme [stock concentration]	Supplier, # Article number
CutSmart buffer [10x]	Supplied together with restriction enzyme
dNTP mix [5 mM]	Robklon GmbH (Berlin, DE), #E2800-04
$MgCl_2$ [25 mM]	Robklon GmbH (Berlin, DE), #E2500-01
NheI-HF® [20.000 U/ml]	New England BioLabs (Ipswich, US), #3131S
PfuUltra II Fusion HotStart DNA Polymerase [2500 U/ml]	Agilent technologies (Santa Clara, US), #600670
PfuUltra II reaction buffer	
T4 ligase [400.000 U/ml] + reaction buffer [10x]	New England BioLabs (Ipswich, US); #M0202S
XhoI [20.000 U/ml]	New England BioLabs (Ipswich, US), #R0146S

2.1.10 Bacterial strains and growth medium

Medium	Composition
Lysogeny broth (LB) medium	10 g/l peptone; 5 g/l yeast extract; 5 g/l NaCl, pH 7.5

For LB agar plates, LB medium was supplemented with 15 g/l of agar and 100 µg/ml kanamycin.

Bacterial strain	Genotype	Supplier
E. coli DH5α	F– Φ80lacZΔM15 Δ(lacZYA-argF) U169 recA1 endA1 hsdR17 (rK–, mK+) phoA supE44 λ– thi-1 gyrA96 relA1	New England BioLabs (Ipswich, US)

2.1.11 siRNA

Table 13: siRNA

Target gene	Supplier, # Article number
Silencer® Select LDHA siRNA	Thermo Fisher Scientific, #4392420, ID: s229664
siGENOME Non-Targeting siRNA Pool #2	Dharmacon, #D-001206-14

2.1.12 Cell culture reagents

Table 14: Cell culture reagents

Reagent	Supplier, # Article number
Arginine-Vasopressin (AVP)	kindly provided by B. Wiesner (Leibniz-Forschungsinstitut für Molekulare Pharmakologie FMP, Berlin-Buch)
Collagenase type II	Biochrom AG (Berlin, DE), #C2-28
Collagen type IV	BD Bioscienes (Heidelberg, DE), #356233
Dexamethasone	Sigma-Aldrich, #D-2915
DMEM, metabolomics assay medium	Sigma-Aldrich, #D5030
DMEM-GlutaMAX™	Life Technologies GmbH (Darmstadt, DE), #21885
DMEM, high glucose	Life Technologies GmbH (Darmstadt, DE), #41965
DMEM/F-12-GlutaMAX™	Life Technologies GmbH (Darmstadt, DE), #31331
DMEM/F-12-GlutaMAX™	Life Technologies GmbH (Darmstadt, DE), #10565
Fetal bovine serum (FBS) superior	Biochrom AG (Berlin, DE), #S0613
Forskolin (FSK)	Biaffin GmbH & Co KG Life Sciences Institute (Kassel, DE); #PKE-FORS-050
Gentamycin	Life Technologies GmbH (Darmstadt, DE), #15710
Hyaluronidase	Sigma-Aldrich, #H6254
Non-essential amino acids	Biochrom AG (Berlin, DE), #K0293
Nystatin	Sigma-Aldrich (St. Louis, US), #N4014
Opti-MEM	Life Technologies GmbH (Darmstadt, DE), #31985

PBS 10x	Life Technologies/ gibco (Darmstadt, DE), #14200
PBS (1x) with Ca^{2+}/Mg^{2+}	GE Healthcare, #H15-001
Penicillin/streptomycin	Biochrom AG (Berlin, DE), #A2212
Transfection reagent Lipofectamine2000	Invitrogen (Carlsbad, US), #11668-019
Transfection reagent Lipofectamine3000	Invitrogen (Carlsbad, US), #L3000-008
Trypsin-EDTA	Biochrom AG (Berlin, DE), #L2153
Ultroser G	Cytogen GmbH (Sinn, DE), #15950-017

2.1.13 Cells and media

Table 15: Cell lines and media

Cell lines	Description	Culture medium	Supplier
C2C12	Mouse myoblast cell line	DMEM, high glucose; 10 % FCS; 1 % penicillin/streptomycin (100 U/ml)	Kindly provided by Prof. Dr. Michael Gotthardt (MDC Berlin)
HEK293	Human embryonic kidney cell line	DMEM-GlutaMAX™; 10 % FCS; 1 % penicillin/streptomycin (100 U/ml)	Deutsche Sammlung von Mikroorganismen und Zellkulturen GmbH (DSMZ; Braunschweig, DE); #ACC305
H9C2	Rat embryonic myoblast cell line	DMEM-GlutaMAX™; 10 % FCS; 1 % penicillin/streptomycin (100 U/ml)	ATCC, LGC Standards GmbH (Wesel, DE) ; #CRL-1446
MCD4	Mouse collecting duct cell line, stably expressing human AQP2 (Iolascon et al., 2007)	DMEM/F-12-GlutaMAX™ (#31331); 5 % FCS, 5 µM dexamethasone	G. Valenti, Dipartimento di Fisiologa Generale ed Ambientale, (Bari, IT)
SH-SY5Y	Human neuroblastoma cell line	DMEM/F-12, GlutaMAX™ (#10565); 10 % FCS; 1 % penicillin/streptomycin (100 U/ml)	DSMZ (Braunschweig, DE); #ACC209
Primary cells			
IMCD	Inner medullary collecting duct cells from rats	DMEM- GlutaMAX™; 1 % non-essential amino acids; 1 % ultroser G; 500 µM dbcAMP, 20 U/ml nystatin; 0.25 µg/ml gentamicin; 4.5 g/l glucose; 100 mM NaCl; 100 mM urea	Primary cells; made inhouse (Faust et al., 2013; K. Maric et al., 1998)
		Metabolomics assay medium: D5030; 100 mM NaCl; 100 mM urea; glutamine (tracer) 2 mM; glucose (tracer) 25 mM; pH 7.4; sterile filtered	

2.1.14 Software

Table 16: Software

Software	Application	Developer
EndNote	Literature manager	Clarivate Analytics (Philadelphia, US)
GraphPad Prism 5	Data presentation and statistical analysis	GraphPad Software, Inc. (La Jolla, US)
Illustrator	Graphics	Adobe Systems, Inc. (San Jose, US)
Image J	Analysis of immunofluorescence pictures	Wayne Rasband (NIH - National Institutes of Health)
Image Studio 2.0	Acquisition and analysis of Western blots	LI-COR Biosciences (Bad-Homburg, DE)
Microsoft Office	Text editing, presentations, spreadsheet	Microsoft (Redmond, US)
ViiA7	Real-time/ Quantitative PCR	Thermo Fisher Scientific (Waltham, MA, US)
ZEN 2011	Confocal microscopy image acquisition and analysis	Carl Zeiss MicroImaging GmbH (Jena, DE)

2.2 Methods

2.2.1 RNA and DNA biology

2.2.1.1 Cloning of DNA fragments into the vector pCMV6-entry

DNA fragments of the human smAKAP-WT/mutant and human AKAP18γ-WT sequences were ordered as GeneStrands (Eurofins Genomics) or GeneArt Strings (Life Technologies), respectively, flanked by suitable restriction sites. 200 ng of reconstituted DNA and 1 µg of vector DNA (pCMV6-entry) were each digested with NheI-HF® and XhoI in 1x CutSmart buffer at 37°C for 1 h. Digested fragments were purified using the NucleoSpin® Extract II kit, with size-exclusion performed as described in the manual. Yield concentrations were measured using the NanoDrop.

2.2.1.2 DNA ligation

For ligation of insert fragments and linearized vector, each 200-300 ng of vector DNA was mixed with the insert DNA in a molar ratio of 1:4 and incubated overnight at 16°C with 400 U of T4 DNA ligase, diluted in T4 ligase reaction buffer. The ligated plasmid was then transformed into bacteria.

2.2.1.3 Site-directed mutagenesis

Point mutations were inserted into plasmid DNA by mutagenesis PCR, using primer pairs with the respective nucleotide mutation (Table 11) and the PCR protocol as shown in Table 18. In order to degrade template DNA prior to transformation into bacteria, plasmid DNA was digested with DpnI restriction enzyme (20 U) for 1 h at 37°C. The enzyme was heat inactivated by incubation at 80°C for 20 min. The mutated plasmid was then transformed into bacteria.

Table 17: Mutagenesis PCR mix

Component	Amount
Template	10-25 ng
PfuII reaction buffer (10x)	5 µl
Primer, fwd (50 µM)	0.4 µl
Primer, rev (50 µM)	0.4 µl
$MgCl_2$	2 µl
dNTP mix	5 µl
PfuII polymerase	1 µl
H_2O	ad 50 µl

Table 18: Mutagenesis PCR protocol

Step	Temperature	Time	Cycles
1	92 °C	2 min	
2	92 °C	30 sec	
3	55 °C	1 min	
4	68 °C	1 min/ kb of template	repeat with step 2, 30x
5	68 °C	double as step 4	
6	4 °C	hold	

2.2.1.4 Bacterial transformation

In order to replicate the construct DNA and perform a selection of clones, plasmid DNA was transformed into chemically competent *E. coli* DH5α by heat shock. Each 5 µl of ligation mix or PCR product was added to the bacteria on ice and incubated for 30 min to allow attachment. Then a heat shock of 40 sec at 42°C was performed, followed by 5 min incubation on ice. The transformed bacteria were grown in normal LB medium for 1 h at 37°C and then plated onto kanamycin-containing agar plates (100 µg/ml) and incubated overnight at 37°C. Single clones were picked and grown in 4 ml LB medium containing 100 µg/ml kanamycin at 37 °C overnight.

2.2.1.5 Isolation and purification of plasmid DNA from *E. coli*

Competent bacteria were transformed with the respective plasmid DNA, clones selected and grown in 4 ml (mini culture) or 200 ml (midi culture) LB medium containing 100 µg/ml kanamycin at 37 °C overnight. Cells were harvested and DNA was isolated using the NucleoSpin® Extract II kit (Mini) or NucleoBond® Xtra Midi / Maxi kit (Midi), according to the manufacturer's instructions.

2.2.1.6 Sequencing

Purified plasmid DNA was sequenced by Source Biosciences (Berlin, DE), employing suitable primers to evaluate the correctness of the cloned construct.

2.2.1.7 Purification of mRNA and transcription into cDNA

Cells were trypsinized, the cell pellet washed with phosphate-buffered saline (PBS) and collected by centrifugation (5 min, 300 x g, RT). Purification of mRNA was performed with the GeneMATRIX Univeral RNA Purification Kit and yield concentrations measured at the

NanoDrop. Each 1 ug of RNA was used for transcription into cDNA by the qScript cDNA Synthesis Kit, applying the PCR program provided in the manual.

2.2.1.8 Quantitative PCR

For quantitative PCR (qPCR), the SYBR Green method was used, which provides universal application for a target gene auf choice. Each cDNA was diluted to 2 ng/µl and mixed with the Power SYBR Green PCR Master Mix and the primer pair of choice (final concentration 350 nM) to a final volume of 20 µl per well of a 384 well plate. For each primer pair, a standard curve was measured in parallel to determine their efficiency. AQP2 mRNA levels were determined as quadruplicates with the ΔΔCt method relative to GAPDH mRNA.

Table 19: Quantitative PCR protocol

Step	Temperature	Time	Cycles
1	95 °C	15 sec	
2	60 °C	1 min	repeat with step 1, 39x

2.2.2 Cell biology

2.2.2.1 Cultivation of mammalian cell lines

The mammalian cell lines C2C12, HEK293, H9c2 and SH-SY5Y were grown in appropriate growth medium (see Table 15), supplemented with 10 % fetal calf serum (FCS). MCD4 medium was supplemented with 5 % FCS and 5 µM dexamethasone. Cells were grown to confluency, washed with PBS (w/o Ca^{2+} and Mg^{2+}) and incubated with 1x Trypsin/EDTA solution at 37 °C until cells detached. Addition of growth medium stopped the enzymatic digest and a defined proportion of cell suspension was transferred into a new sterile cell culture flask containing fresh growth medium.

A. Freezing and thawing of mammalian cells

Cells were grown to confluency, trypsinized and collected in a 15ml falcon tube. After centrifugation (300 x g, 2 min at RT), the cell pellet was resuspended in freezing medium and distributed into 2 ml screw-cap freezing vials. Cells were then placed into a cryo-container that ensured a cooling rate of 1 °C per minute and stored at -80 °C for 24 h. For long-term storage, cell vials were transferred to the gas phase of liquid nitrogen.

Thawing of the cells was done in a 37 °C water bath with slight agitation. Under sterile conditions, cells were transferred into a 15 ml falcon tube with growth medium and centrifuged (300 x g, 2 min at RT) to remove the freezing medium. The cell pellet was

resuspended in growth medium and cells seeded into a T25 or T75 cell culture flask. Cells were grown to confluency and passaged at least twice before experiments were conducted.

2.2.2.2 Cultivation of rat primary inner medullary collecting duct cells

IMCD cells were isolated from rats as published in (Faust *et al.* 2013). In summary, rats (10 to 12 weeks, Wistar Han, Charles River Laboratories, Sulzfeld, DE) were anesthetized, decapitated and the kidneys transferred into cold PBS. Under sterile conditions, inner medullae were isolated, dissected and enzymatically digested with 1 mg/ml of hyaluronidase and 2.2 mg/ml collagenase (type II) for 2 h at 37 °C. Singularized cells were taken up in full growth medium and seeded into collagen type IV coated cell culture plates. After 24 h, medium was changed to remove dead cells and debris. Cells were used starting from day 5 up to day 9. Whenever AQP2 translocation was to be observed, cells were grown 24 h in medium without dibutyryl-cAMP (dbcAMP) and nystatin before stimulation with AVP or FSK.

2.2.2.3 Transfection of mammalian cells

Mammalian cell lines were transfected with small interfering RNA (siRNA) or plasmid DNA using lipofection reagents (Lipofectamine2000 or 3000) or cationic polymers (PEI-Polyethylenimine).

A. Reverse siRNA transfection

MCD4 cells were transfected with siRNA to down-regulate the expression of a protein of interest by RNA interference. Therefore, the double stranded siRNA is inserted into the cells and binds to the RNA-induced silencing complex (RISC). Its antisense strand guides the RISC to the targeted mRNA, which is then degraded.

For transfection, siRNA was diluted in RNAse-free water, mixed with the same volume of lipofectamine2000 pre-diluted in OptiMEM and incubated for 15 min at RT to allow liposome formation. After cells were trypsinized, diluted and seeded into cell culture plates, the liposome-siRNA complex was added to the cells. Cell lysis for Western blot analysis or fixation for immunofluorescence microscopy was performed 72 h after transfection.

B. Plasmid DNA transfection

Transfection of Plasmid DNA was performed to overexpress a protein of interest and investigate its function or protein complex formation in the cellular context.

Cells were seeded 24 h prior to transfection in a way that the cells were 70-80 % confluent on the day of transfection, using medium without antibiotics. For transfection, plasmid DNA was diluted and mixed with diluted transfection reagent, incubated for 15 min at RT and then

added to the cells. The next day, medium was changed to standard growth medium and cells analyzed 48 h post transfection.

2.2.2.4 Immunofluorescence microscopy

Cells were seeded onto 12 mm diameter cover slips placed into 6-well plates or 35 mm cell culture plates and treated with the compounds as indicated. Then, medium was aspired and cells fixed with 10 % trichloroacetic acid (TCA) for 10 min. After careful removal of the fixative and several washing steps with PBS, cells were permeabilized with 0.1% Triton/PBS for 5 min at RT. After intense washing of the cells with PBS, unspecific binding was diminished by incubation with blocking buffer (0.27 % fish skin gelatin/PBS) for 1 h at 37 °C. Incubation with primary antibodies was performed in a wet chamber at 37 °C for 1-2 h, whereby each cover slip was mounted with 35 µl of antibody dilution. After three times washing with PBS, cover slips were incubated with fluorescent secondary antibodies and cell stains (e.g. DAPI) at 37 °C for 1-2 h. Removal of excessive antibody by washing with PBS was followed by immobilization of the cover slips on microscope slides using Immu-Mount. Samples were stored over night at 4 °C to ensure curing. Evaluation and image capturing was performed at the confocal laser scanning microscope (LSM) 780 at the Leibniz-Forschungsinstitut für Molekulare Pharmakologie (FMP, Berlin-Buch).

2.2.3 Protein biology

2.2.3.1 Lactate dehydrogenase activity assay

Lactate dehydrogenase (LDH) activity was measured spectrometrically. At 340 nm wavelength NADH has a second absorption maximum in comparison to NAD^+. Conversion of pyruvate and NADH to lactate and NAD^+ by LDH results in a decrease in A_{340nm}. The rate of this decline correlates with LDH activity. Purified LDH (LDH-H from bovine heart, LDH-M from rabbit muscle) was diluted in Tris-HCl 0.2 M, pH 7.4 and stored on ice. The assay was performed in a 96 well plate, measuring A_{340nm} of one row at a time using a Spectrophotometer. Per well 8 µl enzyme dilution was equilibrated at RT for 5 min. Assay buffer (220 µl/well) with or without cAMP and sodium oxamate (SO, LDH inhibitor) was added with a multi-channel pipette immediately before starting the measurement to ensure parallel start of the enzyme reaction. Absorption at 340 nm was measured 6 times with a shift of 10 sec and the decline in absorption exported as maximal rate [mOD/min]. LDH activity was measured in triplicates and related to control activity [%].

2.2.3.2 Cell lysis

Before lysis, mammalian cells were carefully washed with ice-cold PBS. After complete removal of the PBS, lysis buffer was added and cells scraped on ice. To ensure proper lysis, the suspension was passed through a syringe. After removal of cell debris by centrifugation (5000 x g, 5 min, 4 °C), the lysate was transferred into a clean microtube.

2.2.3.3 Tissue lysis

For tissue preparations, rats/mice were anesthetized, sacrificed by decapitation or cervical dislocation and organs transferred into cold PBS. Isolated organs were homogenized in lysis buffer using a tissue homogenizer. After removal of cell debris by centrifugation (5000 x g, 5 min, 4 °C), the lysates were transferred into a clean microtube.

2.2.3.4 Subcellular Fractionation

The separation of cytosolic and membrane fraction was done by differential detergent fractionation. Cell monolayers were washed once with ice-cold PBS and incubated with fractionation buffer 1 (Table 4) on a horizontal shaker at 4 °C for 15 min. Then cells were scraped and transferred into a microtube. Cytosolic proteins were separated by centrifugation (500 x g, 5 min, 4 °C) and the pellet washed once with buffer 1, followed by centrifugation (500 x g, 5 min, 4 °C). Solubilization of membranous proteins was done by resuspension of the pellet in buffer 2 (Table 4) and incubation for 2 h at 4 °C on a rotator. Centrifugation at 5000 x g and 4 °C for 10 min yielded the membrane fraction in the supernatant. Cytosolic and membrane fractions were analyzed by Western blotting.

2.2.3.5 Bradford assay

The protein concentration of cell and organ lysates was determined by the colorimetric Bradford assay. This method utilizes the protein-dependent color change of Coomassie Brilliant Blue G-250. In a 96-well microtiter plate, 250 µl of Bradford solution was added to 5 µl of lysate and incubated 10 min protected from light. Absorbance was measured with a microplate reader at 595 nm wavelength. Protein concentration was calculated with a standard curve (0.125 - 2 mg/ml) that was measured in parallel.

2.2.3.6 Western Blotting

For protein detection by immunoblot, lysates were denatured in 1x Lämmli sample buffer for 8 min at 95 °C and separated by SDS-polyacrylamide gel electrophoresis (PAGE). To determine the molecular weight of analyzed proteins, Precision Plus Dual Color standard

was applied to each gel. Transfer of the proteins occurred in an electric field, either by wet tank blot (110 V, 2 h) or semi-dry TurboBlot (1.3 A/stack, 25 V, 10 min, BioRad) onto ethanol-activated polyvinylidene fluoride (PVDF) membranes. Blocking of unspecific binding was performed in 1 % BSA in TBS or EasyBlocker (GeneTex) for 1h at room temperature. Membranes were incubated with primary antibody diluted in blocking buffer, rolling overnight at 4 °C. After washing with TBS-T for 3x 10 min, membranes were incubated in secondary antibody coupled to horseradish peroxidase (POD), diluted 1:10.000 in blocking buffer, for at least 1 h at RT. Membranes were washed 3x 10 min with TBS-T and incubated with Immobilon Western Chemiluminescent HRP substrate for detection of proteins in an Odyssey Fc imaging system. Densitometric analysis was performed with the Imager software Li-Cor Image Studio.

2.2.3.7 cAMP pulldown

Cell or tissue lysates were incubated shaking at 30 °C for 30 min with or without cAMP, cGMP, NADH or ATP, before cAMP-agarose beads were added and samples incubated overnight at 4 °C on a rotator. Beads were separated by centrifugation (1000 x g, 2 min, 4 °C) and supernatant samples collected. Beads were washed three times with lysis buffer (1000 x g, 2 min, 4 °C). After the final washing step, the remaining buffer was removed and proteins eluted by addition of Lämmli sample buffer and denaturation at 95 °C for 8 min.

2.2.3.8 Immunoprecipitation

A. Immunoprecipitation of endogenous proteins

ProteinA or -G sepharose-beads were washed once with MLB (Table 4) and incubated for 30 min with the respective immunoprecipitation (IP)-antibody diluted in a small volume of MLB. Then, cell lysates were added and incubated rotating for at least 3 h at 4 °C. Next, beads were washed three times with MLB and proteins eluted from the beads using 0.1 M glycine buffer, pH 2.5. The eluate was neutralized with 1 M Tris, pH 10.6, Lämmli sample buffer was added and samples incubated for 8 min at 95 °C.

B. Flag-IP

For the precipitation of flag-tagged overexpressed protein, anti-FLAG M2 magnetic beads were washed once with TBS, equilibrated in MLB and incubated with cell lysates for at least 3 h. Proteins were eluted from the beads using 0.1 M glycine buffer, pH 2.5 and neutralized with 1 M Tris, pH 10.6. In preparation for Western blotting, Lämmli sample buffer was added and samples incubated for 8 min at 95 °C.

C. AQP2 vesicle isolation

ProteinA-dynabeads were loaded with AQP2 antibody or IgG control in BSA/PBS (10 mg/ml), incubated over night at 4 °C and washed three times with BSA/PBS (1 mg/ml). Cells were stimulated with 30 μM FSK for 30 min or left untreated. In order to keep AQP2-bearing vesicles intact, the cells were scraped with homogenization buffer, transferred to a dounce homogenizer and mechanically disrupted. Post-nuclear supernatant was separated by centrifugation (3000 x g, 15 min, 4 °C) and loaded onto the prepared beads. After incubation for at least 3 h, beads were washed four times with BSA/PBS (1 mg/ml) and proteins eluted by addition of Lämmli sample buffer and denaturation at 95 °C for 8 min.

2.2.3.9 Cell surface protein biotinylation assay

Cell surface expression of proteins was detected by biotinylation and subsequent streptavidin-mediated precipitation, followed by Western blot analysis. IMCD cells were stimulated with SO and/or FSK, washed twice with ice-cold PBS and incubated with biotin (diluted in biotinylation buffer, BB, Table 4) for 1 h at 4 °C. Free biotin was removed by washing twice with BB and cells were incubated with quenching buffer for 10 min at 4 °C. After removal of the buffer, cells were lysed in lysis buffer 1, samples sonicated with 8 pulses and incubated at 37 °C for 20 min. After removal of debris by centrifugation (13.000 rpm, 10 min at 4 °C), the supernatant was loaded onto streptavidin-agarose beads and rotated over night at 4 °C. Next day, beads were washed three times with lysis buffer, proteins eluted with Lämmli sample buffer and analyzed by Western blot.

2.2.3.10 Peptide spot array

Peptides were spot-synthesized as 25mers on a cellulose membrane using the AutoSpot-Robot ASS 222 (Intavis Bioanalytical Instruments AG, Köln, DE).

2.2.3.11 RII overlay

The RII overlay method employs radiolabeled RII subunits that are obtained by auto-phosphorylation of PKA-RII subunits at S96 by its catalytic subunits in the presence of [γ^{32}P]-ATP. RIIα overlay was performed in collaboration with my colleague Dr. Kerstin Zühlke.

Peptide spot membranes were activated in ethanol, briefly washed with *A. dest*. and incubated in blocking buffer (Table 4) for at least 3 h. In parallel, for preparation of the size-exclusion column, swollen sephadex material (G50 medium) was loaded with PBS supplemented with 1 mg/ml BSA. Labeling reaction mix was prepared without ATP (Table 20) and all material transferred to the radioactivity workstation. There, radioactive [γ^{32}P]-ATP and low concentrated ATP were mixed and added to the PKA subunits containing labeling

reaction mix. Incubation for 10 min at RT ensures equilibration of the proteins, before the more concentrated ATP was added to fully activate the auto-phosphorylation reaction. After 1 h incubation on ice, dextran blue was added and radiolabeled RIIα subunits separated from free nucleotides by size-exclusion chromatography. Radiolabeled RIIα elutes with the dextran blue fraction. As negative control, RIIα was pre-incubated with L314E peptide. Radiolabeled RIIα was then added to the membranes and incubated overnight in blocking buffer. Unbound RIIα was removed by washing with blocking buffer (4x, 15 min) and PBS (2x, 10 min). Signals were detected by phosphoimaging.

Table 20: Labeling reaction mix

Proteins	**Final amount**
PKA-RIIα purified protein	14 µg
PKA-C purified protein	3.3 µg
Buffer component	**Final concentration in A. *dest.***
KH_2PO4	25 mM
cAMP	10 µM
$MgCl_2$	10 mM
DTT	0.5 mM
ATP	**Final concentration**
ATP for equilibration	0.1 µM
[γ^{32}P]-ATP	5.55 MBq
ATP for reaction	10 µM

2.2.4 Metabolomics

Analysis of cellular metabolites was performed in cooperation with the group of Prof. Dr. Karsten Hiller at the Braunschweig Integrated Centre of Systems Biology (BRICS, Technical University Braunschweig).

IMCD cells were isolated as described in 2.2.2.2. Medium change was performed on day 1 and 4 after isolation. Freshly isolated IMCD cells (day 4) were transported to Braunschweig, washed with PBS, trypsinized, resuspended in FCS-containing medium to stop the enzyme reaction and spun down for 5 min at 300 xg (RT). The cell pellet was resuspended in growth medium (Table 15) with fresh dbcAMP and seeded into 6 well plates. Next day, the medium was changed to growth medium without dbcAMP. On the second day after seeding the medium was changed to D5030 assay medium set to 600 mOs with NaCl and urea, containing the respective tracers or unlabeled glutamine and glucose as control. Cells were stimulated with 100 nM AVP or left untreated and incubated for the indicated times at 37 °C.

2.2.4.1 Extracellular metabolites

For the analysis of extracellular metabolites, a sample of the supernatant medium was taken, spun down to remove floating cells and debris, and the cleared medium was stored at -20 °C until further analysis. Using the YSI Biochemistry Analyzer (Xylem Inc., Yellow Springs, USA), medium samples were analyzed for lactate, glucose, glutamate and glutamine abundance. For quantification, a standard curve of each metabolite was measured in parallel.

2.2.4.2 Intracellular metabolites

The cells were rinsed with 0.9 % NaCl solution and metabolites extracted on ice by addition of each 400 µl methanol and *A. dest.* supplemented with an internal standard. Cells were scraped, transferred into a microtube containing 400 µl ice-cold chloroform and incubated for 20 min shaking at 4 °C (1400 rpm). Separation of polar and unpolar phases was done by centrifugation (16.000 x g, 5 min, 4 °C). Of the polar (aqueous) phase, 300 µl were transferred into glass vials and solvent vacuum drawn in a vacuum concentrator (CentriVap, Labconco, Kansas City, MO, US). The following steps were conducted by Dr. Andre Wegner and Tobias Ludwig (group of Prof. Dr. Karsten Hiller, University of Braunschweig) as described in (Raffel *et al.* 2017). Briefly, metabolites were analyzed by gas chromatography coupled to mass spectrometry (GC-MS) and chromatograms processed with the MetaboliteDetector software (Hiller *et al.* 2009). Using MetaboliteDetector, mass isotopomer distributions were calculated and corrected for natural isotope abundance.

2.2.5 Statistics

Statistical analyses were carried out using GraphPad Prism 7 software. For the comparison of two groups, unpaired t-test was applied. Results of more than two groups were analyzed by one-way or two-way ANOVA, followed by post hoc multiple comparison tests. Significant differences are indicated as $p \leq 0.05$ = *, $p \leq 0.01$ = **, $p \leq 0.001$ = ***, $p \leq 0.0001$ = ****. Mean values are plotted with standard error of mean (SEM) or standard deviation (SD), as indicated.

3. RESULTS

3.1 Cell models for the investigation of AQP2 trafficking

In order to investigate the redistribution of AQP2 in principal cells, a suitable cell model was needed. The most physiologically relevant cells, in which to study the AQP2 redistribution are primary IMCD cells. They are freshly isolated primary cells from the rat inner medulla, and can be kept in culture for up to two weeks (Faust *et al.* 2013). Following their selection by osmotic pressure, they can be trypsinized and seeded into a multi-plate format, but as they do not proliferate, the cell number is fixed. In order to reduce the number of animals sacrificed, and to gain flexibility, an immortalized cell line, MCD4 cells, originating from mouse collecting duct was used. MCD4 cells are M-1 mouse cortical collecting duct cells that stably express human AQP2 (Iolascon *et al.* 2007). Elevation of intracellular cAMP levels caused by the adenylyl cyclase activator FSK induces a translocation of AQP2 from perinuclear vesicles into the plasma membrane. MCD4 cells, however, do not respond to AVP stimulation, as they lack the V2 receptor. IMCD cells express V2R and AQP2 endogenously, which makes them the more favorable system. However, IMCD transfection efficiency is very low (< 5 %) and high animal numbers are required to produce the cells, so that MCD4 cells were preferred for most of the experiments.

3.2 Global metabolic analysis of AVP-stimulated IMCD cells

Intracellular transport processes require energy to fuel motor proteins that actively move cargo, e.g. along cytoskeletal structures. For the translocation of AQP2-bearing vesicles, however, it is unknown, how the transport is driven. In order to investigate potential global metabolic changes that occur upon stimulation of collecting duct principal cells with AVP, a metabolomics analysis of IMCD cells was performed together with the group of Prof. Dr. Karsten Hiller (Braunschweig Integrated Centre of Systems Biology, BRICS, Technical University Braunschweig). Freshly isolated rat IMCD cells were treated with AVP for 5 min to 6 h or were left untreated. Cells were grown in medium containing stable isotope labeled glucose or glutamine to trace intracellular metabolites. Additionally, changes of metabolites taken up from or secreted into the medium were analyzed to gain insights into the cellular metabolism upon antidiuretic hormone stimulation.

3.2.1 Analysis of extracellular metabolites

Figure 7 summarizes the changes of metabolites in medium from IMCD cells grown with glutamine and glucose tracer for 5, 15, 30, 60, 180, 360 min, each in control conditions and

treated with 100 nM AVP. Medium samples were taken at each time point prior to metabolite extraction and the containing glucose, glutamine, lactate and glutamate measured using the biosensor system YSI Biochemistry Analyzer. Concentration changes were determined by comparison to the medium at time point 0. Reduction of glucose and glutamine in the medium correlates with cellular uptake (Figure 7 A, C); an increase of lactate and glutamate in the medium indicates secretion from the cells (Figure 7 B, D). AVP stimulation for 5, 15 or 30 min did not cause substantial changes in the measured metabolites. Starting from 30 min, however, glucose and glutamine uptake tended to decrease, whereas lactate secretion tended to increase. Glutamate shows only minor changes, so that it is not possible to evaluate changes by AVP stimulation. The tendency of increased lactate secretion and reduced glucose uptake by 30 min of AVP stimulation suggests an increase in lactate dehydrogenase activity.

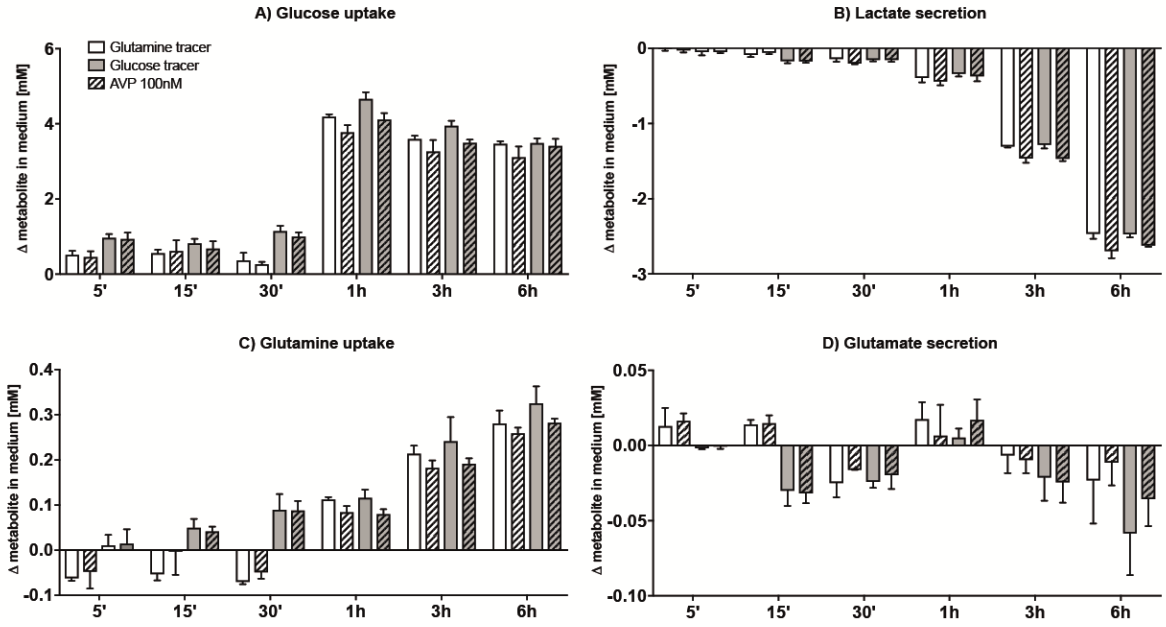

Figure 7: Change of metabolites in IMCD cell culture medium after AVP stimulation. IMCD cells were grown in medium substituted with glutamine (white bars) or glucose (grey bars) tracer for the indicated times. Medium samples of AVP-stimulated (striped bars) and control cells were biochemically analyzed for the abundance of the selected metabolites glucose (A), lactate (B), glutamine (C) and glutamate (D). Positive values represent an uptake of the metabolite from the medium and negative values indicate metabolite secretion into the medium. Bars represent mean values of three technical replicates; error bars indicate standard deviations.

3.2.2 Analysis of intracellular metabolites

Cells were grown in the presence of stable isotope labeled metabolites for 5, 15, 30, 60, 180, 360 min. Total metabolites were extracted and analyzed by GC-MS, which allows detailed tracing of their catabolism products. Alanine, Lactate, Aspartate and Citrate were chosen exemplarily for glycolysis and citric acid cycle (Krebs cycle)-based metabolism of IMCD cells traced with uniform stable-isotope labeled glucose (U-$^{13}C_6$-Glc, Figure 8) or glutamine

(U-$^{13}C_5$-Gln, Figure 9), respectively. Each graph shows the relative mass isotopomer distribution (MID) of the six time points measured. Mass isotopologues M0 to M6 indicate the respective number of labeled carbon atoms incorporated into the metabolite. The schematics shown in Figure 8 A and Figure 9 D guide through the metabolite labeling pattern by U-$^{13}C_6$-Glc and U-$^{13}C_5$-Gln, respectively.

Glycolytic conversion of glucose to pyruvate and further to lactate (Figure 8 D) and alanine (Figure 8 B) is not changed by AVP stimulation of IMCD cells. Mass isotopomer distribution shifts over time from M0 to M3, which indicates efficient glycolytic flux. After 6 h, more than 90 % of lactate was found in the labeled form (Figure 8 D, M3). Overall, aspartate and citrate isotopomer distributions, representative for citric acid cycle flux, also do not change substantially upon AVP stimulation. Aspartate is formed by transamination of oxaloacetate (OAA) and glutamate. As a result, citric acid cycle flux through oxaloacetate leads to a double-labeled (M2) aspartate after the first round and it becomes three times labeled (M3) after the second full cycle (Figure 8 A). Double-labeled citrate (M2) is formed by condensation of unlabeled oxaloacetate with labeled acetyl-CoA by citrate synthase at the entry of the first citric acid cycle. For the 5 and 30 min time points, citrate M2 tends to increase after AVP stimulation, suggesting an increase in citrate synthase activity (Figure 8 E). However, after 15 min of AVP stimulation this increase could not be observed. In the second round, labeled acetyl-CoA forms citrate with a double-labeled OAA, resulting in the isotopomer M4. Citrate M3 is the product of the conversion of pyruvate to oxaloacetate by pyruvate carboxylase and the subsequent condensation with unlabeled acetyl-CoA. Accordingly, citrate M5 is formed by condensation of OAA M3 with labeled acetyl-CoA. Minor changes in citrate M3 (Figure 8 E) at 15 to 30 min of AVP stimulation could indicate a reduction of pyruvate carboxylase activity. Acetyl-CoA serves as an allosteric activator of pyruvate carboxylase. These results suggest that under control conditions acetyl-CoA activates pyruvate carboxylase, which is diminished in the period of 15 to 30 min after AVP stimulation.

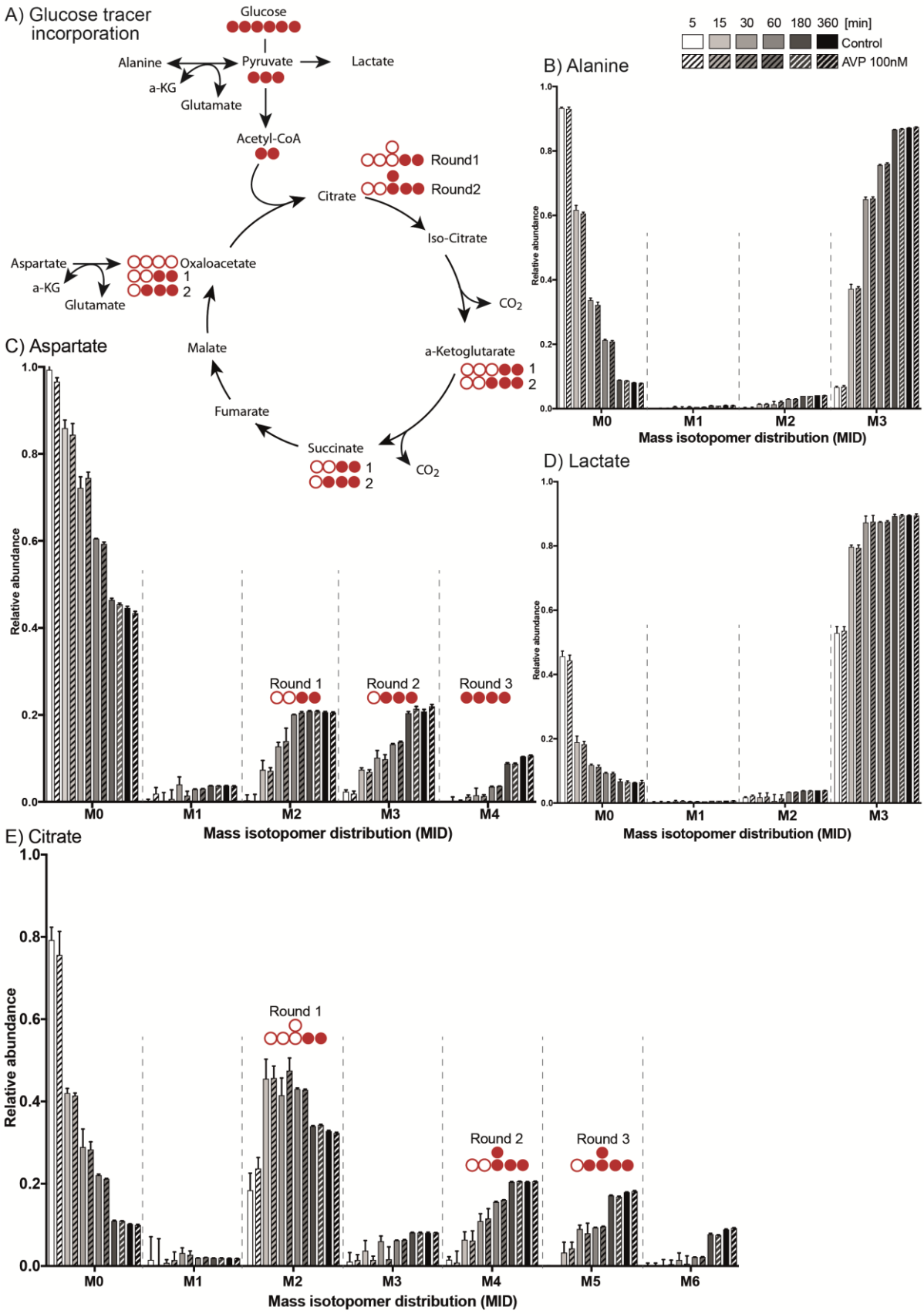

Figure 8: In IMCD cells, the relative intracellular abundance of metabolites traced by ^{13}C-labeled glucose is not changed in response to AVP stimulation. Figure legend see next page

Figure 8: In IMCD cells, the relative intracellular abundance of metabolites traced by ^{13}C- labeled glucose is not changed in response to AVP stimulation. Primary IMCD cells were grown in medium containing uniform stable-isotope labeled glucose (U-$^{13}C_6$-Glc) for the indicated times and were treated with 100 nM AVP (striped bars) or left untreated. Metabolites were extracted, analyzed by GC-MS and concentrations were normalized to an internal standard. Shown is the relative abundance of isotopologues, whereby M0 to M6 indicate the number of labeled carbon atoms incorporated into the metabolite. A) Schematic representation of U-$^{13}C_6$-Glc flux through glycolysis and the citric acid cycle. Filled circles correspond to a labeled carbon atom (^{13}C). Mass isotopomer distribution of Alanine (B) and Lactate (D) show strong enrichment of the isotopologue M3, indicating efficient glycolytic flux. Unlabeled Citrate (C, M0) and Aspartate (E, M0) decrease over time and give rise to up to 6 times labeled isotopologues (M1-M6), corresponding to metabolic flux through the citric acid cycle and the transamination of oxaloacetate to aspartate. Bars represent mean values of three technical replicates; error bars indicate standard deviations.

As expected, the influx of labeled glutamine into the metabolic system does not induce substantial changes in the abundance of labeled alanine (Figure 9 A) or lactate (Figure 9 B) within 6 h. The first cycle of glutamine gives rise to four times labeled aspartate (M4, Figure 9 C) and citrate (M4, Figure 9 E). Accordingly, OAA leaves the second cycle with only two carbon atoms labeled so that its transamination to aspartate or condensation with unlabeled acetyl-CoA to form citrate produces double-labeled metabolites (M2). In line with the results obtained from the glucose tracer experiments, citrate M4 is slightly increased after 30 min of AVP stimulation, indicating an increase in citrate synthase activity compared to control conditions. The shift towards citrate M4 can also be observed in the reduction of unlabeled citrate at this time point (Figure 9 E). The changes in citrate isotopomer distribution observed by both tracers after 30 min of AVP stimulation are summarized in Figure 10. Small changes in the citrate metabolism suggest an elevated citrate synthase activity that could indicate an overall increased energy demand, which is met by elevated mitochondrial respiration. However, this is not in line with the reduced uptake of glucose upon AVP stimulation.

As the experiment was conducted in technical replicates, but not biological replicates, statistical analysis was not done. Nevertheless, the observation of metabolites over 6 h after AVP stimulation gives a good overview about the principal cell metabolism and indicates that AVP stimulation does not substantially change IMCD cell metabolites. As the results were not questionable, for financial reasons and to avoid the unnecessary use of laboratory animals, the experiment was not repeated.

Overall, the metabolomic analysis of IMCD cells indicates that AVP stimulation does not change the global metabolism of collecting duct principal cells. This also shows that principal cells do not globally alter their metabolism to enable translocation of AQP2-bearing vesicles from perinuclear stores into the plasma membrane. Small changes in citrate metabolism upon AVP stimulation of IMCD cells could indicate a temporary increase in ATP demand that is met by elevated mitochondrial respiration after 30 min. However, this is presumably only a secondary effect as translocation of AQP2-bearing vesicles starts within a few seconds of AVP stimulation (Lorenz *et al.* 2003).

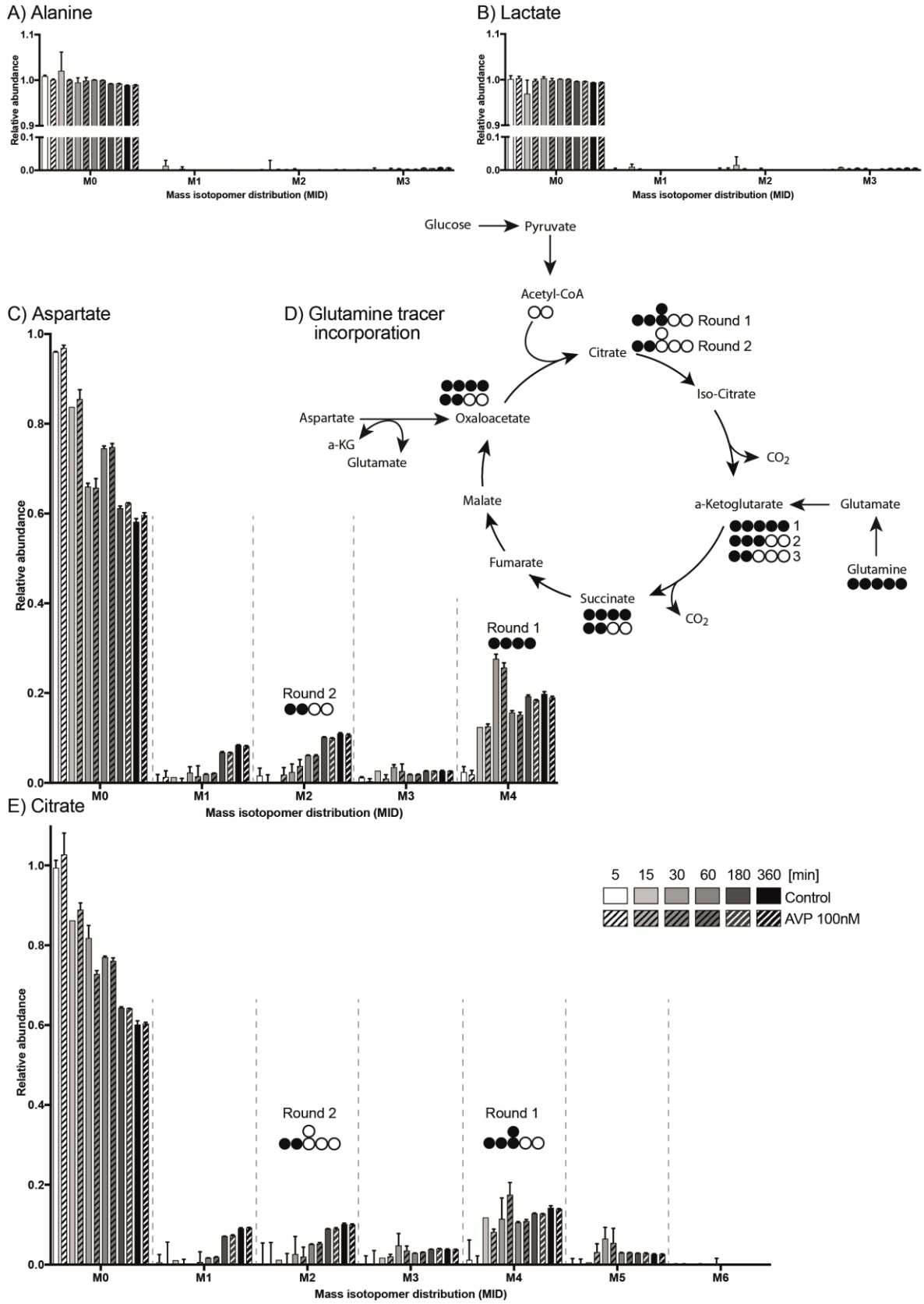

Figure 9: In IMCD cells, the relative intracellular abundance of metabolites traced by ^{13}C-labeled glutamine is not changed in response to AVP stimulation. Figure legend see next page

Figure 9: In IMCD cells, the relative intracellular abundance of metabolites traced by ^{13}C-labeled glutamine is not changed in response to AVP stimulation. Primary IMCD cells were grown in growth medium containing uniform stable-isotope labeled glutamine (U-13C5-Gln) for the indicated times and were treated with 100 nM AVP (striped bars) or left untreated. Metabolites were extracted, analyzed by GC-MS and concentrations were normalized to an internal standard. The relative abundance of isotopologues is shown, in which M0 to M6 indicate the number of labeled carbon atoms incorporated into the metabolite. Mass isotopomer distribution of Alanine (A) and Lactate (B) was overall unchanged. D) Schematic representation of U-13C5-Gln flux through glycolysis and the citric acid cycle. Unlabeled Aspartate (C, M0) and Citrate (E, M0) decrease over time and give rise to 4 and 6 times labeled isotopologues (M1-M4 and M1-M6), respectively. For both metabolites the isotopologue M4 represents the first round of citric acid cycle and M2 is the product of a second cycle. Bars represent mean values of three technical replicates; error bars indicate standard deviations.

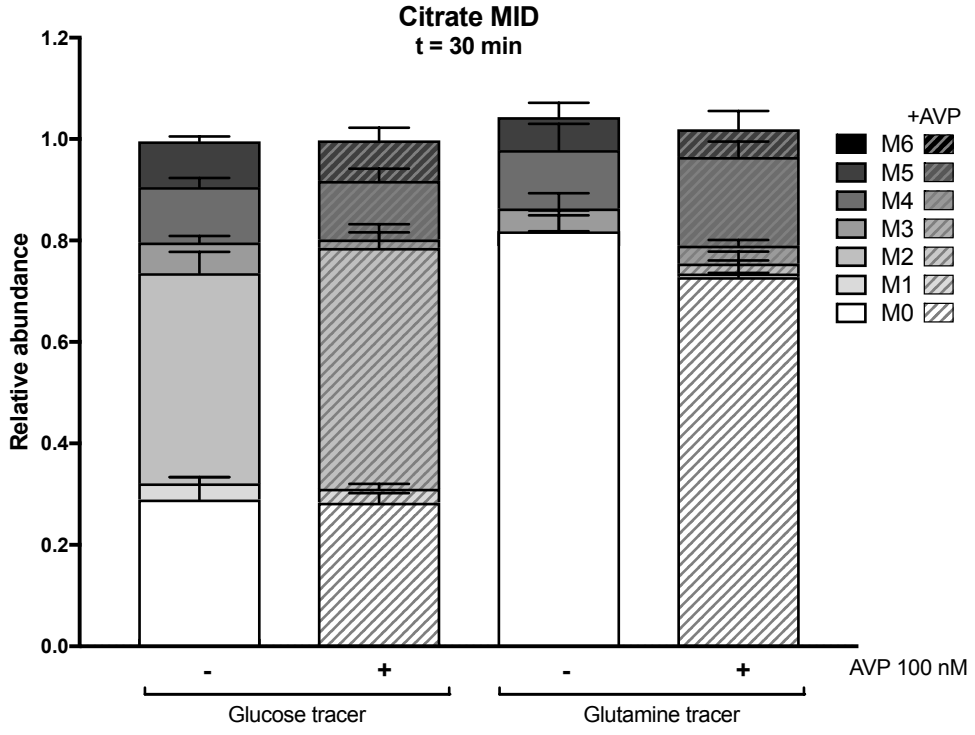

Figure 10: AVP stimulation of IMCD cells causes minimal changes in the mass isotopomer distribution (MID) of citrate. Stimulation of IMCD cells with 100 nM AVP for 30 min (striped bars) changes the MID of citrate that was traced by ^{13}C- labeled glucose and glutamine. The glucose labeling shows a reduction of citrate M3 in favor of an increase of M2 upon AVP stimulation. The analysis of metabolites using the glutamine tracer revealed a shift of citrate M0 to M4 after AVP stimulation. These trends indicate a reduction pf pyruvate carboxylase and an increase of citrate synthase upon AVP stimulation of IMCD cells. Deviation of the sum of the values from 1 is due to negative values that had to be integrated into the calculations as zero. Bars represent mean values of three technical replicates; error bars indicate standard deviations.

3.3 The role of glucose-based metabolism for AQP2 translocation

Studies in neurons have shown that complexes of glycolytic enzymes can be locally restricted within the cytoplasm and that they localize to synaptic vesicles (see chapter 1.2.1), allowing them to locally provide energy for transport processes (Zala *et al.* 2013, Hinckelmann *et al.* 2016). Also for AQP2 translocation, glycolysis is the most common energy source for vesicle transport, as it occurs entirely in the cytoplasm, which ensures that it is accessible to AQP2-bearing vesicles.

In order to assess the validity of the metabolomic analysis, the influence of the inhibition of glycolysis on AQP2 translocation was investigated. The localization of AQP2 after glucose deprivation, 2-deoxyglucose (2DG) glycolysis inhibition, FSK stimulation, or combinations of these, was observed by immunofluorescence microscopy (Figure 11). MCD4 cells were treated with the glucose analog 2DG that is taken up into cells and converted to 2-deoxyglucose-6-phosphate (2DG-6-P) by hexokinase (Wick *et al.* 1957). 2DG-6-P interferes with glycolysis, as it is much slower processed by G6PDH than glucose-6-P so that it remains trapped inside the cell and competitively inhibits glycolytic enzymes. Glutamine and pyruvate concentrations in the medium were left unchanged to not perturb mitochondrial respiration.

In control conditions using standard MCD4 growth medium, AQP2 is located on perinuclear vesicles and FSK induces its redistribution towards and into the plasma membrane (Figure 11 left panel). The tight-junction protein ZO-1 was detected as a marker for plasma membrane localization. The translocation of AQP2 is a dynamic equilibrium of exocytosis-like plasma membrane insertion and endocytic retrieval. As a result, some baseline plasma membrane localization of AQP2 is observed. FSK stimulation shifts the equilibrium towards plasma membrane insertion, but a portion of AQP2 remains in the cytosol.

Glucose starvation alone, or in combination with 5 mM 2DG treatment does not interfere with the FSK-induced AQP2 translocation. However, 5 hours of glucose deprivation reduced the proportion of AQP2 in the plasma membrane below the basal level. Upon FSK stimulation, the AQP2 signal becomes more dispersed throughout the cell, with less prominent plasma membrane localization than in control cells. However, no difference was observed between glucose starvation alone and the additional blockage of glycolysis by 2DG. In both conditions, the cells appeared stressed, which might explain the changes in AQP2 appearance. Cell boundaries appeared irregular and the cell layer showed reduced planarity. For future experiments, the conditions of glucose deprivation and 2DG treatment of MCD4 cells should be further optimized and the use of IMCD cells considered.

In summary, interference with the glucose metabolism does not prevent the translocation of AQP2 from perinuclear vesicles into the plasma membrane, but reduces the steady-state plasma membrane localization of AQP2 in MCD4 cells.

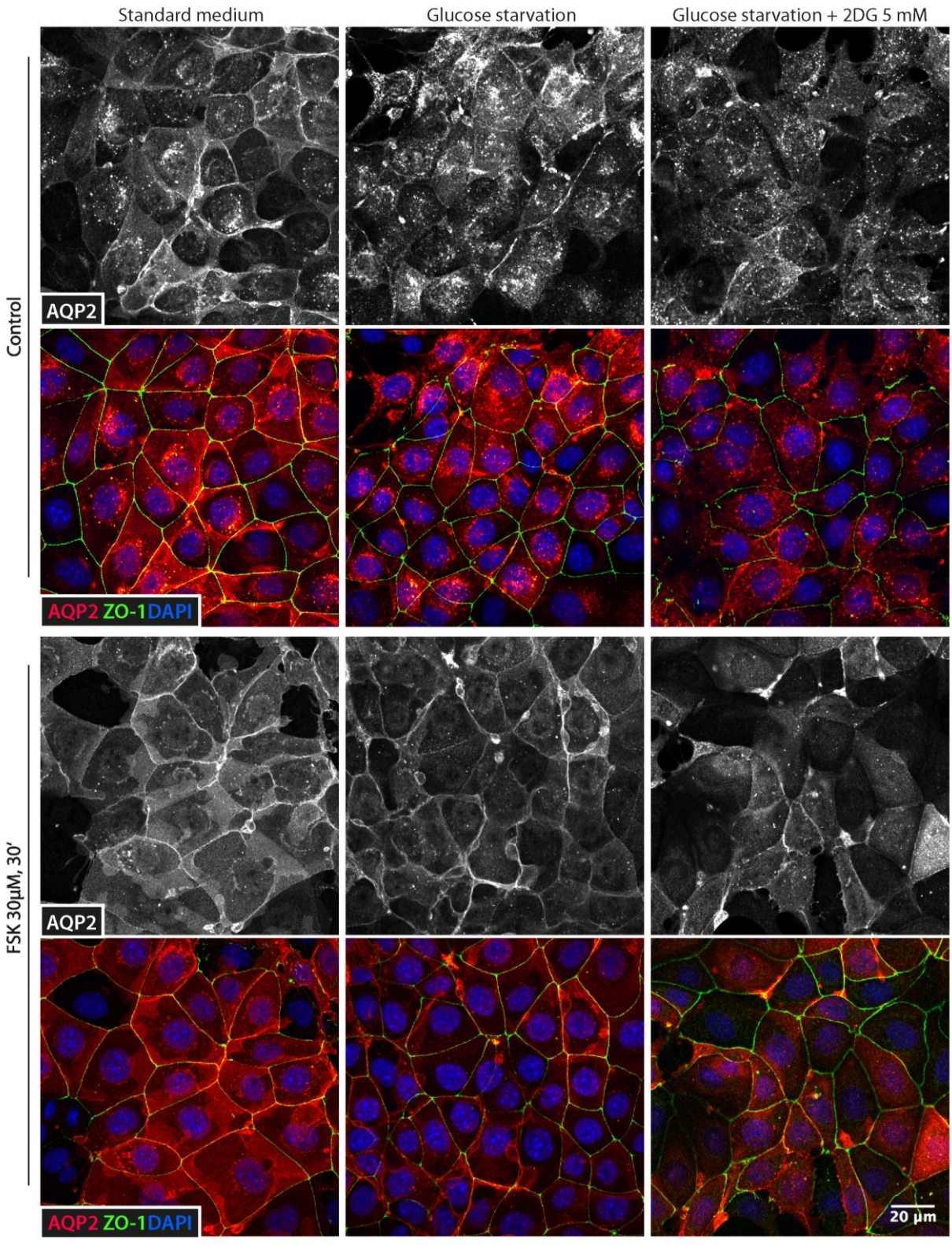

Figure 11: Glycolysis inhibition does not interfere with the trafficking of AQP2 in MCD4 cells. MCD4 cells were grown in normal, or glucose-depleted medium with or without 5 mM 2DG for 5 h. AQP2 translocation was induced by stimulation with 30 µM FSK for 30 min. AQP2 (red) and the tight junction marker ZO-1 (green) were detected using specific antibodies and visualized by Cy2 and Cy5-coupled secondary antibodies, respectively. Co-localization of AQP2 and ZO-1 appears yellow. Nuclei were stained with DAPI and representative images were taken at a confocal microscope. Representative images of one set of two independent experiments are shown. Scale bar 20 µm.

3.4 Putative new AKAPs linking cAMP signaling with metabolic pathways

The control of PKA localization through its association with AKAPs is crucial to the spatiotemporal control of its activity. In addition to tethering PKA in proximity to its substrates, AKAPs coordinate complex signaling hubs that can include phosphodiesterases, and protein phosphatases in addition to other protein components, and they further often define the specific subcellular localization of these multivalent complexes. To date, only a few AKAPs with enzymatic activity have been identified. One example is AKAP-Lbc, which has Rho-GEF activity. Specific interference with the RhoA activation of AKAP-Lbc by the small molecule Scaff10-8 induces AQP2 redistribution towards the plasma membrane in IMCD cells (Schrade *et al.* 2018). Two AKAPs, AKAP18δ and AKAP220, were identified to coordinate the localization of PKA in the regulation of AQP2 trafficking (Henn *et al.* 2004, Okutsu *et al.* 2008). In this work, potentially new AKAPs that regulate AQP2 trafficking through their involvement in metabolic regulation were investigated. The two candidate proteins that were examined were the metabolic enzyme lactate dehydrogenase (LDH) and the proton pump and metabolic sensor vacuolar H^+- ATPase (V-ATPase). The characterization of their AKAP function and their role in AQP2 trafficking will be discussed in the following chapters.

3.5 Candidate 1: Lactate dehydrogenase

LDH reversibly converts pyruvate to lactate in the last step of anaerobic glycolysis. The LDH holoenzyme is a tetramer composed of LDHA and LDHB isoforms, encoded by the *LDHA* and *LDHB* genes, respectively (Figure 12 A). LDHA is also referred to as LDH-M, while LDHB is also known as LDH-H. A further isoform, LDHC, exists, but was not included in here, due to its specific expression in the testis. In predominantly anaerobic tissues, such as skeletal muscle, the M4 homotetramer, which is composed of four LDHA subunits, is the primary isoform (Figure 12 A). When the supply of oxygen is low, the M4 homotetramer favors the conversion of pyruvate to lactate, which replenishes NAD^+ for glycolysis. In contrast, tissues, in which oxygen is not restricted, such as cardiac muscle and brain, use pyruvate for oxidative phosphorylation to produce ATP and predominantly express the H4 homotetramer. H4 is composed of four LDHB subunits and favors the reverse conversion of lactate to pyruvate, as LDHB has a higher affinity for lactate than for pyruvate. The heterotetramers LDH-2, LDH-3 and LDH-4 (Figure 12 A) are expressed in tissues with intermediate oxygen supply, such as kidney and spleen.
In the IMCD metabolomics analysis a trend indicating increased lactate secretion, along with reduced glucose uptake, suggests that AVP stimulation could stimulate lactate dehydrogenase activity. This potential activation of LDH was further examined.

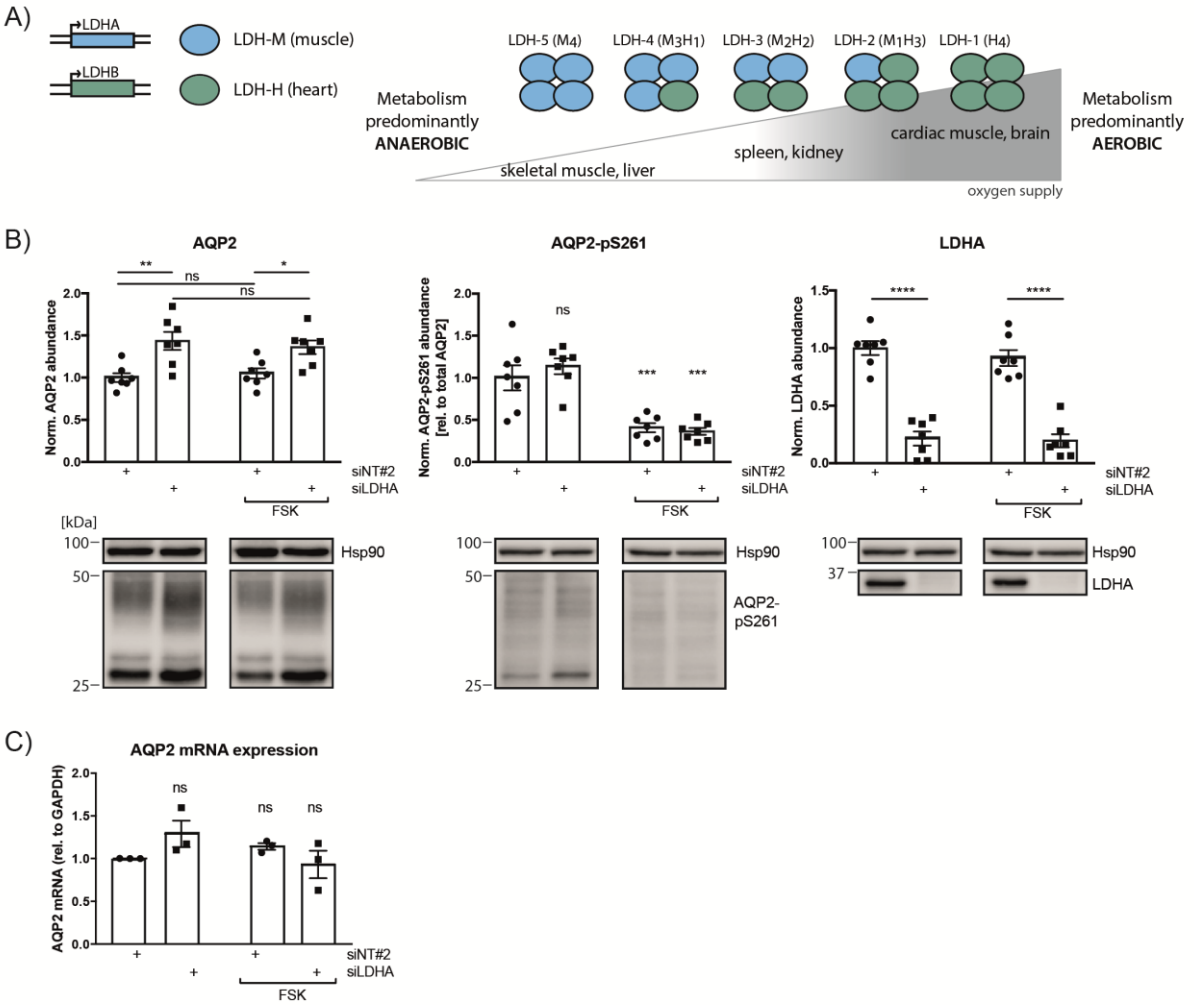

Figure 12: Knockdown of LDHA increases AQP2 protein abundance. A) Schematic representation of LDH isoforms and tissue-specific tetramer composition. B) Mouse collecting duct cells stably expressing human AQP2 (MCD4 cells) were transfected with siRNA against LDHA or a non-targeting control (NT#2) and protein abundance was quantified by densitometric analysis of Western blots. Left panel: Total AQP2 protein abundance increases upon knockdown of LDHA, independent of forskolin (FSK) stimulation. Middle panel: Phosphorylation of AQP2 at S261 is reduced upon FSK stimulation, but unaffected by LDHA knockdown. Right panel: LDHA siRNA efficiently reduces LDHA protein expression. n=7. C) Quantitative PCR of AQP2 mRNA relative to GAPDH. LDHA knockdown does not significantly change AQP2 expression on the transcriptional level. n=3. Mean +/- SEM is plotted. Statistically significant changes were determined using two-way ANOVA, followed by Tukey's multiple comparisons test (Unless indicated differently, untreated non-targeting control was used for reference). Statistics: * - p ≤0.05, ** - p ≤ 0.01, *** - p ≤ 0.001, **** - p ≤ 0.0001.

3.5.1 The role of lactate dehydrogenase in AQP2 translocation

An siRNA-mediated knockdown of LDHA was performed in MCD4 cells and its influence on AQP2 transport was investigated. The LDHA siRNA knockdown efficiently reduces LDHA protein abundance by an average of 80 % compared to a non-targeting control siRNA (NT#2, Figure 12 B). The reduction of LDHA significantly increases the total abundance of AQP2. On average, the LDHA knockdown increases AQP2 protein by 43 % under control conditions and by 30 % upon FSK stimulation. The decrease between control and FSK-stimulated LDHA-knockdown cells is, however, not significant. The increased AQP2 protein abundance is not due to elevated transcription, as AQP2 mRNA measured by quantitative PCR does not

significantly change (Figure 12 C). Transcriptional regulation of AQP2 is unlikely, as in MCD4 cells AQP2 is stably expressed under the control of a SV40 promoter. Thus, another mechanism must be underlying the increase in the AQP2 level that is observed following knockdown of LDHA. The protein abundance of AQP2 is regulated by short-chain-ubiquitination and poly-ubiquitination that target AQP2 for lysosomal or proteasomal degradation, respectively (Kamsteeg *et al.* 2006, Nedvetsky *et al.* 2010). Phosphorylation of AQP2-S261 is a marker for intracellular localization and diminishes upon FSK stimulation. As expected, FSK reduced p-S261 in MCD4 cells by an average of 60 % (Figure 12 B). Inhibition of p38-MAPK reduces p-S261 and increases AQP2 protein stability, indicating that p38-MAPK-mediated phosphorylation at S261 is a prerequisite for ubiquitination and proteasomal degradation (Nedvetsky *et al.* 2010). LDHA knockdown, however, does not influence p-S261 in MCD4 cells, indicating that the regulation of AQP2 protein stability by LDHA involves a different mechanism.

Next, the role of LDHA in AQP2 trafficking was investigated. Immunofluorescence microscopy of MCD4 cells shows that LDHA knockdown does not substantially change AQP2 trafficking (Figure 13 A). LDHA knockdown causes a tendency for decreased perinuclear localization, both under basal conditions as well as after FSK stimulation (Figure 13 A), which would indicate that LDHA is active in the intracellular retention of AQP2-bearing vesicles. As a second method to quantify AQP2 localization, surface biotinylation was performed (Figure 13 B). This assay does not work efficiently for the investigation of AQP2 trafficking in MCD4 cells. Plasma membrane insertion in this cell line is often not complete, meaning that the minor differences in the AQP2 redistribution, which are indicated in the results of the immunofluorescence microscopy experiments, cannot be assessed accurately. To overcome this problem, primary IMCD cells were instead used. However, as IMCD cells cannot be efficiently transfected with siRNA, an inhibitor of LDH, sodium oxamate (SO), was used to limit LDH activity. In an *in vitro* enzyme assay, 10 mM SO reduced LDH activity by about 90 % (Figure 14 C). FSK stimulation robustly induces AQP2 membrane localization, but LDH inhibition does not affect it. The induction of AQP2 membrane translocation that was observed in the LDHA knockdown experiments was not observed in the surface biotinylation experiments using the LDH inhibitor in IMCD cells. This might be due to the species difference between the cell models or indicate that the presence of LDHA protein, but not activity, is required for AQP2 regulation.

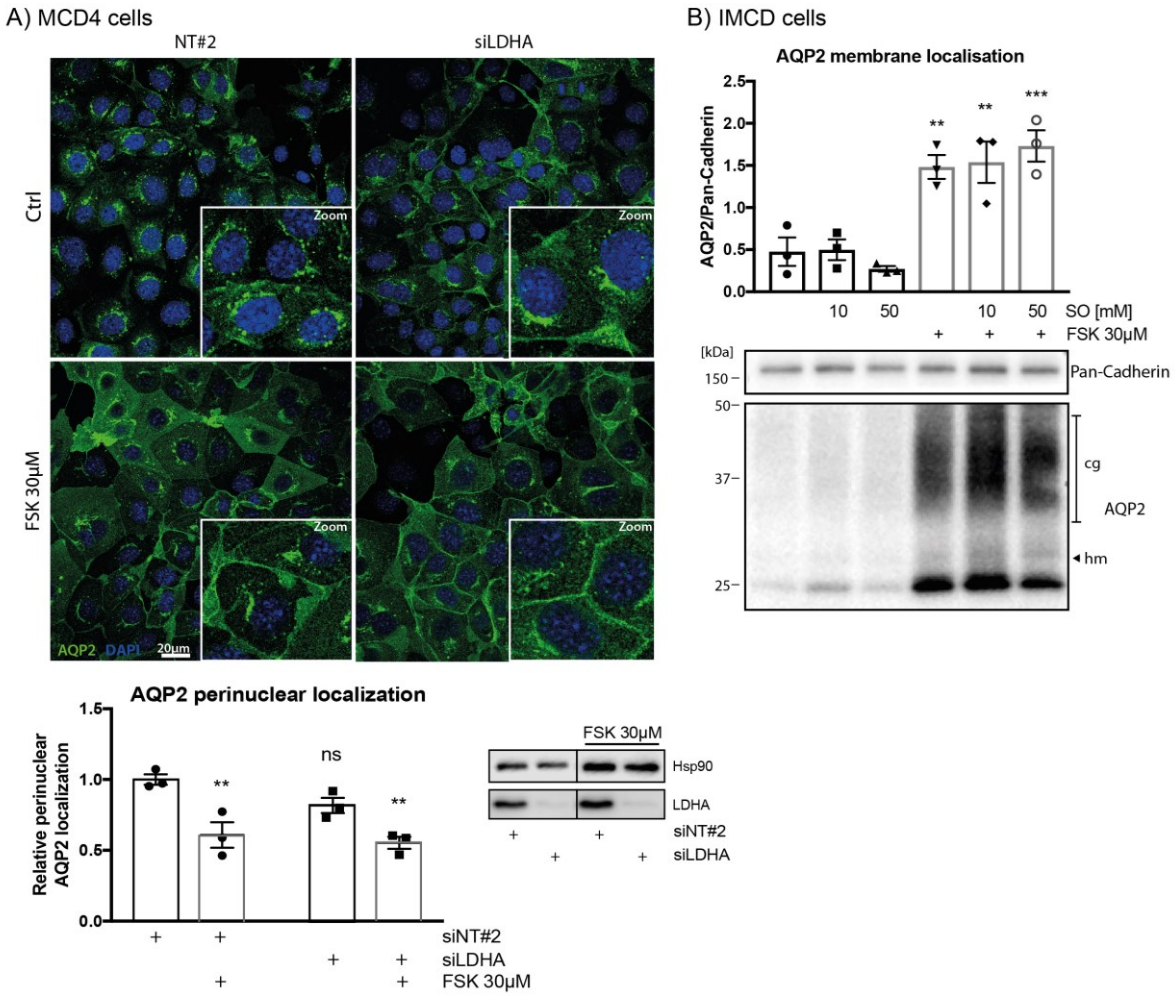

Figure 13: AQP2 trafficking potentially depends on LDHA protein abundance, but not activity. A) Assessment of AQP2 intracellular localization in MCD4 cells by immunofluorescence microscopy shows FSK-induced AQP2 translocation from perinuclear vesicles into the plasma membrane. Knockdown of LDHA, in comparison to the non-targeting control siRNA siNT#2, induces a non-significant trend towards increased plasma membrane localization of AQP2 even without FSK stimulation. B) LDH inhibition in primary IMCD cells does not significantly change AQP2 membrane abundance. IMCD cells were treated with the competitive LDH inhibitor sodium oxamate for 20 h at the given concentrations and plasma membrane localization was assayed by surface biotinylation. Mean +/- SEM is plotted. Statistically significant changes were determined using one-way (B) or two-way ANOVA (A), followed by Dunnett's multiple comparisons test (relative to untreated/non-targeting control). Statistics: * - p ≤0.05, ** - p ≤ 0.01, *** - p ≤ 0.001, **** - p ≤ 0.0001

3.5.2 The role of LDH as an AKAP

In a parallel search for potential new AKAPs, precipitation of PKA regulatory subunits from MCD4 cells and H9c2 cardiac myoblasts was performed using cAMP-agarose pulldown. For these assays, cAMP that is immobilized on agarose beads, is incubated with a cell or tissue lysate in order to precipitate PKA regulatory subunits and potentially co-precipitate AKAPs. As a negative control, free cAMP is added to the lysates to saturate the cAMP binding sites of the PKA regulatory subunits prior to the introduction of the cAMP-agarose beads.
Mass spectrometric analysis identified the co-precipitation of lactate dehydrogenase with R subunits from both cell lines. The results suggest that LDH might have a dual role in the cAMP/PKA/AKAP-dependent AQP2 translocation process and is therefore an interesting candidate, which may link cAMP signaling to metabolism.
In order to verify the results obtained by mass spectrometry, cAMP pulldowns were performed using various tissue and cell lysates. In all tested lysates, cAMP-agarose co-precipitates LDHA along with PKA regulatory subunits (Figure 14 A). LDH requires the cofactor NADH for activity, which is structurally similar to cAMP. Consequently, to rule out direct binding of LDH to cAMP, cAMP pulldowns were repeated with additional pre-saturation of the lysate with NADH and cGMP in concentrations ranging from 15 mM to 200 µM. The cyclic nucleotide cGMP was used to assess general binding to cyclic nucleotides. Binding of LDHA and LDHB to cAMP-agarose was completely abolished by pre-saturation with NADH in all concentrations used (Figure 14 B). As the binding of the regulatory subunits is not abolished by NADH pre-saturation, this indicates that LDH binds directly to cAMP through its NAD^+/H binding site and rejects the hypothesis that LDH acts as an AKAP. A similar binding pattern to that of LDH was observed for the NAD^+/H-dependent dehydrogenase GAPDH, but not for the $NADP^+$/H-dependent glucose-6-phosphate dehydrogenase (G6PDH).
Given that LDH is able to bind cAMP instead of NADH, this suggests that LDH activity could be competitively inhibited by cAMP. An enzyme activity assay using LDH that was purified from rabbit muscle (Figure 14 C, LDH-M/ LDH-5) or bovine heart (LDH-H/ LDH-1) was performed in the presence of cAMP or the pyruvate analog and LDH inhibitor SO, which was used as a positive control. However, significant inhibition of LDH activity occurred only with a cAMP concentration of 10 mM. The LDH enzyme that was purified from skeletal muscle was more sensitive to cAMP than that isolated from heart. The presence of 10 mM cAMP decreased its activity by approximately 40 %, compared to the control, whereas heart LDH only showed a reduction of 20 %. A potential explanation for this could be the presence of a greater proportion of LDHA subunits in skeletal muscle. Due to their higher affinity for pyruvate, LDHA subunits have an overall higher activity in this assay than do LDHB subunits, as the conversion of pyruvate to lactate and the accompanied reduction of NADH to NAD^+ was measured.

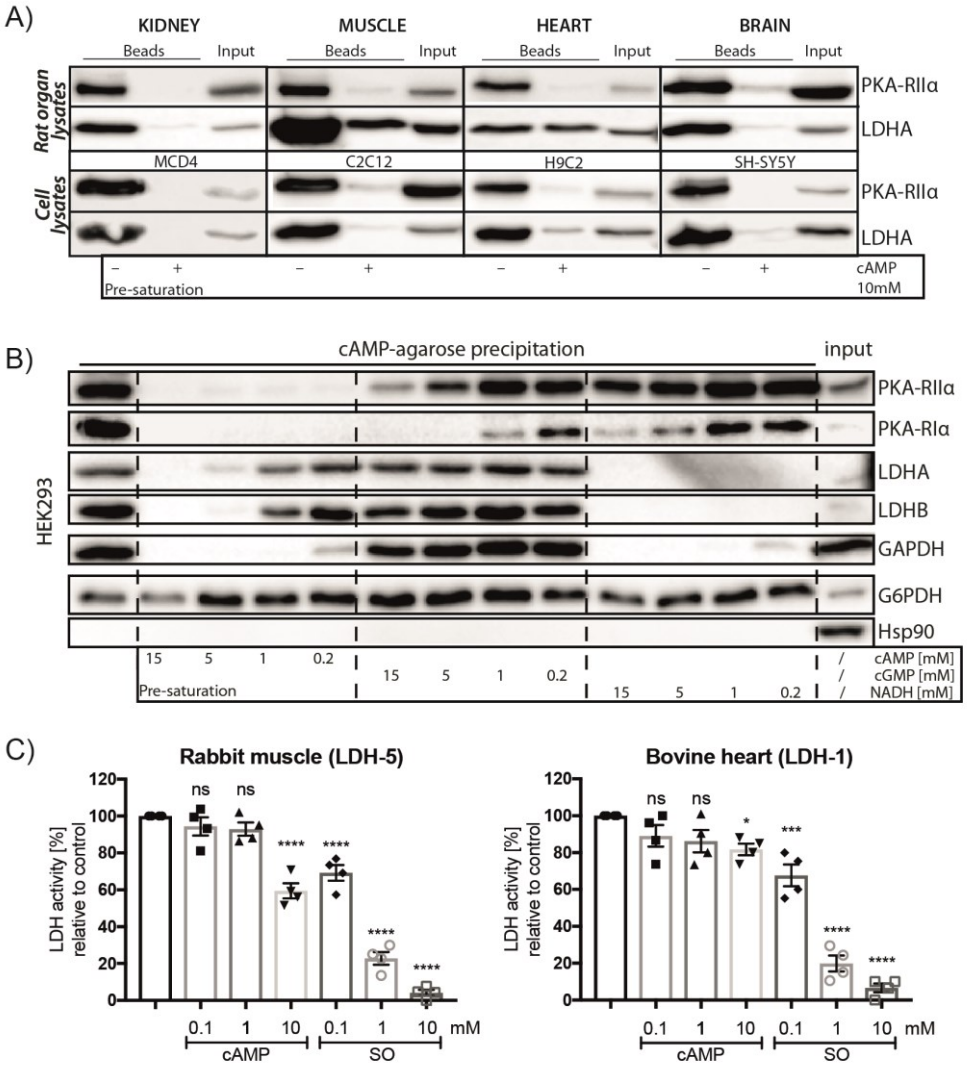

Figure 14: Lactate dehydrogenase (LDH) binds to cAMP, presumably through its NADH binding domain. A) LDHA in lysates from various cell types and organs co-precipitates with PKA-RIIα on cAMP-agarose beads. As negative control, lysates were pre-incubated with 10 mM free cAMP to saturate binding prior to loading of the cAMP-beads. B) LDHA and another NADH-dependent dehydrogenase, GAPDH, bind to cAMP-agarose beads, presumably through their NADH-binding region as pre-saturation with free NADH abolishes the binding more efficiently than cAMP. Binding of the NADPH-dependent G6PDH is not disrupted by any of the nucleotides used for pre-saturation. C) Activity of LDH purified from rabbit muscle (predominantly LDHA isoforms) and bovine heart (predominantly LDHB isoforms) was measured spectrometrically. LDH activity is decreased in the presence of high concentrations of cAMP. SO, a competitive inhibitor of LDH was used as a positive control. Shown are mean values of four independent experiments relative to untreated control. Error bars indicate SEM. Statistics: One-way ANOVA, followed by Dunnett's multiple comparisons test, * - p ≤0.05, *** - p ≤ 0.001, **** - p ≤ 0.0001.

The cAMP pulldown only indirectly shows the interaction between potential AKAPs and PKA regulatory subunits. Due to the ambiguity of the association introduced to the pulldown by the direct binding of LDH to the cAMP-agarose, another method was employed to investigate a potential interaction between LDH and PKA. Immunoprecipitation of PKA-RIIα was performed and co-precipitation of LDH was detected by Western blot. Both LDHA and LDHB co-precipitated with PKA-RIIα. The addition of cAMP to the lysate prior to immunoprecipitation (Figure 15 A) strengthened the interaction.

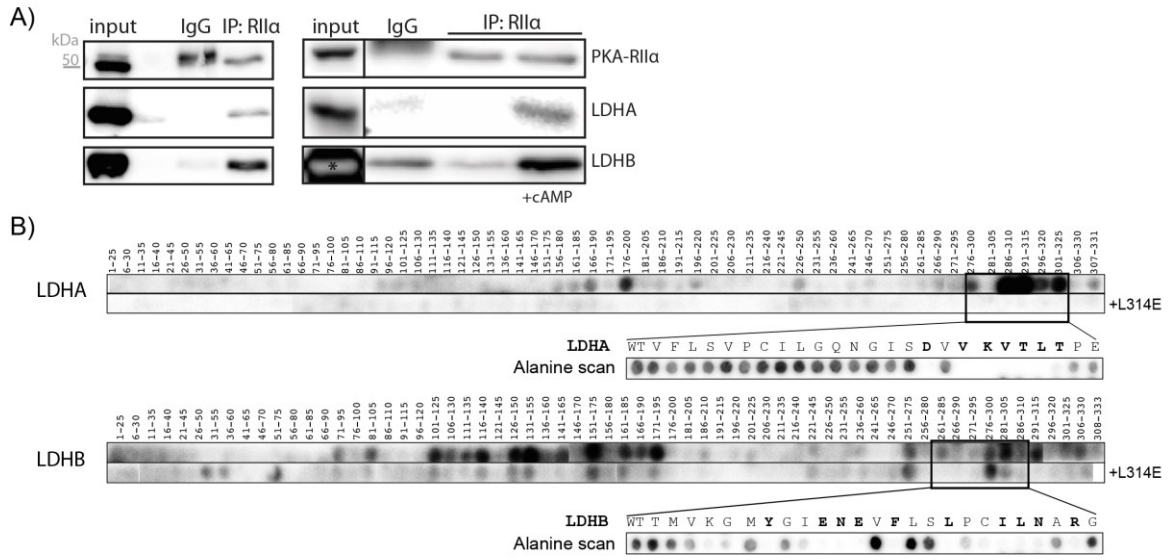

Figure 15: LDH interacts with the PKA regulatory subunit RIIα. A) LDHA and LDHB co-immunoprecipitate with RIIα from MCD4 cells, whereby the interaction is strengthened by addition of cAMP to the lysate prior to precipitation. The asterisk marks an oversaturated band signal. B) Overlay of purified RIIα over mouse LDHA and LDHB 25mer peptide spots identifies two interaction domains in the central and C-terminal part of the proteins. The AKAP18δ-derived peptide L314E interferes with AKAP-PKA interaction and is used as a negative control. Alanine scans, i.e. consecutive replacement of each amino acid by alanine, of the C-terminal interaction domain pinpoints amino acids crucial for the interaction.

The immune-detection of RIIα can overlap with the detection of heavy chains of the antibody used for immunoprecipitation. To circumvent this and develop a robust system to investigate LDH/RIIα interaction in various conditions, expression constructs of both proteins were generated (Appendix, Supplemental methods). RIIα was tagged with green fluorescent protein (GFP) to increase the size of the protein and allow Western blot detection without heavy chain interference. An LDHA expression construct was also created that included a FLAG-tag sequence. The constructs were co-transfected into HEK293 cells and reciprocal immunoprecipitation was performed (Appendix, Figure 29 A). However, due to nonspecific binding of the LDHA-FLAG to the GFP antibody used for immunoprecipitation, this system could not be used to study the LDHA/RIIα interaction. In addition, the co-expression vector pair RIIα-HA/LDHA-FLAG was tested, but again nonspecific co-precipitation of LDHA-FLAG was observed (Appendix, Figure 29 B).

Another option to analyze protein-protein-interactions and pinpoint interaction sites is the peptide spot technology, combined with the overlay of recombinant proteins. For this assay, the entire amino acid (aa) sequence of one of the interaction partners is spot-synthesized as overlapping 20 to 30mer peptides on a cellulose membrane. The spots are then incubated with the purified potential interaction protein. Mouse LDHA and LDHB (NCBI: LDHA NP_034829.1, LDHB NP_032518.1) were spot-synthesized as 25mer peptides with 5 aa

offset and overlaid with radioactively labeled recombinant RIIα. Binding of RIIα to the spots was detected by autoradiography, wherein the spot intensity correlates with the amount of protein bound to the spot. As negative control, the AKAP7-derived peptide L314E was used as a competitor for RIIα binding. Two RIIα binding sites were identified in both LDH isoforms. One of these was in the central portion of the protein and one was in the C terminus. The latter was the focus of further characterization, as this region showed similar binding to RIIα in LDHA and LDHB and is accessible for interaction in the folded protein (structures available for human proteins in RCSB protein database, LDHA: 4OKN and LDHB: 1I0Z). Each amino acid in the 25mer sequence was replaced by alanine to identify which amino acids are crucial for the interaction. This revealed that the LDHA amino acid sequence VKVTLT is necessary for interaction with PKA-RIIα, as replacement of any of these amino acids by alanine results in a diminished RIIα binding. For LDHB the RIIα interaction site is approximately 15 aa upstream of the LDHA-RIIα interaction site. Replacement of more than half of the amino acids abolishes binding of RIIα, but remains to be further characterized.
These peptide array experiments show that PKA-RIIα can directly interact with both LDHA and LDHB *in vitro*, indicating that LDH is a metabolic enzyme with putative AKAP function.

3.5.3 Some metabolic enzymes, but not LDHA, associate with AQP2-bearing vesicles

The aforementioned results showed that LDHA influences AQP2 abundance and presumably also plays a role in its translocation from intracellular vesicles into the plasma membrane. This is potentially due to its interaction with PKA. In order to investigate if LDHA exerts its function in AQP2 trafficking by direct association with AQP2-bearing vesicles, immuno-isolation of AQP2-vesicles from MCD4 cells was performed and LDHA co-localization analyzed by Western blot. However, LDHA could not be detected on AQP2-bearing vesicles in four independent experiments. A representative Western blot is shown in Figure 16 A. Other metabolic enzymes, GAPDH, G6PDH and pyruvate kinase (PKM, muscle isozyme) were found to co-precipitate with AQP2-bearing vesicles (Figure 16 C, D). The strongest and most reproducible binding was observed for G6PDH. Relative to AQP2, G6PDH association with the immune-isolated vesicles significantly increases upon FSK stimulation. Although GAPDH binding seems to be modulated by FSK stimulation as well, binding was observed in the IgG control. For quantification, the IgG control signal was subtracted from the signals of the AQP2-immuno-isolation. Negative values resulting from this normalization were excluded from further analysis (Figure 16 D).

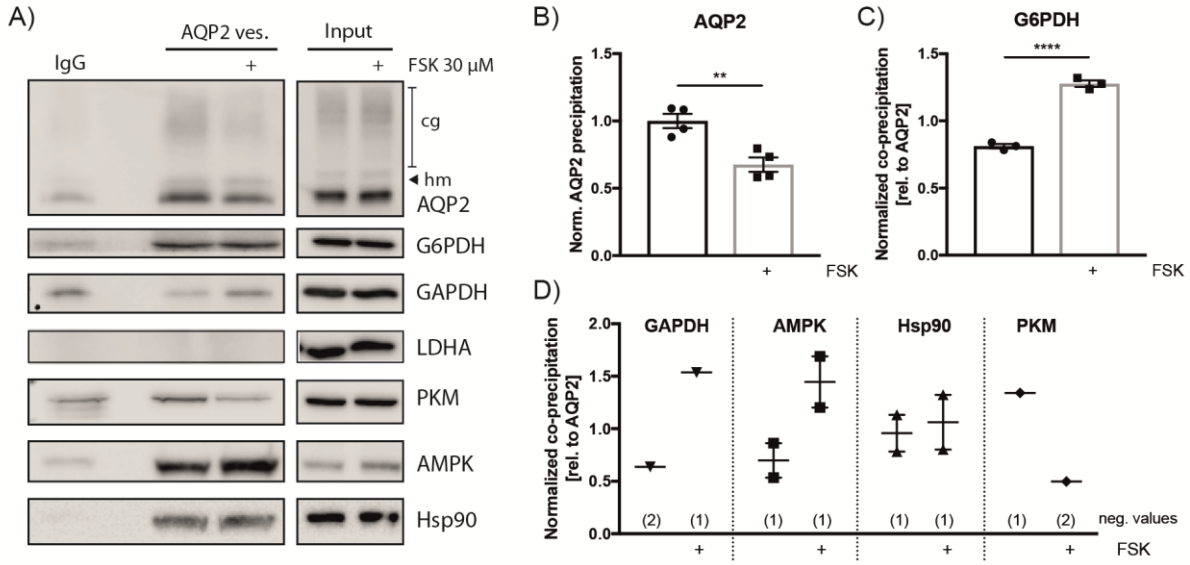

Figure 16: Metabolic enzymes co-precipitate with AQP2-bearing vesicles. A) Western blot detection of AQP2 from immuno-isolated AQP2-bearing vesicles of MCD4 cells show co-localization of the metabolic enzymes G6PDH, GAPDH and PKM, but not LDHA. The metabolic sensor AMPK was co-precipitating, as well as the chaperone Hsp90. Binding of GAPDH seems to be unspecific as it was detected stronger in the negative control (IgG). Shown are representative blots of four independent experiments. B) Quantification of AQP2 precipitation from four independent experiments shows a significant reduction of AQP2-bearing vesicles upon FSK stimulation. C) Quantification of G6PDH co-precipitation relative to AQP2 precipitation from three independent experiments. D) Quantification of co-precipitated proteins on AQP2-bearing vesicles from three independent experiments. Data points not shown had at least one negative value after subtraction of the IgG control signal and were excluded from the calculation. Bars represent mean values +/- SEM. Statistics: Unpaired t-test, ** - $p \leq 0.01$, **** - $p \leq 0.0001$.

The identification of PKM on the AQP2-bearing vesicles is of special interest, as the step of glycolysis catalyzed by PKM generates ATP and could directly fuel motor proteins for vesicle transport. Hinckelmann *et al.* (2016) showed that PKM and PGK co-localize with VAMP2-positive vesicles in neurons to provide an autonomous local ATP supply. However, PGK was not detected on AQP2-bearing vesicles in two independent experiments.

The key metabolic regulator AMPK was also found to co-precipitate with AQP2-bearing vesicles. As it acts antagonistically to PKA, AMPK association with AQP2 vesicles might favor its intracellular localization. Vesicle isolation suggests increased AMPK association upon FSK stimulation. It would be of interest, whether binding of AMPK to the AQP2-bearing vesicles is dependent on its activity. Phosphorylation of AMPK at T172 is a marker for its activation. The preliminary result from so far one experiment indicated reduced binding of p-AMPK resulting from FSK stimulation, which would be in line with the fact that PKA reduces this phosphorylation by introducing a competing phosphorylation at S173 (Djouder *et al.* 2010). Further experiments are needed to understand the role of AMPK in AQP2 vesicle transport.

In addition, the chaperone protein Hsp90 was identified on AQP2-bearing vesicles. Hsp90β was previously identified on AQP2-bearing vesicles (Barile *et al.* 2005), but only the association of Hsp70/Hsc70 with AQP2 was further evaluated. Hsp70 and Hsc70 were

shown to bind AQP2 directly, and this interaction was reduced upon S256 phosphorylation (Lu *et al.* 2007, Zwang *et al.* 2009). However, Hsp70 and Hsp90 act as co-chaperones for processes including steroid receptor maturation (Kimmins *et al.* 2000), and localization of Hsp90 to AQP2-bearing vesicles would be in line with this. Recently, Hsp70 was identified as a regulator of AQP2 abundance through ubiquitination by the E3-ligases CHIP and MDM2. Inhibition of Hsp90 induces an increase in Hsp70 abundance and a reduction of AQP2 in MCD4 cells (Centrone *et al.* 2017). Similarly, Donnelly *et al.* (2013) suggested opposing roles for Hsp70 and Hsp90, regulating proteasomal degradation and protein folding of the distal tubule NaCl cotransporter, respectively. PKA phosphorylates Hsp90 at Thr90, which reduces its interaction with Hsp70, whereas it increases binding of CHIP (Wang *et al.* 2012). This could indicate that AKAP-mediated PKA recruitment to AQP2 vesicles favors AQP2 protein stability by Hsp90 through reduced association with Hsp70. In light of this, Hsp70 recruitment to the AQP2-bearing vesicles under basal conditions and upon FSK stimulation should be further investigated.

3.6 Candidate 2: The vacuolar ATPase

The second candidate for AQP2 regulation in the context of metabolic control is the V-ATPase. In a high-throughput screening that was performed by a former PhD student of our group, 17 700 small molecules were analyzed for their influence on the AQP2 localization in renal principal cells. One of the hits was 4-acetyldiphyllin (4AD), an inhibitor of the V-ATPase. Treatment of MCD4 and primary IMCD cells with 4AD led to an accumulation of AQP2 in the perinuclear region and interfered with AVP/FSK-stimulated redistribution into the plasma membrane (Bogum *et al.* 2013). Acidification of vesicles is decreased upon 4AD treatment of IMCD cells, but the effect is milder than with the common V-ATPase inhibitor Bafilomycin A1 (BafA1). For diphyllin, a published V-ATPase inhibitor of related structure, an IC_{50} value of 17 nM was described, which is only minimally less effective than BafA1, which has an IC_{50} of 4 nM (Sorensen *et al.* 2007).

In IMCD cells, the AVP-induced phosphorylation of AQP2 at S256 was blunted by pre-treatment with 4AD, but overall PKA activity remained unchanged (Bogum *et al.* 2013). Thus, it was hypothesized that V-ATPase might act as an AKAP on AQP2-bearing vesicles, tethering PKA in proximity to its substrate AQP2-S256 and that this interaction is disrupted upon 4AD treatment. In a publication from our group, V-ATPase subunits were identified as hits in a screen for a common AKAP motif, but were neither validated nor characterized (Hundsrucker *et al.* 2010). As depicted in Figure 17 A, the V-ATPase holoenzyme comprises 12 subunits that form the transmembrane proton-gating domain v0 (a, c, d and e) and the ATP hydrolyzing cytosolic domain V1 (A, B, C, D, E, F, G and H).

Reversible dissociation of the V1 subunit controls the activity of the enzyme. This mechanism depends on the intracellular metabolic status, such that V-ATPase also serves as a metabolic sensor (see chapter 1.2.2, Figure 6). Thus, V-ATPase is a potential AKAP that could link cAMP signaling and metabolic control of the AQP2 localization.

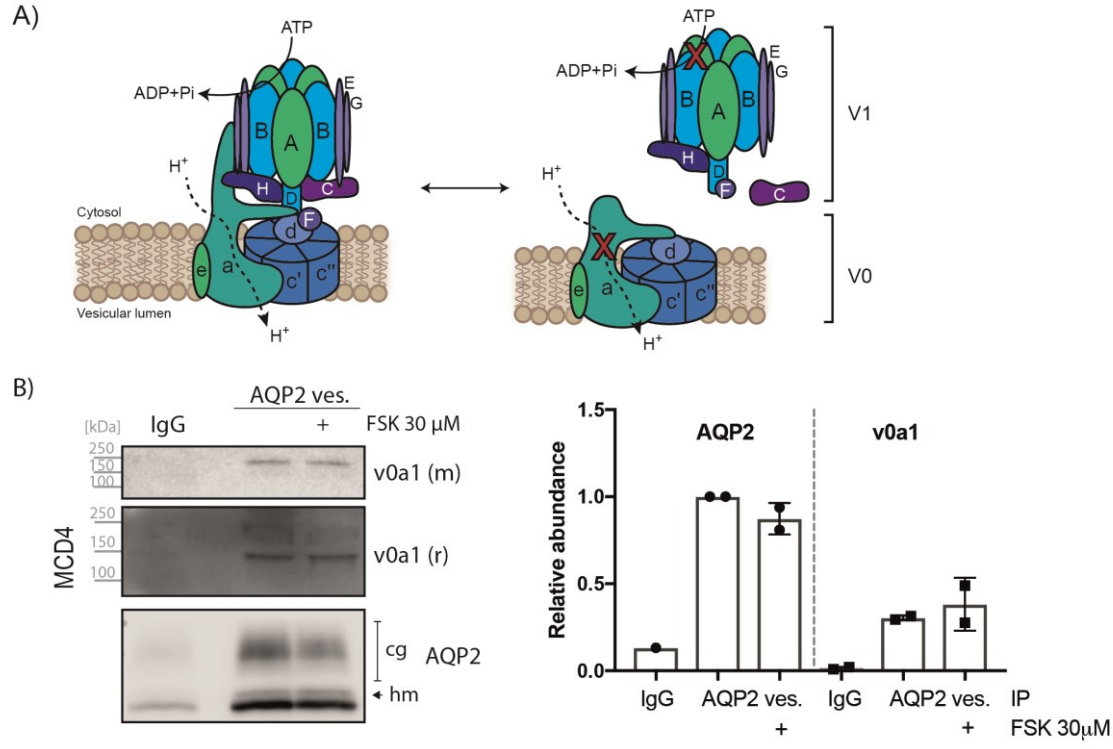

Figure 17: The V-ATPase subunit v0a1 associates with AQP2-bearing vesicles. A) V-ATPase activity can be controlled by regulated dissociation and re-association of the transmembrane domain v0 and the ATP-hydrolyzing subunit V1. The depicted structure is adapted from (Forgac 2007). B) Western blot detection with two different v0a1 antibodies, from mouse (m, #sc-374475) and rabbit (r, #ab105937) identifies co-precipitation of V-ATPase subunit v0a1 on immuno-isolated AQP2 vesicles in control conditions and upon stimulation with 30 µM FSK for 30 min. Right: Quantification of two independent experiments confirms repeated association of v0a1 with AQP2-bearing vesicles. Error bars indicate standard deviations.

3.6.1 V-ATPase v0a1 associates with AQP2-bearing vesicles

As the first step of the characterization of the V-ATPase in the regulation of the AQP2 redistribution, the association of V-ATPase subunits with AQP2-bearing vesicles was investigated. V-ATPase subunit v0a1 was detected on immune-isolated AQP2-bearing vesicles (Figure 17 B). V-ATPase v0a1 co-precipitation was similar or tended to increase upon FSK treatment, whereas the abundance of AQP2 vesicles in general is decreased in this condition. In relation to AQP2 this indicates increased v0a1 localization on AQP2-bearing vesicles upon cAMP elevation. Although further repetitions of the experiment are needed, the localization of V-ATPase on AQP2-bearing vesicles supports the hypothesis that V-ATPase is involved in the regulation of AQP2 translocation and might be an additional AKAP on these vesicles.

A variety of different antibodies against V-ATPase v0a subunits were tested, but did not return a band of consistent apparent site for V-ATPase following SDS-PAGE and Western blotting. As shown in Figure 17, V-ATPase v0a1 was often detected at around 200 kDa, although the size is expected to be 116 kDa (data sheet mouse v0a1 antibody, sc-374475) or 96 kDa (data sheet rabbit v0a1 antibody, #ab105937). Investigations of the subunit v0a isoform distribution in the mouse kidney showed that v0a1 and v0a4 bands were present at approximately 120 kDa (Schulz *et al.* 2007). Studies on the yeast V-ATPase a1 subunit (VPH1) confirm the size of around 120 kDa by Coomassie protein staining of purified protein (Benlekbir *et al.* 2012), despite a predicted protein mass of VPH1 of 95.5 kDa in the UniProt protein database (www.uniprot.org). The band of approximately 120 kDa, detected by the rabbit v0a1 antibody in Figure 17, was thus assumed to be specific. The higher band detected by the mouse anti-v0a1 might be a v0 domain complex containing v0a1 or due to the presence of another protein co-precipitating with the V-ATPase. In addition, V-ATPase v0a subunits can be glycosylated, which could explain the variability of bands with sizes of above 100 kDa (Kartner *et al.* 2013, Esmail *et al.* 2016).

3.6.2 Elucidating the molecular mechanism of 4AD in the control of AQP2 translocation

In the following section, the investigation of the molecular mechanism of 4AD in renal principal cells, in order to discover its inhibitory effect on AQP2 translocation, will be described.

3.6.2.1 The V-ATPase inhibitor 4AD favors v0/V1 subunit association

V-ATPase activity is regulated by dynamic association and dissociation of the major subunits v0 and V1 (Figure 17 A). Functional coupling of the ATPase domain to the transmembrane H^+-translocating domain requires the association of v0/V1. As the interaction between PKA and V-ATPase subunits could be solely taking place in one or the other conformation, the first step was to identify subunit association in response to 4AD treatment. Immunoprecipitation of the v0 subunits v0a1 and v0d1 was performed and the co-precipitation of V1A investigated (Figure 18 A). Surprisingly, inhibition with 4AD strongly favors v0/V1 association. Therefore, the inhibition of V-ATPase function by 4AD cannot be exerted by subunit dissociation.

Co-staining for RIIα indicates an interaction of PKA with the v0a1 and v0d1 subunits (Figure 18 A). Cross-reactivity with the heavy chains of the IP antibody, which can be detected at the same molecular weight as PKA-RIIα, might lead to false positive results.

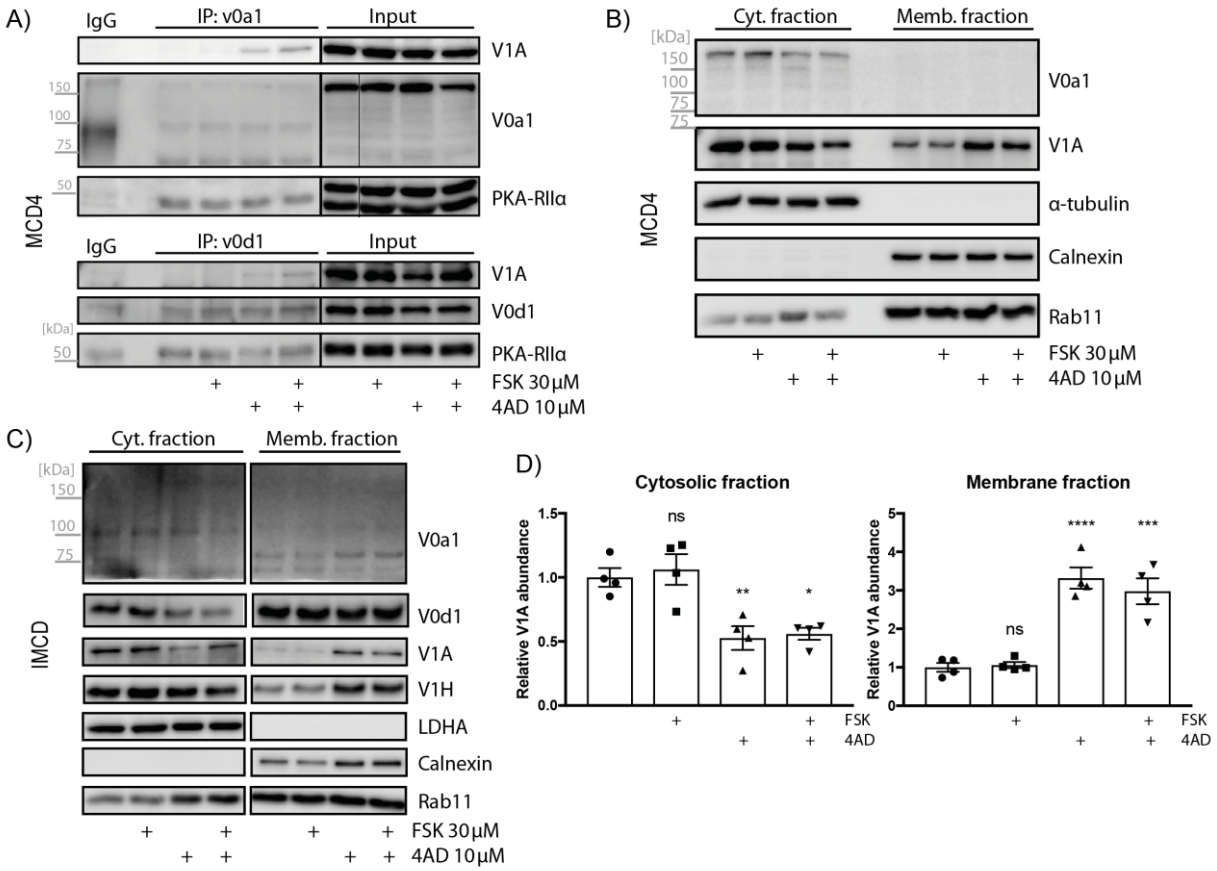

Figure 18: The V-ATPase inhibitor 4AD favors subunit association of the V-ATPase. A) MCD4 cells were treated with 10 µM 4AD for 45 min with and without FSK stimulation in the last 30 min of the incubation. Immunoprecipitation of v0a1 and v0d1 was performed from cell lysates. V-ATPase v0 subunits show increased co-precipitation of subunit V1A upon 4AD treatment, indicating that 4AD induces v0/V1 complex formation. Co-precipitation of PKA-RIIα was observed. In the top western blot image staining was done using a light-chain specific secondary antibody to avoid recognition of the 50 kDa heavy chain. MCD4 (B) and IMCD cells (C) were treated with 4AD (10 µM, 45 min) and FSK (30 µM, 30 min). Differential detergent fractionation separated cytosolic from membrane proteins as confirmed by the cytosolic markers α-tubulin and LDHA. The ER-associated protein Calnexin serves as a membrane marker. V1A detection shows a shift from the cytosolic pool towards the membrane-enriched fraction upon 4AD treatment of MCD4 (B) and IMCD (C) cells. V-ATPase subunit v0a1 detection was problematic in this experiment, but v0d1 detection shows strong and equal abundance of v0 in the membrane fraction (C). D) Quantification of four independent IMCD cell fractionation experiments with 4AD and/or FSK treatment. Error bars indicate SEM. Statistics: One-way ANOVA, followed by Dunnett's multiple comparisons test, * - $p \leq 0.05$, ** - $p \leq 0.01$, *** - $p \leq 0.001$, **** - $p \leq 0.0001$.

A light-chain specific secondary antibody was used for the detection of RIIα co-precipitation with v0a1 (Figure 18 A, top) to circumvent that problem. Co-precipitation with v0a1 appears convincing as the signal is enriched when compared to the IgG control.

4AD does not seem to have an effect on this interaction, which would be in line with the fact that the cytosolic part of v0a1 is accessible in both the disassembled as well as assembled state.

V-ATPase subunit assembly was also assessed by subcellular fractionation of MCD4 and IMCD cells. Cytosolic and membrane-enriched fractions were separated and analyzed by Western blot. The detection of V1A and V1H shifts from the cytosolic fraction to the membrane fraction upon 4AD treatment (Figure 18 B-D). The detection of v0 subunits was

again problematic. Staining for α-tubulin and LDHA as cytosolic markers and Calnexin as membrane marker, however, unequivocally prove the purity of the fractions. For IMCD cell samples, the detection of v0d1 confirms the unchanged predominant membrane localization of v0 subunits. Quantification of IMCD cell fractions (Figure 18 D) from four independent experiments shows a significant reduction of V1A from the cytosolic fraction, along with a significant increase in the amount of V1A found in the membrane-enriched fraction following treatment with 4AD and independent of FSK stimulation.

In order to confirm that the effect is not due to diminished vesicle acidification, the commonly used inhibitor of the V-ATPase, BafA1, was used as a negative control (Appendix, Figure 30). It was previously shown that salicylihalamide, but not BafA1 inhibits V-ATPase in the assembled state (Xie *et al.* 2004). Indeed, in contrast to 4AD, treatment of IMCD cells with BafA1 does not induce v0/V1 association (Figure 30). This suggests that 4AD has an inhibitory mechanism distinct from that of BafA1, but potentially similar to that of salicylihalamide.

3.6.2.2 Treatment of MCD4 and IMCD cells with 4AD increases LC3 lipidation

Bogum *et al.* (2013) showed that phosphorylation of AQP2 at S261 and S269 was unchanged upon 4AD treatment. The expected increase in p-S256 upon FSK stimulation was not observed when IMCD cells were pre-treated with 0.4 and 4 μM 4AD for 30 min. Application of 10 μM 4AD for 45 min, which are the parameters used in the experiments described within this thesis, also did not significantly change the phosphorylation of AQP2-S261 in MCD4 and IMCD cells (Figure 19). As the available antibodies that were tested did not detect the expected increase in p-S256 upon FSK stimulation of MCD4 cells, the phosphorylation of S256 could not be investigated in this thesis.

AMPK activation by phosphorylation at T172 was shown to interfere with AQP2 translocation in renal principal cells (Al-Bataineh *et al.* 2016). Therefore, one could hypothesize that 4AD-mediated activation of AMPK antagonizes PKA-induced plasma membrane localization of AQP2, which would explain the observed translocation defect. In addition, AMPK was identified on AQP2-bearing vesicles, suggesting that is plays a regulatory role in AQP2 trafficking. However, no change in AMPK-pT172 could be observed in MCD4 or IMCD cells. Total levels of AMPK tended to increase in IMCD cells treated with 4AD, but more repetitions would be needed to support this finding.

Another aspect not yet investigated is the reduced acidification of subcellular compartments upon inhibition of V-ATPase by 4AD. Acidification of endosomes and lysosomes depends on V-ATPase activity. Inhibition of V-ATPase blocks the lysosomal degradative pathway at the stage of early endosomes (Hurtado-Lorenzo *et al.* 2006). It was also shown that the V-ATPase inhibitors BafA1 and concanamycin interfere with autophagic flux, which leads to an

accumulation of the autophagy marker lipidated microtubule-associated proteins 1A/1B light chain 3B (MAP1LC3B) or in short LC3-II (Florey *et al.* 2015, Meo-Evoli *et al.* 2015).

In order to investigate whether 4AD exerts a similar effect to these inhibitors, MCD4 and IMCD lysates were analyzed for LC3 lipidation, as indicated by a shift in molecular weight from 16 kDa (LC3-I) to 14 kDa (LC3-II). A robust increase of LC3-II relative to LC3-I was observed in both cell types (Figure 19).

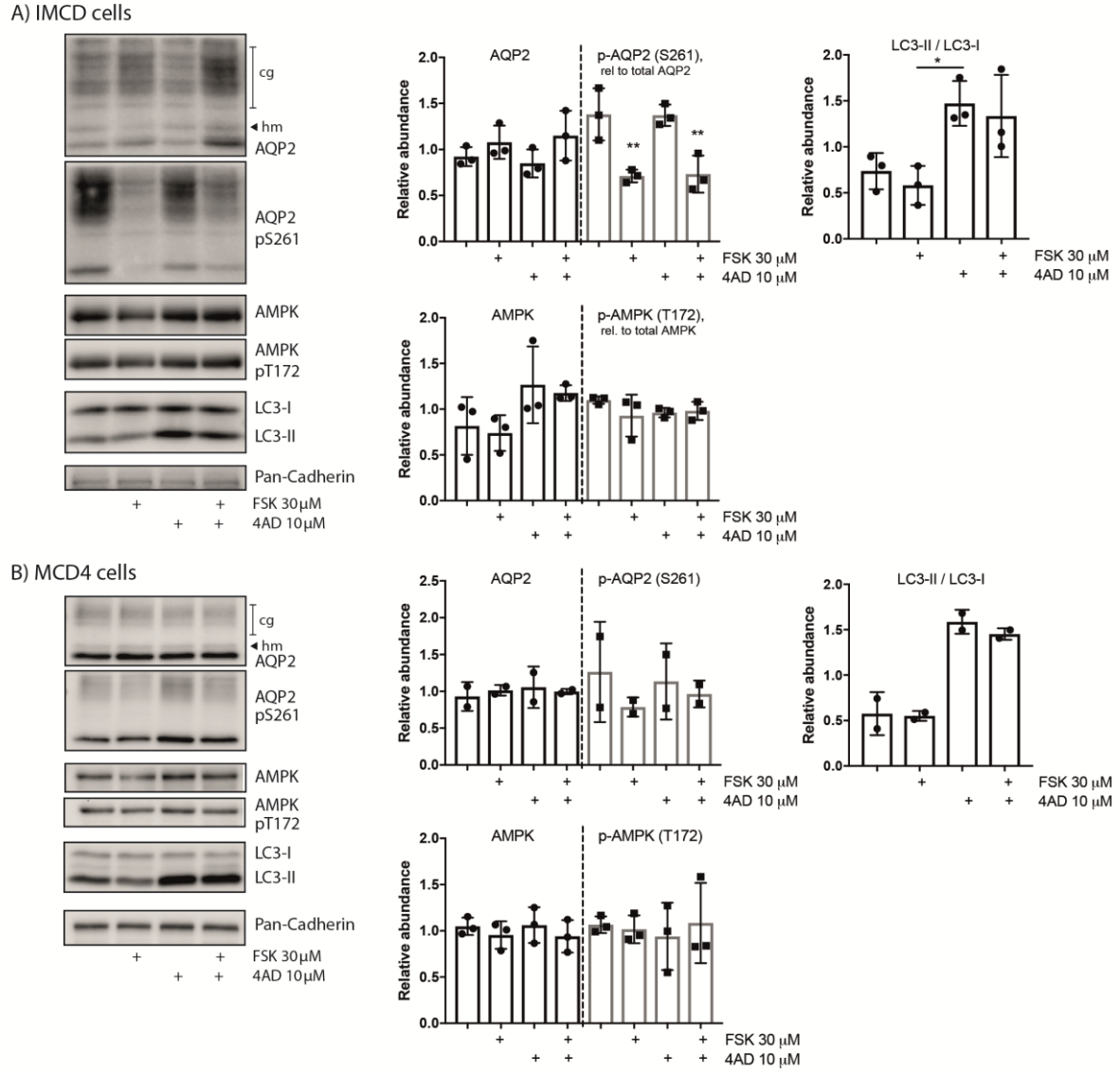

Figure 19: Treatment of IMCD and MCD4 cells with 4AD does not affect the phosphorylation of AMPK-T172 and AQP2-S261. IMCD (A) and MCD4 (B) cells were treated with 30 µM FSK for 30 min, 4AD 10 µM for 45 min or a combination of both and cell lysates were analyzed by Western blot. A) FSK stimulation increases basal levels of AQP2 in IMCD cells and significantly reduces its phosphorylation at S261, whereas 4AD does not affect it. Total levels of AMPK, but not its activating phosphorylation at T172 tend to change upon 4AD treatment. The ratio of LC3-II to LC3-I represents LC3 lipidation during autophagy. 4AD treatment leads to an accumulation of LC3-II. Shown are representative blots of one out of three independent experiments. B) FSK and 4AD do not affect total AQP2 abundance in MCD4 cells. AQP2 phosphorylation at S261 is not reduced upon FSK stimulation of MCD4 cells in one out of two experiments, but combined treatment with 4AD and FSK induces the expected decrease. Total AMPK abundance and phosphorylation at T172 remain unchanged. 4AD induces accumulation of LC3-II. Shown are representative blots of one out of two independent experiments. For the evaluation of AMPK abundance three independent experiments were quantified. Error bars indicate standard deviations. Statistics: One-way ANOVA, followed by Tukey's multiple comparisons test, * - $p \leq 0.05$, ** - $p \leq 0.01$.

3.6.2.3 Treatment of MCD4 cells with 4AD provokes AQP2 translocation into the plasma membrane prior to its accumulation in perinuclear aggregates

AQP2 translocation is a dynamic equilibrium between exocytosis-like plasma membrane insertion and endocytosis-like retrieval. As V-ATPase inhibition affects endocytic processes, AQP2 localization at different time points of 4AD treatment with and without FSK stimulation was observed in MCD4 cells. Although Hurtado-Lorenzo *et al.* (2006) showed that V-ATPase inhibition by BafA1 treatment did not affect recycling through Rab11-positive compartments, which is the recycling pathway that AQP2 undergoes after retrieval from the plasma membrane, AQP2 accumulated in condensed perinuclear areas upon V-ATPase inhibition with 4AD (Bogum *et al.* (2013) and Figure 20 C). Co-staining with a marker for the ER-Golgi intermediate compartment (ERGIC), ERGIC-53, showed increased co-localization of AQP2 with the ERGIC compartment with increasing incubation times with 4AD (Figure 20 C and E). FSK induces AQP2 translocation into the plasma membrane (Figure 20 B), which is in line with decreased ERGIC co-localization (Figure 20 E). The ratio of ERGIC-53 co-localization to all non-ERGIC-53 compartments defines the vesicular fraction of AQP2, and accordingly decreases following FSK stimulation (Figure 20 F). It is also of note that short-term incubation with 4AD reduces the vesicular pool of AQP2. The effect appears even stronger than the FSK stimulation, as 2 min of 4AD treatment results in a reduction of perinuclear AQP2 that is comparable to 10 min of FSK stimulation. By 30 min after application of 4AD, the amount of vesicular AQP2 returns to basal levels, which is consistent with the observations made by Bogum *et al.* (2013). Therefore, 4AD does not generally inhibit AQP2 translocation, but instead may induce it.

The perinuclear accumulation of AQP2 was also observed when cells were first incubated with 4AD, followed by the addition of FSK to induce the translocation. Stimulation with 4AD for 30 min and FSK for 10 min seems to even augment the appearance of bright condensed AQP2 aggregates observed by fluorescence microscopy when compared to 4AD treatment alone (Figure 20 D). This supports the hypothesis that AQP2 shuttles normally to the plasma membrane in the presence of 4AD, which instead blocks the recycling of AQP2 to its basal perinuclear position. Strong membrane localization of AQP2 after 45 min 4AD and 30 min FSK treatment, that is even more defined than that of FSK stimulation alone, suggests membrane accumulation of a sub-pool of AQP2. A reason for that might be the saturation of endosomal pools due to blockage of the recycling pathway that slows down endocytic retrieval of AQP2 from the plasma membrane.

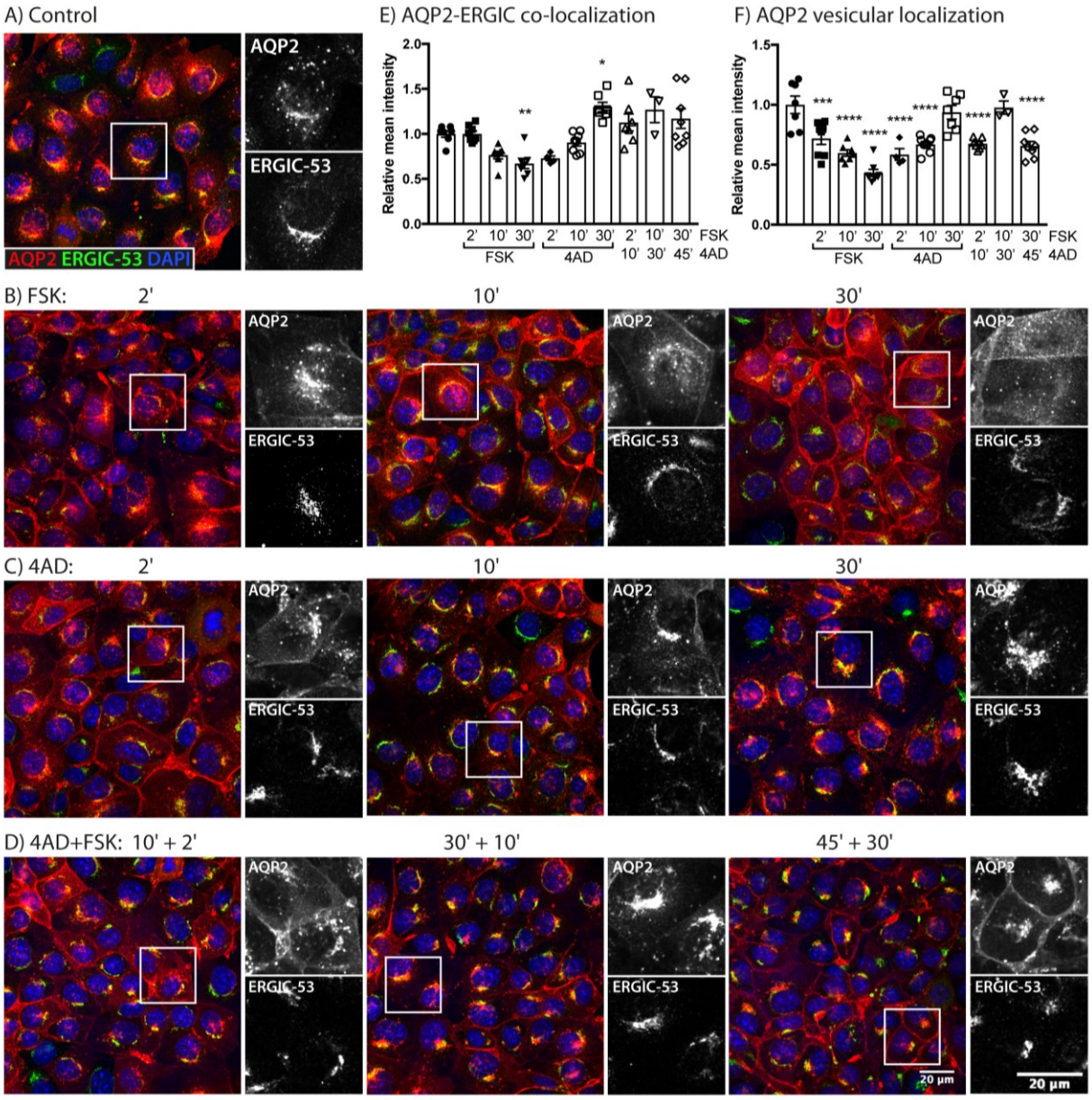

Figure 20: 4AD induces AQP2 translocation into the plasma membrane prior to its accumulation in ERGIC-positive compartments. MCD4 cells were left untreated (A) or stimulated with 30 µM FSK (B) or 10 µM 4AD (C) for 2, 10 and 30 min or treated with 10 µM 4AD for 10, 30 and 45 min followed by FSK stimulation for 2, 10 or 30 min (D). FSK induces the translocation of AQP2 (green) from perinuclear (nuclei blue, DAPI) vesicles into the plasma membrane. Treatment with 4AD leads to AQP2 accumulation in ERGIC (ER-Golgi intermediate compartment, purple)- positive perinuclear clusters starting from 10 min. Short-term 4AD exposure, however, induces AQP2 re-distribution comparable to cells treated with FSK for 10 min. E) Quantitative analysis of AQP2-ERGIC-53 co-localization was observed by immunofluorescence microscopy. Shown are the mean intensities of three to seven images, each showing at least 20 cells that were analyzed with ImageJ, relative to untreated control cells. F) Quantitative analysis of AQP2 localization. The ratio of AQP2 co-localizing with ERGIC-53 to the inverted non-ERGIC pool expresses the proportion of AQP2 located on intracellular vesicles and reduces to its minimum after 30 min of FSK stimulation. Analyzed cell numbers as in E, shown are values relative to the untreated control. Error bars indicate SEM. Statistics: One-way ANOVA, followed by Dunnett's multiple comparisons (relative to untreated control), * - $p \leq 0.05$, ** - $p \leq 0.01$, *** - $p \leq 0.001$, **** - $p \leq 0.0001$

In summary, 4AD inhibits V-ATPase in its assembled state and it presumably has a dual effect on AQP2 trafficking. Short-term 4AD treatment induces translocation of AQP2 from intracellular vesicles into the plasma membrane, whereas longer incubation leads to an accumulation of AQP2 in perinuclear clusters overlapping with the ERGIC.
In addition, preliminary results suggest a role for 4AD in the regulation of the microtubular network (Appendix, Figure 31). Interference with vesicle acidification by 4AD or BafA1 increases the cytosolic pool of α-tubulin, which might be caused by microtubule depolymerization. However, extraction of polymerized tubulin did not show any difference compared to the untreated control (Appendix, Figure 31 B), so that further investigations are needed to unravel the molecular effect of 4AD.

3.6.3 The role of V-ATPase as an AKAP

The immunoprecipitation experiment shown in Figure 18 A indicates complex formation of v0a1 with PKA-RIIα. As a result, the potential AKAP function of v0a1 was investigated using cAMP pulldowns. Figure 21 A confirms co-precipitation of v0a1 with RIIα from rat heart and brain, but not from rat kidney lysate. The observation of precipitation from brain tissue was not further investigated as it falls outside of the cardiovascular focus of this thesis. V-ATPase v0a1 from mouse heart and kidney tissue co-precipitated with PKA-R subunits on cAMP-agarose (Figure 21 B). The discrepancy between rat and mouse kidney tissue might be due to differences in antibody specificity or v0a isoform expression in rat compared to mouse.
Next, the effect of 4AD on V-ATPase subunit interaction with PKA-RIIα was examined. As expected, pre-incubation of mouse kidney tissue with the cell-permeable cAMP analogue dbcAMP (500 μM, 30 min) reduced the binding of PKA-RIIα to cAMP-agarose beads (Figure 21 C). 4AD had no effect on the cAMP-agarose binding of RIIα, v0a1 or V1H. Pre-incubation with 5 mM cAMP only mildly reduced the association of V1H with the cAMP-agarose, which could indicate nonspecific binding. However, binding of V1H was reduced to a comparable extent by dbcAMP pre-incubation, as observed for RIIα. The similar binding pattern of V-ATPase subunits v0a1 and V1H compared to RIIα suggests an interaction with PKA.

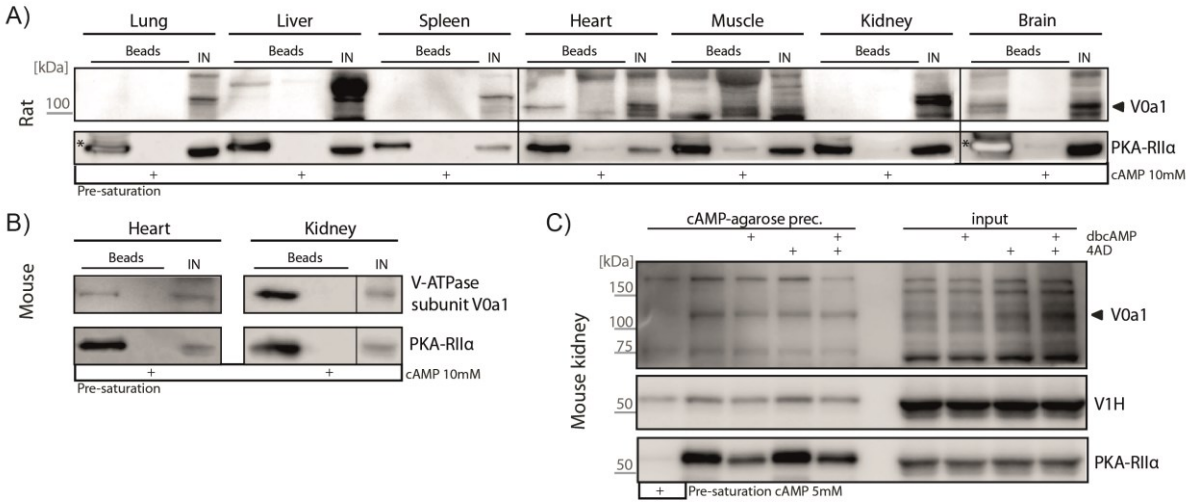

Figure 21: V-ATPase subunits v0a1 and V1H co-precipitate with RIIα and this is independent of 4AD treatment. Precipitation of PKA regulatory subunits with cAMP-agarose identifies potential AKAPs by co-precipitation. Pre-incubation of the lysates with high concentrations of cAMP saturates cAMP binding sites and serves as a negative control. A) Co-precipitation of v0a1 was investigated in seven different rat organ lysates. V0a1 binding was detected from heart and brain samples. Asterisks mark oversaturated band signals. B) Co-precipitation of v0a1 and RIIα on cAMP-agarose from mouse heart and kidney lysates. C) Pre-incubation of mouse kidney slices with 500 μM dbcAMP for 30 min reduces binding of RIIα to cAMP-agarose and accordingly also v0a1 and V1H co-precipitation. Treatment with 10 μM 4AD alone for 45 min or in combination with dbcAMP does not change RIIα, v0a1 or V1H binding.

As described before for LDHA (see 3.5.2), cAMP-agarose pulldowns might yield false positives, so that controls additional to cAMP saturation should be considered. As V-ATPase is an ATP-binding enzyme, in this case ATP was used as additional negative control. Pre-saturation with 1 mM cAMP reduced the co-precipitation of rat heart v0a1 and V1H on cAMP-agarose (Figure 22 A). In comparison to the completely abolished binding with 10 mM cAMP in the pulldown shown in Figure 21 A and B, this already hints at RIIα-independent binding of v0a1 and V1H to the cAMP-agarose. The assumption is supported by the finding that RIIα-binding is almost completely abolished by pre-incubation with 1 mM cAMP. Binding of the V-ATPase subunits is much stronger reduced by pre-incubation with 1 mM ATP, whereas this has only a minor effect on RIIα. NADH pre-incubation and LDHA Western blot detection was used as additional control. NADH does not have an influence on V-ATPase subunit binding. Similar results were obtained with mouse inner medulla samples (Figure 22 B). In the subsets of cAMP and ATP pre-saturated samples, binding of RIIα to the cAMP-agarose is significantly different from binding of the V-ATPase subunits (Figure 22 C). Pre-saturation with ATP leads to a statistically significant reduction of V-ATPase subunit binding.

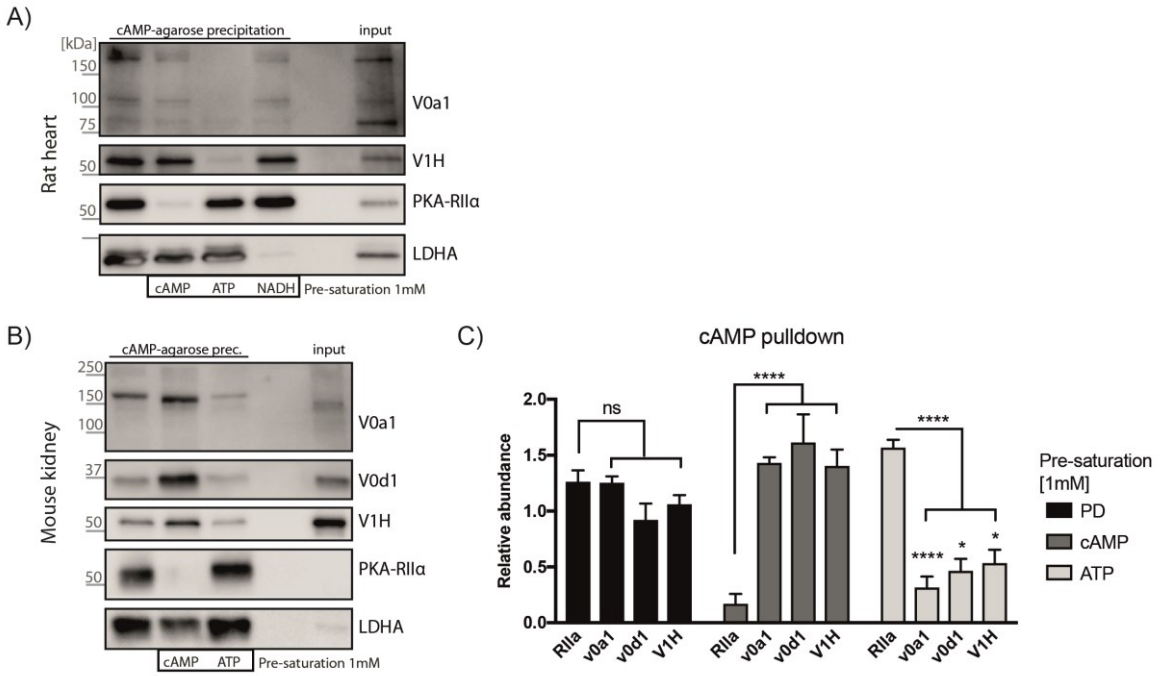

Figure 22: Interaction of V-ATPase subunits with cAMP-agarose is disrupted by ATP pre-saturation. Lysates from rat heart (A) and mouse kidney (B) were pre-incubated with different nucleotides to saturate binding sites. V-ATPase subunit binding to cAMP-agarose is reduced after pre-incubation with cAMP and ATP. Binding of V-ATPase subunits to cAMP-agarose presumably does not occur through PKA-RIIα, as RIIα-binding is only mildly affected by ATP, but almost absent with cAMP. LDHA was used as control for NADH pre-incubation. The seemingly increased binding of V-ATPase subunits upon cAMP pre-saturation (B) is only due to unequal sample loading. C) Quantification of cAMP-pulldown results from three independent experiments performed with mouse kidney lysates. Error bars indicate SEM. Statistics: Two-way ANOVA, followed by Tukey's multiple comparisons test, * - $p \leq 0.05$, ** - $p \leq 0.01$, *** - $p \leq 0.001$, **** - $p \leq 0.0001$

In summary, the V-ATPase subunits v0a1, v0d1 and V1H were identified to bind cAMP-agarose and this interaction is reduced by pre-saturation with ATP. The interaction with cAMP-agarose seems to be direct and not through PKA regulatory subunits. However, due to the control results, this assay is not suitable to evaluate the direct interaction between V-ATPase and PKA-R subunits. In order to analyze the interaction with another method, V-ATPase v0a subunits were spot-synthesized and overlaid with recombinant RIIα (Figure 23). This also allows a comparison between the v0a subunit isoforms a1 to a4. The antibodies used for Western blot detection cannot unequivocally distinguish between all isoforms. Only the cytosolic parts (aa1-397) of the v0a isoforms were spot-synthesized as this region is accessible for interaction partners. The peptides were synthesized both in the normal composition as well as with cysteines exchanged for serines (C>S). This was done to avoid false positive results due to disulfide bonds between the peptides. Binding to the original sequence and the C>S exchanged sequence indicates a true binding event. As described above, the peptide L314E was used as a negative control. For all four isoforms, a binding site for RIIα was identified in the N-terminus between aa 26 and aa 70. However, binding to v0a4 was not reduced upon L314E competition. This either indicates an interaction through an RIIα domain other than the D/D domain or unspecific binding. For v0a4 also the

C>S exchange shows a diminished binding. This is surprising, as the respective spots do not contain cysteines. However, binding intensities may vary throughout the membrane and also between different membranes, so that they are difficult to compare. The finding that there are still faint spots observable, suggests that only the overall signal of the C>S exchanged spots is reduced, but binding still occurs. For v0a1 and a3, reproducible interaction with RIIα was observed. Figure 23 B shows the quantitative analysis of the N-terminal region between aa 16 and aa 75, here indicated as spots #1-8, of v0a1 and v0a3 from four and three independent experiments, respectively. Binding to v0a3 is strongly reduced at spot 4 with a binding intensity not significantly different from the non-binding control spot 1. This is unexpected as the sequence of this spot is only five amino acids different to that of spot 3 and spot 5. Apparently, the sequences flanking spot 4 are crucial for the interaction, potentially conferring the correct folding necessary for RIIα binding.

In summary, the results indicate that V-ATPase v0a subunits can directly interact with PKA-RIIα. The disrupted binding of RIIα to spot 4 of v0a3 indicates amino acids crucial for the interaction. This should be further investigated, e.g. by performing alanine scans.

These results, together with the co-immunoprecipitation of v0a1 with PKA-RIIα indicate that V-ATPase and PKA interact. The interaction seems to be independent of 4AD. The 4AD-induced assembly of the V-ATPase, however, might change the association of other interaction partners and potential PKA substrates with the complex and this might play a role in AQP2 translocation.

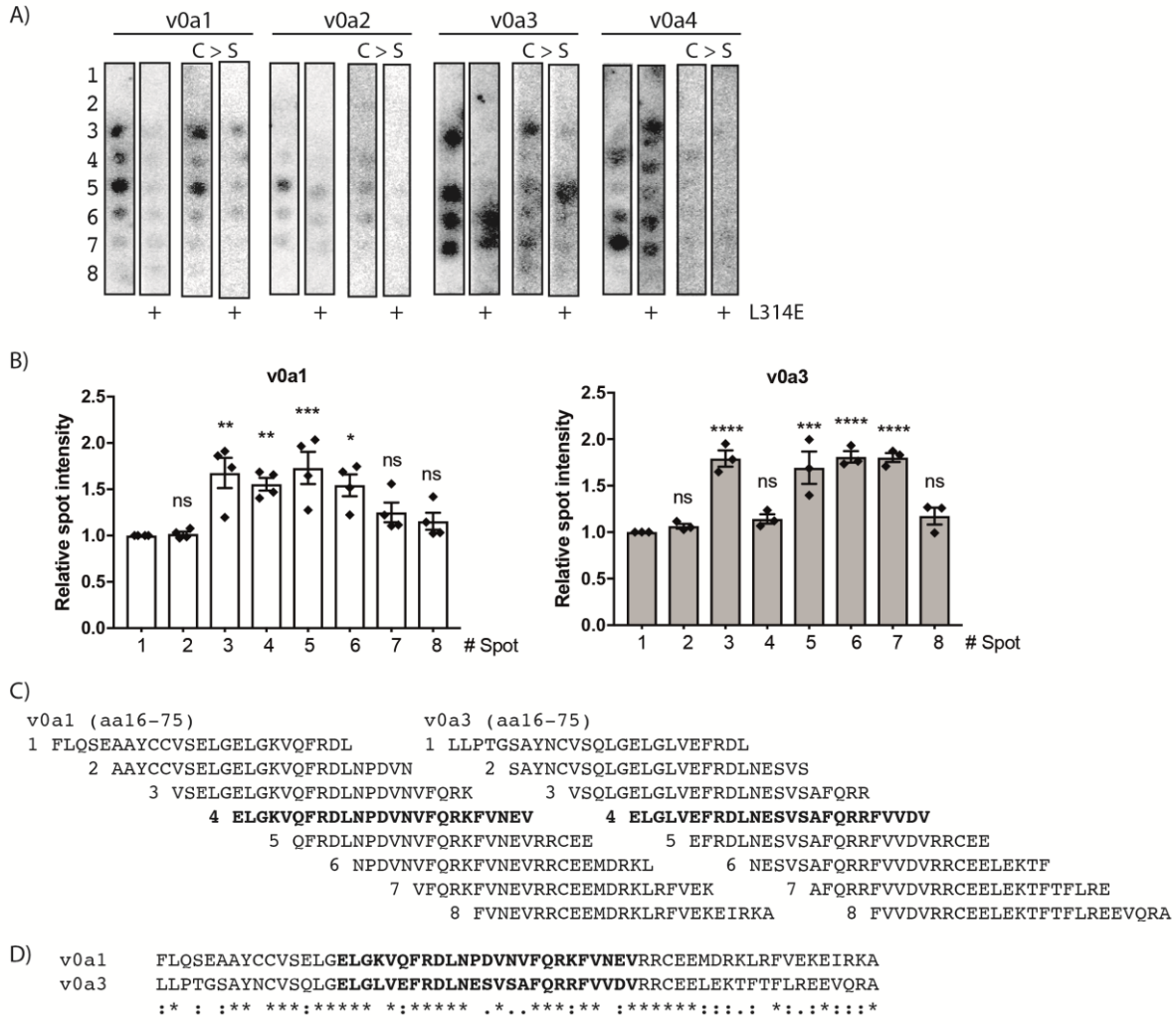

Figure 23: V-ATPase v0a1/2/3/4 subunits have a common PKA-RIIα interaction site. A) Spot-synthesized 25mer peptides of v0a isoforms were overlaid with recombinant RIIα. Spot intensity, as detected by phosphoimaging, is proportional to RIIα binding. As control for false positive signals due to disulfide bridges, sequences were spotted with cysteines exchanged for serines (C>S). L314E is a AKAP7-derived peptide disruptor of AKAP-PKA interactions, here used as a negative control. B) Semi-quantitative analysis of v0a1 and v0a3 spots of amino acids 16 to 75. Results are shown for spots of four (v0a1) and three (v0a3) independent experiments. Error bars indicate SEM. Statistics: One-way ANOVA, followed by Dunnett's multiple comparisons (relative to spot 1), * - $p \leq 0.05$, ** - $p \leq 0.01$, *** - $p \leq 0.001$, **** - $p \leq 0.0001$ C) Amino acid sequences corresponding to the shown v0a1 and v0a3 spots. D) Sequence alignment of v0a1/a3 isoforms conducted with the ClustalW online tool (http://www.genome.jp/tools-bin/clustalw). Asterisks indicate identical amino acids, colons amino acids with very similar properties and a period amino acids of less similar properties.

3.7 Identification of AKAP anchor points defines the AKAP-PKA interaction site

Parts of the results shown in this chapter of the thesis were published in: Götz, F., Y. Roske, M. S. Schulz, K. Autenrieth, D. Bertinetti, K. Faelber, K. Zuhlke, A. Kreuchwig, E. J. Kennedy, G. Krause, O. Daumke, F. W. Herberg, U. Heinemann and E. Klussmann (2016). "AKAP18:PKA-RIIalpha structure reveals crucial anchor points for recognition of regulatory subunits of PKA." Biochem J 473(13): 1881-1894.

The correct localization of AQP2 in renal principal cells relies on the regulation of PKA activity by AKAPs. The interaction between AKAPs and PKA is conveyed by a conserved amphipathic helix formed by the AKAP and the X-type helix bundle of dimerized PKA regulatory subunits that forms the hydrophobic binding cavity. AKAPs can be divided into three subclasses according to their R-binding characteristics: RI-specific, RII-specific and dual specific AKAPs. The general structure of the AKAP motif is HxxHHxxHHxxHHxxHH with x representing any amino acid and H stands for an amino acid with hydrophobic residue. More defined, the AKAP motif for RII-binders was described to be:
(AVLISE)xx(AVLIF)(AVLI)xx(AVLI)(AVLIF)xx(AVLISE), whereby X indicates any amino acid and in parentheses alternative amino acids for a position are given in single letter code (Hundsrucker *et al.* 2010). Recent resolution of an extended AKAP18β:PKA-RIIα-D/D crystal structure by our group elucidated additional hydrophilic anchor points supporting and flanking the amphipathic helix that are crucial for RII binding (Götz *et al.* 2016). The identified anchor points facilitate binding in the correct orientation and stabilize the AKAP:PKA interaction. Sequence alignment proves conservation of the anchor points throughout various AKAPs. Performing an alanine scan peptide spot array of the AKB confirmed the findings *in vitro*. Therefore, 30 amino acids peptides of the AKAP18β-AKB were spot-synthesized on a cellulose membrane with consecutive replacement of each amino acid by alanine and then overlaid with radioactively labelled RIIα as described in 3.4.2. Replacement of each anchor point by alanine reduced RIIα binding by 20 to 40 % and this was further enhanced by simultaneous replacement of all anchor points (Götz *et al.* 2016). In order to confirm the findings in a cellular context, immunoprecipitation and cAMP pulldown experiments were performed from HEK cells overexpressing wildtype and mutant AKAPs. Expression constructs of a RII-specific (AKAP18γ), RI-specific (smAKAP) and a dual-specific AKAP (AKAP1) and their respective anchor point mutants were cloned and expressed in HEK cells as FLAG (DDK)-tagged proteins. Figure 24 B indicates the respective RII- (green) and RI-specific (red) anchor point mutations and their alignment with AKAP18β.

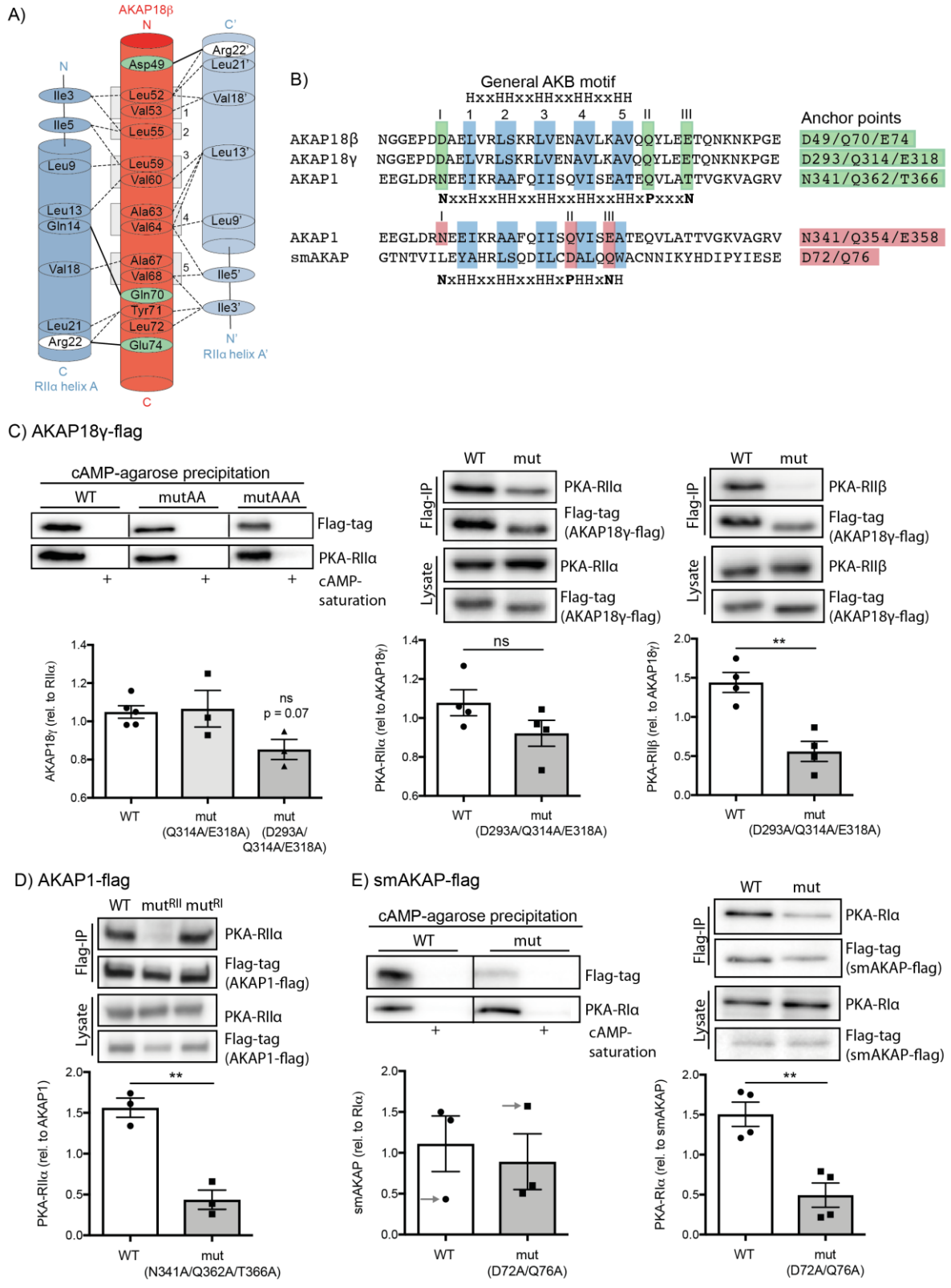

Figure 24: AKAP anchor points are crucial for the interaction with PKA regulatory subunits. Parts of the figure are modified from (Götz *et al.* 2016). A) Schematic representation of the interaction of AKAP18β (red) with RIIα helices A (blue) and A' (light blue). Marked in green are the polar residues of the anchor points that strengthen the AKAP-PKA interaction. The numbered grey boxes indicate hydrophobic residues of the amphipathic helix that bind RIIα and form the canonical AKAP motif. Dashed lines represent hydrophobic interactions; solid lines indicate polar interactions. B) Sequence alignment of the analyzed AKAPs with AKAP18 β. Highlighted are the classic AKB motif patches 1-5 (blue) and the identified anchor points I-III (green for RII binding, red for RI binding). Figure legend continues on the next page.

C-E) Reciprocal precipitation of R subunits by cAMP-agarose pulldown and flag-IP of selected AKAPs identifies deficient binding upon mutation of the identified anchor points in AKAP18γ (C), AKAP1 (D) and smAKAP (E). Error bars indicate SEM. Statistics: One-way ANOVA, unpaired t-test, * - $p \leq 0.05$, ** - $p \leq 0.01$.

Precipitation of PKA-R subunits was performed by cAMP pulldown and co-precipitation of the FLAG-tagged AKAP was detected by WB. It is of note that for quantification, the AKAP signal was related to the RIα or RIIα WB signal according to their specificity, although all types of R subunits bind to the cAMP-agarose. RI or RII-specificity cannot be distinguished with this experiment. The AKAP18γ triple mutant D293A/Q314A/E318A showed reduced binding to cAMP-agarose compared to AKAP18γ-WT (Figure 24 C, left). Binding of smAKAP-D72A/Q76A to cAMP-agarose was severely reduced in two out of three experiments (Figure 24 E, left). The third repetition shows the opposite (Figure 24 E, arrows), which is presumably due to a quantification problem. Expression of the mutant smAKAP was much weaker than that of WT-smAKAP in that experiment. Therefore, co-precipitation of smAKAP on cAMP-agarose relative to the total abundance of the expressed protein appeared increased. Nevertheless, the two experiments with comparable expression levels of the constructs indicate that smAKAP anchor point mutation strongly interferes with R subunit binding on cAMP-agarose.

As cAMP pulldowns are not suitable for the assessment of R subunit specificity, immunoprecipitation *via* the FLAG-tag of the constructs was performed and the interactions with R subunits evaluated by WB detection. Binding of RIIα to the AKAP18γ triple mutant was only slightly reduced compared to the WT protein (Figure 24 C, middle). However, the mutations interfered more with RIIβ interaction (Figure 24 C, right). The statistically significant reduction of RIIβ, but not RIIα binding might be due to a lower affinity of AKAP18 for RIIβ that enables easier disruption of the binding by sequence manipulation at the anchor points. Binding of RIIα to the RII-specific anchor point mutant of AKAP1 was strongly reduced compared to both WT and RI-specific anchor point mutant (Figure 24 D). Co-precipitation of RIα with AKAP1 could not be observed reproducibly, so that the RI-specific anchor point mutations could not be further investigated. A first indication for the proof of concept that anchor points define subunit specificity in dual-specific AKAPs, however, is the finding that RIIα binding to AKAP1 is not affected by mutation of the RI-specific anchor sites. Yet, this needs to be reproduced and also RI co-precipitation established before any scientific conclusion can be drawn. Anchor point mutation of smAKAP significantly interferes with RIα binding. Thus, the findings of the cAMP pulldown could be confirmed, indicating that the experiment showing opposing results is an outlier and can be excluded from the evaluation. Summarized, the results of the co-precipitation experiments show that mutation of the newly identified polar anchor points to alanine strongly interferes with R subunit binding of AKAPs with different R subunit specificity.

4. DISCUSSION

4.1 Metabolic control of the AQP2 shuttle

4.1.1 AQP2 redistribution does not require global metabolic changes

The results of the global metabolic analysis of IMCD cells indicate that no major changes of the cellular metabolism are needed to allow the AVP-induced translocation of AQP2 from intracellular vesicles into the plasma membrane. Flux through general metabolic pathways, such as glycolysis and citric acid cycle, was not substantially changed upon AVP. However, minor changes of the metabolite citrate, temporally limited to 30 min after stimulation, indicate that IMCD cells undergo some metabolic modifications at the entry of the citric acid cycle upon stimulation of the AQP2 translocation with AVP.

Upon stimulation of IMCD cells with AVP for 15 to 30 min, the citrate isotopomer M3, derived from stable isotope labelled glucose, was reduced compared to control cells. This indicates reduced pyruvate carboxylase (PC) activity. PC catalyzes the carboxylation of pyruvate to OAA in mitochondria. Its major function is the replenishment of OAA as an intermediate in the citric acid cycle. In addition to its role in anaplerosis, PC is needed for the supply of phosphoenolpyruvate (PEP) in gluconeogenic tissues, e.g. the liver and renal cortex. Reduced PC activity upon AVP stimulation could indicate less removal of metabolites from the citric acid cycle, in concert with a reduced need for replenishment. A reduced activity of PC would also result in an accumulation of pyruvate and its conversion to lactate. Lactate secretion from AVP-stimulated IMCD cells was marginally increased compared to control cells, but this was not observed by the intracellular analysis of labeled lactate.

The pyruvate that is not converted to OAA enters the citric acid cycle *via* decarboxylation to acetyl-CoA by the pyruvate dehydrogenase (PDH) complex. PDH fuels the citric acid cycle and is inhibited by high levels of ATP, NADH and acetyl-CoA. In contrast, acetyl-CoA allosterically activates PC. Hence, reduced levels of acetyl-CoA can result in lower PC activity compared to control conditions. Acetyl-CoA was not assessed, but the results from the measurement of citrate isotopologues suggest an increase in citrate synthase activity after 30 min of AVP stimulation. This indicates that the pool of acetyl-CoA was shifted towards incorporation into the citric acid cycle, so that less acetyl-CoA was available for PC activation in AVP-stimulated cells compared to control cells.

It is of note that the changes observed and discussed herein were only little and are not confirmed by biological repetition of the experiment. Nevertheless are the findings from the glucose tracer samples in line with those using the glutamine tracer. Overall, sample variability was low between the three technical replicates. As the experiment was of good

quality and clearly answered the question whether the IMCD metabolism is globally modified by AVP stimulation, a repetition of the experiment was not necessary.

In addition to the metabolomic analysis of IMCD cells, insight into metabolic mechanisms that regulate the AQP2 shuttle was gained by a siRNA-based screening for kinases in the control of AQP2 translocation, performed by another member of the group, Dr. Dörte Faust (Faust 2014). One of the kinases whose absence interfered with AQP2 redistribution into the plasma membrane was the glycolytic enzyme phosphofructokinase 1 (PFKP).

Citrate inhibits citrate synthase by product inhibition, but also phosphofructokinase (PFK) as a negative feedback mechanism to reduce glycolytic flux. An assumption would be that increased levels of citrate, through elevated citrate synthase activity, reduce PFK activity upon cAMP elevation. However, this is not in line with the deficient AQP2 shuttle upon PFKP knockdown. Yet, both observations represent disparate time points within the regulation. While the metabolic analysis shows only differences within 30 min of stimulation, AQP2 translocation modulated by PFK knockdown was evaluated as an end point measurement at 72 h after siRNA transfection, so that the cells had time to adapt their metabolism to the loss of PFK. PFK might be generally required for the induction of AQP2 translocation, but citrate accumulation after 30 min of stimulation could act as a negative feedback to return glycolysis back to basal levels.

Glucose uptake from the medium appeared to be reduced starting from 30 min of AVP stimulation with total maximal uptake after 1 h of incubation. This time point also showed the strongest difference to untreated control cells. In order to analyze glucose uptake, MCD4 cells were treated with the glucose analogue 2DG that can be taken up by the cell and converted to glucose-6-phosphate by hexokinase, but is not further metabolized. However, blockage of glycolysis upstream of PFK by the use of 2DG did not result in a defective AQP2 shuttle.

In conclusion, the metabolic analysis of IMCD cells shows small differences in citrate metabolism after 30 min of AVP stimulation. This is concurrent with the time point usually chosen for observation of AQP2 translocation. It is of note that plasma membrane insertion of AQP2 already starts 20 sec after AVP stimulation in IMCD cells (Lorenz *et al.* 2003). MCD4 cells showed increased membrane localization of AQP2 after 2 min of cAMP elevation with FSK (Figure 20 B). Thus, the observed changes in the IMCD metabolism could also serve to re-establish basal conditions. Overall, no major changes in cellular metabolism were observed upon AVP stimulation, indicating that the metabolic regulation is rather local and does not translate into global metabolic changes.

4.1.2 A role for lactate dehydrogenase A in the control of AQP2 protein abundance

LDH catalyzes the reversible conversion of pyruvate to lactate in anaerobic glycolysis, which is paralleled by NADH oxidation to NAD^+. If oxygen levels are low, cellular respiration cannot efficiently use oxidative phosphorylation to produce ATP from pyruvate. Instead, LDH converts pyruvate to lactate and replenishes NAD^+, which is needed for glycolysis. Glycolysis does not yield as much ATP as mitochondrial respiration, only 2 ATP per glucose molecule compared to 36, but occurs much faster. Cancer cells perform this switch in metabolism even in the presence of oxygen, known as the Warburg effect (reviewed by Koppenol *et al.* 2011).
The knockdown of LDHA by RNA interference increased the total abundance of AQP2 at the protein level, but not at the mRNA level. This indicates that reduction of LDHA stabilizes the AQP2 protein, possibly by decreasing its degradation. It also suggests that LDHA is involved in targeting AQP2 for degradation. It was shown that AQP2 poly-ubiquitination targets its proteasomal degradation (Nedvetsky *et al.* 2010), whereas short-chain ubiquitination induces its endocytic retrieval from the plasma membrane and lysosomal degradation (Kamsteeg *et al.* 2006). Further investigations are needed to evaluate the potential role of LDHA in the proteasomal or lysosomal degradation of AQP2. A Western blot analysis of the ubiquitination status of immuno-isolated AQP2 from MCD4 cells, might reveal changes in the ubiquitin chain length between control cells and cells in which LDHA was down-regulated by RNA interference. A recent study showed that the C terminus of HSC70-Interacting Protein (CHIP/Stub1), together with Hsp70, organizes E3 ubiquitin ligases for the control of AQP2 ubiquitination and degradation (Centrone *et al.* 2017). Thus, the ubiquitination of AQP2 and its potential association with Hsp70 upon LDHA knockdown should also be investigated.
Knockdown of LDHA tends to increase the membrane accumulation of AQP2 in untreated cells and to elevate the translocation in FSK-stimulated MCD4 cells. The increased abundance of AQP2 might cause a shift of the dynamic equilibrium of AQP2 localization towards membrane insertion. The validity of this hypothesis was investigated by surface biotinylation of IMCD cells, which show a more pronounced membrane insertion of AQP2 upon cAMP elevation, compared to the rather diffused cytosolic distribution in MCD4 cells. This makes IMCD cells the better model system for investigating the AQP2 shuttle and is also the reason, why surface biotinylation was performed from IMCD cells and not from MCD4 cells. Freshly isolated primary IMCD cells are fully differentiated cells and in a non-proliferating state. Thus, it is difficult to obtain adequate transfection efficiencies for biochemical experiments using standard cationic or liposomal transfection reagents. An alternative approach for the analysis of AQP2 by immunofluorescence microscopy is the use of fluorescently labeled siRNAs. In that way, transfected cells can be visualized and selectively analyzed. Another approach would be the use of shRNA, expressed with a fluorescent protein reporter, but the design of efficient shRNA constructs might be tedious.

Also, other methods for siRNA delivery as electroporation and viral particles could be considered. Here, an inhibitor of LDH was used to evaluate how functional interference with LDH affects AQP2 redistribution. However, there was no change in the amount of AQP2 that was exposed to the surface of IMCD cells upon LDH inhibition with SO. The stimulation with FSK induced the plasma membrane localization and was used as a positive control. The LDH inhibitor SO is a structural analog of pyruvate. As LDHA has a higher affinity for pyruvate than LDHB, SO interferes more with LDHA than LDHB activity. In this way it is similar to the knockdown of LDHA, but cannot reflect changes caused by LDHA protein interaction. This could explain why the effect of LDHA knockdown on AQP2 membrane localization was not reproduced in IMCD surface biotinylation.

4.1.3 Metabolic enzymes associate with AQP2-bearing vesicles

The metabolic analysis of IMCD and MCD4 cells suggests that AQP2-vesicle transport does not depend on global metabolic changes. Association of metabolic enzymes with AQP2-bearing vesicles could locally regulate AQP2 trafficking. This interaction could be permanent and modulated by local changes in enzyme activity, or regulated through conditional association with the vesicles.

To address these possibilities, MCD4 cells were stimulated with FSK or left untreated and AQP2-bearing vesicles were immuno-isolated. Of the proteins associated with AQP2-bearing vesicles, G6PDH and AMPK were the most promising for the metabolic regulation of the cAMP-mediated AQP2 redistribution. AMPK itself is not a metabolically active enzyme, but a central regulator of cellular energy supply. Energy shortage causes an accumulation of AMP and ADP, which activate AMPK to up-regulate ATP-generating pathways, while restraining ATP-consuming pathways (Moore *et al.* 1991, Gowans *et al.* 2013). The potential role of G6PDH and AMPK in AQP2 trafficking will be discussed below.

Although LDHA and PFKP were found to modulate AQP2 abundance and intracellular localization, respectively, association of these enzymes with AQP2-bearing vesicles was not observed. It is possible that their binding to the vesicles is only transient or too weak to be detected by this method. Their effect on AQP2 could also be exerted through other proteins that regulate AQP2 stability and transport, e.g. ubiquitin ligases or regulators of the actin cytoskeleton to only give two examples. Actin filaments form a physical barrier for vesicle transport. Their disruption was shown to allow AQP2 movement to the plasma membrane without the key trigger, cAMP elevation (Klussmann *et al.* 2001).

A general problem of the AQP2-vesicle immuno-isolation was the lack of a reliable negative control. The use of nonspecific IgGs led to co-precipitation of candidate proteins. This would indicate that the observed interaction is unspecific. However, often also AQP2 was detected in the negative control. Thus, it was not possible to discriminate between unspecific binding

to the IgG control or the residual AQP2. An approach to circumvent this problem is the use of the precursor cell line of MCD4, M1, as a negative control. The M1 cell line has the same properties as MCD4 cells, but does not stably express human AQP2. Endogenous levels of AQP2 are low in M1 cells. The use of M1 cells as negative control could help to evaluate the binding of GAPDH and PKM to the AQP2-bearing vesicles, as both proteins were found abundant in the IgG control. Of the proteins identified on AQP2-bearing vesicles in this thesis, the ER-specific Hsp90β isozyme and the V-ATPase subunit v0a were already found in a large-scale mass spectrometry-approach of rat inner medullary collecting ducts to be associated with AQP2-bearing vesicles (Barile *et al.* 2005).

4.1.3.1 G6PDH

G6PDH catalyzes the conversion of glucose-6-phosphate to 6-phospho-gluconolactone, along with the reduction of $NADP^+$ to NADPH, in the first step of the pentose phosphate pathway (PPP). NADPH is required for oxidative stress control to enable glutathione reduction, and for the lipid biosynthesis by the fatty acid synthase complex. PKA negatively regulates G6PDH activity, potentially through its phosphorylation, which decreases NADPH levels and augments oxidative stress in diabetic hyperglycemia, and eventually causes diabetic nephropathy (Zhang *et al.* 2000, Xu *et al.* 2005). In addition, cAMP signaling through PKA and cAMP-responsive element modulator (CREM) reduces G6PDH abundance at the transcriptional level (Leopold *et al.* 2007).

Co-precipitation of G6PDH with AQP2-bearing vesicles from MCD4 cells increased upon FSK stimulation. Elevation of the intracellular cAMP concentration by FSK activates PKA, which, in turn, favors G6PDH phosphorylation and decreases G6PDH activity. Thus, co-localization of G6PDH with PKA on AQP2-bearing vesicles could decrease its activity. How tethering of G6PDH to the vesicles could favor the translocation, however, remains to be established. It would be of interest to investigate, if G6PDH knockdown induces AQP2 translocation into the plasma membrane, even without cAMP elevation.

NADPH is required for the mevalonate synthesis by HMG-CoA reductase. This enzymatic reaction is the pharmacological target of statins, which are a class of cholesterol-lowering drugs for the prevention of cardiovascular diseases. In renal principal cells, statins elevate water reabsorption from primary urine independently of V2R stimulation, which brought them into the focus for the treatment of NDI. Mevalonate is a precursor for the synthesis of isoprenoids and in that way required for the iso-prenylation of RhoA and Rab proteins, which ensures their membrane targeting and activity. Statins interfere with RhoA activity in renal principal cells and cause membrane accumulation of AQP2 through the disassembly of the actin cytoskeleton and decreased AQP2 endocytosis (Tamma *et al.* 2001, Li *et al.* 2011, reviewed by Bonfrate *et al.* 2015).

A PKA-mediated reduction of G6PDH activity on AQP2-bearing vesicles could locally interfere with RhoA activity to facilitate the AQP2 redistribution (Figure 25). This would be a secondary and more long-term effect to the direct PKA phosphorylation of RhoA at S188, which causes RhoA inhibition through increased RhoA- RhoGDP dissociation inhibitor (RhoGDI) interaction (Lang *et al.* 1996, Tamma *et al.* 2003). RhoGDIs inhibit Rho proteins by interference with their GDP to GTP nucleotide exchange and their membrane localization, which are both required for the activity of Rho proteins (reviewed by Dovas *et al.* 2005).
COX-2 inhibitors interfere with the conversion of arachidonic acid to prostaglandins and favor AQP2-mediated water retention in NDI patients (Pattaragarn *et al.* 2003). Arachidonic acid decreases G6PDH expression through an AMPK-dependent process that involves the PI3-kinase pathway and p38-MAPK activation (Talukdar *et al.* 2005, Kohan *et al.* 2009). Thus, in addition to the regulation through prostaglandins, the antidiuretic effect of COX-2 inhibitors might be caused by accumulation of arachidonic acid, which decreases G6PDH abundance and facilitates AQP2 translocation. This hypothesis, however, needs to be confirmed experimentally.

4.1.3.2 AMPK

AMPK was found on AQP2-bearing vesicles in this project. It has an antagonistic role to PKA in the regulation of AQP2 localization (Al-Bataineh *et al.* 2016). Activation of AMPK by the AMP-analog 5-aminoimidazole-4-carboxamide-1-β-d-ribofuranoside (AICAR) interferes with FSK-induced plasma membrane localization of AQP2 in mouse cortical collecting duct cells. However, AICAR also prevented the increase of total AQP2 abundance upon long-term FSK stimulation, which indicates that the apparent decrease of translocation could also be due to overall reduced AQP2 levels (Al-Bataineh *et al.* 2016). AICAR-mediated AMPK activation interferes with dDAVP-induced AQP2 phosphorylation at S269, whereas it induces p-S261. This supports the hypothesis that AMPK favors AQP2 intracellular localization. However, it is of note that the cell system used for this experiment does not represent the expected decrease in p-S261 upon dDAVP stimulation. This indicates that the cell model used for the experiment might not be suitable to investigate the phosphorylation status of AQP2 (Al-Bataineh *et al.* 2016).
In contrast to these findings, recent investigations with the anti-diabetic drug and AMPK activator metformin indicate that metformin treatment improves urinary concentrating ability in NDI mouse and rat models (Efe *et al.* 2016). An *in vitro* phosphorylation assay indicates that AMPK directly phosphorylates AQP2, which might be the underlying mechanism of metformin-stimulated apical membrane accumulation of AQP2 (Klein *et al.* 2016).

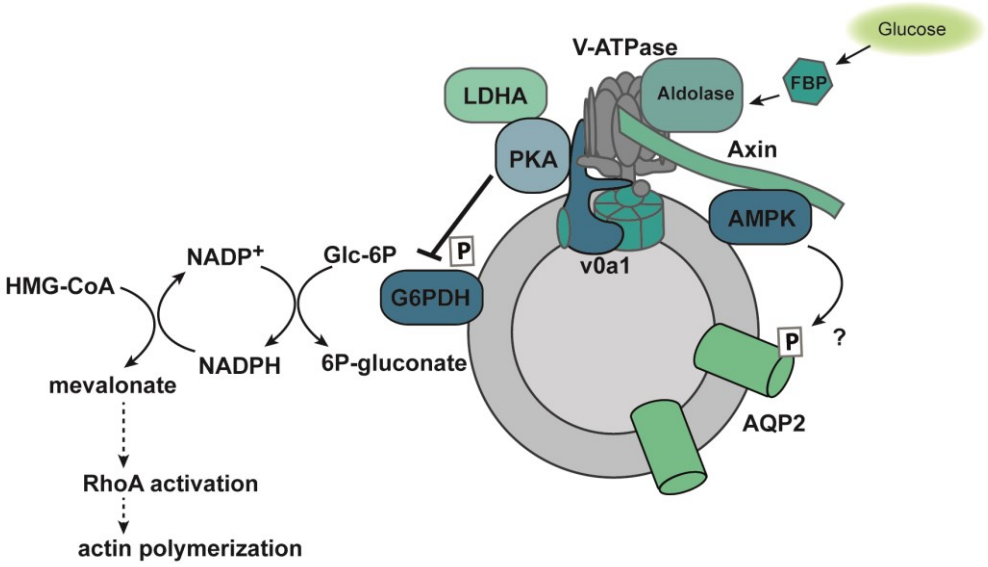

Figure 25: Model of a metabolic sensor complex on AQP2-bearing vesicles In this thesis, G6PDH, AMPK and V-ATPase v0a1 were identified on AQP2-vesicles and they might play a role in metabolic regulation of cAMP-mediated AQP2 translocation. Local inactivation of AMPK through PKA phosphorylation at T173 potentially interferes with AQP2 phosphorylation by AMPK, which in turn reduces the perinuclear localization of AQP2. The involvement of axin and aldolase is only hypothesized, as their localization to V-ATPase on lysosomal vesicles was described for the regulation of AMPK (Zhang *et al.* 2014, Zhang *et al.* 2017). For details regarding the V-ATPase-organized metabolic complex on lysosomes, see chapter 1.2.2.

The binding of AMPK to AQP2-bearing vesicles was increased upon FSK stimulation. On the vesicles AMPK resides in proximity to AKAP-tethered PKA, suggesting that PKA inhibitory phosphorylation of AMPK at S173 could be part of the regulatory mechanism. This phosphorylation interferes with the phosphorylation at T172, which is required for AMPK activation. Western blot detection of AMPK-pT172 on AQP2-vesicles with a phospho-specific antibody will help to elucidate, whether FSK stimulation changes the phosphorylation status of AMPK-T172. A decreased phosphorylation of T172 would be in line with the compartmentalization of active PKA on the AQP2-bearing vesicles. For the regulation of AQP2 translocation this would indicate that active AMPK favors perinuclear positioning and PKA-mediated down-regulation of AMPK activity is required for translocation into the plasma membrane. As it is still unknown at which site AQP2 is phosphorylated by AMPK, it is not possible to deduce its molecular effect. In line with the findings of Al-Bataineh *et al.* (2016) and the results of this thesis, AMPK could be responsible for AQP2 phosphorylation at S261. Yet, this is in contrast with the apical accumulation upon metformin treatment. A potential explanation for this would be that metformin, compared to AICAR, does not directly and exclusively activate AMPK. Instead, the primary target of metformin is the mitochondrial complex I, but it was also described to inhibit mitochondrial glycerophosphate dehydrogenase and hexokinase-II (Owen *et al.* 2000, Salani *et al.* 2013, Madiraju *et al.*

2014). In addition, metformin treatment was performed over 4 days, whereas collecting duct cells were stimulated with AICAR for only 4 h (Al-Bataineh *et al.* 2016, Efe *et al.* 2016).
Taken together, AMPK and G6PDH are interesting new players in the regulation of AQP2 trafficking. Further investigations are needed to understand their role for the interplay between renal principal cell metabolism and cAMP-regulated AQP2 translocation.

4.2 Characterizing the function of V-ATPase in the control of AQP2

Inhibition of V-ATPase is pursued for the treatment of diseases, such as cancer, osteoporosis and certain viral infections, in which excessive or unwanted acidification by V-ATPase is observed (reviewed by Hernandez *et al.* 2012, Qin *et al.* 2012, Muller *et al.* 2014). The first specific inhibitors of V-ATPase were the plecomacrolides bafilomycin and concanamycin, which are still commonly used for research purposes (Bowman *et al.* 1988, Drose *et al.* 1993). As they bind the highly conserved c subunit of the transmembrane v0 domain to impede proton translocation, plecomacrolides cannot distinguish between V-ATPases of different organisms (Bowman *et al.* 2002, Huss *et al.* 2002). For a therapeutic use, inhibitors with higher specificity and stability are sought. The benzolactone enamide salicylihalamide specifically inhibits the V-ATPase of animals, but not yeast. It also binds to the v0 domain, yet at a site different from bafilomycin (Xie *et al.* 2004). In the opposite sense, inhibitors that specifically target fungal V-ATPase have been developed for antimycotic therapy (reviewed by Hayek *et al.* 2014). In order to increase the specificity of V-ATPase inhibitors, advances were made in the identification and targeting of tissue-specific subunits, for example to target the osteoclast-specific a3 isoform for the treatment of osteopetrosis (Kartner *et al.* 2010).
The natural plant-derived V-ATPase inhibitor diphyllin has improved characteristics for the treatment of bone resorption compared to bafilomycin, as it shows reduced osteoblast cytotoxicity (Sorensen *et al.* 2007). More recently, diphyllin was also tested for antiviral therapeutic strategies. Impaired endosomal acidification caused by V-ATPase inhibition interferes with viral particle fusion and by that reduces viral susceptibility (Chen *et al.* 2013).
A V-ATPase inhibitor that is structurally related to diphyllin, 4-acetyldiphyllin (4AD), was identified to interfere with the AVP-induced AQP2 redistribution in renal principal cells. Although it is less potent than bafilomycin, 4AD significantly reduces vesicle acidification in MCD4 cells (Bogum *et al.* 2013). In this thesis, 4AD increased the autophagic marker LC3-II in IMCD and MCD4 cells, similar to what is known for other V-ATPase inhibitors (Meo-Evoli *et al.* 2015). This indicates that autophagic vesicles, which cannot be cleared, due to impaired vesicle acidification, accumulate in endo-lysosomal compartments. V-ATPase has been assumed to control both (auto)phagosome-lysosome fusion and acidification-dependent lysosomal functions (Peri *et al.* 2008). However, the recent work of Mauvezin and

colleagues (2015) suggests that bafilomycin inhibits the fusion event through inhibition of a secondary target, the sarco/endoplasmic reticulum Ca^{2+} ATPase (SERCA). The authors conclude that inhibition of the V-ATPase is only responsible for impaired lysosomal acidification, but not vesicle fusion (Mauvezin *et al.* 2015). It remains to be investigated, whether 4AD also inhibits SERCA, or if 4AD is a more specific inhibitor and only targets the V-ATPase.

The results of the immunoprecipitation and differential detergent fractionation experiments in this thesis (Figure 18 and Appendix Figure 30) indicate that 4AD acts through a mechanism distinct from bafilomycin. Treatment with 4AD, but not bafilomycin, favors the assembly of the v0 and V1 subunits of the V-ATPase, similar to what was shown for salicylihalamide (Xie *et al.* 2004). The inhibition of V-ATPase in its assembled form might also indicate a different mode of action as this interferes with v0 subunit accessibility. In the last years, a role for V-ATPase in the regulation of vesicle fusion independent of its proton pumping activity emerged (reviewed by El Far *et al.* 2011). The c subunit hexamer of the v0 transmembrane domain forms a proteolipid pore that interacts with the v-SNARE VAMP2 and regulates Ca^{2+}-induced synaptic vesicle fusion (Di Giovanni *et al.* 2010). Figure 26 schematically depicts this regulatory mechanism. The subunit v0a also plays a role in neurotransmission by regulating the formation of the SNARE fusion complex (Hiesinger *et al.* 2005, Wang *et al.* 2014). The pH-dependent disassembly of the V-ATPase presumably serves as a switch between vesicle loading and exocytosis of synaptic vesicles (Poea-Guyon *et al.* 2013). VAMP2 is located on AQP2-bearing vesicles and required for FSK-mediated plasma membrane insertion of AQP2 (Gouraud *et al.* 2002, Barile *et al.* 2005, Procino *et al.* 2008). Thus, the mode of action of 4AD could be through the stabilization of the assembled V-ATPase holoenzyme that not only

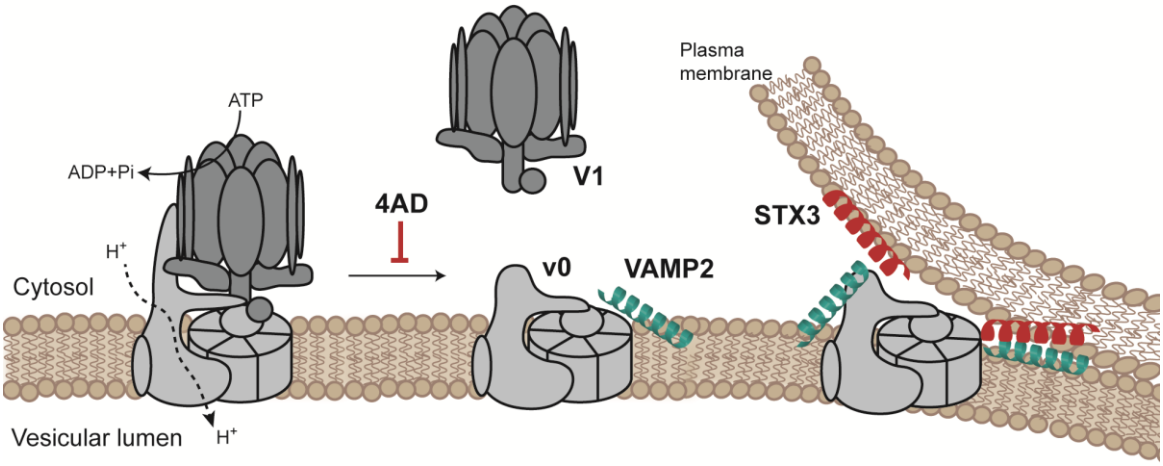

Figure 26: 4AD inhibits the V-ATPase in its assembled state. The inhibitory mechanism of 4AD is different from the common V-ATPase inhibitor bafilomycin and favors the v0-V1 assembly of the V-ATPase. In that way, 4AD might impede the interaction of the v0 domain with proteins of the SNARE machinery, such as VAMP2. This could interfere with AQP2-bearing vesicle exocytosis at the stage of plasma membrane fusion, which was shown to depend on VAMP2 and STX3 (Procino 2008) .

interferes with its activity, but also impedes interaction of v0 with the SNARE machinery for fusion of AQP2-bearing vesicles with the apical plasma membrane in renal principal cells.

Incubation of MCD4 cells with 4AD for 30 min resulted in the accumulation of AQP2 in condensed perinuclear compartments, which overlapped with the ERGIC marker ERGIC-53. This is similar to what was observed by bafilomycin treatment of proximal tubule LLC-PK1 cells expressing AQP2 (Gustafson *et al.* 2000). The results of this thesis indicate that 4AD treatment does not interfere with the translocation of AQP2 into the plasma membrane, as treatment with 4AD followed by FSK stimulation causes AQP2 accumulation in both the plasma membrane and the ERGIC53-positive compartment. This suggests that in the presence of 4AD, AQP2 shuttles into the plasma membrane upon cAMP elevation, undergoes endocytic retrieval, but is not able to pass through the recycling compartment. In addition, short-term incubation with 4AD induced AQP2 redistribution into the plasma membrane to a similar extent or even stronger than FSK stimulation observed at the same time point. These findings suggest that V-ATPase inhibition by 4AD not only causes an intracellular accumulation of AQP2 that fails to recycle, but also affects mechanisms regulating plasma membrane transport of AQP2.

The work of Gustafson and colleagues showed that incubation of the AQP2-expressing LLC-PK1 cells at 20°C also caused the accumulation of AQP2 in a trans-Golgi compartment, similar to what was seen with bafilomycin (Gustafson *et al.* 2000). This indicates the involvement of microtubular structures, which disassemble in the cold (Breton *et al.* 1998). Subcellular fractionation of IMCD cells showed a significantly increased pool of α-tubulin in the cytosolic fraction upon 4AD treatment, which was reproduced by the use of bafilomycin, indicating that the effect is due to V-ATPase inhibition, and is not specific for 4AD (Appendix Figure 31). This could indicate that V-ATPase inhibition causes disassembly of the microtubular network. However, the amount of polymerized tubulin did not change upon 4AD treatment in two independent experiments. This is in line with the finding that microtubules are required for perinuclear positioning of AQP2 rather than for its transport to the plasma membrane. Disruption of microtubules by nocodazole reduces the perinuclear pool of AQP2 (Vossenkamper *et al.* 2007). Applying a 4°C cold shock to MDCK cells induces the reversible redistribution of AQP2 into the basolateral membrane in parallel to, but not dependent on microtubule disruption (Yui *et al.* 2013). Further investigations are needed to understand how V-ATPase inhibition modifies the microtubular network in renal principal cells. The effect on tubulin observed herein might also be only secondary to the inhibition of the V-ATPase. In yeast, the V-ATPase inhibitor Iejimalide C was shown to disassemble the actin cytoskeleton as a secondary effect to impaired pH homeostasis (Kazami *et al.* 2014). However, interference with the actin network could also be caused by structural changes, such as v0-V1 association, as the V-ATPase subunits B and C can directly interact with F-actin (Holliday

et al. 2000, Vitavska *et al.* 2005). The role of the C subunit in this regulation is of particular interest as it can dissociate from the disassembled V1 domain and was shown to stabilize F-actin (Vitavska *et al.* 2005). 4AD inhibits the V-ATPase in its assembled state, so that reduced interaction between V1C and F-actin in proximity to AQP2-bearing vesicles could locally destabilize F-actin fibers and enable AQP2 transport to the plasma membrane.
In conclusion, 4AD influences AQP2 localization in MCD4 and IMCD cells through a dual mechanism. The strengthened interaction between v0 and V1 could interfere with stabilization of the actin cytoskeleton by V1 subunits. In that way, 4AD-induced actin disassembly could mediate the initial redistribution of AQP2 into the plasma membrane. Accumulation of AQP2 in recycling compartments upon longer 4AD treatment indicates that acidification of intracellular vesicles is required for AQP2 recycling.

4.3 Evaluation of the potential AKAP function of LDH and V-ATPase isoforms

A standard assay for the identification of new AKAPs is the cAMP pulldown, which efficiently precipitates all R subunits of PKA and can co-precipitate interaction partners of PKA. Application of different cAMP-agarose resins that vary in spacer length and cAMP modifications, can affect the yield of different R subunits (Bertinetti *et al.* 2009). The use of agonistic or antagonistic cAMP analogs that induce or repress the dissociation of the catalytic subunits from the PKA holoenzyme, respectively, can limit the subsets of PKA interaction proteins that are co-precipitated (Hanke *et al.* 2011). As cAMP is highly abundant on the agarose beads, even less efficient binding proteins, such as nucleotide binding proteins, can be precipitated. This was also observed in this project (Figure 14) and for such proteins the assay cannot determine PKA binding. As an alternative, co-immunoprecipitation was performed. The results suggest that LDH and V-ATPase are in a complex with PKA-RIIα (Figure 15). However, reproducibility and RIIα detection, without the IgG heavy chain signal, need to be further improved to unequivocally confirm the interaction of LDH and PKA by immunoprecipitation. The co-expression of both potential interaction partners and reciprocal immunoprecipitation through their epitope tags, such as FLAG, myc or HA, fused to the protein of interest, was pursued to circumvent the mentioned problems. However, due to unspecific co-precipitation of LDHA-FLAG with both GFP and HA antibodies, this approach was not successful. Another way to reduce the detection of the heavy chains of the immunoprecipitation antibody is the covalent coupling of the antibody to the resin, which should be employed for future experiments.

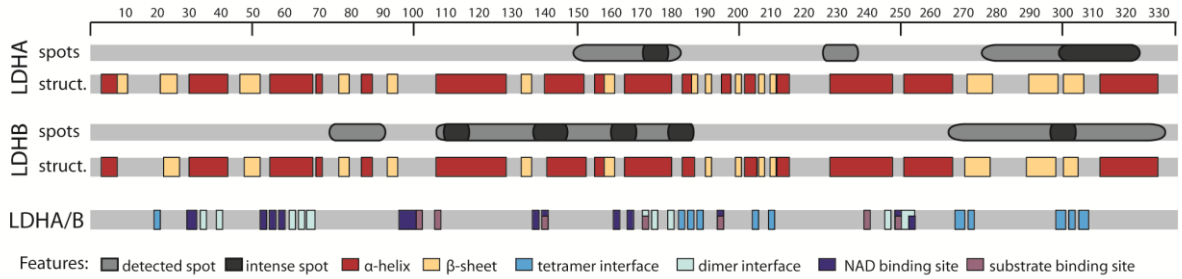

Figure 27: Potential PKA-RIIα interaction sites on LDHA and LDHB. The entire mouse protein sequences (NCBI: LDHA NP_034829.1, LDHB NP_032518.1) were spot-synthesized. Spots detected by overlay with radioactively labeled RIIα are depicted in medium grey (for original spots see **Figure 15**). Of those, spots with highest intensity are shown in dark grey. Human LDH shares 94 % identity with mouse. Features are shown from human LDH, due to better availability of structural data. Secondary structure according to RCSB PDB (https://www.rcsb.org/) P00338 (human LDHA) and P07195 (human LDHB), other protein features according to NCBI NP_005557.1 (human LDHA) and NP_002291.1 (human LDHB).

A method to investigate the direct interaction of two proteins is the peptide spot array technology, in which a protein sequence is spot-synthesized on a cellulose membrane as overlapping oligomers. Overlay with radioactively labelled RIIα allows detection of the protein sequences that interact with RIIα by autoradiography and does not depend on the specificity of an antibody for detection. For LDHA, LDHB and V-ATPase v0a subunits interaction with RIIα was observed. Figure 27 depicts the identified PKA-RIIα interaction sites on LDHA and LDHB in alignment with known protein features. The canonical PKA binding motif of AKAPs forms an α-helix. Comparison of the detected spots with the LDH secondary structure might reveal regions of interest for the identification of an AKAP function. Scanning the LDH protein sequence for the canonical AKAP motif [AVLISE]-x-x-[AVLIF]-[AVLI]-x-x-[AVLI]-[AVLIF]-x-x-[AVLISE], using the PROSITE online tool (http://prosite.expasy.org/scanprosite/), did not reveal an AKAP motif. However, small modifications of the motif revealed two similar motifs between aa118 and 128 (_KF**II**PN**IV**KY**S**) and between aa140 and 150 (_VD**IL**TY**VA**WK**I**) in the LDHA structure, of which the first one is conserved in LDHB (_KF**II**PQ**IV**KY**S**). RIIα-binding was observed to both sequence regions of the LDHB peptide spots, but not to the corresponding LDHA spots (Figure 27). The helix spanning aa111 to 128 is accessible for protein binding in the three-dimensional fold (human LDHB RCSB PDB entry 1I0Z) and in proximity to the LDH C terminus, which also showed RIIα binding in the peptide spot array.
This suggests that LDHB interacts with PKA through a binding site formed by amino acids of the central and C-terminal part of the LDHB protein sequence. It remains to be investigated, whether binding of PKA-RIIα to LDHA occurs through a similar site and the binding was only too weak to be detected or to a site different from the one in LDHB. In order to identify also the binding site on PKA, the RIIα sequence should be spot-synthesized and overlaid with recombinant LDHA and LDHB.

For V-ATPase subunit v0a2, two bioinformatic screenings identified a putative helical AKAP motif (Hundsrucker *et al.* 2010, Burgers *et al.* 2015). One of the identified sequences overlapped with the interaction site identified in this thesis (Figure 28). The binding site detected here additionally employed amino acids in the unstructured region upstream of the α-helix. This indicates that the interaction site identified here by peptide spot array is not a canonical AKAP motif. However, as binding was confirmed in four independent experiments, the V-ATPase might interact with PKA in a non-canonical manner. The interaction site should be further analyzed, for example by alanine scan, to identify amino acids crucial for binding.

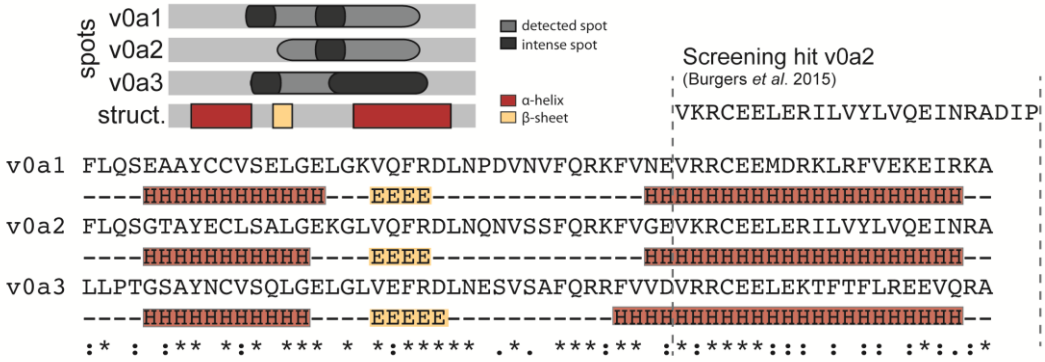

Figure 28: Potential PKA interaction site of V-ATPase subunits v0a1/v0a2/v0a3. Shown are schemes of the PKA-v0a interaction site, which was identified by peptide spot array overlaid with radioactively labeled PKA-RIIα (see results chapter **Figure 23**). Detected spots are depicted in mid grey, intense binding is highlighted with dark grey. Shown in the scheme and in alignment with the protein sequences is the secondary structure as predicted by the online service Jpred (http://www.compbio.dundee.ac.uk/jpred/).

4.4 Hydrophilic anchor points modulate the AKAP-PKA interaction

A new crystal structure of the PKA-D/D domain in complex with an extended AKAP18 AKB domain revealed polar anchor points that stabilize the binding of the amphipathic AKAP helix (Götz *et al.* 2016). These anchor points potentially support docking of the AKAP into the D/D domain with the correct orientation. Sequence alignment of several AKAPs with RI, RII or dual specificity revealed a different anchor point pattern for RI or RII specific interaction. For RII-specific AKAPs, anchor points II and III were identified C-terminally to the hydrophobic amino acids of patch five of the AKAP helix, whereas the RI-specific anchor points II and III lie in between patches three and five (Figure 24 B and Götz *et al.* (2016)). However, a shift of the helical register for RI binding, compared to RII binding, moves anchor point III of RI binders in the same location as anchor point II in the RII interaction (Sarma *et al.* 2010, Götz *et al.* 2016). This indicates that the stabilizing function of this anchor point is similar in RI and RII binding AKAPs. The characterization of the anchor points in a cellular context was part of this thesis. Therefore, expression constructs of an RII- and RI-specific AKAP and of one with dual specificity were generated with and without substitutions of the anchor points for alanine, and their ability to bind PKA regulatory subunits investigated by cAMP pulldown and

co-immunoprecipitation. Mutation of the three anchor points of the RII-specific AKAP18γ reduced the binding to RIIα, which was, however, not statistically significant. In contrast, binding to RIIβ was significantly decreased. This is potentially due to the lower affinity of AKAP18γ to RIIβ, compared to RIIα, which allows easier interference with RIIβ than RIIα. This difference could be exploited for the specific targeting of the AKAP18γ-RIIβ interaction by disruptor peptides or small molecules. For example in the forebrain, RIIβ is about 10 times more abundant than the RIIα isoform (Walker-Gray *et al.* 2017). Breast and prostate cancer also show increased expression of RIIβ, whereas RIIα expression is equally high in various tumor tissues (https://www.proteinatlas.org/).

Substitution of the two anchor points for alanine identified significantly decreased RIα binding of the RI-specific smAKAP. For the dual specific AKAP1, two sets of anchor point mutations were introduced that should interfere with RII- or RI-binding. Detecting the co-precipitation of RIIα with AKAP1-FLAG revealed reduced binding to the mutant AKAP1, which has all three RII-specific anchor sites substituted for alanine, compared to AKAP1-WT. Preliminary data indicate that mutation of the RI-specific anchor points does not interfere with RIIα binding. This suggests that manipulation of subunit-specific anchor points may allow specific disruption of the AKAP1-RI or AKAP1-RII interaction. Investigation of the RI binding ability of WT and mutant AKAP1 was not possible, due to the lack of RIα and RIβ antibodies that detect the co-precipitation of RI subunits with AKAP1.

The results of the co-precipitation studies prove that the identified polar anchor points are crucial components of AKAP-PKA interactions.

5. OUTLOOK

This thesis highlights interesting new players involved in the control of AQP2 translocation in renal principal cells that act at the interface of cAMP signaling and metabolic regulation. Local metabolic control of the vesicle transport process might be regulated by V-ATPase through the organization of a metabolic sensor complex involving AMPK on AQP2-bearing vesicles. It remains to be investigated, whether the components of the sensor complex on lysosomes, such as aldolase and axin (Zhang *et al.* 2017), are also part of the complex on AQP2-bearing vesicles.

The putative AKAP function of the V-ATPase subunit v0a observed in this thesis might tether PKA to the complex. In that way, the main effector of cAMP signaling would be linked to the regulation of metabolite sensing. Further investigations are required to understand the role of PKA phosphorylation in the local metabolic control of AQP2-bearing vesicles and how this function might translate into AQP2 trafficking.

A putative PKA substrate is the pentose-phosphate pathway enzyme G6PDH, which was also identified on AQP2-bearing vesicles. In order to evaluate the impact of G6PDH on AQP2 trafficking, knockdown by RNA interference and assessment of the AQP2 translocation by immunofluorescence microscopy will reveal whether down-regulation of G6PDH increases AQP2 plasma membrane localization. As the phosphorylation by PKA decreases G6PDH activity in diabetic kidneys (Xu *et al.* 2005), it would be of interest whether this inhibition also occurs on AQP2-bearing vesicles. The measurement of G6PDH enzyme activity in MCD4 cells, with and without FSK stimulation, or even the local activity on isolated vesicles could be sought. In addition, G6PDH activity is linked to the synthesis of isoprenoids through the regulation of HMG-CoA reductase activity by NADPH. Activation of RhoA by isoprenylation interferes with AQP2 trafficking (Klussmann *et al.* 2001, Li *et al.* 2011). These observations point to a possible novel role of G6PDH in the regulation of AQP2 trafficking by control of RhoA activity, but require further experimental assessment.

In addition, the role of AMPK activity in AQP2 trafficking should be elucidated. For example, activation of AMPK by AICAR or inhibition of AMPK by dorsomorphin could be employed to study the effect of AMPK activity on AQP2 localization in the cell models MCD4 and IMCD cells. A similar approach would be the overexpression or knockdown of AMPK, which could be performed with MCD4 cells.

The novel molecular pathways and regulatory proteins for the control of AQP2 trafficking identified in this thesis might support the development of pharmacological agents that target AQP2 localization for therapeutic purposes, e.g. for the treatment of water balance disorders as nephrogenic diabetes insipidus or for the reduction of water load in heart failure patients.

APPENDIX

I. Supplemental material and methods

I.1 Supplemental material

Table 21: Supplemental reagents

Reagent	Supplier, Article number (#)
Bafilomycin A1	Sigma-Aldrich, #B1793
Nocodazole	Sigma-Aldrich, #M1404
Taxol/ Paclitaxel	Calbiochem, #580556

Table 22: Supplemental antibodies

Primary antibody	Application	Species	Supplier, Article number (#)
β-tubulin	WB	rabbit	Cell Signaling Technology, #2128
γ-tubulin	WB	rabbit	Abcam, #ab179503
GFP	IP	mouse	Takara Clontech, Living colors, #JL-8
GFP	WB	rabbit	GeneTex, #GTX113617
HA-tag	WB	mouse	BioLegend, #MMS-101P
p84	WB	mouse	GeneTex, #GTX70220

Table 23: Primer for insertion of a HA-tag into RIIα-pEGFP-N1

Target gene	Modification	Orientation	Sequence
PKA-RIIα (pEGFP-N1)	**AgeI site** HA-tag	fwd	TGTAC AAGCA TTCGA GAGGC
		rev	CATTA T**ACCG GT**CTA AGCGT AATCT GGAAC ATCGT ATGGG TATGG ATCCC GCTGC CC

I.2 Supplemental methods

I.2.1 Cloning of mammalian expression plasmids

Human LDHA cDNA was ordered as GeneArt Strings fragment (Life Technologies) flanked by NheI and XhoI restriction sites that were used for insertion into the pCMV6-entry vector (2.2.1.1, for sequence see III.8). RIIα was previously cloned into the pEGFP-N1 vector (Takara Clontech, Saint-Germain-en-Laye, FR) by a member of the lab. The construct was modified to obtain a HA-tagged version as follows: A fragment of RIIα containing an ApaI restriction site was amplified by PCR (2.2.1.3) using an elongated reverse primer that carried the sequence for the HA-tag and a AgeI restriction site (Table 23). After DpnI digest, the

PCR product and the RIIα-pEGFP plasmid were cut with the restriction enzymes ApaI (New England BioLabs, US, #R0114S) and AgeI (New England BioLabs, US, #R0552S), purified using the NucleoSpin® Extract II kit (Macherey-Nagel) and ligated as described in 2.2.1.2.

I.2.2 GFP-IP

GFP-IP was performed as described for endogenous protein (2.2.3.8 A).

I.2.3 HA-IP

For the precipitation of HA-tagged overexpressed protein, anti-HA magnetic beads (Pierce, Thermo Fisher Scientific, #88836) were washed twice with TBS-T and incubated with cell lysates for 2 h. Then, beads were washed three times with TBS-T, followed by one washing step with *A. dest*. Proteins were eluted from the beads using 0.1 M glycine buffer, pH 2.5 and neutralized with 1 M Tris, pH 10.6. In preparation for Western blotting, Lämmli sample buffer was added and samples incubated for 8 min at 95 °C.

I.2.4 Extraction of polymerized tubulin

Tubulin extraction was performed according to Vossenkamper *et al.* (2007). Briefly, cells were washed with PBS, lysed with tubulin extraction buffer [20 mM PIPES (pH 6.8), 140 mM NaCl, 1 mM $MgCl_2$, 1 mM EGTA, 0.5 % Nonidet P-40 (NP40), 0.5 mM PMSF, 0.4 mM taxol, in *A. dest.*] and centrifuged at 13.000 x g for 10 min at RT to separate the NP40-insoluble polymerized tubulin (pellet) from its monomeric form (supernatant). In preparation for Western blotting, Lämmli sample buffer was added to the pellets and samples incubated for 8 min at 95 °C.

II. Supplemental results

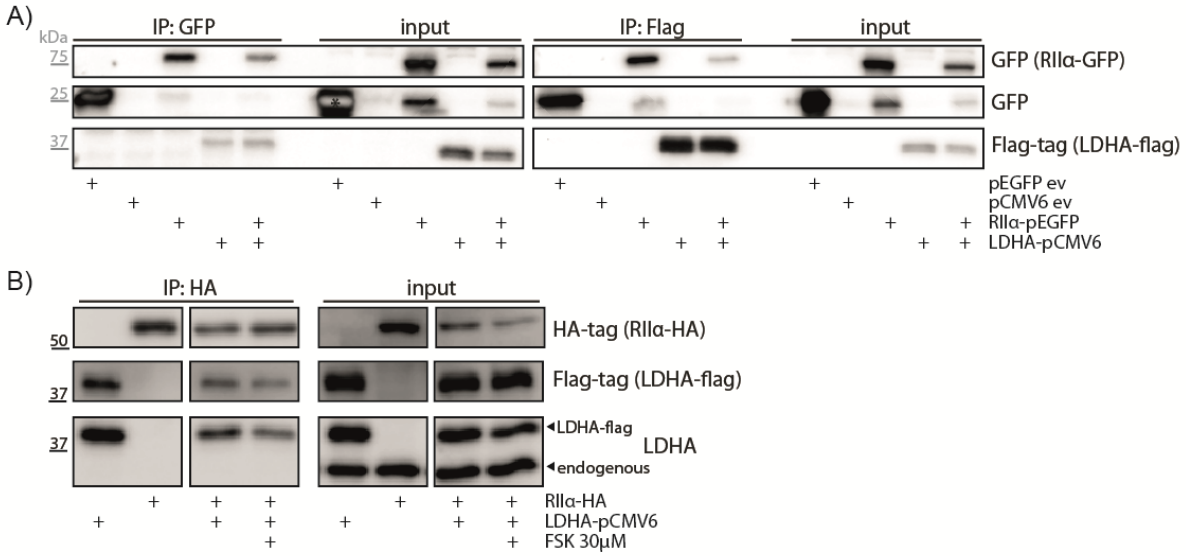

Figure 29: Double overexpression system to study the LDHA-PKA interaction. A) Overexpression of empty vector controls for GFP (pEGFP) or Flag (pCMV6), GFP-tagged RIIα, Flag-tagged LDHA or the combination of RIIα-GFP and LDHA-Flag in HEK cells, followed by GFP- and Flag-IP. Western blot detection shows efficient precipitation of GFP and RIIα-GFP and co-precipitation of LDHA-flag after double overexpression. However, the flag-tagged construct also co-precipitates with the GFP-antibody in the control condition of only LDHA-flag expression. Vice versa, RIIα-GFP co-precipitates with Flag-IP in the double overexpression setting, but also with only RIIα-GFP being expressed. B) Overexpression of HA-tagged RIIα, LDHA-flag, both in combination with or without FSK stimulation in HEK cells, followed by HA-IP. LDHA-flag co-precipitates with HA-IP in control conditions (only LDHA-flag expressed) and after co-expression with RIIα-HA.

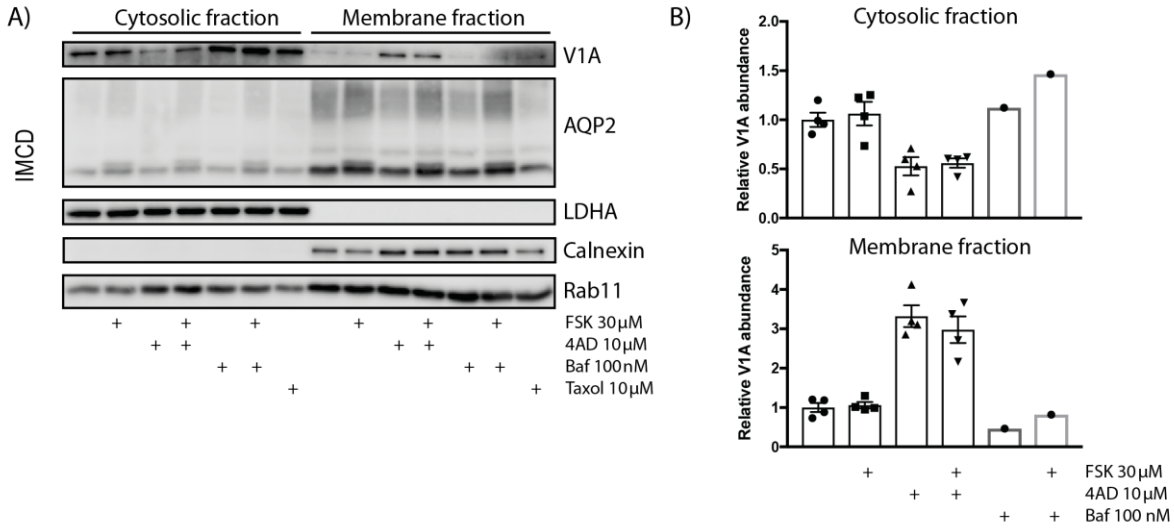

Figure 30: V-ATPase inhibition by 4AD, but not BafA1 favors V-ATPase assembly. A) Subcellular differential detergent fractionation of IMCD cells shows increased V-ATPase V1 association with membranes upon treatment with 10 µM 4AD for 45 min, but not with Bafilomycin A1 (Baf, 100 nM, 45 min), indicating that V-ATPase inhibition by 4AD induces subunit assembly, whereas inhibition by BafA1 does not modulate it. B) Quantitative results of four independent experiments for FSK and 4AD stimulation and one data point for BafA1 treatment with or without FSK stimulation. Error bars indicate SEM.

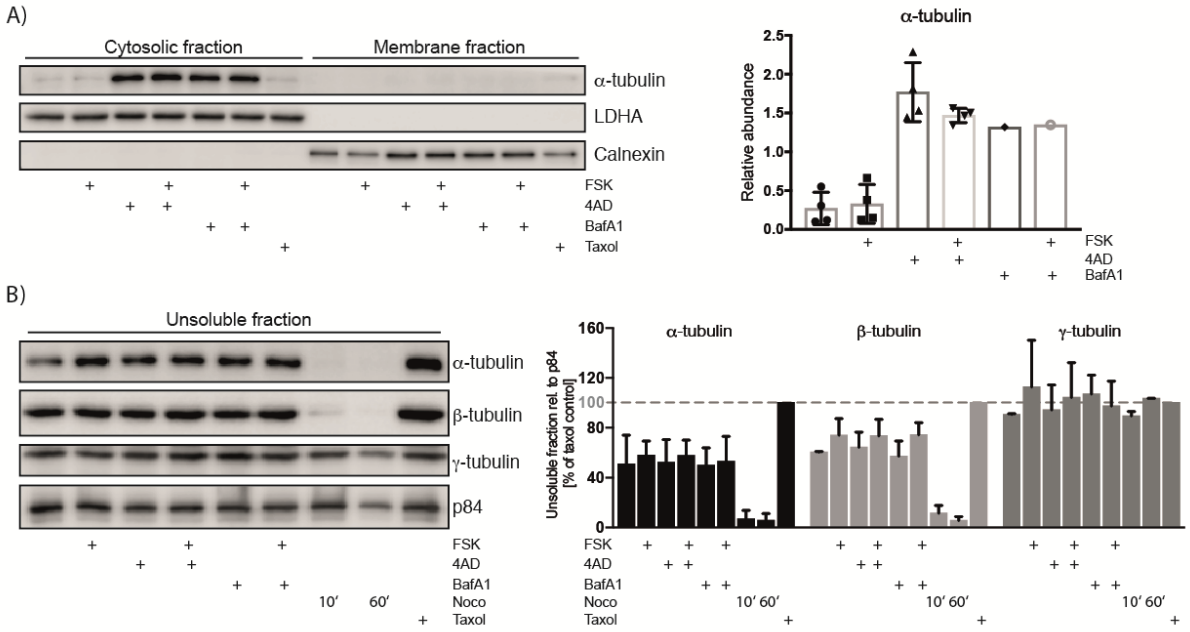

Figure 31: V-ATPase inhibition by 4AD or BafA1 increases α-tubulin in the cytosolic fraction, which is not due to decreased tubulin polymerization. A) Subcellular differential detergent fractionation of IMCD cells shows increased cytosolic pools of α-tubulin after stimulation with FSK (30 μM, 30 min) and/or the V-ATPase inhibitors 4AD (10 μM, 45 min) and BafA1 (100 nM, 45 min). LDHA was used as a cytosolic marker, Calnexin as a membrane marker. Right: Quantitative results of four independent experiments for FSK and 4AD stimulation and one data point for BafA1 treatment with and without FSK stimulation. B) Insoluble fraction of tubulin extraction corresponds to polymerized α-/β-tubulin. Treatment of the cells with the microtubule-disrupting agent nocodazole (30 μM, 10 and 60 min) serves as a negative control. Taxol treatment (10 μM, 60 min) stabilizes microtubules and is used as a positive control. Right: Quantification of α-, β-, and γ- tubulin as percent of taxol control of two independent experiments. γ- tubulin does not assemble into microtubules and is only shown as control. Tubulin abundance in the insoluble pool was normalized to the nuclear matrix protein p84.

III. Plasmid sequences

Inserted genes of interest are given in bold; tags are underlined. All genes are cloned into the vector pCMV6-entry, so that only once the whole sequence is given. Following sequences start from the CMV promoter and end after the stop codon.

III.1 AKAP18γ-WT in pCMV6-entry

AACAAAATATTAACGCTTACAATTTCCATTCGCCATTCAGGCTGCGCAACTGTTGGGAAGGGCGATCGGTGCGGGCCTCT
TCGCTATTACGCCAGCTGGCGAAAGGGGGATGTGCTGCAAGGCGATTAAGTTGGGTAACGCCAGGGTTTTCCCAGTCACG
ACGTTGTAAAACGACGGCCAGTGCCAAGCTGATCTATACATTGAATCAATATTGGCAATTAGCCATATTAGTCATTGGTT
ATATAGCATAAATCAATATTGGCTATTGGCCATTGCATACGTTGTATCTATATCATAATATGTACATTTATATTGGCTCA
TGTCCAATATGACCGCCATGTTGACATTGATTATTGACTAGTTATTAATAGTAATCAATTACGGGGTCATTAGTTCATAG
CCCATATATGGAGTTCCGCGTTACATAACTTACGGTAAATGGCCCGCCTGGCTGACCGCCCAACGACCCCCGCCCATTGA
CGTCAATAATGACGTATGTTCCCATAGTAACGCCAATAGGGACTTTCCATTGACGTCAATGGGTGGAGTATTTACGGTAA
ACTGCCCACTTGGCAGTACATCAAGTGTATCATATGCCAAGTCCGCCCCCTATTGACGTCAATGACGGTAAATGGCCCGC
CTGGCATTATGCCCAGTACATGACCTTACGGGACTTTCCTACTTGGCAGTACATCTACGTATTAGTCATCGCTATTACCA
TGGTGATGCGGTTTTGGCAGTACACCAATGGGCGTGGATAGCGGTTTGACTCACGGGGATTTCCAAGTCTCCACCCCATT
GACGTCAATGGGAGTTTGTTTTGGCACCAAAATCAACGGGACTTTCCAAAATGTCGTAATAACCCCGCCCCGTTGACGCA
AATGGGCGGTAGGCGTGTACGGTGGGAGGTCTATATAAGCAGAGCTCGTTTAGTGAACCGTCAGAATTTTGTAATACGAC
TCACTATAGGGCGGCCGGGAATTCGTCGACTGGATCCGGTACCGAGGAGATCTGCCGCCGCGATCGCCGGCGCGCCAGAT
CTCAAGCTTAACTAGctagc**ATGGAGCGCCCCGAAGCGGGAGGAATTAATTCCAATGAGTGTGAAAATGTATCAAGAAAA**
AAGAAAATGTCAGAGGAATTTGAAGCCAATACTATGGATTCTCTGGTAGACATGCCATTTGCTACTGTAGATATTCAGGA
TGACTGTGGAATCACTGATGAACCTCAAATAAATTTGAAGAGAAGTCAAGAAAATGAATGGGTCAAGAGTGATCAAGTAA
AGAAGAGGAAAAAAAAGAGAAAAGATTATCAACCCAACTATTTCCTGTCCATTCCAATCACCAACAAAGAGATTATAAAA
GGAATTAAGATCCTGCAGAATGCAATAATACAACAAGATGAGCGACTGGCCAAAGCAATGGTCAGTGATGGTTCCTTTCA
TATTACCCTGCTGGTGATGCAATTATTAAATGAAGATGAAGTAAACATTGGTATTGATGCTCTTTTGGAATTGAAACCAT
TCATAGAAGAACTCCTCCAGGGAAAACATTTGACTTTGCCCTTTCAAGGGATTGGTACTTTTGGAAATCAGGTTGGATTT
GTGAAGCTGGCAGAAGGAGATCATGTAAACTCACTTTTGGAGATAGCAGAGACTGCAAATAGGACATTTCAAGAAAAAGG
CATCCTGGTAGGAGAGAGCAGAAGTTTTAAACCTCATTTGACCTTCATGAAGTTGTCAAAATCACCGTGGCTCCGTAAGA
ATGGAGTGAAAAAAATAGATCCTGATTTATATGAAAAGTTTATCAGTCACAGATTTGGAGAAGAAATATTATATCGCATA
GATCTTTGCTCCATGCTGAAGAAAAAACAAAGTAATGGTTATTATCACTGTGAATCTTCCATTGTGATTGGTGAAAAGAA
CGGAGGGGAGCCCGATGACGCTGAACTAGTAAGGCTCAGTAAGAGGCTGGTGGAGAACGCGGTGCTCAAGGCTGTCCAGC
AGTATCTGGAGGAAACACAGAATAAAAACAAGCCGGGGGAGGGGAGCTCTGTGAAAACCGAAGCAGCTGATCAGAATGGC
AATGACAATGAGAACAACAGGAAACtcgaGCAGAAACTCATCTCAGAAGAGGATCTGGCAGCAAATGATATCCTGGATTA
CAAGGATGACGACGATAAGGTTTAAACGGCCGGCCGCGGTCATAGCTGTTTCCTGAACAGATCCCGGGTGGCATCCCTGT
GACCCCTCCCCAGTGCCTCTCCTGGCCCTGGAAGTTGCCACTCCAGTGCCCACCAGCCTTGTCCTAATAAAATTAAGTTG
CATCATTTTGTCTGACTAGGTGTCCTTCTATAATATTATGGGGTGGAGGGGGGTGGTATGGAGCAAGGGGCAAGTTGGGA
AGACAACCTGTAGGGCCTGCGGGGTCTATTGGGAACCAAGCTGGAGTGCAGTGGCACAATCTTGGCTCACTGCAATCTCC
GCCTCCTGGGTTCAAGCGATTCTCCTGCCTCAGCCTCCCGAGTTGTTGGGATTCCAGGCATGCATGACCAGGCTCAGCTA
ATTTTTGTTTTTTTGGTAGAGACGGGGTTTCACCATATTGGCCAGGCTGGTCTCCAACTCCTAATCTCAGGTGATCTACC
CACCTTGGCCTCCCAAATTGCTGGGATTACAGGCGTGAACCACTGCTCCCTTCCCTGTCCTTCTGATTTTAAAATAACTA
TACCAGCAGGAGGACGTCCAGACACAGCATAGGCTACCTGGCCATGCCCAACCGGTGGGACATTTGAGTTGCTTGCTTGG
CACTGTCCTCTCATGCGTTGGGTCCACTCAGTAGATGCCTGTTGAATTGGGTACGCGGCCAGCGGCGAGCGGTATCAGCT
CACTCAAAGGCGGTAATACGGTTATCCACAGAATCAGGGGATAACGCAGGAAAGAACATGTGAGCAAAAGGCCAGCAAAA
GGCCAGGAACCGTAAAAAGGCCGCGTTGCTGGCGTTTTTCCATAGGCTCCGCCCCCCTGACGAGCATCACAAAAATCGAC
GCTCAAGTCAGAGGTGGCGAAACCCGACAGGACTATAAAGATACCAGGCGTTTCCCCCTGGAAGCTCCCTCGTGCGCTCT
CCTGTTCCGACCCTGCCGCTTACCGGATACCTGTCCGCCTTTCTCCCTTCGGGAAGCGTGGCGCTTTCTCATAGCTCACG
CTGTAGGTATCTCAGTTCGGTGTAGGTCGTTCGCTCCAAGCTGGGCTGTGTGCACGAACCCCCCGTTCAGCCCGACCGCT
GCGCCTTATCCGGTAACTATCGTCTTGAGTCCAACCCGGTAAGACACGACTTATCGCCACTGGCAGCAGCCACTGGTAAC
AGGATTAGCAGAGCGAGGTATGTAGGCGGTGCTACAGAGTTCTTGAAGTGGTGGCCTAACTACGGCTACACTAGAAGAAC
AGTATTTGGTATCTGCGCTCTGCTGAAGCCAGTTACCTTCGGAAAAAGAGTTGGTAGCTCTTGATCCGGCAAACAAACCA
CCGCTGGTAGCGGTGGTTTTTTTGTTTGCAAGCAGCAGATTACGCGCAGAAAAAAAGGATCTCAAGAAGATCCTTTGATC
TTTTCTACGGGGTCTGACGCTCAGTGGAACGAAAACTCACGTTAAGGGATTTTGGTCATGAGATTATCAAAAAGGATCTT
CACCTAGATCCTTTTAAATTAAAAATGAAGTTTTAAATCAATCTAAAGTATATATGAGTAACCTGAGGCTATGGCAGGGC
CTGCCGCCCCGACGTTGGCTGCGAGCCCTGGGCCTTCACCCGAACTTGGGGGGTGGGGTGGGGAAAAGGAAGAAACGCGG
GCGTATTGGCCCCAATGGGGTCTCGGTGGGGTATCGACAGAGTGCCAGCCCTGGGACCGAACCCCGCGTTTATGAACAAA
CGACCCAACACCGTGCGTTTTATTCTGTCTTTTTATTGCCGTCATAGCGCGGGTTCCTTCCGGTATTGTCTCCTTCCGTG
TTTCAGTTAGCCTCCCCCTAGGGTGGGCGAAGAACTCCAGCATGAGATCCCCGCGCTGGAGGATCATCCAGCCGGCGTCC
CGGAAAACGATTCCGAAGCCCAACCTTTCATAGAAGGCGGCGGTGGAATCGAAATCTCGTGATGGCAGGTTGGGCGTCGC
TTGGTCGGTCATTTCGAACCCCAGAGTCCCGCTCAGAAGAACTCGTCAAGAAGGCGATAGAAGGCGATGCGCTGCGAATC
GGGAGCGGCGATACCGTAAAGCACGAGGAAGCGGTCAGCCCATTCGCCGCCAAGCTCTTCAGCAATATCACGGGTAGCCA
ACGCTATGTCCTGATAGCGATCCGCCACACCCAGCCGGCCACAGTCGATGAATCCAGAAAAGCGGCCATTTTCCACCATG
ATATTCGGCAAGCAGGCATCGCCATGGGTCACGACGAGATCCTCGCCGTCGGGCATGCTCGCCTTGAGCCTGGCGAACAG
TTCGGCTGGCGCGAGCCCCTGATGCTCTTCGTCCAGATCATCCTGATCGACAAGACCGGCTTCCATCCGAGTACGTGCTC
GCTCGATGCGATGTTTCGCTTGGTGGTCGAATGGGCAGGTAGCCGGATCAAGCGTATGCAGCCGCCGCATTGCATCAGCC

ATGATGGATACTTTCTCGGCAGGAGCAAGGTGAGATGACAGGAGATCCTGCCCCGGCACTTCGCCCAATAGCAGCCAGTC
CCTTCCCGCTTCAGTGACAACGTCGAGCACAGCTGCGCAAGGAACGCCCGTCGTGGCCAGCCACGATAGCCGCGCTGCCT
CGTCTTGCAGTTCATTCAGGGCACCGGACAGGTCGGTCTTGACAAAAAGAACCGGGCGCCCCTGCGCTGACAGCCGGAAC
ACGGCGGCATCAGAGCAGCCGATTGTCTGTTGTGCCCAGTCATAGCCGAATAGCCTCTCCACCCAAGCGGCCGGAGAACC
TGCGTGCAATCCATCTTGTTCAATCATGCGAAACGATCCTCATCCTGTCTCTTGATCGATCTTTGCAAAAGCCTAGGCCT
CCAAAAAAGCCTCCTCACTACTTCTGGAATAGCTCAGAGGCCGAGGCGGCCTCGGCCTCTGCATAAATAAAAAAAATTAG
TCAGCCATGGGGCGGAGAATGGGCGGAACTGGGCGGAGTTAGGGGCGGGATGGGCGGAGTTAGGGGCGGGACTATGGTTG
CTGACTAATTGAGATGCATGCTTTGCATACTTCTGCCTGCTGGGGAGCCTGGGGACTTTCCACACCCTAACTGACACACATTCCACAG
TTGAGATGCATGCTTTGCATACTTCTGCCTGCTGGGGAGCCTGGGGACTTTCCACACCCTAACTGACACACATTCCACAG
CTGGTTCTTTCCGCCTCAGGACTCTTCCTTTTTCAATATTATTGAAGCATTTATCAGGGTTATTGTCTCATGAGCGGATA
CATATTTGAATGTATTTAGAAAAATAAACAAATAGGGGTTCCGCGCACATTTCCCCGAAAAGTGCCACCTGACGCGCCCT
GTAGCGGCGCATTAAGCGCGGCGGGTGTGGTGGTTACGCGCAGCGTGACCGCTACACTTGCCAGCGCCCTAGCGCCCGCT
CCTTTCGCTTTCTTCCCTTCCTTTCTCGCCACGTTCGCCGGCTTTCCCCGTCAAGCTCTAAATCGGGGGCTCCCTTTAGG
GTTCCGATTTAGTGCTTTACGGCACCTCGACCCCAAAAAACTTGATTAGGGTGATGGTTCACGTAGTGGGCCATCGCCCT
GATAGACGGTTTTTCGCCCTTTGACGTTGGAGTCCACGTTCTTTAATAGTGGACTCTTGTTCCAAACTGGAACAACACTC
AACCCTATCTCGGTCTATTCTTTTGATTTATAAGGGATTTTGCCGATTTCGGCCTATTGGTTAAAAAATGAGCTGATTTA
ACAAAAATTTAACGCGAATTTT

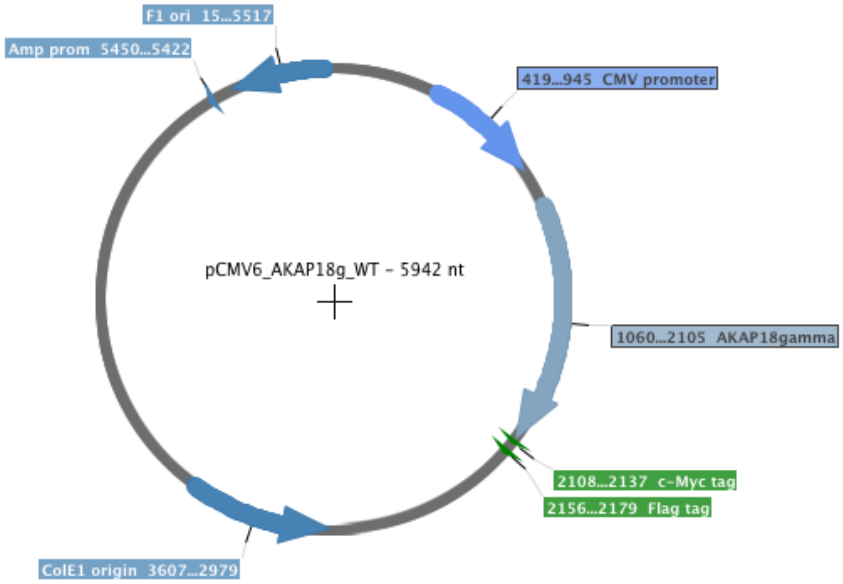

Figure 32: Vector map of AKAP18γ-WT-pCMV6

III.2 AKAP18γ-(D293A/Q314A/E318A) in pCMV6-entry

CGTTACATAACTTACGGTAAATGGCCCGCCTGGCTGACCGCCCAACGACCCCCGCCCATTGA
CGTCAATAATGACGTATGTTCCCATAGTAACGCCAATAGGGACTTTCCATTGACGTCAATGGGTGGAGTATTTACGGTAA
ACTGCCCACTTGGCAGTACATCAAGTGTATCATATGCCAAGTCCGCCCCCTATTGACGTCAATGACGGTAAATGGCCCGC
CTGGCATTATGCCCAGTACATGACCTTACGGGACTTTCCTACTTGGCAGTACATCTACGTATTAGTCATCGCTATTACCA
TGGTGATGCGGTTTTGGCAGTACACCAATGGGCGTGGATAGCGGTTTGACTCACGGGGATTTCCAAGTCTCCACCCCATT
GACGTCAATGGGAGTTTGTTTTGGCACCAAAATCAACGGGACTTTCCAAAATGTCGTAATAACCCCGCCCCGTTGACGCA
AATGGGCGGTAGGCGTGTACGGTGGGAGGTCTATATAAGCAGAGCTCGTTTAGTGAACCGTCAGAATTTTGTAATACGAC
TCACTATAGGGCGGCCGGGAATTCGTCGACTGGATCCGGTACCGAGGAGATCTGCCGCCGCGATCGCCGGCGCGCCAGAT
CTCAAGCTTAACTAGCTAGC**ATGGAGCGCCCCGAAGCGGGAGGAATTAATTCCAATGAGTGTGAAAATGTATCAAGAAAA**
AAGAAAATGTCAGAGGAATTTGAAGCCAATACTATGGATTCTCTGGTAGACATGCCATTTGCTACTGTAGATATTCAGGA
TGACTGTGGAATCACTGATGAACCTCAAATAAATTTGAAGAGAAGTCAAGAAAATGAATGGGTCAAGAGTGATCAAGTAA
AGAAGAGGAAAAAAAAGAGAAAAGATTATCAACCCAACTATTTCCTGTCCATTCCAATCACCAACAAAGAGATTATAAAA
GGAATTAAGATCCTGCAGAATGCAATAATACAACAAGATGAGCGACTGGCCAAAGCAATGGTCAGTGATGGTTCCTTTCA
TATTACCCTGCTGGTGATGCAATTATTAAATGAAGATGAAGTAAACATTGGTATTGATGCTCTTTTGGAATTGAAACCAT
TCATAGAAGAACTCCTCCAGGGAAAACATTTGACTTTGCCCTTTCAAGGGATTGGTACTTTTGGAAATCAGGTTGGATTT
GTGAAGCTGGCAGAAGGAGATCATGTAAACTCACTTTTGGAGATAGCAGAGACTGCAAATAGGACATTTCAAGAAAAAGG
CATCCTGGTAGGAGAGAGCAGAAGTTTTAAACCTCATTTGACCTTCATGAAGTTGTCAAAATCACCGTGGCTCCGTAAGA
ATGGAGTGAAAAAAATAGATCCTGATTTATATGAAAAGTTTATCAGTCACAGATTTGGAGAAGAAATATTATATCGCATA
GATCTTTGCTCCATGCTGAAGAAAAAACAAAGTAATGGTTATTATCACTGTGAATCTTCCATTGTGATTGGTGAAAAGAA
CGGAGGGGAGCCCGATGCCGCTGAACTAGTAAGGCTCAGTAAGAGGCTGGTGGAGAACGCGGTGCTCAAGGCTGTCCAGG
CGTATCTGGAGGCAACACAGAATAAAAACAAGCCGGGGGAGGGGAGCTCTGTGAAAACCGAAGCAGCTGATCAGAATGGC
AATGACAATGAGAACAACAGGAAACTCGAGCAGAAACTCATCTCAGAAGAGGATCTGGCAGCAAATGATATCCTGGATTA

CAAGGATGACGACGATAAGGTTTAA

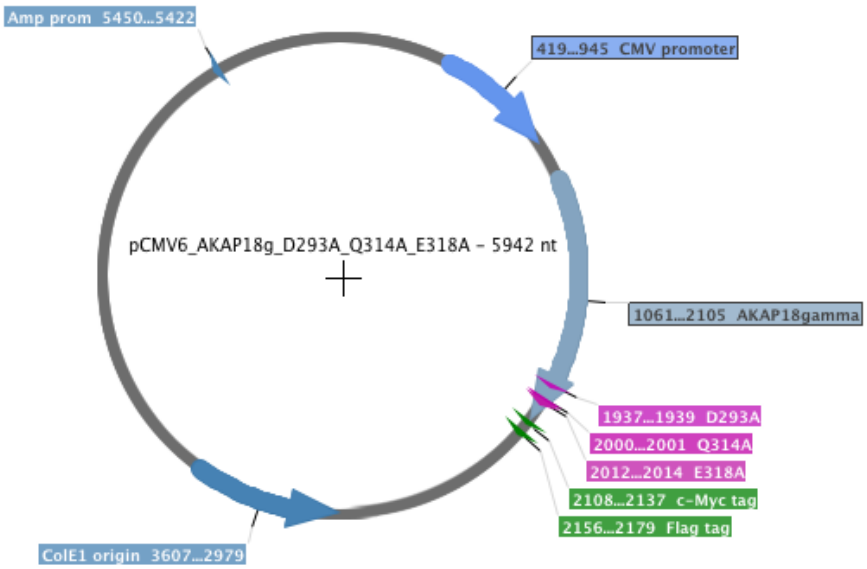

Figure 33: Vector map of AKAP18γ- (D293A/Q314A/E318A)-pCMV6

III.3 smAKAP-WT in pCMV6-entry

CGTTACATAACTTACGGTAAATGGCCCGCCTGGCTGACCGCCCAACGACCCCCGCCCATTGA
CGTCAATAATGACGTATGTTCCCATAGTAACGCCAATAGGGACTTTCCATTGACGTCAATGGGTGGAGTATTTACGGTAA
ACTGCCCACTTGGCAGTACATCAAGTGTATCATATGCCAAGTCCGCCCCCTATTGACGTCAATGACGGTAAATGGCCCGC
CTGGCATTATGCCCAGTACATGACCTTACGGGACTTTCCTACTTGGCAGTACATCTACGTATTAGTCATCGCTATTACCA
TGGTGATGCGGTTTTGGCAGTACACCAATGGGCGTGGATAGCGGTTTGACTCACGGGGATTTCCAAGTCTCCACCCCATT
GACGTCAATGGGAGTTTGTTTTGGCACCAAAATCAACGGGACTTTCCAAAATGTCGTAATAACCCCGCCCCGTTGACGCA
AATGGGCGGTAGGCGTGTACGGTGGGAGGTCTATATAAGCAGAGCTCGTTTAGTGAACCGTCAGAATTTTGTAATACGAC
TCACTATAGGGCGGCCGGGAATTCGTCGACTGGATCCGGTACCGAGGAGATCTGCCGCCGCGATCGCCGGCGCGCCAGAT
CTCAAGCTTAACTAGCTAGC**ATGGGCTGCATGAAATCAAAGCAAACTTTCCCATTTCCTACCATATATGAAGGTGAGAAG**
CAGCATGAGAGTGAAGAACCCTTTATGCCAGAAGAGAGATGTCTACCTAGGATGGCTTCTCCAGTTAATGTCAAAGAGGA
AGTGAAGGAACCTCCAGGGACCAATACTGTGATCTTGGAATATGCACACCGCCTGTCTCAGGATATCTTGTGTGATGCCT
TGCAGCAATGGGCATGCAATAACATCAAGTACCATGACATTCCATACATTGAGAGTGAGGGGCCTCTCGAGCAGAAACTC
ATCTCAGAAGAGGATCTGGCAGCAAATGATATCCTGGATTACAAGGATGACGACGATAAGGTTTAA

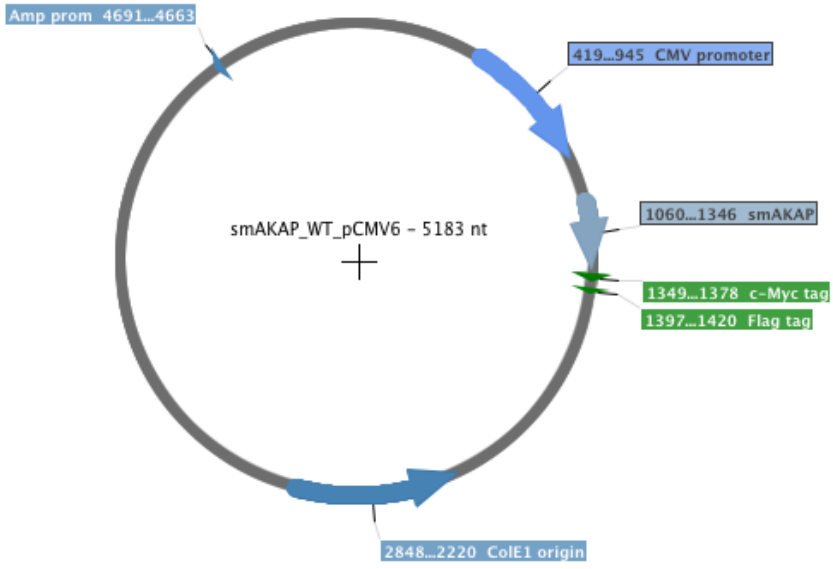

Figure 34: Vector map of smAKAP-WT-pCMV6

III.4 smAKAP-(D72A/Q76A) in pCMV6-entry

CGTTACATAACTTACGGTAAATGGCCCGCCTGGCTGACCGCCCAACGACCCCCGCCCATTGA
CGTCAATAATGACGTATGTTCCCATAGTAACGCCAATAGGGACTTTCCATTGACGTCAATGGGTGGAGTATTTACGGTAA
ACTGCCCACTTGGCAGTACATCAAGTGTATCATATGCCAAGTCCGCCCCCTATTGACGTCAATGACGGTAAATGGCCCGC
CTGGCATTATGCCCAGTACATGACCTTACGGGACTTTCCTACTTGGCAGTACATCTACGTATTAGTCATCGCTATTACCA
TGGTGATGCGGTTTTGGCAGTACACCAATGGGCGTGGATAGCGGTTTGACTCACGGGGATTTCCAAGTCTCCACCCCATT
GACGTCAATGGGAGTTTGTTTTGGCACCAAAATCAACGGGACTTTCCAAAATGTCGTAATAACCCCGCCCCGTTGACGCA
AATGGGCGGTAGGCGTGTACGGTGGGAGGTCTATATAAGCAGAGCTCGTTTAGTGAACCGTCAGAATTTTGTAATACGAC
TCACTATAGGGCGGCCGGGAATTCGTCGACTGGATCCGGTACCGAGGAGATCTGCCGCCGCGATCGCCGGCGCGCCAGAT
CTCAAGCTTAACTAGCTAGC**ATGGGCTGCATGAAATCAAAGCAAACTTTCCCATTTCCTACCATATATGAAGGTGAGAAG**
CAGCATGAGAGTGAAGAACCCTTTATGCCAGAAGAGAGATGTCTACCTAGGATGGCTTCTCCAGTTAATGTCAAAGAGGA
AGTGAAGGAACCTCCAGGGACCAATACTGTGATCTTGGAATATGCACACCGCCTGTCTCAGGATATCTTGTGTGCTGCCT
TGCAGGCATGGGCATGCAATAACATCAAGTACCATGACATTCCATACATTGAGAGTGAGGGGCCTCTCGAGCAGAAACTC
ATCTCAGAAGAGGATCTGGCAGCAAATGATATCCTGGATTACAAGGATGACGACGATAAGGTTTAA

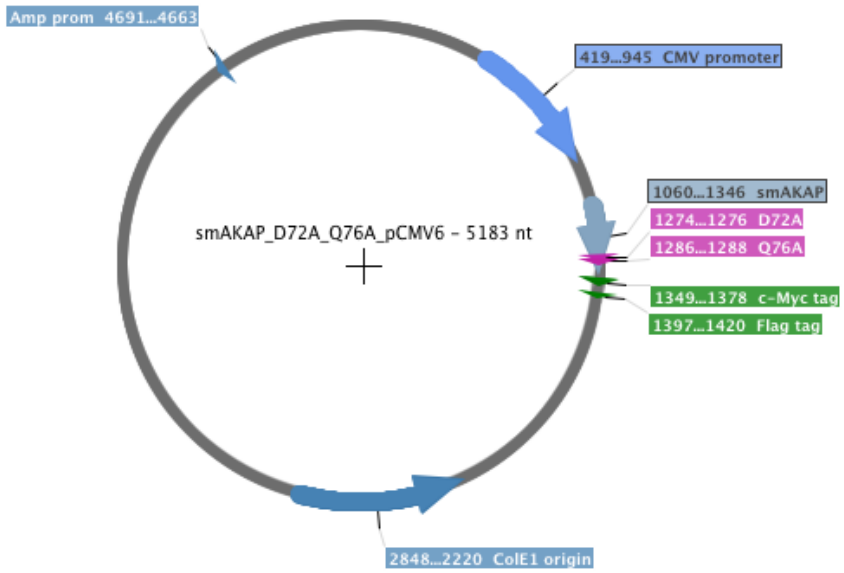

Figure 35: Vector map of smAKAP- (D72A/Q76A)-pCMV6

III.5 AKAP1-WT in pCMV6-entry

CGTTACATAACTTACGGTAAATGGCCCGCCTGGCTGACCGCCCAACGACCCCCGCCCATTGA
CGTCAATAATGACGTATGTTCCCATAGTAACGCCAATAGGGACTTTCCATTGACGTCAATGGGTGGAGTATTTACGGTAA
ACTGCCCACTTGGCAGTACATCAAGTGTATCATATGCCAAGTCCGCCCCCTATTGACGTCAATGACGGTAAATGGCCCGC
CTGGCATTATGCCCAGTACATGACCTTACGGGACTTTCCTACTTGGCAGTACATCTACGTATTAGTCATCGCTATTACCA
TGGTGATGCGGTTTTGGCAGTACACCAATGGGCGTGGATAGCGGTTTGACTCACGGGGATTTCCAAGTCTCCACCCCATT
GACGTCAATGGGAGTTTGTTTTGGCACCAAAATCAACGGGACTTTCCAAAATGTCGTAATAACCCCGCCCCGTTGACGCA
AATGGGCGGTAGGCGTGTACGGTGGGAGGTCTATATAAGCAGAGCTCGTTTAGTGAACCGTCAGAATTTTGTAATACGAC
TCACTATAGGGCGGCCGGGAATTCGTCGACTGGATCCGGTACCGAGGAGATCTGCCGCCGCGatCGCC**ATGGCAATCCAG**
TTCCGTTCGCTCTTCCCCTTGGCATTGCCTGGGATGCTGGCGCTCCTCGGCTGGTGGTGGTTTTTCTCTCGTAAAAAAGG
CCATGTCAGCAGCCATGATGAGCAGCAGGTGGAGGCTGGTGCTGTGCAGCTGAGGGCTGACCCTGCCATCAAGGAACCTC
TCCCCGTGGAAGACGTCTGTCCCAAAGTAGTGTCCACACCCCCCAGTGTCACAGAGCCTCCAGAAAAGGAACTGTCCACC
GTGAGCAAGCTGCCTGCAGAGCCCCCAGCATTGCTCCAGACACACCCACCTTGCCGAAGATCAGAGTCCTCGGGCATTCT
TCCTAACACCACAGACATGAGATTGCGACCAGGAACACGCAGAGATGACAGTACAAAGCTGGAGCTAGCCCTGACAGGTG
GTGAAGCCAAATCGATTCCTCTAGAGTGCCCCCTTTCATCCCCAAAGGGTGTACTATTCTCCAGCAAATCAGCTGAGGTG
TGTAAGCAAGATTCCCCCTTCAGCAGGGTGCCAAGGAAGGTCCAGCCAGGCTACCCCGTAGTCCCCGCAGAGAAGCGTAG
CTCTGGGGAGAGGGCAAGAGAGACAGGTGGGGCCGAAGGGACTGGTGATGCCGTGTTGGGGGAAAAGGTGCTTGAAGAAG
CTCTGTTGTCTCGGGAGCATGTCTTGGAATTGGAGAACAGCAAGGGCCCCAGCCTGGCCTCTTTAGAGGGGGAAGAAGAT
AAGGGGAAGAGCAGCTCATCCCAGGTGGTGGGGCCAGTGCAGGAGGAAGAGTATGTAGCAGAGAAGTTGCCAAGTAGGTT
CATCGAGTCGGCTCACACAGAGCTGGCAAAGGACGATGCGGCGCCAGCACCCCCAGTCGCAGACGCCAAAGCCCAGGATA
GAGGTGTCGAGGGAGAACTGGGCAATGAGGAGAGCTTGGATAGAAATGAGGAGGGCTTGGATAGAAATGAGGAGGGCTTG
GATAGAAATGAGGAGAGCTTGGATAGAAATGAGGAGGGCTTGGATAGAAATGAGGAGATTAAGCGGGCTGCCTTCCAGAT
AATCTCCCAAGTGATCTCAGAAGCAACCGAACAGGTGCTGGCCACCACGGTTGGCAAGGTTGCAGGTCGTGTGTGTCAGG

CCAGTCAGCTCCAAGGGCAGAAGGAAGAGAGCTGTGTCCCAGTTCACCAGAAAACTGTCTTGGGCCCAGACACTGCGGAG
CCTGCCACAGCAGAGGCAGCTGTTGCCCCGCCGGATGCTGGCCTCCCCTTGCCAGGCCTACCAGCAGAGGGCTCACCACC
ACCAAAGACCTACGTGAGCTGCCTGAAGAGCCTTCTGTCCAGCCCCACCAAGGACAGTAAGCCAAATATCTCTGCACACC
ACATCTCCCTGGCCTCCTGCCTGGCACTGACCACCCCCAGTGAAGAGTTGCCGGACCGGGCAGGCATCCTGGTGGAAGAT
GCCACCTGTGTCACCTGCATGTCAGACAGCAGCCAAAGTGTCCCTTTGGTGGCTTCTCCAGGACACTGCTCAGATTCTTT
CAGCACTTCAGGGCTTGAAGACTCTTGCACAGAGACCAGCTCGAGCCCCAGGGACAAGGCCATCACCCCGCCACTGCCAG
AAAGTACTGTGCCCTTCAGCAATGGGGTGCTGAAGGGGGAGTTGTCAGACTTGGGGGCTGAGGATGGATGGACCATGGAT
GCGGAAGCAGATCATTCAGGAGGTTCTGACAGGAACAGCATGGATTCCGTGGATAGCTGTTGCAGTCTCAAGAAGACTGA
GAGCTTCCAAAATGCCCAGGCAGGCTCCAACCCTAAGAAGGTCGACCTCATCATCTGGGAGATCGAGGTGCCAAAGCACT
TAGTCGGTCGGCTAATTGGCAAGCAGGGGCGCTATGTGAGTTTTCTGAAGCAAACATCTGGTGCCAAGATCTACATTTCA
ACCCTGCCTTACACCCAGAGCGTCCAGATCTGCCACATAGAAGGCTCTCAACATCATGTAGACAAAGCGCTGAACTTGAT
TGGGAAGAAGTTCAAAGAGCTGAACCTCACCAATATCTACGCTCCCCCATTGCCTTCACTGGCACTGCCTTCTCTGCCGA
TGACATCCTGGCTCATGCTGCCTGATGGCATCACCGTGGAGGTCATTGTGGTCAACCAGGTCAATGCCGGGCACCTGTTC
GTGCAGCAGCACACACACCCTACCTTCCACGCGCTGCGCAGCCTCGACCAGCAGATGTACCTCTGTTACTCTCAGCCTGG
AATCCCCACCTTGCCCACCCCAGTGGAAATAACGGTCATCTGTGCCGCCCCTGGTGCGGACGGGGCCTGGTGGCGAGCCC
AAGTGGTTGCCTCCTACGAGGAGACCAACGAAGTGGAGATTCGATACGTGGACTACGGCGGATATAAGAGGGTGAAAGTA
GACGTGCTCCGGCAAATCAGGTCTGACTTTGTCACCCTGCCGTTTCAGGGAGCAGAAGTCCTTCTGGACAGTGTGATGCC
CCTGTCAGACGATGACCAGTTTTCACCGGAAGCAGATGCCGCCATGAGCGAGATGACGGGGAATACAGCACTGCTTGCTC
AGGTGACAAGTTACAGTCCAACTGGTCTTCCTCTGATTCAGCTGTGGAGTGTGGTTGGAGATGAAGTGGTGTTGATAAAC
CGGTCCCTGGTGGAGCGAGGCCTTGCCCAGTGGGTAGACAGCTACTACACAAGCCTTAcgcgTACGCGGCCGCTC<u>GAGCA</u>
<u>GAAACTCATCTCAGAAGAGGATCTG</u>GCAGCAAATGATATCCTG<u>GATTACAAGGATGACGACGATAAG</u>GTTTAA

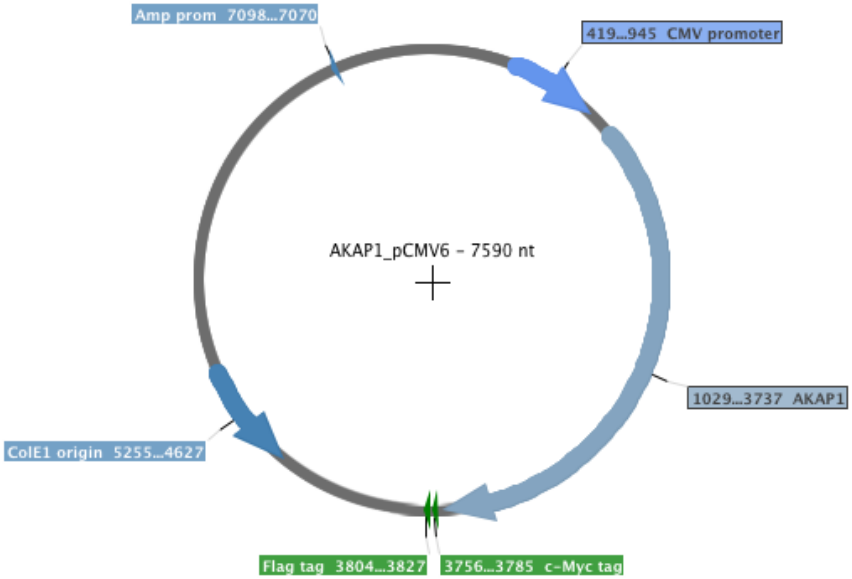

Figure 36: Vector map of AKAP1-WT-pCMV6

III.6 AKAP1-(N341A/Q362A/T366A) in pCMV6-entry

CGTTACATAACTTACGGTAAATGGCCCGCCTGGCTGACCGCCCAACGACCCCCGCCCATTGA
CGTCAATAATGACGTATGTTCCCATAGTAACGCCAATAGGGACTTTCCATTGACGTCAATGGGTGGAGTATTTACGGTAA
ACTGCCCACTTGGCAGTACATCAAGTGTATCATATGCCAAGTCCGCCCCCTATTGACGTCAATGACGGTAAATGGCCCGC
CTGGCATTATGCCCAGTACATGACCTTACGGGACTTTCCTACTTGGCAGTACATCTACGTATTAGTCATCGCTATTACCA
TGGTGATGCGGTTTTGGCAGTACACCAATGGGCGTGGATAGCGGTTTGACTCACGGGGATTTCCAAGTCTCCACCCCATT
GACGTCAATGGGAGTTTGTTTTGGCACCAAAATCAACGGGACTTTCCAAAATGTCGTAATAACCCCGCCCCGTTGACGCA
AATGGGCGGTAGGCGTGTACGGTGGGAGGTCTATATAAGCAGAGCTCGTTTAGTGAACCGTCAGAATTTTGTAATACGAC
TCACTATAGGGCGGCCGGGAATTCGTCGACTGGATCCGGTACCGAGGAGATCTGCCGCCGCGatCGCC**ATGGCAATCCAG**
TTCCGTTCGCTCTTCCCCTTGGCATTGCCTGGGATGCTGGCGCTCCTCGGCTGGTGGTGGTTTTTCTCTCGTAAAAAAGG
CCATGTCAGCAGCCATGATGAGCAGCAGGTGGAGGCTGGTGCTGTGCAGCTGAGGGCTGACCCTGCCATCAAGGAACCTC
TCCCCGTGGAAGACGTCTGTCCCAAAGTAGTGTCCACACCCCCCAGTGTCACAGAGCCTCCAGAAAAGGAACTGTCCACC
GTGAGCAAGCTGCCTGCAGAGCCCCCAGCATTGCTCCAGACACACCCACCTTGCCGAAGATCAGAGTCCTCGGGCATTCT
TCCTAACACCACAGACATGAGATTGCGACCAGGAACACGCAGAGATGACAGTACAAAGCTGGAGCTAGCCCTGACAGGTG
GTGAAGCCAAATCGATTCCTCTAGAGTGCCCCCTTTCATCCCCAAAGGGTGTACTATTCTCCAGCAAATCAGCTGAGGTG
TGTAAGCAAGATTCCCCCTTCAGCAGGGTGCCAAGGAAGGTCCAGCCAGGCTACCCCGTAGTCCCCGCAGAGAAGCGTAG
CTCTGGGGAGAGGGCAAGAGAGACAGGTGGGGCCGAAGGGACTGGTGATGCCGTGTTGGGGGAAAAGGTGCTTGAAGAAG

CTCTGTTGTCTCGGGAGCATGTCTTGGAATTGGAGAACAGCAAGGGCCCCAGCCTGGCCTCTTTAGAGGGGGAAGAAGAT
AAGGGGAAGAGCAGCTCATCCCAGGTGGTGGGGCCAGTGCAGGAGGAAGAGTATGTAGCAGAGAAGTTGCCAAGTAGGTT
CATCGAGTCGGCTCACACAGAGCTGGCAAAGGACGATGCGGCGCCAGCACCCCCAGTCGCAGACGCCAAAGCCCAGGATA
GAGGTGTCGAGGGAGAACTGGGCAATGAGGAGAGCTTGGATAGAAATGAGGAGGGCTTGGATAGAAATGAGGAGGGCTTG
GATAGAAATGAGGAGAGCTTGGATAGAAATGAGGAGGGCTTGGATAGAGCTGAGGAGATTAAGCGGGCTGCCTTCCAGAT
AATCTCCCAAGTGATCTCAGAAGCAACTGAAGCGGTGCTGGCCGCCACGGTTGGCAAGGTTGCAGGTCGTGTGTGTCAGG
CCAGTCAGCTCCAAGGGCAGAAGGAAGAGAGCTGTGTCCCAGTTCACCAGAAAACTGTCTTGGGCCCAGACACTGCGGAG
CCTGCCACAGCAGAGGCAGCTGTTGCCCCGCCGGATGCTGGCCTCCCCTTGCCAGGCCTACCAGCAGAGGGCTCACCACC
ACCAAAGACCTACGTGAGCTGCCTGAAGAGCCTTCTGTCCAGCCCCACCAAGGACAGTAAGCCAAATATCTCTGCACACC
ACATCTCCCTGGCCTCCTGCCTGGCACTGACCACCCCCAGTGAAGAGTTGCCGGACCGGGCAGGCATCCTGGTGGAAGAT
GCCACCTGTGTCACCTGCATGTCAGACAGCAGCCAAAGTGTCCCTTTGGTGGCTTCTCCAGGACACTGCTCAGATTCTTT
CAGCACTTCAGGGCTTGAAGACTCTTGCACAGAGACCAGCTCGAGCCCCAGGGACAAGGCCATCACCCCGCCACTGCCAG
AAAGTACTGTGCCCTTCAGCAATGGGGTGCTGAAGGGGGAGTTGTCAGACTTGGGGGCTGAGGATGGATGGACCATGGAT
GCGGAAGCAGATCATTCAGGAGGTTCTGACAGGAACAGCATGGATTCCGTGGATAGCTGTTGCAGTCTCAAGAAGACTGA
GAGCTTCCAAAATGCCCAGGCAGGCTCCAACCCTAAGAAGGTCGACCTCATCATCTGGGAGATCGAGGTGCCAAAGCACT
TAGTCGGTCGGCTAATTGGCAAGCAGGGGCGCTATGTGAGTTTTCTGAAGCAAACATCTGGTGCCAAGATCTACATTTCA
ACCCTGCCTTACACCCAGAGCGTCCAGATCTGCCACATAGAAGGCTCTCAACATCATGTAGACAAAGCGCTGAACTTGAT
TGGGAAGAAGTTCAAAGAGCTGAACCTCACCAATATCTACGCTCCCCCATTGCCTTCACTGGCACTGCCTTCTCTGCCGA
TGACATCCTGGCTCATGCTGCCTGATGGCATCACCGTGGAGGTCATTGTGGTCAACCAGGTCAATGCCGGGCACCTGTTC
GTGCAGCAGCACACACACCCTACCTTCCACGCGCTGCGCAGCCTCGACCAGCAGATGTACCTCTGTTACTCTCAGCCTGG
AATCCCCACCTTGCCCACCCCAGTGGAAATAACGGTCATCTGTGCCGCCCCTGGTGCGGACGGGGCCTGGTGGCGAGCCC
AAGTGGTTGCCTCCTACGAGGAGACCAACGAAGTGGAGATTCGATACGTGGACTACGGCGGATATAAGAGGGTGAAAGTA
GACGTGCTCCGGCAAATCAGGTCTGACTTTGTCACCCTGCCGTTTCAGGGAGCAGAAGTCCTTCTGGACAGTGTGATGCC
CCTGTCAGACGATGACCAGTTTTCACCGGAAGCAGATGCCGCCATGAGCGAGATGACGGGGAATACAGCACTGCTTGCTC
AGGTGACAAGTTACAGTCCAACTGGTCTTCCTCTGATTCAGCTGTGGAGTGTGGTTGGAGATGAAGTGGTGTTGATAAAC
CGGTCCCTGGTGGAGCGAGGCCTTGCCCAGTGGGTAGACAGCTACTACACAAGCCTTAcgcgTACGCGGCCGCTCGAGCA
GAAACTCATCTCAGAAGAGGATCTGGCAGCAAATGATATCCTGGATTACAAGGATGACGACGATAAGGTTTAA

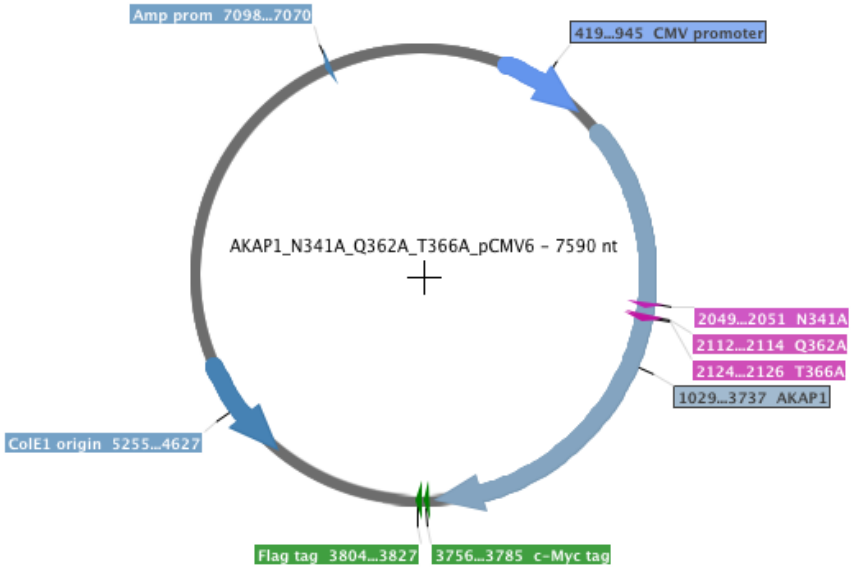

Figure 37: Vector map of AKAP1- (N341A/Q362A/T366A)-pCMV6

III.7 AKAP1-(N341A/Q354A/E358A) in pCMV6-entry

CGTTACATAACTTACGGTAAATGGCCCGCCTGGCTGACCGCCCAACGACCCCCGCCCATTGA
CGTCAATAATGACGTATGTTCCCATAGTAACGCCAATAGGGACTTTCCATTGACGTCAATGGGTGGAGTATTTACGGTAA
ACTGCCCACTTGGCAGTACATCAAGTGTATCATATGCCAAGTCCGCCCCCTATTGACGTCAATGACGGTAAATGGCCCGC
CTGGCATTATGCCCAGTACATGACCTTACGGGACTTTCCTACTTGGCAGTACATCTACGTATTAGTCATCGCTATTACCA
TGGTGATGCGGTTTTGGCAGTACACCAATGGGCGTGGATAGCGGTTTGACTCACGGGGATTTCCAAGTCTCCACCCCATT
GACGTCAATGGGAGTTTGTTTTGGCACCAAAATCAACGGGACTTTCCAAAATGTCGTAATAACCCCGCCCCGTTGACGCA
AATGGGCGGTAGGCGTGTACGGTGGGAGGTCTATATAAGCAGAGCTCGTTTAGTGAACCGTCAGAATTTTGTAATACGAC
TCACTATAGGGCGGCCGGGAATTCGTCGACTGGATCCGGTACCGAGGAGATCTGCCGCCGCGatCGCC**ATGGCAATCCAG**
TTCCGTTCGCTCTTCCCCTTGGCATTGCCTGGGATGCTGGCGCTCCTCGGCTGGTGGTGGTTTTTCTCTCGTAAAAAAGG
CCATGTCAGCAGCCATGATGAGCAGCAGGTGGAGGCTGGTGCTGTGCAGCTGAGGGCTGACCCTGCCATCAAGGAACCTC
TCCCCGTGGAAGACGTCTGTCCCAAAGTAGTGTCCACACCCCCCAGTGTCACAGAGCCTCCAGAAAAGGAACTGTCCACC
GTGAGCAAGCTGCCTGCAGAGCCCCCAGCATTGCTCCAGACACACCCACCTTGCCGAAGATCAGAGTCCTCGGGCATTCT
TCCTAACACCACAGACATGAGATTGCGACCAGGAACACGCAGAGATGACAGTACAAAGCTGGAGCTAGCCCTGACAGGTG

GTGAAGCCAAATCGATTCCTCTAGAGTGCCCCCTTTCATCCCCAAAGGGTGTACTATTCTCCAGCAAATCAGCTGAGGTG
TGTAAGCAAGATTCCCCCTTCAGCAGGGTGCCAAGGAAGGTCCAGCCAGGCTACCCCGTAGTCCCCGCAGAGAAGCGTAG
CTCTGGGGAGAGGGCAAGAGAGACAGGTGGGGCCGAAGGGACTGGTGATGCCGTGTTGGGGGAAAAGGTGCTTGAAGAAG
CTCTGTTGTCTCGGGAGCATGTCTTGGAATTGGAGAACAGCAAGGGCCCCAGCCTGGCCTCTTTAGAGGGGGAAGAAGAT
AAGGGGAAGAGCAGCTCATCCCAGGTGGTGGGGCCAGTGCAGGAGGAAGAGTATGTAGCAGAGAAGTTGCCAAGTAGGTT
CATCGAGTCGGCTCACACAGAGCTGGCAAAGGACGATGCGGCGCCAGCACCCCCAGTCGCAGACGCCAAAGCCCAGGATA
GAGGTGTCGAGGGAGAACTGGGCAATGAGGAGAGCTTGGATAGAAATGAGGAGGGCTTGGATAGAAATGAGGAGGGCTTG
GATAGAAATGAGGAGAGCTTGGATAGAAATGAGGAGGGCTTGGATAGAGCTGAGGAGATTAAGCGGGCTGCCTTCCAGAT
AATCTCCGCAGTGATCTCAGCAGCAACCGAACAGGTGCTGGCCACCACGGTTGGCAAGGTTGCAGGTCGTGTGTGTCAGG
CCAGTCAGCTCCAAGGGCAGAAGGAAGAGAGCTGTGTCCCAGTTCACCAGAAAACTGTCTTGGGCCCAGACACTGCGGAG
CCTGCCACAGCAGAGGCAGCTGTTGCCCCGCCGGATGCTGGCCTCCCCTTGCCAGGCCTACCAGCAGAGGGCTCACCACC
ACCAAAGACCTACGTGAGCTGCCTGAAGAGCCTTCTGTCCAGCCCCACCAAGGACAGTAAGCCAAATATCTCTGCACACC
ACATCTCCCTGGCCTCCTGCCTGGCACTGACCACCCCCAGTGAAGAGTTGCCGGACCGGGCAGGCATCCTGGTGGAAGAT
GCCACCTGTGTCACCTGCATGTCAGACAGCAGCCAAAGTGTCCCTTTGGTGGCTTCTCCAGGACACTGCTCAGATTCTTT
CAGCACTTCAGGGCTTGAAGACTCTTGCACAGAGACCAGCTCGAGCCCCAGGGACAAGGCCATCACCCCGCCACTGCCAG
AAAGTACTGTGCCCTTCAGCAATGGGGTGCTGAAGGGGGAGTTGTCAGACTTGGGGGCTGAGGATGGATGGACCATGGAT
GCGGAAGCAGATCATTCAGGAGGTTCTGACAGGAACAGCATGGATTCCGTGGATAGCTGTTGCAGTCTCAAGAAGACTGA
GAGCTTCCAAAATGCCCAGGCAGGCTCCAACCCTAAGAAGGTCGACCTCATCATCTGGGAGATCGAGGTGCCAAAGCACT
TAGTCGGTCGGCTAATTGGCAAGCAGGGGCGCTATGTGAGTTTTCTGAAGCAAACATCTGGTGCCAAGATCTACATTTCA
ACCCTGCCTTACACCCAGAGCGTCCAGATCTGCCACATAGAAGGCTCTCAACATCATGTAGACAAAGCGCTGAACTTGAT
TGGGAAGAAGTTCAAAGAGCTGAACCTCACCAATATCTACGCTCCCCCATTGCCTTCACTGGCACTGCCTTCTCTGCCGA
TGACATCCTGGCTCATGCTGCCTGATGGCATCACCGTGGAGGTCATTGTGGTCAACCAGGTCAATGCCGGGCACCTGTTC
GTGCAGCAGCACACACACCCTACCTTCCACGCGCTGCGCAGCCTCGACCAGCAGATGTACCTCTGTTACTCTCAGCCTGG
AATCCCCACCTTGCCCACCCCAGTGGAAATAACGGTCATCTGTGCCGCCCCTGGTGCGGACGGGGCCTGGTGGCGAGCCC
AAGTGGTTGCCTCCTACGAGGAGACCAACGAAGTGGAGATTCGATACGTGGACTACGGCGGATATAAGAGGGTGAAAGTA
GACGTGCTCCGGCAAATCAGGTCTGACTTTGTCACCCTGCCGTTTCAGGGAGCAGAAGTCCTTCTGGACAGTGTGATGCC
CCTGTCAGACGATGACCAGTTTTCACCGGAAGCAGATGCCGCCATGAGCGAGATGACGGGGAATACAGCACTGCTTGCTC
AGGTGACAAGTTACAGTCCAACTGGTCTTCCTCTGATTCAGCTGTGGAGTGTGGTTGGAGATGAAGTGGTGTTGATAAAC
CGGTCCCTGGTGGAGCGAGGCCTTGCCCAGTGGGTAGACAGCTACTACACAAGCCTTAcgcgTACGCGGCCGCTCGAGCA
GAAACTCATCTCAGAAGAGGATCTGGCAGCAAATGATATCCTGGATTACAAGGATGACGACGATAAGGTTTAA

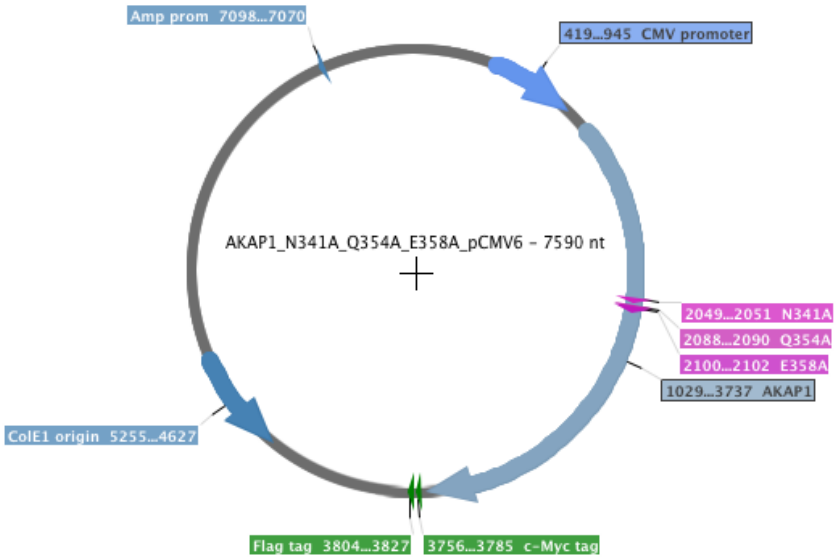

Figure 38: Vector map of AKAP1- (N341A/Q354A/E358A)-pCMV6

III.8 LDHA in pCMV6-entry

CGTTACATAACTTACGGTAAATGGCCCGCCTGGCTGACCGCCCAACGACCCCCGCCCATTGA
CGTCAATAATGACGTATGTTCCCATAGTAACGCCAATAGGGACTTTCCATTGACGTCAATGGGTGGAGTATTTACGGTAA
ACTGCCCACTTGGCAGTACATCAAGTGTATCATATGCCAAGTCCGCCCCCTATTGACGTCAATGACGGTAAATGGCCCGC
CTGGCATTATGCCCAGTACATGACCTTACGGGACTTTCCTACTTGGCAGTACATCTACGTATTAGTCATCGCTATTACCA
TGGTGATGCGGTTTTGGCAGTACACCAATGGGCGTGGATAGCGGTTTGACTCACGGGGATTTCCAAGTCTCCACCCCATT
GACGTCAATGGGAGTTTGTTTTGGCACCAAAATCAACGGGACTTTCCAAAATGTCGTAATAACCCCGCCCCGTTGACGCA
AATGGGCGGTAGGCGTGTACGGTGGGAGGTCTATATAAGCAGAGCTCGTTTAGTGAACCGTCAGAATTTTGTAATACGAC
TCACTATAGGGCGGCCGGGAATTCGTCGACTGGATCCGGTACCGAGGAGATCTGCCGCCGCGATCGCCGGCGCGCCAGAT
CTCAAGCTTAACTAGctagC**ATGGGCGAGCCCAGCGGCGGCTACACATATACCCAGACCAGCATCTTCCTGTTCCACGCC**
AAGATCCCTTTCGGCAGCAAGAGCAACATGGCCACCCTGAAGGACCAGCTGATCTACAACCTGCTGAAAGAGGAACAGAC

CCCCCAGAACAAGATCACCGTCGTGGGAGTGGGCGCCGTGGGAATGGCCTGTGCCATCAGCATCCTGATGAAGGACCTGG
CCGACGAGCTGGCCCTGGTGGACGTGATCGAGGACAAGCTGAAGGGCGAGATGATGGACCTGCAGCACGGCAGCCTGTTT
CTGCGGACCCCCAAGATCGTGTCCGGCAAGGACTACAACGTGACCGCCAACAGCAAGCTCGTGATCATCACCGCAGGCGC
CAGACAGCAGGAAGGCGAGAGCAGACTGAACCTGGTGCAGCGGAACGTGAACATCTTCAAGTTCATCATCCCCAACGTCG
TGAAGTACAGCCCCAACTGCAAGCTGCTGATCGTGTCTAACCCCGTGGACATCCTGACCTACGTGGCCTGGAAGATCAGC
GGCTTCCCCAAGAACAGAGTGATCGGCAGCGGCTGCAACCTGGACAGCGCCCGGTTCAGATACCTGATGGGCGAGAGACT
GGGCGTGCACCCTCTGTCTTGTCACGGCTGGGTGCTGGGAGAGCACGGCGATAGTTCTGTGCCTGTGTGGAGCGGCATGA
ACGTGGCAGGCGTGTCCCTGAAAACCCTGCACCCTGACCTGGGCACCGACAAGGACAAAGAACAGTGGAAAGAGGTGCAC
AAACAGGTGGTGGAAAGCGCCTACGAAGTGATCAAGCTGAAAGGCTACACCAGCTGGGCCATCGGCCTGAGCGTGGCAGA
TCTGGCCGAGAGCATCATGAAGAACCTGCGGAGAGTGCACCCCGTGTCCACCATGATCAAGGGCCTGTACGGAATCAAGG
ACGACGTGTTCCTGTCCGTGCCCTGCATCCTGGGCCAGAACGGCATCAGCGACCTCGTGAAAGTGACCCTGACCAGCGAG
GAAGAGGCCCGGCTGAAGAAGTCCGCCGATACCCTGTGGGGCATCCAGAAAGAGCTGCAGTTCCTCGAGCAGAAACTCAT
CTCAGAAGAGGATCTGGCAGCAAATGATATCCTGGATTACAAGGATGACGACGATAAGGTTTAA

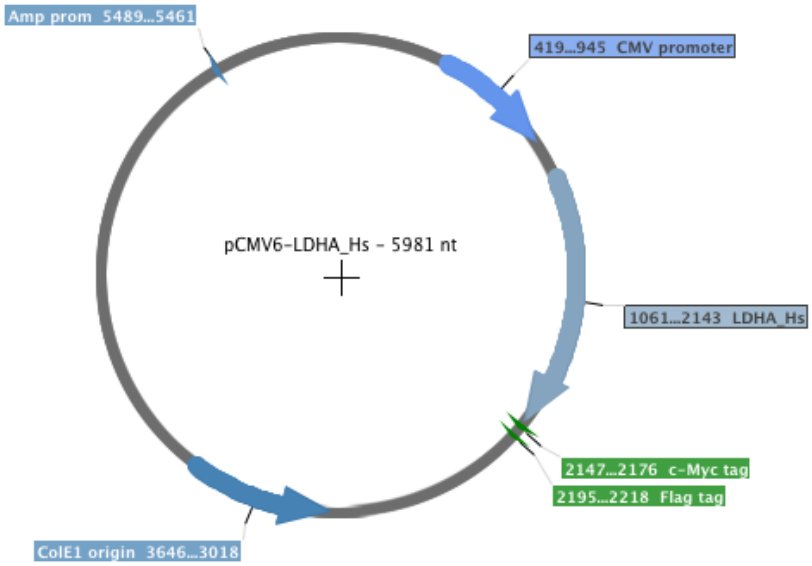

Figure 39: Vector map of LDHA-pCMV6

III.9 RIIα in pEGFP-N1

tagttattaatagtaatcaattacggggtcattagttcatagcccatatatggagttccgcgttacataacttacggtaa
atggcccgcctggctgaccgcccaacgacccccgcccattgacgtcaataatgacgtatgttcccatagtaacgccaata
gggactttccattgacgtcaatgggtggagtatttacggtaaactgcccacttggcagtacatcaagtgtatcatatgcc
aagtacgccccctattgacgtcaatgacggtaaatggcccgcctggcattatgcccagtacatgaccttatgggactttc
ctacttggcagtacatctacgtattagtcatcgctattaccatggtgatgcggttttggcagtacatcaatgggcgtgga
tagcggtttgactcacggggatttccaagtctccaccccattgacgtcaatgggagtttgttttggcaccaaaatcaacg
ggactttccaaaatgtcgtaacaactccgccccattgacgcaaatgggcggtaggcgtgtacggtgggaggtctatataa
gcagagctggtttagtgaaccgtcagatccgctagcgctaccggactcagatctcgaG**ATGAGCCACATCCAGATCCCGC**
CGGGGCTCACGGAGCTGCTGCAGGGCTACACGGTGGAGGTGCTGCGACAGCAGCCGCCTGACCTCGTCGAATTCGCAGTG
GAGTACTTCACCCGCCTGCGCGAGGCCCGCGCCCCAGCCTCAGTCCTGCCCGCCGCCACCCCACGCCAGAGCCTGGGCCA
CCCCCCGCCAGAACCCGGCCCGGACCGTGTCGCCGACGCCAAAGGGGACAGCGAGTCGGAGGAGGACGAGGACTTGGAAG
TTCCAGTTCCTAGCAGATTTAATAGACGAGTATCAGTCTGTGCTGAGACCTATAACCCTGATGAGGAAGAGGAAGATACA
GATCCAAGGGTGATTCATCCTAAAACTGATGAACAGAGATGCAGACTTCAGGAAGCTTGCAAAGATATTCTCCTTTTCAA
AAATCTTGATCAGGAACAGCTTTCTCAAGTTCTCGATGCCATGTTTGAAAGGATAGTCAAAGCTGATGAGCATGTCATTG
ACCAAGGAGATGATGGAGACAACTTTTATGTCATAGAACGGGGAACTTATGACATTTTAGTAACAAAAGATAATCAAACC
CGCTCTGTTGGTCAATATGACAACCGTGGCAGTTTTGGAGAACTAGCTCTGATGTACAACACCCCGAGAGCTGCTACCAT
TGTTGCTACCTCAGAAGGCTCCCTTTGGGGACTGGACCGGGTGACTTTTAGAAGAATCATAGTGAAAAATAATGCAAAGA
AGAGGAAGATGTTTGAATCATTTATTGAGTCTGTGCCCCTCCTTAAATCACTAGAGGTGTCAGAACGAATGAAGATTGTG
GATGTAATAGGAGAGAAGATCTATAAGGATGGAGAACGCATAATCACTCAGGGTGAAAAGGCTGATAGCTTTTACATCAT
AGAGTCTGGCGAAGTGAGCATCTTGATTAGAAGCAGGACTAAATCAAACAAGGATGGTGGGAACCAGGAGGTCGAGATTG
CCCGCTGCCATAAGGGGCAGTACTTTGGAGAGCTTGCCCTGGTCACCAACAAACCCAGAGCTGCCTCAGCTTATGCAGTT
GGAGATGTCAAATGCTTAGTTATGGATGTACAAGCATTCGAGAGGCTTCTGGGGCCCTGCATGGACATCATGAAGAGGAA
CATCTCACACTATGAGGAACAGCTGGTGAAGATGTTTGGCTCCAGCGTGGATCTGGGCAACCTCGGGCAGCGGgatccac
cggtcgccaccatggtgagcaagggcgaggagctgttcaccggggtggtgcccatcctggtcgagctggacggcgacgta
aacggccacaagttcagcgtgtccggcgagggcgagggcgatgccacctacggcaagctgaccctgaagttcatctgcac
caccggcaagctgcccgtgccctggcccaccctcgtgaccaccctgacctacggcgtgcagtgcttcagccgctaccccg
accacatgaagcagcacgacttcttcaagtccgccatgcccgaaggctacgtccaggagcgcaccatcttcttcaaggac
gacggcaactacaagacccgcgccgaggtgaagttcgagggcgacaccctggtgaaccgcatcgagctgaagggcatcga

cttcaaggaggacggcaacatcctggggcacaagctggagtacaactacaacagccacaacgtctatatcatggccgaca
agcagaagaacggcatcaaggtgaacttcaagatccgccacaacatcgaggacggcagcgtgcagctcgccgaccactac
cagcagaacaccccatcggcgacggccccgtgctgctgcccgacaaccactacctgagcacccagtccgccctgagcaa
agaccccaacgagaagcgcgatcacatggtcctgctggagttcgtgaccgccgccgggatcactctcggcatggacgagc
tgtacaagtaaagcggccgcgactctagatcataatcagccataccacatttgtagaggtttacttgctttaaaaaacc
tcccacacctcccccctgaacctgaaacataaaatgaatgcaattgttgttgttaacttgtttattgcagcttataatggt
tacaaataaagcaatagcatcacaaatttcacaaataaagcatttttttcactgcattctagttgtggtttgtccaaact
catcaatgtatcttaaggcgtaaattgtaagcgttaatattttgttaaaattcgcgttaaatttttgttaaatcagctca
ttttttaaccaataggccgaaatcggcaaaatcccttataaatcaaaagaatagaccgagatagggttgagtgttgttcc
agtttggaacaagagtccactattaaagaacgtggactccaacgtcaaagggcgaaaaaccgtctatcagggcgatggcc
cactacgtgaaccatcaccctaatcaagttttttggggtcgaggtgccgtaaagcactaaatcggaaccctaaagggagc
ccccgatttagagcttgacggggaaagccggcgaacgtggcgagaaaggaagggaagaaagcgaaaggagcgggcgctag
ggcgctggcaagtgtagcggtcacgctgcgcgtaaccaccacacccgccgcgcttaatgcgccgctacagggcgcgtcag
gtggcacttttcggggaaatgtgcgcggaacccctatttgtttatttttctaaatacattcaaatatgtatccgctcatg
agacaataaccctgataaatgcttcaataatattgaaaaaggaagagtcctgaggcggaaagaaccagctgtggaatgtg
tgtcagttagggtgtggaaagtccccaggctccccagcaggcagaagtatgcaaagcatgcatctcaattagtcagcaac
caggtgtggaaagtccccaggctccccagcaggcagaagtatgcaaagcatgcatctcaattagtcagcaaccatagtcc
cgcccctaactccgcccatcccgcccctaactccgcccagttccgcccattctccgccccatggctgactaatttttttt
atttatgcagaggccgaggccgcctcggcctctgagctattccagaagtagtgaggaggctttttggaggcctaggctt
ttgcaaagatcgatcaagagacaggatgaggatcgtttcgcatgattgaacaagatggattgcacgcaggttctccggcc
gcttgggtggagaggctattcggctatgactgggcacaacagacaatcggctgctctgatgccgccgtgttccggctgtc
agcgcaggggcgcccggttctttttgtcaagaccgacctgtccggtgccctgaatgaactgcaagacgaggcagcgcggc
tatcgtggctggccacgacgggcgttccttgcgcagctgtgctcgacgttgtcactgaagcgggaagggactggctgcta
ttgggcgaagtgccggggcaggatctcctgtcatctcaccttgctcctgccgagaaagtatccatcatggctgatgcaat
gcggcggctgcatacgcttgatccggctacctgcccattcgaccaccaagcgaaacatcgcatcgagcgagcacgtactc
ggatggaagccggtcttgtcgatcaggatgatctggacgaagagcatcaggggctcgcgccagccgaactgttcgccagg
ctcaaggcgagcatgcccgacggcgaggatctcgtcgtgacccatggcgatgcctgcttgccgaatatcatggtggaaaa
tggccgcttttctggattcatcgactgtggccggctgggtgtggcggaccgctatcaggacatagcgttggctacccgtg
atattgctgaagagcttggcggcgaatgggctgaccgcttcctcgtgctttacggtatcgccgctcccgattcgcagcgc
atcgccttctatcgccttcttgacgagttcttctgagcgggactctggggttcgaaatgaccgaccaagcgacgcccaac
ctgccatcacgagatttcgattccaccgccgccttctatgaaaggttgggcttcggaatcgttttccgggacgccggctg
gatgatcctccagcgcggggatctcatgctggagttcttcgcccaccctagggggaggctaactgaaacacggaaggaga
caataccggaaggaacccgcgctatgacggcaataaaaagacagaataaaacgcacggtgttgggtcgtttgttcataaa
cgcggggttcggtcccagggctggcactctgtcgataccccaccgagaccccattggggccaatacgcccgcgtttcttc
cttttccccaccccacccccaagttcgggtgaaggcccagggctcgcagccaacgtcgggggcggcaggccctgccatag
cctcaggttactcatatatactttagattgatttaaaacttcatttttaatttaaaaggatctaggtgaagatccttttt
gataatctcatgaccaaaatcccttaacgtgagttttcgttccactgagcgtcagaccccgtagaaaagatcaaaggatc
ttcttgagatcctttttttctgcgcgtaatctgctgcttgcaaacaaaaaaaccaccgctaccagcggtggtttgtttgc
cggatcaagagctaccaactctttttccgaaggtaactggcttcagcagagcgcagataccaaatactgtccttctagtg
tagccgtagttaggccaccacttcaagaactctgtagcaccgcctacatacctcgctctgctaatcctgttaccagtggc
tgctgccagtggcgataagtcgtgtcttaccgggttggactcaagacgatagttaccggataaggcgcagcggtcgggct
gaacgggggttcgtgcacacagcccagcttggagcgaacgacctacaccgaactgagatacctacagcgtgagctatga
gaaagcgccacgcttcccgaagggagaaaggcggacaggtatccggtaagcggcagggtcggaacaggagagcgcacgag
ggagcttccagggggaaacgcctggtatctttatagtcctgtcgggtttcgccacctctgacttgagcgtcgatttttgt
gatgctcgtcaggggggcggagcctatggaaaaacgccagcaacgcggcctttttacggttcctggccttttgctggcct
tttgctcacatgttctttcctgcgttatcccctgattctgtggataaccgtattaccgccatgcat

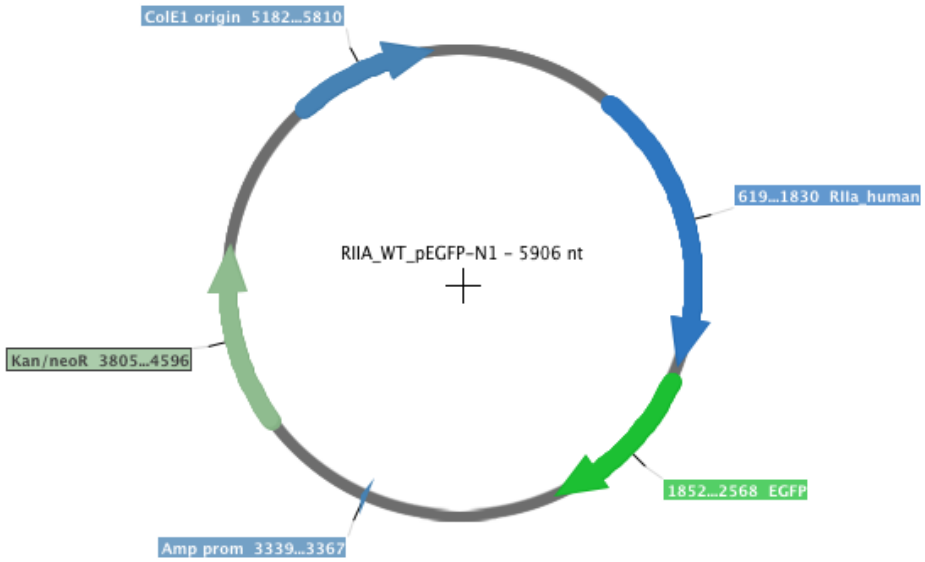

Figure 40: Vector map of RIIα-pEGFP-N1

III.10 RIIα with HA-tag (in pEGFP-N1 as backbone vector)

Sequence starting from RIIα gene until stop codon

ATGAGCCACATCCAGATCCCGCCGGGGCTCACGGAGCTGCTGCAGGGCTACACGGTGGAGGTGCTGCGACAGCAGCCGCC
TGACCTCGTCGAATTCGCAGTGGAGTACTTCACCCGCCTGCGCGAGGCCCGCGCCCCAGCCTCAGTCCTGCCCGCCGCCA
CCCCACGCCAGAGCCTGGGCCACCCCCCGCCAGAACCCGGCCCGGACCGTGTCGCCGACGCCAAAGGGGACAGCGAGTCG
GAGGAGGACGAGGACTTGGAAGTTCCAGTTCCTAGCAGATTTAATAGACGAGTATCAGTCTGTGCTGAGACCTATAACCC
TGATGAGGAAGAGGAAGATACAGATCCAAGGGTGATTCATCCTAAAACTGATGAACAGAGATGCAGACTTCAGGAAGCTT
GCAAAGATATTCTCCTTTTCAAAAATCTTGATCAGGAACAGCTTTCTCAAGTTCTCGATGCCATGTTTGAAAGGATAGTC
AAAGCTGATGAGCATGTCATTGACCAAGGAGATGATGGAGACAACTTTTATGTCATAGAACGGGGAACTTATGACATTTT
AGTAACAAAAGATAATCAAACCCGCTCTGTTGGTCAATATGACAACCGTGGCAGTTTTGGAGAACTAGCTCTGATGTACA
ACACCCCGAGAGCTGCTACCATTGTTGCTACCTCAGAAGGCTCCCTTTGGGGACTGGACCGGGTGACTTTTAGAAGAATC
ATAGTGAAAAATAATGCAAAGAAGAGGAAGATGTTTGAATCATTTATTGAGTCTGTGCCCCTCCTTAAATCACTAGAGGT
GTCAGAACGAATGAAGATTGTGGATGTAATAGGAGAGAAGATCTATAAGGATGGAGAACGCATAATCACTCAGGGTGAAA
AGGCTGATAGCTTTTACATCATAGAGTCTGGCGAAGTGAGCATCTTGATTAGAAGCAGGACTAAATCAAACAAGGATGGT
GGGAACCAGGAGGTCGAGATTGCCCGCTGCCATAAGGGGCAGTACTTTGGAGAGCTTGCCCTGGTCACCAACAAACCCAG
AGCTGCCTCAGCTTATGCAGTTGGAGATGTCAAATGCTTAGTTATGGATGTACAAGCATTCGAGAGGCTTCTGGggccCT
GCATGGACATCATGAAGAGGAACATCTCACACTATGAGGAACAGCTGGTGAAGATGTTTGGCTCCAGCGTGGATCTGGGC
AACCTCGGGCAGCGGgatccaTACCCATACGATGTTCCAGATTACGCTTAG

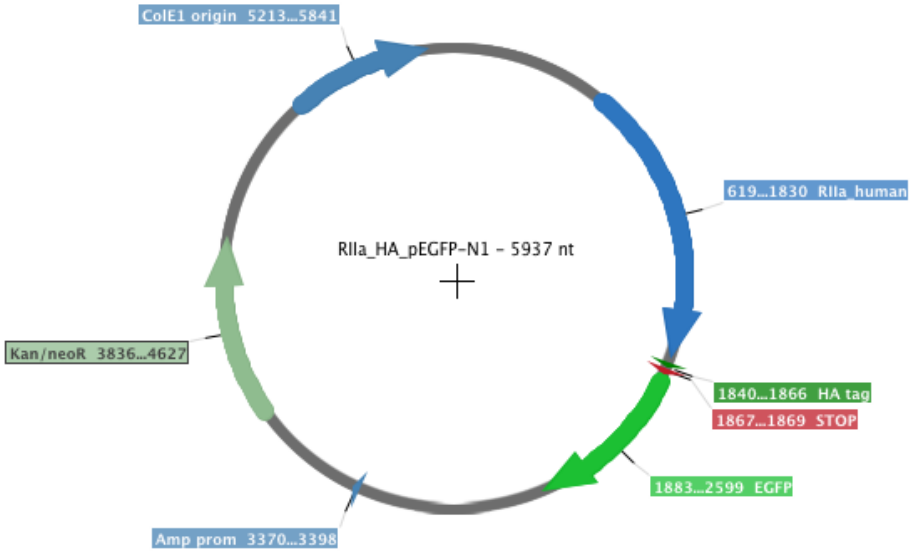

Figure 41: Vector map of RIIα-HA in pEGFP-N1

LITERATURE

Al-Bataineh, M. M., H. Li, K. Ohmi, F. Gong, A. L. Marciszyn, S. Naveed, X. Zhu, D. Neumann, Q. Wu, L. Cheng, R. A. Fenton, N. M. Pastor-Soler and K. R. Hallows (2016). "Activation of the metabolic sensor AMP-activated protein kinase inhibits aquaporin-2 function in kidney principal cells." Am J Physiol Renal Physiol **311**(5): F890-F900.

Alzamora, R., M. M. Al-Bataineh, W. Liu, F. Gong, H. Li, R. F. Thali, Y. Joho-Auchli, R. A. Brunisholz, L. M. Satlin, D. Neumann, K. R. Hallows and N. M. Pastor-Soler (2013). "AMP-activated protein kinase regulates the vacuolar H+-ATPase via direct phosphorylation of the A subunit (ATP6V1A) in the kidney." Am J Physiol Renal Physiol **305**(7): F943-956.

Alzamora, R., R. F. Thali, F. Gong, C. Smolak, H. Li, C. J. Baty, C. A. Bertrand, Y. Auchli, R. A. Brunisholz, D. Neumann, K. R. Hallows and N. M. Pastor-Soler (2010). "PKA regulates vacuolar H+-ATPase localization and activity via direct phosphorylation of the a subunit in kidney cells." J Biol Chem **285**(32): 24676-24685.

Arnspang, E. C., F. H. Login, J. S. Koffman, P. Sengupta and L. N. Nejsum (2016). "AQP2 Plasma Membrane Diffusion Is Altered by the Degree of AQP2-S256 Phosphorylation." Int J Mol Sci **17**(11).

Arthur, J., J. Huang, N. Nomura, W. W. Jin, W. Li, X. Cheng, D. Brown and H. J. Lu (2015). "Characterization of the putative phosphorylation sites of the AQP2 C terminus and their role in AQP2 trafficking in LLC-PK1 cells." Am J Physiol Renal Physiol **309**(8): F673-679.

Bar-Peled, L., L. D. Schweitzer, R. Zoncu and D. M. Sabatini (2012). "Ragulator is a GEF for the rag GTPases that signal amino acid levels to mTORC1." Cell **150**(6): 1196-1208.

Barile, M., T. Pisitkun, M. J. Yu, C. L. Chou, M. J. Verbalis, R. F. Shen and M. A. Knepper (2005). "Large scale protein identification in intracellular aquaporin-2 vesicles from renal inner medullary collecting duct." Mol Cell Proteomics **4**(8): 1095-1106.

Bech, A. P., J. F. M. Wetzels and T. Nijenhuis (2018). "Effects of sildenafil, metformin, and simvastatin on ADH-independent urine concentration in healthy volunteers." Physiol Rep **6**(7): e13665.

Benlekbir, S., S. A. Bueler and J. L. Rubinstein (2012). "Structure of the vacuolar-type ATPase from Saccharomyces cerevisiae at 11-A resolution." Nat Struct Mol Biol **19**(12): 1356-1362.

Berl, T., F. Quittnat-Pelletier, J. G. Verbalis, R. W. Schrier, D. G. Bichet, J. Ouyang, F. S. Czerwiec and S. Investigators (2010). "Oral tolvaptan is safe and effective in chronic hyponatremia." J Am Soc Nephrol **21**(4): 705-712.

Bernier, V., M. Lagace, M. Lonergan, M. F. Arthus, D. G. Bichet and M. Bouvier (2004). "Functional rescue of the constitutively internalized V2 vasopressin receptor mutant R137H by the pharmacological chaperone action of SR49059." Mol Endocrinol **18**(8): 2074-2084.

Bertinetti, D., S. Schweinsberg, S. E. Hanke, F. Schwede, O. Bertinetti, S. Drewianka, H. G. Genieser and F. W. Herberg (2009). "Chemical tools selectively target components of the PKA system." BMC Chem Biol **9**: 3.

Bichet, D. G. and D. Bockenhauer (2016). "Genetic forms of nephrogenic diabetes insipidus (NDI): Vasopressin receptor defect (X-linked) and aquaporin defect (autosomal recessive and dominant)." Best Pract Res Clin Endocrinol Metab **30**(2): 263-276.

Bogum, J., D. Faust, K. Zuhlke, J. Eichhorst, M. C. Moutty, J. Furkert, A. Eldahshan, M. Neuenschwander, J. P. von Kries, B. Wiesner, C. Trimpert, P. M. Deen, G. Valenti, W. Rosenthal and E. Klussmann (2013). "Small-molecule screening identifies modulators of aquaporin-2 trafficking." J Am Soc Nephrol **24**(5): 744-758.

Bonfrate, L., G. Procino, D. Q. Wang, M. Svelto and P. Portincasa (2015). "A novel therapeutic effect of statins on nephrogenic diabetes insipidus." J Cell Mol Med **19**(2): 265-282.

Bouley, R., S. Breton, T. Sun, M. McLaughlin, N. N. Nsumu, H. Y. Lin, D. A. Ausiello and D. Brown (2000). "Nitric oxide and atrial natriuretic factor stimulate cGMP-dependent membrane insertion of aquaporin 2 in renal epithelial cells." J. Clin. Invest. **106**(9): 1115-1126.

Bowman, B. J. and E. J. Bowman (2002). "Mutations in subunit C of the vacuolar ATPase confer resistance to bafilomycin and identify a conserved antibiotic binding site." J Biol Chem **277**(6): 3965-3972.

Bowman, E. J., A. Siebers and K. Altendorf (1988). "Bafilomycins: a class of inhibitors of membrane ATPases from microorganisms, animal cells, and plant cells." Proc Natl Acad Sci U S A **85**(21): 7972-7976.

Breton, S. and D. Brown (1998). "Cold-induced microtubule disruption and relocalization of membrane proteins in kidney epithelial cells." J Am Soc Nephrol **9**(2): 155-166.

Brond, L., K. M. Mullertz, M. Torp, J. Nielsen, M. Graebe, N. Hadrup, S. Nielsen, S. Christensen and T. E. Jonassen (2013). "Congestive heart failure in rats is associated with increased collecting duct vasopressin sensitivity and vasopressin type 2 receptor reexternalization." Am J Physiol Renal Physiol **305**(11): F1547-1554.

Burgers, P. P., M. A. van der Heyden, B. Kok, A. J. Heck and A. Scholten (2015). "A systematic evaluation of protein kinase A-A-kinase anchoring protein interaction motifs." Biochemistry **54**(1): 11-21.

Centrone, M., M. Ranieri, A. Di Mise, S. P. Berlingerio, A. Russo, P. M. T. Deen, O. Staub, G. Valenti and G. Tamma (2017). "AQP2 Abundance is Regulated by the E3-Ligase CHIP Via HSP70." Cell Physiol Biochem **44**(2): 515-531.

Chambrey, R., I. Kurth, J. Peti-Peterdi, P. Houillier, J. M. Purkerson, F. Leviel, M. Hentschke, A. A. Zdebik, G. J. Schwartz, C. A. Hubner and D. Eladari (2013). "Renal intercalated cells are rather energized by a proton than a sodium pump." Proc Natl Acad Sci U S A **110**(19): 7928-7933.

Chan, W. Y. (1973). "A study on the mechanism of vasopressin escape: effects of chronic vasopressin and overhydration on renal tissue osmolality and electrolytes in dogs." J Pharmacol Exp Ther **184**(1): 244-251.

Chen, H. W., J. X. Cheng, M. T. Liu, K. King, J. Y. Peng, X. Q. Zhang, C. H. Wang, S. Shresta, R. T. Schooley and Y. T. Liu (2013). "Inhibitory and combinatorial effect of diphyllin, a v-ATPase blocker, on influenza viruses." Antiviral Res **99**(3): 371-382.

Cheung, P. W., L. Ueberdiek, J. Day, R. Bouley and D. Brown (2017). "Protein phosphatase 2C is responsible for VP-induced dephosphorylation of AQP2 serine 261." Am J Physiol Renal Physiol **313**(2): F404-F413.

Choi, H. J., H. J. Jung and T. H. Kwon (2015). "Extracellular pH affects phosphorylation and intracellular trafficking of AQP2 in inner medullary collecting duct cells." Am J Physiol Renal Physiol **308**(7): F737-748.

de Groot, B. L., T. Frigato, V. Helms and H. Grubmuller (2003). "The mechanism of proton exclusion in the aquaporin-1 water channel." J Mol Biol **333**(2): 279-293.

de Mattia, F., P. J. Savelkoul, E. J. Kamsteeg, I. B. Konings, P. van der Sluijs, R. Mallmann, A. Oksche and P. M. Deen (2005). "Lack of arginine vasopressin-induced phosphorylation of aquaporin-2 mutant AQP2-R254L explains dominant nephrogenic diabetes insipidus." J Am Soc Nephrol **16**(10): 2872-2880.

Deen, P. M., H. Croes, R. A. van Aubel, L. A. Ginsel and C. H. van Os (1995). "Water channels encoded by mutant aquaporin-2 genes in nephrogenic diabetes insipidus are impaired in their cellular routing." J Clin Invest **95**(5): 2291-2296.

Dema, A., E. Perets, M. S. Schulz, V. A. Deak and E. Klussmann (2015). "Pharmacological targeting of AKAP-directed compartmentalized cAMP signalling." Cell Signal **27**(12): 2474-2487.

Di Giovanni, J., S. Boudkkazi, S. Mochida, A. Bialowas, N. Samari, C. Leveque, F. Youssouf, A. Brechet, C. Iborra, Y. Maulet, N. Moutot, D. Debanne, M. Seagar and O. El Far (2010). "V-ATPase membrane sector associates with synaptobrevin to modulate neurotransmitter release." Neuron **67**(2): 268-279.

DiGiovanni, S. R., S. Nielsen, E. I. Christensen and M. A. Knepper (1994). "Regulation of collecting duct water channel expression by vasopressin in Brattleboro rat." Proc Natl Acad Sci U S A **91**(19): 8984-8988.

Djouder, N., R. D. Tuerk, M. Suter, P. Salvioni, R. F. Thali, R. Scholz, K. Vaahtomeri, Y. Auchli, H. Rechsteiner, R. A. Brunisholz, B. Viollet, T. P. Makela, T. Wallimann, D. Neumann and W. Krek

(2010). "PKA phosphorylates and inactivates AMPKalpha to promote efficient lipolysis." EMBO J **29**(2): 469-481.

Dollerup, P., T. M. Thomsen, L. N. Nejsum, M. Faerch, M. Osterbrand, N. Gregersen, S. Rittig, J. H. Christensen and T. J. Corydon (2015). "Partial nephrogenic diabetes insipidus caused by a novel AQP2 variation impairing trafficking of the aquaporin-2 water channel." BMC Nephrol **16**: 217.

Donnelly, B. F., P. G. Needham, A. C. Snyder, A. Roy, S. Khadem, J. L. Brodsky and A. R. Subramanya (2013). "Hsp70 and Hsp90 multichaperone complexes sequentially regulate thiazide-sensitive cotransporter endoplasmic reticulum-associated degradation and biogenesis." J Biol Chem **288**(18): 13124-13135.

Dovas, A. and J. R. Couchman (2005). "RhoGDI: multiple functions in the regulation of Rho family GTPase activities." Biochem J **390**(Pt 1): 1-9.

Drose, S., K. U. Bindseil, E. J. Bowman, A. Siebers, A. Zeeck and K. Altendorf (1993). "Inhibitory effect of modified bafilomycins and concanamycins on P- and V-type adenosinetriphosphatases." Biochemistry **32**(15): 3902-3906.

Ecelbarger, C. A., S. Nielsen, B. R. Olson, T. Murase, E. A. Baker, M. A. Knepper and J. G. Verbalis (1997). "Role of renal aquaporins in escape from vasopressin-induced antidiuresis in rat." J Clin Invest **99**(8): 1852-1863.

Ecelbarger, C. A., J. Terris, G. Frindt, M. Echevarria, D. Marples, S. Nielsen and M. A. Knepper (1995). "Aquaporin-3 water channel localization and regulation in rat kidney." Am J Physiol Renal Physiol **269**(5 Pt 2): F663-672.

Efe, O., J. D. Klein, L. M. LaRocque, H. Ren and J. M. Sands (2016). "Metformin improves urine concentration in rodents with nephrogenic diabetes insipidus." JCI Insight **1**(11).

Efeyan, A., R. Zoncu, S. Chang, I. Gumper, H. Snitkin, R. L. Wolfson, O. Kirak, D. D. Sabatini and D. M. Sabatini (2013). "Regulation of mTORC1 by the Rag GTPases is necessary for neonatal autophagy and survival." Nature **493**(7434): 679-683.

El Far, O. and M. Seagar (2011). "A role for V-ATPase subunits in synaptic vesicle fusion?" J Neurochem **117**(4): 603-612.

Esmail, S., Y. Yao, N. Kartner, J. Li, R. A. Reithmeier and M. F. Manolson (2016). "N-Linked Glycosylation Is Required for Vacuolar H(+) -ATPase (V-ATPase) a4 Subunit Stability, Assembly, and Cell Surface Expression." J Cell Biochem **117**(12): 2757-2768.

Farsi, Z., R. Jahn and A. Woehler (2017). "Proton electrochemical gradient: Driving and regulating neurotransmitter uptake." Bioessays **39**(5).

Faust, D. (2014). Identification of proteins controlling AQP2 translocation by large-scale siRNA screening of the mouse kinome. Doktorarbeit, Freie Universität Berlin.

Faust, D., A. Geelhaar, B. Eisermann, J. Eichhorst, B. Wiesner, W. Rosenthal and E. Klussman (2013). "Culturing primary rat inner medullary collecting duct cells." J Vis Exp(76).

Feldman, B. J., S. M. Rosenthal, G. A. Vargas, R. G. Fenwick, E. A. Huang, M. Matsuda-Abedini, R. H. Lustig, R. S. Mathias, A. A. Portale, W. L. Miller and S. E. Gitelman (2005). "Nephrogenic syndrome of inappropriate antidiuresis." N Engl J Med **352**(18): 1884-1890.

Fenton, R. A., H. B. Moeller, J. D. Hoffert, M. J. Yu, S. Nielsen and M. A. Knepper (2008). "Acute regulation of aquaporin-2 phosphorylation at Ser-264 by vasopressin." Proc Natl Acad Sci U S A **105**(8): 3134-3139.

Fernandez-Llama, P., C. A. Ecelbarger, J. A. Ware, P. Andrews, A. J. Lee, R. Turner, S. Nielsen and M. A. Knepper (1999). "Cyclooxygenase inhibitors increase Na-K-2Cl cotransporter abundance in thick ascending limb of Henle's loop." Am J Physiol **277**(2 Pt 2): F219-226.

Florey, O., N. Gammoh, S. E. Kim, X. Jiang and M. Overholtzer (2015). "V-ATPase and osmotic imbalances activate endolysosomal LC3 lipidation." Autophagy **11**(1): 88-99.

Foretz, M., S. Hebrard, J. Leclerc, E. Zarrinpashneh, M. Soty, G. Mithieux, K. Sakamoto, F. Andreelli and B. Viollet (2010). "Metformin inhibits hepatic gluconeogenesis in mice independently of the LKB1/AMPK pathway via a decrease in hepatic energy state." J Clin Invest **120**(7): 2355-2369.

Forgac, M. (2007). "Vacuolar ATPases: rotary proton pumps in physiology and pathophysiology." Nat Rev Mol Cell Biol **8**(11): 917-929.

Frokiaer, J., D. Marples, M. A. Knepper and S. Nielsen (1996). "Bilateral ureteral obstruction downregulates expression of vasopressin-sensitive AQP-2 water channel in rat kidney." Am J Physiol **270**(4 Pt 2): F657-668.

Fushimi, K., S. Sasaki and F. Marumo (1997). "Phosphorylation of serine 256 is required for cAMP-dependent regulatory exocytosis of the aquaporin-2 water channel." J. Biol. Chem. **272**(23): 14800-14804.

Fushimi, K., S. Uchida, Y. Hara, Y. Hirata, F. Marumo and S. Sasaki (1993). "Cloning and expression of apical membrane water channel of rat kidney collecting tubule." Nature **361**(6412): 549-552.

Gheorghiade, M., W. A. Gattis, C. M. O'Connor, K. F. Adams, Jr., U. Elkayam, A. Barbagelata, J. K. Ghali, R. L. Benza, F. A. McGrew, M. Klapholz, J. Ouyang, C. Orlandi, Acute and I. Chronic Therapeutic Impact of a Vasopressin Antagonist in Congestive Heart Failure (2004). "Effects of tolvaptan, a vasopressin antagonist, in patients hospitalized with worsening heart failure: a randomized controlled trial." JAMA **291**(16): 1963-1971.

Goji, K., M. Kuwahara, Y. Gu, M. Matsuo, F. Marumo and S. Sasaki (1998). "Novel mutations in aquaporin-2 gene in female siblings with nephrogenic diabetes insipidus: evidence of disrupted water channel function." J Clin Endocrinol Metab **83**(9): 3205-3209.

Gold, M. G., B. Lygren, P. Dokurno, N. Hoshi, G. McConnachie, K. Tasken, C. R. Carlson, J. D. Scott and D. Barford (2006). "Molecular basis of AKAP specificity for PKA regulatory subunits." Mol Cell **24**(3): 383-395.

Goldberg, H., P. Clayman and K. Skorecki (1988). "Mechanism of Li inhibition of vasopressin-sensitive adenylate cyclase in cultured renal epithelial cells." Am J Physiol **255**(5 Pt 2): F995-1002.

Gong, F., R. Alzamora, C. Smolak, H. Li, S. Naveed, D. Neumann, K. R. Hallows and N. M. Pastor-Soler (2010). "Vacuolar H+-ATPase apical accumulation in kidney intercalated cells is regulated by PKA and AMP-activated protein kinase." Am J Physiol Renal Physiol **298**(5): F1162-1169.

Götz, F., Y. Roske, M. S. Schulz, K. Autenrieth, D. Bertinetti, K. Faelber, K. Zuhlke, A. Kreuchwig, E. J. Kennedy, G. Krause, O. Daumke, F. W. Herberg, U. Heinemann and E. Klussmann (2016). "AKAP18:PKA-RIIalpha structure reveals crucial anchor points for recognition of regulatory subunits of PKA." Biochem J **473**(13): 1881-1894.

Gouraud, S., A. Laera, G. Calamita, M. Carmosino, G. Procino, O. Rossetto, R. Mannucci, W. Rosenthal, M. Svelto and G. Valenti (2002). "Functional involvement of VAMP/synaptobrevin-2 in cAMP-stimulated aquaporin 2 translocation in renal collecting duct cells." J. Cell. Sci. **115**(Pt 18): 3667-3674.

Gowans, G. J., S. A. Hawley, F. A. Ross and D. G. Hardie (2013). "AMP is a true physiological regulator of AMP-activated protein kinase by both allosteric activation and enhancing net phosphorylation." Cell Metab **18**(4): 556-566.

Guet, D., K. Mandal, M. Pinot, J. Hoffmann, Y. Abidine, W. Sigaut, S. Bardin, K. Schauer, B. Goud and J. B. Manneville (2014). "Mechanical role of actin dynamics in the rheology of the Golgi complex and in Golgi-associated trafficking events." Curr Biol **24**(15): 1700-1711.

Guo, Q., Y. Wang, P. Tripathi, K. R. Manda, M. Mukherjee, M. Chaklader, P. F. Austin, K. Surendran and F. Chen (2015). "Adam10 mediates the choice between principal cells and intercalated cells in the kidney." J Am Soc Nephrol **26**(1): 149-159.

Gustafson, C. E., T. Katsura, M. McKee, R. Bouley, J. E. Casanova and D. Brown (2000). "Recycling of AQP2 occurs through a temperature- and bafilomycin-sensitive trans-Golgi-associated compartment." Am J Physiol Renal Physiol **278**(2): F317-F326.

Hall, J. E., J. P. Montani, L. L. Woods and H. L. Mizelle (1986). "Renal escape from vasopressin: role of pressure diuresis." Am J Physiol **250**(5 Pt 2): F907-916.

Hallows, K. R., R. Alzamora, H. Li, F. Gong, C. Smolak, D. Neumann and N. M. Pastor-Soler (2009). "AMP-activated protein kinase inhibits alkaline pH- and PKA-induced apical vacuolar H+-ATPase accumulation in epididymal clear cells." Am J Physiol Cell Physiol **296**(4): C672-681.

Hanke, S. E., D. Bertinetti, A. Badel, S. Schweinsberg, H. G. Genieser and F. W. Herberg (2011). "Cyclic nucleotides as affinity tools: phosphorothioate cAMP analogues address specific PKA subproteomes." N Biotechnol **28**(4): 294-301.

Hasler, U., U. S. Jeon, J. A. Kim, D. Mordasini, H. M. Kwon, E. Feraille and P. Y. Martin (2006). "Tonicity-responsive enhancer binding protein is an essential regulator of aquaporin-2 expression in renal collecting duct principal cells." J Am Soc Nephrol **17**(6): 1521-1531.

Hasler, U., V. Leroy, U. S. Jeon, R. Bouley, M. Dimitrov, J. A. Kim, D. Brown, H. M. Kwon, P. Y. Martin and E. Feraille (2008). "NF-kappaB modulates aquaporin-2 transcription in renal collecting duct principal cells." J. Biol. Chem. **283**(42): 28095-28105.

Hayashi, M., S. Sasaki, H. Tsuganezawa, T. Monkawa, W. Kitajima, K. Konishi, K. Fushimi, F. Marumo and T. Saruta (1994). "Expression and distribution of aquaporin of collecting duct are regulated by vasopressin V2 receptor in rat kidney." J Clin Invest **94**(5): 1778-1783.

Hayek, S. R., S. A. Lee and K. J. Parra (2014). "Advances in targeting the vacuolar proton-translocating ATPase (V-ATPase) for anti-fungal therapy." Front Pharmacol **5**: 4.

He, L., E. Chang, J. Peng, H. An, S. M. McMillin, S. Radovick, C. A. Stratakis and F. E. Wondisford (2016). "Activation of the cAMP-PKA pathway Antagonizes Metformin Suppression of Hepatic Glucose Production." J Biol Chem **291**(20): 10562-10570.

Henn, V., B. Edemir, E. Stefan, B. Wiesner, D. Lorenz, F. Theilig, R. Schmitt, L. Vossebein, G. Tamma, M. Beyermann, E. Krause, F. W. Herberg, G. Valenti, S. Bachmann, W. Rosenthal and E. Klussmann (2004). "Identification of a novel A-kinase anchoring protein 18 isoform and evidence for its role in the vasopressin-induced aquaporin-2 shuttle in renal principal cells." J Biol Chem **279**(25): 26654-26665.

Herberg, F. W., A. Maleszka, T. Eide, L. Vossebein and K. Tasken (2000). "Analysis of A-kinase anchoring protein (AKAP) interaction with protein kinase A (PKA) regulatory subunits: PKA isoform specificity in AKAP binding." J Mol Biol **298**(2): 329-339.

Hernandez, A., G. Serrano-Bueno, J. R. Perez-Castineira and A. Serrano (2012). "Intracellular proton pumps as targets in chemotherapy: V-ATPases and cancer." Curr Pharm Des **18**(10): 1383-1394.

Hiesinger, P. R., A. Fayyazuddin, S. Q. Mehta, T. Rosenmund, K. L. Schulze, R. G. Zhai, P. Verstreken, Y. Cao, Y. Zhou, J. Kunz and H. J. Bellen (2005). "The v-ATPase V0 subunit a1 is required for a late step in synaptic vesicle exocytosis in Drosophila." Cell **121**(4): 607-620.

Hiller, K., J. Hangebrauk, C. Jager, J. Spura, K. Schreiber and D. Schomburg (2009). "MetaboliteDetector: comprehensive analysis tool for targeted and nontargeted GC/MS based metabolome analysis." Anal Chem **81**(9): 3429-3439.

Hinckelmann, M. V., A. Virlogeux, C. Niehage, C. Poujol, D. Choquet, B. Hoflack, D. Zala and F. Saudou (2016). "Self-propelling vesicles define glycolysis as the minimal energy machinery for neuronal transport." Nat Commun **7**: 13233.

Hirokawa, N., R. Sato-Yoshitake, N. Kobayashi, K. K. Pfister, G. S. Bloom and S. T. Brady (1991). "Kinesin associates with anterogradely transported membranous organelles in vivo." J Cell Biol **114**(2): 295-302.

Hirokawa, N., R. Sato-Yoshitake, T. Yoshida and T. Kawashima (1990). "Brain dynein (MAP1C) localizes on both anterogradely and retrogradely transported membranous organelles in vivo." J Cell Biol **111**(3): 1027-1037.

Hoffert, J. D., R. A. Fenton, H. B. Moeller, B. Simons, D. Tchapyjnikov, B. W. McDill, M. J. Yu, T. Pisitkun, F. Chen and M. A. Knepper (2008). "Vasopressin-stimulated Increase in Phosphorylation at Ser269 Potentiates Plasma Membrane Retention of Aquaporin-2." J. Biol. Chem. **283**(36): 24617-24627.

Hoffert, J. D., J. Nielsen, M. J. Yu, T. Pisitkun, S. M. Schleicher, S. Nielsen and M. A. Knepper (2007). "Dynamics of aquaporin-2 serine-261 phosphorylation in response to short-term vasopressin treatment in collecting duct." Am J Physiol Renal Physiol **292**(2): F691-700.

Holliday, L. S., M. Lu, B. S. Lee, R. D. Nelson, S. Solivan, L. Zhang and S. L. Gluck (2000). "The amino-terminal domain of the B subunit of vacuolar H+-ATPase contains a filamentous actin binding site." J Biol Chem **275**(41): 32331-32337.

Horton, C. E., Jr., M. T. Davisson, J. B. Jacobs, G. T. Bernstein, A. B. Retik and J. Mandell (1988). "Congenital progressive hydronephrosis in mice: a new recessive mutation." J Urol **140**(5 Pt 2): 1310-1315.

Hozawa, S., E. J. Holtzman and D. A. Ausiello (1996). "cAMP motifs regulating transcription in the aquaporin 2 gene." Am J Physiol Renal Physiol **270**(6 Pt 1): C1695-1702.

Hundsrucker, C., P. Skroblin, F. Christian, H. M. Zenn, V. Popara, M. Joshi, J. Eichhorst, B. Wiesner, F. W. Herberg, B. Reif, W. Rosenthal and E. Klussmann (2010). "Glycogen synthase kinase 3beta interaction protein functions as an A-kinase anchoring protein." J Biol Chem **285**(8): 5507-5521.

Hurtado-Lorenzo, A., M. Skinner, J. El Annan, M. Futai, G. H. Sun-Wada, S. Bourgoin, J. Casanova, A. Wildeman, S. Bechoua, D. A. Ausiello, D. Brown and V. Marshansky (2006). "V-ATPase interacts with ARNO and Arf6 in early endosomes and regulates the protein degradative pathway." Nat Cell Biol **8**(2): 124-136.

Huss, M., G. Ingenhorst, S. Konig, M. Gassel, S. Drose, A. Zeeck, K. Altendorf and H. Wieczorek (2002). "Concanamycin A, the specific inhibitor of V-ATPases, binds to the V(o) subunit c." J Biol Chem **277**(43): 40544-40548.

Ikemoto, A., D. G. Bole and T. Ueda (2003). "Glycolysis and glutamate accumulation into synaptic vesicles. Role of glyceraldehyde phosphate dehydrogenase and 3-phosphoglycerate kinase." J Biol Chem **278**(8): 5929-5940.

Iolascon, A., V. Aglio, G. Tamma, rsquo, M. Apolito, F. Addabbo, G. Procino, M. C. Simonetti, G. Montini, L. Gesualdo, E. W. Debler, M. Svelto and G. Valenti (2007). "Characterization of Two Novel Missense Mutations in the AQP2 Gene Causing Nephrogenic Diabetes Insipidus." Nephron Physiol. **105**(3): p33-p41.

Ishida, A., Y. Noda and T. Ueda (2009). "Synaptic vesicle-bound pyruvate kinase can support vesicular glutamate uptake." Neurochem Res **34**(5): 807-818.

Jang, S., J. C. Nelson, E. G. Bend, L. Rodriguez-Laureano, F. G. Tueros, L. Cartagenova, K. Underwood, E. M. Jorgensen and D. A. Colon-Ramos (2016). "Glycolytic Enzymes Localize to Synapses under Energy Stress to Support Synaptic Function." Neuron **90**(2): 278-291.

Joanny, J. F. and J. Prost (2009). "Active gels as a description of the actin-myosin cytoskeleton." HFSP J **3**(2): 94-104.

Johanns, M., Y. C. Lai, M. F. Hsu, R. Jacobs, D. Vertommen, J. Van Sande, J. E. Dumont, A. Woods, D. Carling, L. Hue, B. Viollet, M. Foretz and M. H. Rider (2016). "AMPK antagonizes hepatic glucagon-stimulated cyclic AMP signalling via phosphorylation-induced activation of cyclic nucleotide phosphodiesterase 4B." Nat Commun **7**: 10856.

Jung, J. S., G. M. Preston, B. L. Smith, W. B. Guggino and P. Agre (1994). "Molecular structure of the water channel through aquaporin CHIP. The hourglass model." J Biol Chem **269**(20): 14648-14654.

Kamsteeg, E. J., A. S. Duffield, I. B. M. Konings, J. Spencer, P. Pagel, P. M. T. Deen and M. J. Caplan (2007). "MAL decreases the internalization of the aquaporin-2 water channel." Proc Natl Acad Sci U S A **104**(42): 16696-16701.

Kamsteeg, E. J., I. Heijnen, C. H. van Os and P. M. Deen (2000). "The subcellular localization of an aquaporin-2 tetramer depends on the stoichiometry of phosphorylated and nonphosphorylated monomers." J. Biol. Chem. **151**(4): 919-930.

Kamsteeg, E. J., G. Hendriks, M. Boone, I. B. Konings, V. Oorschot, P. van der Sluijs, J. Klumperman and P. M. Deen (2006). "Short-chain ubiquitination mediates the regulated endocytosis of the aquaporin-2 water channel." Proc Natl Acad Sci U S A **103**(48): 18344-18349.

Kamsteeg, E. J., T. A. Wormhoudt, J. P. Rijss, C. H. van Os and P. M. Deen (1999). "An impaired routing of wild-type aquaporin-2 after tetramerization with an aquaporin-2 mutant explains dominant nephrogenic diabetes insipidus." EMBO J **18**(9): 2394-2400.

Kane, P. M. (1995). "Disassembly and reassembly of the yeast vacuolar H(+)-ATPase in vivo." J Biol Chem **270**(28): 17025-17032.

Kartner, N., Y. Yao, A. Bhargava and M. F. Manolson (2013). "Topology, glycosylation and conformational changes in the membrane domain of the vacuolar H+-ATPase a subunit." J Cell Biochem **114**(7): 1474-1487.

Kartner, N., Y. Yao, K. Li, G. J. Crasto, A. Datti and M. F. Manolson (2010). "Inhibition of osteoclast bone resorption by disrupting vacuolar H+-ATPase a3-B2 subunit interaction." J Biol Chem **285**(48): 37476-37490.

Katsura, T., C. E. Gustafson, D. A. Ausiello and D. Brown (1997). "Protein kinase A phosphorylation is involved in regulated exocytosis of aquaporin-2 in transfected LLC-PK1 cells." Am J Physiol **272**(6 Pt 2): F817-822.

Katsura, T., J. M. Verbavatz, J. Farinas, T. Ma, D. A. Ausiello, A. S. Verkman and D. Brown (1995). "Constitutive and regulated membrane expression of aquaporin 1 and aquaporin 2 water channels in stably transfected LLC-PK1 epithelial cells." Proc Natl Acad Sci U S A **92**(16): 7212-7216.

Kazami, S., M. Takaine, H. Itoh, T. Kubota, J. Kobayashi and T. Usui (2014). "Iejimalide C is a potent V-ATPase inhibitor, and induces actin disorganization." Biol Pharm Bull **37**(12): 1944-1947.

Kim, G. H., N. W. Choi, J. Y. Jung, J. H. Song, C. H. Lee, C. M. Kang and M. A. Knepper (2008). "Treating lithium-induced nephrogenic diabetes insipidus with a COX-2 inhibitor improves polyuria via upregulation of AQP2 and NKCC2." Am J Physiol Renal Physiol **294**(4): F702-709.

Kimmins, S. and T. H. MacRae (2000). "Maturation of steroid receptors: an example of functional cooperation among molecular chaperones and their associated proteins." Cell Stress Chaperones **5**(2): 76-86.

Kishore, B. K. and C. M. Ecelbarger (2013). "Lithium: a versatile tool for understanding renal physiology." Am J Physiol Renal Physiol **304**(9): F1139-1149.

Klein, J. D., Y. Wang, M. A. Blount, P. A. Molina, L. M. LaRocque, J. A. Ruiz and J. M. Sands (2016). "Metformin, an AMPK activator, stimulates the phosphorylation of aquaporin 2 and urea transporter A1 in inner medullary collecting ducts." Am J Physiol Renal Physiol **310**(10): F1008-1012.

Klussmann, E., K. Maric, B. Wiesner, M. Beyermann and W. Rosenthal (1999). "Protein Kinase A Anchoring Proteins Are Required for Vasopressin-mediated Translocation of Aquaporin-2 into Cell Membranes of Renal Principal Cells." J Biol Chem **274**(8): 4934-4938.

Klussmann, E., G. Tamma, D. Lorenz, B. Wiesner, K. Maric, F. Hofmann, K. Aktories, G. Valenti and W. Rosenthal (2001). "An inhibitory role of Rho in the vasopressin-mediated translocation of aquaporin-2 into cell membranes of renal principal cells." J Biol Chem **276**(23): 20451-20457.

Kohan, A. B., I. Talukdar, C. M. Walsh and L. M. Salati (2009). "A role for AMPK in the inhibition of glucose-6-phosphate dehydrogenase by polyunsaturated fatty acids." Biochem Biophys Res Commun **388**(1): 117-121.

Koppenol, W. H., P. L. Bounds and C. V. Dang (2011). "Otto Warburg's contributions to current concepts of cancer metabolism." Nat Rev Cancer **11**(5): 325-337.

Kortenoeven, M. L., H. Schweer, R. Cox, J. F. Wetzels and P. M. Deen (2012). "Lithium reduces aquaporin-2 transcription independent of prostaglandins." Am J Physiol Cell Physiol **302**(1): C131-140.

Kosinska Eriksson, U., G. Fischer, R. Friemann, G. Enkavi, E. Tajkhorshid and R. Neutze (2013). "Subangstrom resolution X-ray structure details aquaporin-water interactions." Science **340**(6138): 1346-1349.

Kuwahara, M., K. Iwai, T. Ooeda, T. Igarashi, E. Ogawa, Y. Katsushima, I. Shinbo, S. Uchida, Y. Terada, M. F. Arthus, M. Lonergan, T. M. Fujiwara, D. G. Bichet, F. Marumo and S. Sasaki (2001). "Three families with autosomal dominant nephrogenic diabetes insipidus caused by aquaporin-2 mutations in the C-terminus." Am J Hum Genet **69**(4): 738-748.

Lang, P., F. Gesbert, M. Delespine-Carmagnat, R. Stancou, M. Pouchelet and J. Bertoglio (1996). "Protein kinase A phosphorylation of RhoA mediates the morphological and functional effects of cyclic AMP in cytotoxic lymphocytes." EMBO J **15**(3): 510-519.

Leopold, J. A., A. Dam, B. A. Maron, A. W. Scribner, R. Liao, D. E. Handy, R. C. Stanton, B. Pitt and J. Loscalzo (2007). "Aldosterone impairs vascular reactivity by decreasing glucose-6-phosphate dehydrogenase activity." Nat Med **13**(2): 189-197.

Levinsky, N. G., D. G. Davidson and R. W. Berliner (1959). "Changes in urine concentration during prolonged administration of vasopressin and water." Am J Physiol **196**(2): 451-456.

Li, J. H., C. L. Chou, B. Li, O. Gavrilova, C. Eisner, J. Schnermann, S. A. Anderson, C. X. Deng, M. A. Knepper and J. Wess (2009). "A selective EP4 PGE2 receptor agonist alleviates disease in a new mouse model of X-linked nephrogenic diabetes insipidus." J Clin Invest **119**(10): 3115-3126.

Li, W., Y. Zhang, R. Bouley, Y. Chen, T. Matsuzaki, P. Nunes, U. Hasler, D. Brown and H. A. Lu (2011). "Simvastatin enhances aquaporin-2 surface expression and urinary concentration in vasopressin-deficient Brattleboro rats through modulation of Rho GTPase." Am J Physiol Renal Physiol **301**(2): F309-318.

Li, Y., S. Shaw, E. J. Kamsteeg, A. Vandewalle and P. M. Deen (2006). "Development of lithium-induced nephrogenic diabetes insipidus is dissociated from adenylyl cyclase activity." J Am Soc Nephrol **17**(4): 1063-1072.

Liberman, R., S. Bond, M. G. Shainheit, M. J. Stadecker and M. Forgac (2014). "Regulated assembly of vacuolar ATPase is increased during cluster disruption-induced maturation of dendritic cells through a phosphatidylinositol 3-kinase/mTOR-dependent pathway." J Biol Chem **289**(3): 1355-1363.

Lloyd, D. J., F. W. Hall, L. M. Tarantino and N. Gekakis (2005). "Diabetes insipidus in mice with a mutation in aquaporin-2." PLoS Genet **1**(2): e20.

Lorenz, D., A. Krylov, D. Hahm, V. Hagen, W. Rosenthal, P. Pohl and K. Maric (2003). "Cyclic AMP is sufficient for triggering the exocytic recruitment of aquaporin-2 in renal epithelial cells." EMBO reports **4**(1): 88-93.

Los, E. L., P. M. Deen and J. H. Robben (2010). "Potential of nonpeptide (ant)agonists to rescue vasopressin V2 receptor mutants for the treatment of X-linked nephrogenic diabetes insipidus." J Neuroendocrinol **22**(5): 393-399.

Lu, H., T. X. Sun, R. Bouley, K. Blackburn, M. McLaughlin and D. Brown (2004a). "Inhibition of endocytosis causes phosphorylation (S256)-independent plasma membrane accumulation of AQP2." Am J Physiol Renal Physiol **286**(2): F233-243.

Lu, H. A. J., T. X. Sun, T. Matsuzaki, X. H. Yi, J. Eswara, R. Bouley, M. McKee and D. Brown (2007). "Heat Shock Protein 70 Interacts with Aquaporin-2 and Regulates Its Trafficking." J Biol Chem **282**(39): 28721-28732.

Lu, M., L. S. Holliday, L. Zhang, W. A. Dunn, Jr. and S. L. Gluck (2001). "Interaction between aldolase and vacuolar H+-ATPase: evidence for direct coupling of glycolysis to the ATP-hydrolyzing proton pump." J Biol Chem **276**(32): 30407-30413.

Lu, M., Y. Y. Sautin, L. S. Holliday and S. L. Gluck (2004b). "The glycolytic enzyme aldolase mediates assembly, expression, and activity of vacuolar H+-ATPase." J Biol Chem **279**(10): 8732-8739.

Lujan, B., C. Kushmerick, T. D. Banerjee, R. K. Dagda and R. Renden (2016). "Glycolysis selectively shapes the presynaptic action potential waveform." J Neurophysiol **116**(6): 2523-2540.

Maday, S., A. E. Twelvetrees, A. J. Moughamian and E. L. Holzbaur (2014). "Axonal transport: cargo-specific mechanisms of motility and regulation." Neuron **84**(2): 292-309.

Madiraju, A. K., D. M. Erion, Y. Rahimi, X. M. Zhang, D. T. Braddock, R. A. Albright, B. J. Prigaro, J. L. Wood, S. Bhanot, M. J. MacDonald, M. J. Jurczak, J. P. Camporez, H. Y. Lee, G. W. Cline, V. T. Samuel, R. G. Kibbey and G. I. Shulman (2014). "Metformin suppresses gluconeogenesis by inhibiting mitochondrial glycerophosphate dehydrogenase." Nature **510**(7506): 542-546.

Maric, K., A. Oksche and W. Rosenthal (1998). "Aquaporin-2 expression in primary cultured rat inner medullary collecting duct cells." Am J Physiol Renal Physiol **275**(5 Pt 2): F796-801.

Marples, D., S. Christensen, E. I. Christensen, P. D. Ottosen and S. Nielsen (1995). "Lithium-induced downregulation of aquaporin-2 water channel expression in rat kidney medulla." J Clin Invest **95**(4): 1838-1845.

Marples, D., T. A. Schroer, N. Ahrens, A. Taylor, M. A. Knepper and S. Nielsen (1998). "Dynein and dynactin colocalize with AQP2 water channels in intracellular vesicles from kidney collecting duct." Am J Physiol Renal Physiol **274**(2 Pt 2): F384-394.

Marr, N., D. G. Bichet, S. Hoefs, P. J. Savelkoul, I. B. Konings, F. De Mattia, M. P. Graat, M. F. Arthus, M. Lonergan, T. M. Fujiwara, N. V. Knoers, D. Landau, W. J. Balfe, A. Oksche, W. Rosenthal, D. Muller, C. H. Van Os and P. M. Deen (2002). "Cell-biologic and functional analyses of five new Aquaporin-2 missense mutations that cause recessive nephrogenic diabetes insipidus." J Am Soc Nephrol **13**(9): 2267-2277.

Marr, N., E. J. Kamsteeg, M. van Raak, C. H. van Os and P. M. Deen (2001). "Functionality of aquaporin-2 missense mutants in recessive nephrogenic diabetes insipidus." Pflugers Arch **442**(1): 73-77.

Matsumura, Y., S. Uchida, T. Rai, S. Sasaki and F. Marumo (1997). "Transcriptional regulation of aquaporin-2 water channel gene by cAMP." J Am Soc Nephrol **8**(6): 861-867.

Mauvezin, C., P. Nagy, G. Juhasz and T. P. Neufeld (2015). "Autophagosome-lysosome fusion is independent of V-ATPase-mediated acidification." Nat Commun **6**: 7007.

McDill, B. W., S. Z. Li, P. A. Kovach, L. Ding and F. Chen (2006). "Congenital progressive hydronephrosis (cph) is caused by an S256L mutation in aquaporin-2 that affects its phosphorylation and apical membrane accumulation." Proc Natl Acad Sci U S A **103**(18): 6952-6957.

Meng, S., J. Cao, Q. He, L. Xiong, E. Chang, S. Radovick, F. E. Wondisford and L. He (2015). "Metformin activates AMP-activated protein kinase by promoting formation of the alphabetagamma heterotrimeric complex." J Biol Chem **290**(6): 3793-3802.

Meo-Evoli, N., E. Almacellas, F. A. Massucci, A. Gentilella, S. Ambrosio, S. C. Kozma, G. Thomas and A. Tauler (2015). "V-ATPase: a master effector of E2F1-mediated lysosomal trafficking, mTORC1 activation and autophagy." Oncotarget **6**(29): 28057-28070.

Miller, R. A., Q. Chu, J. Xie, M. Foretz, B. Viollet and M. J. Birnbaum (2013). "Biguanides suppress hepatic glucagon signalling by decreasing production of cyclic AMP." Nature **494**(7436): 256-260.

Moeller, H. B., T. S. Aroankins, J. Slengerik-Hansen, T. Pisitkun and R. A. Fenton (2014). "Phosphorylation and ubiquitylation are opposing processes that regulate endocytosis of the water channel aquaporin-2." J Cell Sci **127**(Pt 14): 3174-3183.

Moeller, H. B., N. MacAulay, M. A. Knepper and R. A. Fenton (2009). "Role of multiple phosphorylation sites in the COOH-terminal tail of aquaporin-2 for water transport: evidence against channel gating." Am J Physiol Renal Physiol **296**(3): F649-657.

Moeller, H. B., J. Praetorius, M. R. Rutzler and R. A. Fenton (2010). "Phosphorylation of aquaporin-2 regulates its endocytosis and protein-protein interactions." Proc Natl Acad Sci U S A **107**(1): 424-429.

Moore, F., J. Weekes and D. G. Hardie (1991). "Evidence that AMP triggers phosphorylation as well as direct allosteric activation of rat liver AMP-activated protein kinase. A sensitive mechanism to protect the cell against ATP depletion." Eur J Biochem **199**(3): 691-697.

Morello, J. P., A. Salahpour, A. Laperriere, V. Bernier, M. F. Arthus, M. Lonergan, U. Petaja-Repo, S. Angers, D. Morin, D. G. Bichet and M. Bouvier (2000). "Pharmacological chaperones rescue cell-surface expression and function of misfolded V2 vasopressin receptor mutants." J Clin Invest **105**(7): 887-895.

Mulders, S. M., N. V. Knoers, A. F. Van Lieburg, L. A. Monnens, E. Leumann, E. Wuhl, E. Schober, J. P. Rijss, C. H. Van Os and P. M. Deen (1997). "New mutations in the AQP2 gene in nephrogenic diabetes insipidus resulting in functional but misrouted water channels." J Am Soc Nephrol **8**(2): 242-248.

Muller, K. H., G. A. Spoden, K. D. Scheffer, R. Brunnhofer, J. K. De Brabander, M. E. Maier, L. Florin and C. P. Muller (2014). "Inhibition by cellular vacuolar ATPase impairs human papillomavirus uncoating and infection." Antimicrob Agents Chemother **58**(5): 2905-2911.

Murase, T., Y. Tian, X. Y. Fang and J. G. Verbalis (2003). "Synergistic effects of nitric oxide and prostaglandins on renal escape from vasopressin-induced antidiuresis." Am J Physiol Regul Integr Comp Physiol **284**(2): R354-362.

Nedvetsky, P. I., E. Stefan, S. Frische, K. Santamaria, B. Wiesner, G. Valenti, J. A. Hammer, S. Nielsen, J. R. Goldenring, W. Rosenthal and E. Klussmann (2007). "A Role of Myosin Vb and Rab11-FIP2 in the Aquaporin-2 Shuttle." Traffic **8**(2): 110-123.

Nedvetsky, P. I., V. Tabor, G. Tamma, S. Beulshausen, P. Skroblin, A. Kirschner, K. Mutig, M. Boltzen, O. Petrucci, A. Vossenkamper, B. Wiesner, S. Bachmann, W. Rosenthal and E. Klussmann (2010). "Reciprocal Regulation of Aquaporin-2 Abundance and Degradation by Protein Kinase A and p38-MAP Kinase." J Am Soc Nephrol **21**(10): 1645-1656.

Nejsum, L. N., M. Zelenina, A. Aperia, J. Frokiaer and S. Nielsen (2005). "Bidirectional regulation of AQP2 trafficking and recycling: involvement of AQP2-S256 phosphorylation." Am J Physiol Renal Physiol **288**(5): F930-938.

Nielsen, S., B. L. Smith, E. I. Christensen, M. A. Knepper and P. Agre (1993). "CHIP28 water channels are localized in constitutively water-permeable segments of the nephron." J Cell Biol **120**(2): 371-383.

Noda, Y., S. Horikawa, E. Kanda, M. Yamashita, H. Meng, K. Eto, Y. Li, M. Kuwahara, K. Hirai, C. Pack, M. Kinjo, S. Okabe and S. Sasaki (2008). "Reciprocal interaction with G-actin and tropomyosin is essential for aquaporin-2 trafficking." J. Biol. Chem. **182**(3): 587-601.

Noda, Y., S. Horikawa, Y. Katayama and S. Sasaki (2004). "Water channel aquaporin-2 directly binds to actin." Biochem Biophys Res Commun **322**(3): 740-745.

Okutsu, R., T. Rai, A. Kikuchi, M. Ohno, K. Uchida, S. Sasaki and S. Uchida (2008). "AKAP220 colocalizes with AQP2 in the inner medullary collecting ducts." Kidney Int **74**(11): 1429-1433.

Olesen, E. T., M. R. Rutzler, H. B. Moeller, H. A. Praetorius and R. A. Fenton (2011). "Vasopressin-independent targeting of aquaporin-2 by selective E-prostanoid receptor agonists alleviates nephrogenic diabetes insipidus." Proc Natl Acad Sci U S A.

Owen, M. R., E. Doran and A. P. Halestrap (2000). "Evidence that metformin exerts its anti-diabetic effects through inhibition of complex 1 of the mitochondrial respiratory chain." Biochem J **348 Pt 3**: 607-614.

Pandit, K., P. Mukhopadhyay, S. Ghosh and S. Chowdhury (2011). "Natriuretic peptides: Diagnostic and therapeutic use." Indian J Endocrinol Metab **15 Suppl 4**: S345-353.

Pastor-Soler, N., V. Beaulieu, T. N. Litvin, N. Da Silva, Y. Chen, D. Brown, J. Buck, L. R. Levin and S. Breton (2003). "Bicarbonate-regulated adenylyl cyclase (sAC) is a sensor that regulates pH-dependent V-ATPase recycling." J Biol Chem **278**(49): 49523-49529.

Pattaragarn, A. and U. S. Alon (2003). "Treatment of congenital nephrogenic diabetes insipidus by hydrochlorothiazide and cyclooxygenase-2 inhibitor." Pediatr Nephrol **18**(10): 1073-1076.

Paunescu, T. G., N. Da Silva, L. M. Russo, M. McKee, H. A. Lu, S. Breton and D. Brown (2008). "Association of soluble adenylyl cyclase with the V-ATPase in renal epithelial cells." Am J Physiol Renal Physiol **294**(1): F130-138.

Paunescu, T. G., M. Ljubojevic, L. M. Russo, C. Winter, M. M. McLaughlin, C. A. Wagner, S. Breton and D. Brown (2010). "cAMP stimulates apical V-ATPase accumulation, microvillar elongation, and proton extrusion in kidney collecting duct A-intercalated cells." Am J Physiol Renal Physiol **298**(3): F643-654.

Pearce, D., R. Soundararajan, C. Trimpert, O. B. Kashlan, P. M. Deen and D. E. Kohan (2015). "Collecting duct principal cell transport processes and their regulation." Clin J Am Soc Nephrol **10**(1): 135-146.

Peri, F. and C. Nusslein-Volhard (2008). "Live imaging of neuronal degradation by microglia reveals a role for v0-ATPase a1 in phagosomal fusion in vivo." Cell **133**(5): 916-927.

Poea-Guyon, S., M. R. Ammar, M. Erard, M. Amar, A. W. Moreau, P. Fossier, V. Gleize, N. Vitale and N. Morel (2013). "The V-ATPase membrane domain is a sensor of granular pH that controls the exocytotic machinery." J Cell Biol **203**(2): 283-298.

Procino, G., C. Barbieri, M. Carmosino, G. Tamma, S. Milano, L. De Benedictis, M. G. Mola, Y. Lazo-Fernandez, G. Valenti and M. Svelto (2011). "Fluvastatin modulates renal water reabsorption

in vivo through increased AQP2 availability at the apical plasma membrane of collecting duct cells." Pflugers Arch. - Eur. J. Physiol.

Procino, G., C. Barbieri, G. Tamma, L. De Benedictis, J. E. Pessin, M. Svelto and G. Valenti (2008). "AQP2 exocytosis in the renal collecting duct -- involvement of SNARE isoforms and the regulatory role of Munc18b." J Cell Sci **121**(Pt 12): 2097-2106.

Procino, G., M. Carmosino, O. Marin, A. M. Brunati, A. Contri, L. A. Pinna, R. Mannucci, S. Nielsen, T. H. Kwon, M. Svelto and G. Valenti (2003). "Ser-256 phosphorylation dynamics of Aquaporin 2 during maturation from the ER to the vesicular compartment in renal cells." FASEB J **17**(13): 1886-1888.

Qin, A., T. S. Cheng, N. J. Pavlos, Z. Lin, K. R. Dai and M. H. Zheng (2012). "V-ATPases in osteoclasts: structure, function and potential inhibitors of bone resorption." Int J Biochem Cell Biol **44**(9): 1422-1435.

Raffel, S., M. Falcone, N. Kneisel, J. Hansson, W. Wang, C. Lutz, L. Bullinger, G. Poschet, Y. Nonnenmacher, A. Barnert, C. Bahr, P. Zeisberger, A. Przybylla, M. Sohn, M. Tonjes, A. Erez, L. Adler, P. Jensen, C. Scholl, S. Frohling, S. Cocciardi, P. Wuchter, C. Thiede, A. Florcken, J. Westermann, G. Ehninger, P. Lichter, K. Hiller, R. Hell, C. Herrmann, A. D. Ho, J. Krijgsveld, B. Radlwimmer and A. Trumpp (2017). "BCAT1 restricts alphaKG levels in AML stem cells leading to IDHmut-like DNA hypermethylation." Nature **551**(7680): 384-388.

Rao, R., M. Z. Zhang, M. Zhao, H. Cai, R. C. Harris, M. D. Breyer and C. M. Hao (2005). "Lithium treatment inhibits renal GSK-3 activity and promotes cyclooxygenase 2-dependent polyuria." Am J Physiol Renal Physiol **288**(4): F642-649.

Rena, G., E. R. Pearson and K. Sakamoto (2013). "Molecular mechanism of action of metformin: old or new insights?" Diabetologia **56**(9): 1898-1906.

Riethmuller, C., H. Oberleithner, M. Wilhelmi, J. Franz, E. Schlatter, J. Klokkers and B. Edemir (2008). "Translocation of aquaporin-containing vesicles to the plasma membrane is facilitated by actomyosin relaxation." Biophys J **94**(2): 671-678.

Robben, J. H., M. L. Kortenoeven, M. Sze, C. Yae, G. Milligan, V. M. Oorschot, J. Klumperman, N. V. Knoers and P. M. Deen (2009). "Intracellular activation of vasopressin V2 receptor mutants in nephrogenic diabetes insipidus by nonpeptide agonists." Proc Natl Acad Sci U S A **106**(29): 12195-12200.

Robben, J. H., M. Sze, N. V. Knoers and P. M. Deen (2007). "Functional rescue of vasopressin V2 receptor mutants in MDCK cells by pharmacochaperones: relevance to therapy of nephrogenic diabetes insipidus." Am J Physiol Renal Physiol **292**(1): F253-260.

Rojek, A., E. M. Fuchtbauer, T. H. Kwon, J. Frokiaer and S. Nielsen (2006). "Severe urinary concentrating defect in renal collecting duct-selective AQP2 conditional-knockout mice." Proc Natl Acad Sci U S A **103**(15): 6037-6042.

Salani, B., C. Marini, A. D. Rio, S. Ravera, M. Massollo, A. M. Orengo, A. Amaro, M. Passalacqua, S. Maffioli, U. Pfeffer, R. Cordera, D. Maggi and G. Sambuceti (2013). "Metformin impairs glucose consumption and survival in Calu-1 cells by direct inhibition of hexokinase-II." Sci Rep **3**: 2070.

Sarma, G. N., F. S. Kinderman, C. Kim, S. von Daake, L. Chen, B. C. Wang and S. S. Taylor (2010). "Structure of D-AKAP2:PKA RI complex: insights into AKAP specificity and selectivity." Structure **18**(2): 155-166.

Savelkoul, P. J., F. De Mattia, Y. Li, E. J. Kamsteeg, I. B. Konings, P. van der Sluijs and P. M. Deen (2009). "p.R254Q mutation in the aquaporin-2 water channel causing dominant nephrogenic diabetes insipidus is due to a lack of arginine vasopressin-induced phosphorylation." Hum Mutat **30**(10): E891-903.

Schnermann, J., C. L. Chou, T. Ma, T. Traynor, M. A. Knepper and A. S. Verkman (1998). "Defective proximal tubular fluid reabsorption in transgenic aquaporin-1 null mice." Proc Natl Acad Sci U S A **95**(16): 9660-9664.

Schrade, K., J. Troger, A. Eldahshan, K. Zuhlke, K. R. Abdul Azeez, J. M. Elkins, M. Neuenschwander, A. Oder, M. Elkewedi, S. Jaksch, K. Andrae, J. Li, J. Fernandes, P. M. Muller, S. Grunwald, S. F. Marino, T. Vukicevic, J. Eichhorst, B. Wiesner, M. Weber, M. Kapiloff, O. Rocks, O. Daumke, T.

Wieland, S. Knapp, J. P. von Kries and E. Klussmann (2018). "An AKAP-Lbc-RhoA interaction inhibitor promotes the translocation of aquaporin-2 to the plasma membrane of renal collecting duct principal cells." PLoS One **13**(1): e0191423.

Schrier, R. W., P. Gross, M. Gheorghiade, T. Berl, J. G. Verbalis, F. S. Czerwiec, C. Orlandi and S. Investigators (2006). "Tolvaptan, a selective oral vasopressin V2-receptor antagonist, for hyponatremia." N Engl J Med **355**(20): 2099-2112.

Schulz, N., M. H. Dave, P. A. Stehberger, T. Chau and C. A. Wagner (2007). "Differential localization of vacuolar H+-ATPases containing a1, a2, a3, or a4 (ATP6V0A1-4) subunit isoforms along the nephron." Cell Physiol Biochem **20**(1-4): 109-120.

Shi, P. P., X. R. Cao, J. Qu, K. A. Volk, P. Kirby, R. A. Williamson, J. B. Stokes and B. Yang (2007). "Nephrogenic diabetes insipidus in mice caused by deleting COOH-terminal tail of aquaporin-2." Am J Physiol Renal Physiol **292**(5): F1334-1344.

Simon, H., Y. Gao, N. Franki and R. M. Hays (1993). "Vasopressin depolymerizes apical F-actin in rat inner medullary collecting duct." Am J Physiol Renal Physiol **265**(3 Pt 1): C757-762.

Sorensen, M. G., K. Henriksen, A. V. Neutzsky-Wulff, M. H. Dziegiel and M. A. Karsdal (2007). "Diphyllin, a novel and naturally potent V-ATPase inhibitor, abrogates acidification of the osteoclastic resorption lacunae and bone resorption." J Bone Miner Res **22**(10): 1640-1648.

Soylu, A., B. Kasap, N. Ogun, Y. Ozturk, M. Turkmen, L. Hoefsloot and S. Kavukcu (2005). "Efficacy of COX-2 inhibitors in a case of congenital nephrogenic diabetes insipidus." Pediatr Nephrol **20**(12): 1814-1817.

Stefan, E., B. Wiesner, G. S. Baillie, R. Mollajew, V. Henn, D. Lorenz, J. Furkert, K. Santamaria, P. Nedvetsky, C. Hundsrucker, M. Beyermann, E. Krause, P. Pohl, I. Gall, A. N. MacIntyre, S. Bachmann, M. D. Houslay, W. Rosenthal and E. Klussmann (2007). "Compartmentalization of cAMP-dependent signaling by phosphodiesterase-4D is involved in the regulation of vasopressin-mediated water reabsorption in renal principal cells." J Am Soc Nephrol **18**(1): 199-212.

Stodkilde, L., R. Norregaard, R. A. Fenton, G. Wang, M. A. Knepper and J. Frokiaer (2011). "Bilateral ureteral obstruction induces early downregulation and redistribution of AQP2 and phosphorylated AQP2." Am J Physiol Renal Physiol **301**(1): F226-235.

Stone, K. A. (1999). "Lithium-induced nephrogenic diabetes insipidus." J Am Board Fam Pract **12**(1): 43-47.

Storm, R., E. Klussmann, A. Geelhaar, W. Rosenthal and K. Maric (2003). "Osmolality and solute composition are strong regulators of AQP2 expression in renal principal cells." Am J Physiol Renal Physiol **284**(1): F189-198.

Stransky, L. A. and M. Forgac (2015). "Amino Acid Availability Modulates Vacuolar H+-ATPase Assembly." J Biol Chem **290**(45): 27360-27369.

Su, Y., A. Zhou, R. S. Al-Lamki and F. E. Karet (2003). "The a-subunit of the V-type H+-ATPase interacts with phosphofructokinase-1 in humans." J Biol Chem **278**(22): 20013-20018.

Sun, T. X., A. Van Hoek, Y. Huang, R. Bouley, M. McLaughlin and D. Brown (2002). "Aquaporin-2 localization in clathrin-coated pits: inhibition of endocytosis by dominant-negative dynamin." Am J Physiol Renal Physiol **282**(6): F998-1011.

Talukdar, I., W. Szeszel-Fedorowicz and L. M. Salati (2005). "Arachidonic acid inhibits the insulin induction of glucose-6-phosphate dehydrogenase via p38 MAP kinase." J Biol Chem **280**(49): 40660-40667.

Tamma, G., E. Klussmann, K. Maric, K. Aktories, M. Svelto, W. Rosenthal and G. Valenti (2001). "Rho inhibits cAMP-induced translocation of aquaporin-2 into the apical membrane of renal cells." Am J Physiol Renal Physiol **281**(6): F1092-1101.

Tamma, G., E. Klussmann, G. Procino, M. Svelto, W. Rosenthal and G. Valenti (2003). "cAMP-induced AQP2 translocation is associated with RhoA inhibition through RhoA phosphorylation and interaction with RhoGDI." J Cell Sci **116**(Pt 8): 1519-1525.

Tang, Y., D. Scott, U. Das, D. Gitler, A. Ganguly and S. Roy (2013). "Fast vesicle transport is required for the slow axonal transport of synapsin." J Neurosci **33**(39): 15362-15375.

Tchapyjnikov, D., Y. Li, T. Pisitkun, J. D. Hoffert, M. J. Yu and M. A. Knepper (2010). "Proteomic profiling of nuclei from native renal inner medullary collecting duct cells using LC-MS/MS." Physiol Genomics **40**(3): 167-183.

Terris, J., C. A. Ecelbarger, D. Marples, M. A. Knepper and S. Nielsen (1995). "Distribution of aquaporin-4 water channel expression within rat kidney." Am J Physiol **269**(6 Pt 2): F775-785.

Tian, Y., K. Sandberg, T. Murase, E. A. Baker, R. C. Speth and J. G. Verbalis (2000). "Vasopressin V2 receptor binding is down-regulated during renal escape from vasopressin-induced antidiuresis." Endocrinology **141**(1): 307-314.

Tisdale, E. J. (2001). "Glyceraldehyde-3-phosphate dehydrogenase is required for vesicular transport in the early secretory pathway." J Biol Chem **276**(4): 2480-2486.

Tisdale, E. J. (2002). "Glyceraldehyde-3-phosphate dehydrogenase is phosphorylated by protein kinase Ciota /lambda and plays a role in microtubule dynamics in the early secretory pathway." J Biol Chem **277**(5): 3334-3341.

Tisdale, E. J., F. Azizi and C. R. Artalejo (2009). "Rab2 utilizes glyceraldehyde-3-phosphate dehydrogenase and protein kinase C{iota} to associate with microtubules and to recruit dynein." J Biol Chem **284**(9): 5876-5884.

Tisdale, E. J., C. Kelly and C. R. Artalejo (2004). "Glyceraldehyde-3-phosphate dehydrogenase interacts with Rab2 and plays an essential role in endoplasmic reticulum to Golgi transport exclusive of its glycolytic activity." J Biol Chem **279**(52): 54046-54052.

Tristan, C., N. Shahani, T. W. Sedlak and A. Sawa (2011). "The diverse functions of GAPDH: views from different subcellular compartments." Cell Signal **23**(2): 317-323.

Trombetta, E. S., M. Ebersold, W. Garrett, M. Pypaert and I. Mellman (2003). "Activation of lysosomal function during dendritic cell maturation." Science **299**(5611): 1400-1403.

Umenishi, F., T. Narikiyo, A. Vandewalle and R. Schrier (2006). "cAMP regulates vasopressin-induced AQP2 expression via protein kinase A-independent pathway." Biochim Biophys Acta **1758**(8): 1100-1105.

Valenti, G., G. Procino, M. Carmosino, A. Frigeri, R. Mannucci, I. Nicoletti and M. Svelto (2000). "The phosphatase inhibitor okadaic acid induces AQP2 translocation independently from AQP2 phosphorylation in renal collecting duct cells." J Cell Sci **113 (Pt 11)**: 1985-1992.

Valtin, H., W. H. Sawyer and H. W. Sokol (1965). "Neurohypophysial principles in rats homozygous and heterozygous for hypothalamic diabetes insipidus (Brattleboro strain)." Endocrinology **77**(4): 701-706.

Verney, E. B. (1947). "The antidiuretic hormone and the factors which determine its release." Proc R Soc Lond B Biol Sci **135**(878): 25-106.

Vitavska, O., H. Merzendorfer and H. Wieczorek (2005). "The V-ATPase subunit C binds to polymeric F-actin as well as to monomeric G-actin and induces cross-linking of actin filaments." J Biol Chem 280(2): 1070-1076.

Vossenkamper, A., P. I. Nedvetsky, B. Wiesner, J. Furkert, W. Rosenthal and E. Klussmann (2007). "Microtubules are needed for the perinuclear positioning of aquaporin-2 after its endocytic retrieval in renal principal cells." Am J Physiol Cell Physiol 293(3): C1129-1138.

Vukicevic, T., M. Schulz, D. Faust and E. Klussmann (2016). "The Trafficking of the Water Channel Aquaporin-2 in Renal Principal Cells-a Potential Target for Pharmacological Intervention in Cardiovascular Diseases." Front Pharmacol **7**: 23.

Walker-Gray, R., F. Stengel and M. G. Gold (2017). "Mechanisms for restraining cAMP-dependent protein kinase revealed by subunit quantitation and cross-linking approaches." Proc Natl Acad Sci U S A **114**(39): 10414-10419.

Walz, T., T. Hirai, K. Murata, J. B. Heymann, K. Mitsuoka, Y. Fujiyoshi, B. L. Smith, P. Agre and A. Engel (1997). "The three-dimensional structure of aquaporin-1." Nature **387**(6633): 624-627.

Wang, C. C., C. P. Ng, H. Shi, H. C. Liew, K. Guo, Q. Zeng and W. Hong (2010). "A role for VAMP8/endobrevin in surface deployment of the water channel aquaporin 2." Mol. Cell. Biol. **30**(1): 333-343.

Wang, D., D. Epstein, O. Khalaf, S. Srinivasan, W. R. Williamson, A. Fayyazuddin, F. A. Quiocho and P. R. Hiesinger (2014). "Ca2+-Calmodulin regulates SNARE assembly and spontaneous neurotransmitter release via v-ATPase subunit V0a1." J Cell Biol **205**(1): 21-31.

Wang, X., X. A. Lu, X. Song, W. Zhuo, L. Jia, Y. Jiang and Y. Luo (2012). "Thr90 phosphorylation of Hsp90alpha by protein kinase A regulates its chaperone machinery." Biochem J **441**(1): 387-397.

Whiting, J. L., L. Ogier, K. A. Forbush, P. Bucko, J. Gopalan, O. M. Seternes, L. K. Langeberg and J. D. Scott (2016). "AKAP220 manages apical actin networks that coordinate aquaporin-2 location and renal water reabsorption." Proc Natl Acad Sci U S A **113**(30): E4328-4337.

Wick, A. N., D. R. Drury, H. I. Nakada and J. B. Wolfe (1957). "Localization of the primary metabolic block produced by 2-deoxyglucose." J Biol Chem **224**(2): 963-969.

Wolosker, H., D. O. de Souza and L. de Meis (1996). "Regulation of glutamate transport into synaptic vesicles by chloride and proton gradient." J Biol Chem **271**(20): 11726-11731.

Woods, A., S. R. Johnstone, K. Dickerson, F. C. Leiper, L. G. Fryer, D. Neumann, U. Schlattner, T. Wallimann, M. Carlson and D. Carling (2003). "LKB1 is the upstream kinase in the AMP-activated protein kinase cascade." Curr Biol **13**(22): 2004-2008.

Xie, X. S., D. Padron, X. Liao, J. Wang, M. G. Roth and J. K. De Brabander (2004). "Salicylihalamide A inhibits the V0 sector of the V-ATPase through a mechanism distinct from bafilomycin A1." J Biol Chem **279**(19): 19755-19763.

Xu, D. L., P. Y. Martin, M. Ohara, J. St John, T. Pattison, X. Meng, K. Morris, J. K. Kim and R. W. Schrier (1997). "Upregulation of aquaporin-2 water channel expression in chronic heart failure rat." J Clin Invest **99**(7): 1500-1505.

Xu, Y., B. W. Osborne and R. C. Stanton (2005). "Diabetes causes inhibition of glucose-6-phosphate dehydrogenase via activation of PKA, which contributes to oxidative stress in rat kidney cortex." Am J Physiol Renal Physiol **289**(5): F1040-1047.

Yang, B., A. Gillespie, E. J. Carlson, C. J. Epstein and A. S. Verkman (2001). "Neonatal mortality in an aquaporin-2 knock-in mouse model of recessive nephrogenic diabetes insipidus." J Biol Chem **276**(4): 2775-2779.

Yasui, M., S. M. Zelenin, G. Celsi and A. Aperia (1997). "Adenylate cyclase-coupled vasopressin receptor activates AQP2 promoter via a dual effect on CRE and AP1 elements." Am J Physiol Renal Physiol **272**(4 Pt 2): F443-450.

Yoshida, M., Y. Iwasaki, M. Asai, T. Nigawara and Y. Oiso (2004). "Gene therapy for central diabetes insipidus: effective antidiuresis by muscle-targeted gene transfer." Endocrinology **145**(1): 261-268.

Yu, M. J., R. L. Miller, P. Uawithya, M. M. Rinschen, S. Khositseth, D. W. W. Braucht, C. L. Chou, T. Pisitkun, R. D. Nelson and M. A. Knepper (2009). "Systems-level analysis of cell-specific AQP2 gene expression in renal collecting duct." Proc Natl Acad Sci U S A **106**(7): 2441-2446.

Yui, N., H. A. Lu, Y. Chen, N. Nomura, R. Bouley and D. Brown (2013). "Basolateral targeting and microtubule-dependent transcytosis of the aquaporin-2 water channel." Am J Physiol Cell Physiol **304**(1): C38-48.

Zala, D., M. V. Hinckelmann, H. Yu, M. M. Lyra da Cunha, G. Liot, F. P. Cordelieres, S. Marco and F. Saudou (2013). "Vesicular glycolysis provides on-board energy for fast axonal transport." Cell **152**(3): 479-491.

Zhang, C. S., S. A. Hawley, Y. Zong, M. Li, Z. Wang, A. Gray, T. Ma, J. Cui, J. W. Feng, M. Zhu, Y. Q. Wu, T. Y. Li, Z. Ye, S. Y. Lin, H. Yin, H. L. Piao, D. G. Hardie and S. C. Lin (2017). "Fructose-1,6-bisphosphate and aldolase mediate glucose sensing by AMPK." Nature **548**(7665): 112-116.

Zhang, C. S., B. Jiang, M. Li, M. Zhu, Y. Peng, Y. L. Zhang, Y. Q. Wu, T. Y. Li, Y. Liang, Z. Lu, G. Lian, Q. Liu, H. Guo, Z. Yin, Z. Ye, J. Han, J. W. Wu, H. Yin, S. Y. Lin and S. C. Lin (2014). "The lysosomal v-ATPase-Ragulator complex is a common activator for AMPK and mTORC1, acting as a switch between catabolism and anabolism." Cell Metab **20**(3): 526-540.

Zhang, Y., I. L. Pop, N. G. Carlson and B. K. Kishore (2012). "Genetic deletion of the P2Y2 receptor offers significant resistance to development of lithium-induced polyuria accompanied by alterations in PGE2 signaling." Am J Physiol Renal Physiol **302**(1): F70-77.

Zhang, Y. L., H. Guo, C. S. Zhang, S. Y. Lin, Z. Yin, Y. Peng, H. Luo, Y. Shi, G. Lian, C. Zhang, M. Li, Z. Ye, J. Ye, J. Han, P. Li, J. W. Wu and S. C. Lin (2013). "AMP as a low-energy charge signal autonomously initiates assembly of AXIN-AMPK-LKB1 complex for AMPK activation." Cell Metab **18**(4): 546-555.

Zhang, Z., K. Apse, J. Pang and R. C. Stanton (2000). "High glucose inhibits glucose-6-phosphate dehydrogenase via cAMP in aortic endothelial cells." J Biol Chem **275**(51): 40042-40047.

Zoncu, R., L. Bar-Peled, A. Efeyan, S. Wang, Y. Sancak and D. M. Sabatini (2011). "mTORC1 senses lysosomal amino acids through an inside-out mechanism that requires the vacuolar H(+)-ATPase." Science **334**(6056): 678-683.

Zwang, N. A., J. D. Hoffert, T. Pisitkun, H. B. Moeller, R. A. Fenton and M. A. Knepper (2009). "Identification of Phosphorylation-Dependent Binding Partners of Aquaporin-2 Using Protein Mass Spectrometry." J. Proteome Res. **8**(3): 1540-1554.

PUBLICATION LIST

Articles

Review articles

Dema, A.*, E. Perets*, **M. S. Schulz***, V. A. Deak and E. Klussmann (2015). "Pharmacological targeting of AKAP-directed compartmentalized cAMP signalling." Cell Signal **27**(12): 2474-2487.

Vukicevic, T.*, **M. Schulz***, D. Faust and E. Klussmann (2016). "The Trafficking of the Water Channel Aquaporin-2 in Renal Principal Cells - a Potential Target for Pharmacological Intervention in Cardiovascular Diseases." Front Pharmacol **7**: 23.

*authors contributed equally

Original work

Götz, F., Y. Roske, **M. S. Schulz**, K. Autenrieth, D. Bertinetti, K. Faelber, K. Zuhlke, A. Kreuchwig, E. J. Kennedy, G. Krause, O. Daumke, F. W. Herberg, U. Heinemann and E. Klussmann (2016). "AKAP18:PKA-RIIalpha structure reveals crucial anchor points for recognition of regulatory subunits of PKA." Biochem J **473**(13): 1881-1894.

Manuscripts

Csályi, K. D.*, T. Rharass*, M. H. Q. Phan, **M. S. Schulz**, P. J. Wakula-Heinzel, K. N. Mhatre, D. Plotnick, A. A. Werdich, H. Zauber, M. Sury, M. Selbach, F. R. Heinzel, C. A. MacRae, E. Klußmann and D. Panáková. “AKAP2-PKA compartmentalization by alternative Wnt/GPCR signaling regulates L-type Ca^{2+} channel.”

*authors contributed equally

Talks

“Stem Cell Technology – focus on kidney research”
Group retreat AG Rosenthal / Klussmann, Heringsdorf, 30.06. – 02.07.2014
“New A-kinase Anchoring Proteins Controlling Renal Principal Cell And Cardiac Myocyte Functions or How to find an AKAP”
TransCard Retreat, Valencia, 29.06. - 02.07.2017
“Analysis of metabolic pathways controlling cAMP-regulated AQP2 redistribution in renal principal cells”
Wollenberger students seminar, MDC Berlin, 14.05.2018

Poster presentations

TransCard Retreat, Neuruppin, 26.11. – 28.11.2014
MDC & FMP PhD Retreat, Bad Saarow, 15.10. – 17.10.2015
Tag der Biotechnologie, TU Berlin, 14.07.2016
TransCard Retreat, Bad Saarow, 18.09. - 21.09.2016
MDC & FMP PhD Retreat, Ringhotel Schorfheide, 22.09. - 24.09.2016
5th International Meeting on Anchored cAMP Signaling Pathways, Zermatt, 6.10. - 9.10.2016